AGARD FLIGHT TEST INSTRUMENTATION SERIES

VOLUME 7. STRAIN GUAGE MEASUREMENTS ON AIRCRAFT

ADVISORY GROUP FOR AEROSPACE
RESEARCH AND DEVELOPMENT

PREPARED FOR
NORTH ATLANTIC TREATY ORGANIZATION

APRIL 1976

AGARDograph No.160

AGARD Flight Test Instrumentation Series
Volume 7
on
Strain Gauge Measurements on Aircraft

by

E.Kottkamp, H.Wilhelm and D.Kohl

REPORT DOCUMENTATION PAGE

1. Recipient's Reference	2. Originator's Reference	3. Further Reference	4. Security Classification of Document
	AGARD-AG-160 Volume 7	ISBN 92-835-1215-4	UNCLASSIFIED

5. Originator Advisory Group for Aerospace Research and Development
North Atlantic Treaty Organization
7 rue Ancelle, 92200 Neuilly sur Seine France

6. Title

STRAIN GAUGE MEASUREMENTS ON AIRCRAFT

7. Presented at

8. Author(s) E.Kottkamp, H.Wilhelm and D.Kohl

9. Date April 1976

10. Author's Address VFW-Fokker Test Laboratories
Lemwerder
Federal Republic of Germany

11. Pages 150

13. Keywords/Descriptors

Aircraft
Strain measurement
Loads (forces)
Flight tests
Airborne equipment

14. UDC 620.17:533.6.054:629.73.05

15. Abstract

This AGARDograph is the seventh of the AGARD Flight Test Instrumentation Series, and is intended to give the test engineer a comprehensive description of the different aspects of strain and load measurements on aircraft. These measurements are of outstanding importance as they are the only practical means of determining material stresses during ground and flight tests.

This AGARDograph has been sponsored by the Flight Mechanics Panel of AGARD.

10-7

14

(3) */dodsd+110;12111,1111

1) AD-784 944
2) 1/3/14/2
4) PC$5.50/MF$2.25
5) Advisory Group for Aerospace Research and Development, Paris (France).
6) AGARD Flight Test Instrumentation Series. Volume 6. Open and Closed Loop Accelerometers, (10) by I. McLaren. (11) Jul 74, (12) 46p
14) AGARD-ograph-160-Vol-6
21) See also Volume 4, AD-771 192.
NATO furnished. * Royal Aircraft Establishment, Bedford (England).

wpg 9/27 GRA 74-23

*51

DO NOT PUNCH

Added Entry

Release Date

74.12.13

Check List for Fields

	DC	SA
1	/	
2		
4	/	
5	/	
6	/	
8		
9		
10		
11		
12		
14		
15		
16		
17		
18		
19		
21		
22		
23		
25		
27		
29		
30		
33		
34		
35		/

23) Descriptors

*Aircraft,
*Flight tests,
*Accelerometers,
Instrumentation,
Open loop systems,
Closed loop systems,
Transducers,
Calibration,
[illegible],

25) Identifiers

/

27) Abstract: See reverse ( ) Page (s) - 1

29) Inventory 1

30) Annotated Title

33) Dist. Code 1

34) Serial 6

35) Code 400 043

FORM NTIS-59 (REV. 5-71)

U.S. DEPARTMENT OF COMMERCE
NATIONAL TECHNICAL INFORMATION SERVICE

DOCUMENT PROCESSING WORKSHEET

USCOMM-DC 41420-P71

R

AGARD-AG-160
Volume 7

NORTH ATLANTIC TREATY ORGANIZATION

ADVISORY GROUP FOR AEROSPACE RESEARCH AND DEVELOPMENT

(ORGANISATION DU TRAITE DE L'ATLANTIQUE NORD)

AGARDograph No.160 Vol.7

STRAIN GAUGE MEASUREMENTS ON AIRCRAFT

by

E.Kottkamp, H.Wilhelm and D.Kohl

Volume 7

of the

AGARD FLIGHT TEST INSTRUMENTATION SERIES

Edited by

K.C.Sanderson and A.Pool

This AGARDograph has been sponsored by the Flight Mechanics Panel of AGARD.

THE MISSION OF AGARD

The mission of AGARD is to bring together the leading personalities of the NATO nations in the fields of science and technology relating to aerospace for the following purposes:

- Exchanging of scientific and technical information;
- Continuously stimulating advances in the aerospace sciences relevant to strengthening the common defence posture;
- Improving the co-operation among member nations in aerospace research and development;
- Providing scientific and technical advice and assistance to the North Atlantic Military Committee in the field of aerospace research and development;
- Rendering scientific and technical assistance, as requested, to other NATO bodies and to member nations in connection with research and development problems in the aerospace field;
- Providing assistance to member nations for the purpose of increasing their scientific and technical potential;
- Recommending effective ways for the member nations to use their research and development capabilities for the common benefit of the NATO community.

The highest authority within AGARD is the National Delegates Board consisting of officially appointed senior representatives from each member nation. The mission of AGARD is carried out through the Panels which are composed of experts appointed by the National Delegates, the Consultant and Exchange Program and the Aerospace Applications Studies Program. The results of AGARD work are reported to the member nations and the NATO Authorities through the AGARD series of publications of which this is one.

Participation in AGARD activities is by invitation only and is normally limited to citizens of the NATO nations.

Published April 1976

ISBN 92-835-1215-4

620.17:533.6.054:629.73.05

Printed by Technical Editing and Reproduction Ltd
Harford House, 7–9 Charlotte St, London W1P 1HD

PREFACE

Soon after its foundation in 1952, the Advisory Group for Aeronautical Research and Development recognized the need for a comprehensive publication on flight test techniques and the associated instrumentation. Under the direction of the AGARD Flight Test Panel (now the Flight Mechanics Panel), a Flight Test Manual was published in the years 1954 to 1956. The Manual was divided into four volumes: I. Performance, II. Stability and Control, III. Instrumentation Catalog, and IV. Instrumentation Systems.

Since then flight test instrumentation has developed rapidly in a broad field of sophisticated techniques. In view of this development the Flight Test Instrumentation Committee of the Flight Mechanics Panel was asked in 1968 to update Volumes III and IV of the Flight Test Manual. Upon the advice of the Committee, the Panel decided that Volume III would not be continued and that Volume IV would be replaced by a series of separately published monographs on selected subjects of flight test instrumentation: the AGARD Flight Test Instrumentation Series. The first volume of the Series gives a general introduction to the basic principles of flight test instrumentation engineering and is composed from contributions by several specialized authors. Each of the other volumes provides a more detailed treatise by a specialist on a selected instrumentation subject. Mr W.D.Mace and Mr A.Pool were willing to accept the responsibility of editing the Series, and Prof. D.Bosman assisted them in editing the introductory volume. In 1975 Mr K.C.Sanderson succeeded Mr Mace as an editor. AGARD was fortunate in finding competent editors and authors willing to contribute their knowledge and to spend considerable time in the preparation of this Series.

It is hoped that this Series will satisfy the existing need for specialized documentaion in the field of flight test instrumentation and as such may promote a better understanding between the flight test engineer and the instrumentation and data processing specialists. Such understanding is essential for the efficient design and execution of flight test programs.

The efforts of the Flight Test Instrumentation Committee members and the assistance of the Flight Mechanics Panel in the preparation of this Series are greatly appreciated.

T. VAN OOSTEROM
Member of the Flight Mechanics Panel
Chairman of the Flight Test
Instrumentation Committee

CONTENTS

		Page No
PREFACE		iii
LIST OF SYMBOLS		ix
1.0	INTRODUCTION	1
1.1	Measuring strains on aircraft	1
1.2	Strain measurements by means of strain gauges	2
1.3	Other transducers	3
1.4	Application of strain gauges	4
2.0	PHYSICAL BACKGROUND	5
2.1	The behaviour of metallic materials under load	5
2.1.1	Metallic materials under static load	5
2.1.1.1	Longitudinal stress and deformation	5
2.1.1.2	Shear deformation and stress	7
2.1.1.3	States of stress	7
2.1.1.4	Mohr's circle for stress	8
2.1.1.5	Mohr's circle for strain or deformation	9
2.1.2	Metallic materials under cycling load	9
2.1.3	Dynamic loading	10
2.2	Physical fundamentals of strain gauges	10
2.2.1	Elasticity of metal conductors	10
2.2.2	Thermal expansion of metal conductors	10
2.2.3	Current conduction in a metal conductor	11
2.2.4	Change in resistance of an unsupported wire under tensile and thermal loads	11
2.2.4.1	Strain sensitivity	11
2.2.4.2	Temperature sensitivity	13
2.2.5	Strain sensitivity of a bonded strain gauge	13
2.2.5.1	A model for illustrating the strain relations in a bonded strain gauge	13
2.2.5.1.1	Transfer of a strain from the component to the supporting layer	13
2.2.5.1.2	Transfer of strain from the supporting layer to the measuring wire	15
2.2.5.1.3	Conclusions	15
2.2.6	Thermal behaviour of a bonded strain gauge under mechanical load	15
2.2.7	Semi-conductor strain gauges	16
2.2.7.1	Correlation between electric conductivity and mechanical strain	17
2.2.7.1.1	p- and n-type conductivity of semi-conductors	17
2.2.7.1.2	The piezoelectric effect	17

		Page No
2.2.7.1.3	Strain sensitivity of a bonded semi-conductor strain gauge	17
2.2.7.1.4	Thermal behaviour of a bonded semi-conductor strain gauge	17
2.2.8	Determination of the gauge factor k	18
3.0	THE MEASUREMENT OF RESISTANCE CHANGES OF STRAIN GAUGES	18
3.1	Current and voltage distribution in a Wheatstone bridge	20
3.2	Practical application of the Wheatstone bridge	22
3.2.1	Choice of the supply voltage with respect to power dissipation	22
3.2.2	Choice of the output signal conditioning equipment	22
3.2.3	Power dissipation in the bridge resistors	22
3.3	Behaviour of the Wheatstone bridge in unbalanced conditions	23
3.3.1	Quarter-active bridge	23
3.3.1.1	Temperature compensation	24
3.3.1.2	Three-wire method	25
3.3.2	Half-active bridge	25
3.3.3	Full-active bridge	26
3.4	Bridge balancing and compensation	26
3.4.1	Bridge balancing	26
3.4.2	Compensation	28
3.5	Bridge power supply	28
3.5.1	Voltage control	28
3.5.2	Current control	28
3.5.3	Separate-arm-controlled current supply	28
3.5.4	A.C. voltage supply	28
3.6	Immunity from electrical and magnetic disturbances	29
3.6.1	Common-mode voltages	29
3.6.2	Electrical and magnetic disturbances	29
3.7	Filtering	29
4.0	ERROR ESTIMATION FOR STRAIN GAUGES WITH METALLIC MEASURING GRIDS	29
4.1	Resistance tolerances of strain gauges	29
4.2	Gauge factor k	30
4.2.1	Gauge factor tolerances	30
4.2.2	Transverse strain sensitivity t	30
4.3	Errors caused by hysteresis and non-linearity	31
4.4	Maximum static elasticity of strain gauges	31
4.5	Creep effects	31
4.6	The temperature coefficient of a strain gauge	31

		Page No
4.7	Fatigue strength of a strain gauge	31
4.8	Effects of the thickness of the adhesive layer	32
4.9	Angular errors during application of the strain gauge	32
4.10	The stiffening effect	32
4.11	Insulation resistance effect	32
4.12	Averaging effect of the strain gauge over the entire measuring grid area	32
4.13	Estimation of the total errors	33
5.0	TYPES OF STRAIN GAUGES	33
5.1	Strain gauge configuration	33
5.2	Grid types and shapes	33
5.2.1	Wire-grid strain gauge	33
5.2.2	Flat-coil gauges	33
5.2.3	Cross-bridge gauges	33
5.2.4	Metal-foil gauges	34
5.2.5	Strain gauges with metal supporting materials	34
5.3	Supporting materials and their configuration	34
5.3.1	Strain gauges with paper supporting material	35
5.3.2	Strain gauges with epoxy or phenolic resin supporting material	35
5.3.3	Strain gauges with polyimide-foil supporting material	35
5.3.4	Strain gauges with glass-fibre-reinforced supporting material	35
5.3.5	Strain gauges for large strains	35
5.4	Vapour-deposited strain gauges	37
6.0	APPLICATION OF STRAIN GAUGES FOR STATIC AND DYNAMIC SHORT AND LONG TERM MEASUREMENTS UNDER NORMAL CONDITIONS	37
6.1	Preliminary remarks	37
6.1.1	Technical boundary conditions	37
6.1.2	Organizational boundary conditions	37
6.2	Material selection	38
6.3	Pre-treatment of bonding areas	40
6.3.1	Pre-cleaning	40
6.3.2	Mechanical pre-treatment	40
6.3.3	Chemical pre-treatment	40
6.4	Adhesives	40
6.4.1	Cold-setting adhesives	40
6.4.1.1	Acrylic resin adhesives	41
6.4.1.2	Cyanoacrylates	41

		Page No.
6.4.1.3	Other adhesives	41
6.4.2	Hot-setting adhesives	42
6.4.2.1	Epoxy resins	42
6.4.2.2	Phenolic resins	42
6.4.2.3	Polyimide resins	42
6.4.2.4	Ceramic adhesives	42
6.4.2.5	Special procedures	43
6.5	Wiring technique	43
6.6	Protective materials	43
6.7	General instructions	44
7.0	STRAIN GAUGES FOR SPECIAL APPLICATIONS	45
7.1	Measurement of multi-axial strain conditions and determination of mechanical stress conditions	45
7.1.1	Triaxial rosettes	46
7.1.1.1	$0^{\circ}/45^{\circ}/90^{\circ}$ rosettes	46
7.1.1.2	$0^{\circ}/60^{\circ}/120^{\circ}$ rosettes	50
7.1.2	Biaxial rosettes	52
7.1.3	Shear stress measurements with 90° rosettes	54
7.1.4	Boundary conditions for the application of rosettes	54
7.1.5	Error estimations for measurements with strain gauge rosettes	54
7.1.5.1	Errors of material constants	54
7.1.5.2	Orientation errors	55
7.1.5.3	Systematic errors	56
7.2	Measurement of strain behaviour by means of strain gauge chains	58
7.3	Strain gauges for flexural strain measurements	60
7.4	Strain gauges for membrane stress measurements	60
7.5	Strain gauges for the determination of residual stresses	61
7.6	Stress gauges	61
7.7	Measurement of material fatigue	62
7.8	Measurement of crack propagation	63
7.9	Measurement of large strains	63
7.10	Special procedures for strain gauge application	63
7.10.1	Self-adherent strain gauges	63
7.10.2	Pressure application of strain gauges	64
7.11	Strain transformers	64

		Page No
7.12	Geometrical arrangement and electrical interconnection to realize special measuring effects	65
7.13	Measurement of strains on and in fibre-reinforced components	67
7.14	Interconnection of strain gauge bridges for the measurement of defined load elements (structural measurements)	68
7.14.1	Basic mathematical relations	68
7.14.2	Calibration process	70
7.14.3	Interconnection of bridges	70
7.15	High-frequency strain measurements	71
7.16	Strain gauges of excessive lengths	71
7.17	Interferometric strain gauges	71
8.0	USE OF STRAIN GAUGES UNDER EXTREME ENVIRONMENTAL CONDITIONS	72
8.1	Use at extreme temperatures	72
8.1.1	Technical configurations of strain gauges for extreme temperatures and their attachment to the component	72
8.1.2	Influences of lead-wire resistances	73
8.1.3	Apparent strains	73
8.1.4	Dependence of the gauge factor k on temperature	75
8.1.5	Hysteresis: maximum static strain	75
8.1.6	Summary of the most important temperature characteristics	76
8.2	Use under hydrostatic pressure	76
8.3	Use under nuclear radiation	76
8.4	Use in magnetic fields	77
8.5	Use of strain gauges under vacuum conditions	78
9.0	INSTRUMENTATION OF TWO VAK 191 B AIRCRAFT WITH FLIGHT LOAD MEASURING SYSTEMS	78
9.1	Selection of components	78
9.2	Installation technique	79
9.2.1	Location of strain gauges	79
9.2.2	Installation of the strain gauge bridges	80
9.2.3	Installation time requirements	80
9.3	Calibration	80
9.4	Results	81
	REFERENCES	82
	FIGURES AND DIAGRAMS	87

LIST OF SYMBOLS
(Subscripts are explained in the text)

Symbol	Unit	Meaning
a	-	Reference direction of rosettes
A	mm^2	Cross-sectional area
d	mm	Diameter
e_o	-	Unit charge
E	N/mm^2	Modulus of elasticity
f	Hz	Frequency
F	N	Force
G	N/mm^2	Shear modulus
I	amp	Electric current
j	-	Complex operator
k	-	Gauge factor of a strain gauge
K	-	Degree Kelvin
ℓ	mm	Length
n	-	Free electrons/unit volume
R	Ω	Electrical resistance
S	-	Standard deviation
T	K	Temperature
$\overline{u}$	-	Electron mobility
U	volt	Electrical potential
x	mm	Length of supporting layer
α	-	Orientation angle of a rosette
α_R	K^{-1}	Temperature coefficient of resistance
α_T	K^{-1}	Temperature coefficient of expansion
β	radian	Orientation error
δ	radian	Shear angle
ϵ	$\mu m/m$	Principal strain
μ	-	Poisson's ratio
ξ	mm	Length of strain wire
ρ	$\mu\Omega/cm$	Specific resistance
σ	N/mm^2	Mechanical stress
τ	N/mm^2	Shear stress
ϕ	radian	Stress angle
χ	Ω^{-1}	Conductivity
ψ	radian	Section angle
ω	rad/sec	Angular velocity
Ω	-	Ohms

STRAIN GAUGE MEASUREMENTS ON AIRCRAFT

by
E Kottkamp, H Wilhelm, D Kohl
VFW-Fokker Test Laboratories
Lemwerder
Federal Republic of Germany

1.0 INTRODUCTION

This publication is intended to give the test engineer a comprehensive description of the different aspects of strain and load measurements on aircraft. These measurements are of outstanding importance as they are the only practical means of determining material stresses during ground and flight tests.

As stresses cannot be measured directly but must be derived by calculation from strain measurements, an introduction to the fundamental physical and mechanical laws is given. This is essential as the strain gauge is directly bonded to the specimen to be tested so that its surface becomes part of the measurement system. Strain gauge behaviour can therefore only be understood on the basis of some fundamental knowledge of these physical and mechanical laws. The main concentration is on the directly applicable methods but nevertheless some not directly applicable equations and techniques are mentioned, thereby demonstrating:

- some straightforward techniques which look attractive but have proven unsatisfactory for various reasons;
- special old and new strain measuring techniques which may become attractive in the future (e.g. for orbital spacecraft) so that the reader will know know the basic principles.

Once the strain has been exactly transferred from the surface of the specimen to the grid of the strain gauge, the quality of the measurement is determined by the accuracy of recording the resistance change. Techniques for recording resistance changes are therefore discussed. The main emphasis is put on the description of the Wheatstone bridge, but other circuit techniques are also considered.

After discussion of possible errors, the various types of strain gauges and adhesives are described. Practical advice is given on their application. In order to allow the test engineer some judgement in less usual cases, special applications of strain gauges are explained. This is followed by a consideration of the strain gauge behaviour under adverse environmental conditions (e.g. extreme low and high temperatures). Finally, an example is given of equipping an aircraft with a flight load measuring system.

The contents of this volume allow the test engineer to select the correct method for strain measurements. For special problems, the basic mathematical relationships are given to allow him to use more detailed calculations. Where special applications are needed the contents of this book give an understanding of the basic principles. This allows the necessary effort to be estimated and indicates the relevant documentation.

1.1 Measuring of strains on aircraft

The techniques for measuring strains, which are the subject of this paper, refer mainly to measurements within the scope of flight testing. However, the greater part of of the contents of this book is also applicable to non-aeronautical measurements.

A transducer used for measuring strains on a typical aircraft during flight nas to fulfil the following requirements:

1.	Strain range	0 to ±10000µm/m
2.	Transverse sensitivity	has to be negligible
3.	Accuracy of the measuring system	
	uncalibrated	±5% (as compared with the full-range value)
	calibrated	±3% (as compared with the full-range value)
4.	Resolution of the system	±10 µm/m
5.	Life	
	period of application	up to several years
	load cycles	up to 10^7 load cycles with varying amplitude
6.	Frequency range	0 to 2,000 Hz (in exceptional cases higher)
7.	Temperature range	200 K to 400 K (in exceptional cases higher)

8.	Pressure range	independent of pressure
9.	Other environmental conditions	high alternating load with regard to temperature and humidity chemically corrosive environment (e.g. for tank measurements) physically hostile environment (e.g. mechanical loads)
10.	Installation conditions	the effect on the test specimen of the application method and mechanical or thermal behaviour must be negligible. can be applied easily even in limited space
11.	Measuring techniques	easy connection even in the case of numerous measuring points. Fast data logging and processing must be possible
12.	Price and installation costs	must be low

Among all the available transducers, the strain gauge is the only one which is able to fulfil most of the above requirements.

1.2 Strain measurements by means of strain gauges

The characteristic feature of an electrical strain gauge is the change in its electrical resistance with the change in strain. It is therefore possible to determine the strain change by measuring this resistance change. If the strain in a component has to be determined, a strain gauge is bonded to the component and the resistance change is measured when different loads are applied to the component(Fig 1.2-1).The strain gauge must therefore be securely bonded to the surface of the component. Optimum application of strain gauges requires a comparatively detailed knowledge of the physical fundamentals so that the significance of numerous marginal conditions can be correctly estimated.

This paper will deal with these fundamentals, but also with some fundamentals of materials (Chapter 2) and with several aspects of measurement techniques (Chapter 3).

First, however, the basic characteristics of a strain gauge measurement system will be described. The relation between the resistance change ΔR of the strain gauge and the strain is expressed by

$$\frac{\Delta R}{R} = k \frac{\Delta \ell}{\ell} = k \cdot \varepsilon \qquad (1.2\text{-}1)$$

The gauge factor k (see Section 2.2) is a constant. The determination of the resistance change is almost exclusively carried out by means of the Wheatstone bridge circuit (Fig 1.2-2, see also Chapter 3).

In the balanced condition ($I = 0$) the relation is

$$\frac{R_1}{R_2} = \frac{R_3}{R_4} \quad \text{or} \quad R_1 = R_2 \frac{R_3}{R_4} \qquad (1.2\text{-}2)$$

The resistor R_1 is the strain gauge and R_2 a calibrated variable resistor. The balanced condition can be achieved by varying R_2 . Balancing is carried out in the strained and unstrained condition so that the resistance change ΔR_1 relative to the unstrained condition is proportional to the strain.

ΔR_1 can be determined by balancing the Wheatstone bridge and reading the value of ΔR_2.

$$\text{Then } \Delta R_1 = (R_2 + \Delta R_2) \frac{R_3}{R_4} - R_2 \frac{R_3}{R_4} \qquad (1.2\text{-}3)$$

$$\text{So} \quad \Delta R_1 = \Delta R_2 \frac{R_3}{R_4} \quad \text{hence} \quad \frac{\Delta R_1}{R_1} = \frac{\Delta R_2}{R_2}$$

$$\text{In turn } k \cdot \varepsilon = \frac{\Delta R_1}{R_1} = \frac{\Delta R_2}{R_2} \text{ so that } \varepsilon \text{ can be determined.}$$

The balancing method is not practicable for an in-flight strain gauge measurement; the output voltage of the unbalanced bridge is therefore measured (Fig 1.2-3).

The following approximation is applicable:

$$\frac{U_m}{U_s} = \frac{1}{4}\left(\frac{\Delta R_1}{R_1} - \frac{\Delta R_2}{R_2} - \frac{\Delta R_3}{R_3} + \frac{\Delta R_4}{R_4}\right) \qquad (1.2\text{-}4)$$

U_m = bridge output voltage

U_s = bridge supply voltage

The resistors R_1, R_2, R_3 and R_4 can all be strain gauges. With the same gauge factor k for all strain gauges the following relation results for a Wheatstone bridge with four strain gauges:

$$\frac{U_m}{U_s} = \frac{1}{4}\left(\varepsilon_{11} - \varepsilon_{22} - \varepsilon_{33} + \varepsilon_{44} \cdot k\right) \qquad (1.2\text{-}5)$$

with $k \cdot \varepsilon_{ii} = \frac{\Delta R_i}{R_i}$

Once the strain of the specimen has been determined for the direction of the strain gauge, the corresponding stress σ can be calculated by applying Hookes law.

1.3 Other transducers

In general and especially for flight measurements the strain gauge plays a leading role in the determination of strains and stresses. In certain special cases, however, it may be reasonable to occasionally use other transducers. As they are not generally applied in flight testing, they will be presented here only with a brief description of their fundamental mode of operation.

The oldest transducers known are the mechanically operating extensometers (Fig 1.3-1) where the change in length between a fixed and movable blade is converted into a rotary motion. Because of the large measuring length required, the sensitivity to vibration, the relatively complex assembly and the poor suitability for dynamic applications, devices of this or similar kinds are no longer used today.

If the pointer is replaced by a light beam as in Fig 1.3-2, we have the well known Martens extensometer. Because of its less complicated set-up, this device has some advantages when compared to the mechanical arrangement.

Another non-electrical transducer worth mentioning here is the pneumatic transducer. In its original form it was designed as a re-usable transducer. Fig 1.3-3 shows a version with a differential pressure outlet. Investigations by the US Army are aimed at the development of a strain gauge comparable to the electrical strain gauge in its application and stress behaviour. These could result in some improvements for flight measurements, in particular when electrical measuring equipment can only be used in a protected system due to safety reasons or when electronic auxiliary devices are dispensed with. (Ref (1)).

However, most of the transducers used besides strain gauges are based on electrical principles.

The first device to be mentioned in this connection is the inductance transducer which is also used, in its varying versions (Figs 1.3-4a-f), as a re-usable transducer for measuring large distances. Its advantages are high sensitivity, sturdiness and simple electrical circuit requirements.

Vibration and position sensitivity can lead to detrimental effects. In the medium frequency range (20-50 Hz) contact resonances occur and at high frequencies (>50 Hz) the transducer cannot be used at all because of the carrier frequency supply problems. The same applies to the vibrating-wire transducer (Fig 1.3-5). It is used in those cases where a high zero stability is required.

For some time, capacitance type transducers have been available on the market especially for application at extremely high temperatures. A typical type is shown in Fig 1.3-6. The disadvantage of this transducer lies in obtaining signal conditioning hardware to meet the requirements of a flight environment.

It is also possible to use piezoelectric transducers for dynamic measurements. However, due to the extremely high degree of temperature sensitivity, applications are very limited.

Finally, the surface coating methods must be mentioned briefly. The best-known and mostly used procedure is the brittle lacquer method. The lacquer is applied in the unstressed condition. When tension strain is applied, and this is the only possible application, cracks will occur. The direction of the cracks indicates the stress direction and their density the stress level. Thus the determination of the areas of maximum stress is the main field of application. For a more detailed analysis, strain gauges can then be applied in such areas. The above description demonstrates that the method is only applicable for one load cycle. (Various cases of application are shown in Figs 1.3-7A-D). Compared to it, the photoelastic method is not subjected to such limitations. For this method an optically active material is applied to the surface of the test specimen. The refraction characteristics of this material change when stressed. They can be made visible with optical equipment and then photographed. In a subsequent analysis, the stresses occurring can be determined qualitatively and, with limited accuracy, quantitatively in their distribution over the surface.

References: (1) (25), (B3), (B4), (B5), (B6).

1.4 Application of strain gauges

Basically a strain gauge is a device which measures strain in a single direction at the surface of a component. Though in some applications this strain may be the primary quantity to be determined, in most cases strain measurements are used to obtain information about the stresses that occur in the components to which the strain gauges are bonded or about the forces which act on such components. In the latter case, more information needs to be combined with the strain measurement.

The simplest case is a one-dimensional stress state, e.g. an infinitely long homogeneous bar of constant cross section loaded by a longitudinal force. Then a single strain gauge measuring in the longitudinal direction can be used to measure the strain. The stress will also be in the longitudinal direction and can be determined from the strain if the Young's modulus and the Poisson's ratio for the material are known. The force can be calculated by multiplying the stress by the cross-sectional area of the bar.

One-dimensional stress states rarely occur in practice, but a two-dimensional stress state can often be used as an adequate model for actual stress distributions. In this case the positions of the strain gauges must be carefully chosen, taking into account the stresses which are of interest. In some cases a single strain gauge will provide sufficient information, for instance in the case of a bar under pure bending; then a strain gauge at the point of greatest curvature can measure the maximum strain and the stress distribution in the bar can be calculated from it. In many cases, however, two or more strain gauges will be necessary to supply the information necessary to calculate the stresses. If the principal directions are known, strains of interest can usually be measured by a $0^{o}/90^{o}$ rosette. If the principal directions are not known, three-armed rosettes or a combination of three separate strain gauges will be required.

In the general case of a three-dimensional stress state it is necessary to define beforehand the stresses that must be measured. Often it is possible to use a two-dimensional approximation for the part that is of special interest. But in other cases a truly three-dimensional model must be made of the component and strain gauges will have to be applied at several specific spots.

In many applications where only the load is of interest, the calculation of the load via stress is replaced by a direct calibration of strain gauge output against load. This is, for instance, common practice for all strain gauges used in transducers. The same method but with multiple strain gauges and multiple applied loads, is used for measuring structural loads in aircraft.

2.0 PHYSICAL BACKGROUND

An appropriate application of the strain gauge and the conclusive interpretation of the measurement results are only possible with a thorough knowledge of the strain gauge system.

One part of this system is the material to be tested. Section 2.1 describes the elementary laws of the behaviour of metallic materials under load. Due to the outstanding importance of metallic materials, other materials (such as fibre reinforced materials) will be dealt with later in Section 7.13.

The other important part is the measuring grid of a strain gauge. The fundamental correlations between the load on the measuring grid and its electrical behaviour is described in Section 2.2 Metallic measuring grids as well as semi-conductor measuring grids are described here.

2.1 The behaviour of metallic materials under load

Each metallic body shows a specific behaviour under the influence of external loads. Up to a certain load elastic deformation takes place, i.e. the deformation disappears after unloading. However, if the load is increased beyond this point, first plastic deformation and then fracture occurs. The correlations between load and deformation are described in Chapters 2 and 7. Section 2.1 describes only the mathematical analysis of the different states of stress and deformation. Known principal directions (and principal stresses or strains) are the basis for the analysis. Using the formulae given here, stress can be determined for each direction of interest from a knowledge of the strain.

The field of experimental stress analysis, on the other hand, is described in Section 7.1. Here the principal directions and principal stresses and/or principal strains have to be found from the measured values of, for example, three strain gauges. In this case the directions of the strain gauges serve as the reference system.

2.1.1 Metallic materials under static load

2.1.1.1 Longitudinal deformation and stress

If we consider a simple circular bar under tension having a cross-sectional area A and loaded with longitudinal force F, as in Fig 2.1-1, assuming a uniform force distribution over the entire cross section, the force divided by the cross-sectional area is defined as the stress σ:

$$\sigma = \frac{F}{A} \qquad (2.1\text{-}1)$$

Under load F the length ℓ of the bar changes by $\Delta\ell$ from ℓ_0 to ℓ_1, $\ell_1 = \ell_0 + \Delta\ell$. The change in length divided by the length ℓ_0 is defined as the longitudinal strain:

$$\varepsilon_\ell = \frac{\Delta\ell}{\ell_0} = \frac{\ell_1 - \ell_0}{\ell_0} \qquad (2.1\text{-}2)$$

Under load F the diameter of the bar changes by Δd from d_0 to d_1, $d_1 = d_0 - \Delta d$. The change in diameter divided by the diameter d_0 is defined as the transverse strain or transverse contraction:

$$\varepsilon_t = \frac{-\Delta d}{d_0} = \frac{d_1 - d_0}{d_0} \qquad (2.1\text{-}3)$$

The relation between transverse strain ε_t and longitudinal strain ε_ℓ is a material constant. The value

$$\frac{-\varepsilon_t}{\varepsilon_\ell} = \mu = \frac{\ell_0}{d_0} \cdot \frac{-\Delta d}{\Delta\ell}$$

known as Poisson's ratio, will generally be about 0.3 for metals.

With respect to the area this leads to

$$\frac{\partial A}{\partial \ell} = \frac{\pi}{4} \frac{\partial (d^2)}{\partial \ell} = \frac{-A}{\ell_0 d_0} \frac{\ell_0}{\Delta\ell} \frac{\Delta d}{\Delta\ell} = \frac{-A}{\ell_0} \; 2\mu$$

If the bar is successively submitted to increasing loads and the values of σ are plotted against the values of ε, the result is a stress-strain diagram. The σ values are determined with reference to the original cross section A_0. The dashed line in Fig 2.1-2 shows the σ values as a function of the actual cross section. The latter is of no further importance and is shown only for illustrative purposes.

Up to σ_p (proportional limit) the curve shows a linear section; then there is a slight non-linearity up to the elastic limit σ_E. Up to this limit the material shows no remarkable permanent deformation. If the load is increased beyond σ_E, the material will be deformed permanently. When it deforms without requiring a further increase in load, the yield point σ_F is reached.

After completion of the yielding, the load can be increased until the stress reaches its maximum possible value σ_B, the ultimate stress; then fracture occurs. Fig 2.1-2 shows the σ-ε diagram for mild steel; for many other materials the limits indicated are not as marked as in this case. Some materials, for instance, have a very small linear part, others hardly show any yielding at all during load. The σ-ε diagrams together with many other parameters are published in material handbooks.

As stated above, the σ-ε diagram shows a linear part from $\sigma = -\sigma_p$ to $+\sigma_p$. In this linear part

$$\sigma = E\,\varepsilon \qquad (2.1\text{-}4)$$

thus

$$\frac{\sigma}{\varepsilon} = E \qquad (2.1\text{-}5)$$

where E is the modulus of elasticity, also called Young's modulus. The value $\frac{\sigma}{\varepsilon} = E$ is constant for the linear part mentioned above.

This linear range is known as Hooke's law range; equation (2.1-5)is therefore called Hooke's law for the uniaxial state of stress.

The modulus of elasticity E is, like μ, a material constant.Some typical parameters of materials used in aircraft are given in Table 2.1-1. The exact values, however, have to be taken from material handbooks.

The range beyond σ_E is of less importance for this paper as the limit load will not be exceeded during flight and this load has to be reached without yielding of materials. This will be demonstrated by static fracture tests. In some components, however, the actual stress is larger than σ_E, for instance in the vicinity of cracks, but this is part of fatigue life investigations.

Table 2.1-1: Some typical parameters of materials used in aircraft. (The exact values have to be taken from the material standards).

Material	Young's modulus E (N/mm^2)	Poisson's ratio μ	Specific weight (g/cm^3)	σ_E (N/mm^2)	σ_B (N/mm^2)	α_T ($\mu m/m/K$)
Al, 99.5% work hardened	72000	0.34	2.7	50-70	110-140	23
Al-Cu-Mg	74000	∿0.30	2.8	300	420-580	23
Ti, pure, work hardened	110000	∿0.36	4.5	400-500	∿700	9
Titanium Ti Al6 V4	115000	∿0.32	4.5	750-850	900-1150	9
Steel (1% C)	210000	0.28-0.30	7.84	180-200	350-400	12
Cr-Ni-steel 18% Cr, 8% Ni	195000	∿0.43	7.88	300-400	550-750	16

2.1.1.2 Shear deformation and stress

Fig 2.1-3 illustrates another kind of load by showing an element of a shear-stressed panel to which the shear stresses τ, which always occur in pairs, are applied. Under load, the element is deformed by the angle γ; the panel side lengths, however, remain constant. If, in this case, the shear stresses τ are plotted as a function of the shear angle γ, the result is the τ-γ diagram which is very similar to the σ-ε diagram and shows the same type of limits as the latter. The notation generally used for the Hooke's law range $-\tau_p$ to $+\tau_p$ is

$$\frac{\tau}{\gamma} = G \qquad (2.1\text{-}6)$$

where G is the shear modulus.

This covers the basic laws of the linear theory of elasticity of metallic materials, showing that the elastic behaviour of a metallic body can be defined by the parameters E, μ and G. These three magnitudes are governed by the relation

$$G = \frac{E}{2(1 + \mu)} \qquad (2.1\text{-}7)$$

Thus, it is possible to determine a third magnitude by means of two known magnitudes, i.e. the linear theory of elasticity requires two material constants.

2.1.1.3 States of stress

A spherical element, cut from the inside of a three-dimensional body, will form an ellipsoid if subjected to external loads. Maximum changes in length will occur in three mutually perpendicular directions of this ellipsoid, the so-called principal directions. In these directions the minimum and maximum stress values occur defined as so-called principal stresses. In all other directions not only changes in length but also angular displacements occur. A triaxial state of stress then exists.

The relations between principal stresses and principal strains in the principal directions are defined by Hooke's law for the triaxial state of stress

$$\varepsilon_1 = \frac{1}{E}\left[\sigma_1 - \mu(\sigma_2 + \sigma_3)\right] \qquad (2.1\text{-}8)$$

$$\varepsilon_2 = \frac{1}{E}\left[\sigma_2 - \mu(\sigma_1 + \sigma_3)\right] \qquad (2.1\text{-}9)$$

$$\varepsilon_3 = \frac{1}{E}\left[\sigma_3 - \mu(\sigma_1 + \sigma_2)\right] \qquad (2.1\text{-}10)$$

or

$$\sigma_1 = \frac{E}{1 + \mu}\left[\varepsilon_1 + \frac{\mu}{1 - 2\mu}(\varepsilon_1 + \varepsilon_2 + \varepsilon_3)\right] \qquad (2.1\text{-}11)$$

$$\sigma_2 = \frac{E}{1 + \mu}\left[\varepsilon_2 + \frac{\mu}{1 - 2\mu}(\varepsilon_1 + \varepsilon_2 + \varepsilon_3)\right] \qquad (2.1\text{-}12)$$

$$\sigma_3 = \frac{E}{1 + \mu}\left[\varepsilon_3 + \frac{\mu}{1 - 2}(\varepsilon_1 + \varepsilon_2 + \varepsilon_3)\right] \qquad (2.1\text{-}13)$$

Assuming that no stresses occur perpendicular to the component surface (exception: inner surface of a pressurized tank), the relations of the plane or two-dimensional state of stress are valid for this surface. Take $\sigma_3 = 0$, then:

$$\varepsilon_1 = \frac{1}{E}(\sigma_1 - \mu\sigma_2) \qquad (2.1\text{-}14$$

$$\varepsilon_2 = \frac{1}{E}(\sigma_2 - \mu\sigma_1) \qquad (2.1\text{-}15)$$

$$\varepsilon_3 = \frac{\mu}{\mu - 1}(\varepsilon_1 + \varepsilon_2) = \frac{-\mu}{E}(\sigma_1 + \sigma_2) \qquad (2.1\text{-}16)$$

or

$$\sigma_1 = \frac{E}{1 - \mu^2}(\varepsilon_1 + \mu\varepsilon_2) \qquad (2.1\text{-}17)$$

$$\sigma_2 = \frac{E}{1 - \mu^2}(\varepsilon_2 + \mu\varepsilon_1) \qquad (2.1\text{-}18)$$

Thus strains in all three principal directions can occur even at a biaxial state of stress.

The notations (2.1-8) to(2.1-18) are related to the principal directions of a stress state, but these are also notations for Hooke's law related to arbitrary directions.

The notation for any set of perpendicular coordinates in the biaxial state of stress can be found by changing the indices in equations (2.1-14) to (2.1-18) in the following way:

$$\varepsilon_1 \hat{=} \varepsilon_a \qquad \sigma_1 \hat{=} \sigma_a$$

$$\varepsilon_2 \hat{=} \varepsilon_b \qquad \sigma_2 \hat{=} \sigma_b$$

$$\varepsilon_3 \hat{=} \varepsilon_c$$

σ_a and σ_b indicate the stresses, ε_a, ε_b, and ε_c the strains in the arbitrary directions (see also Section 7.1).

2.1.1.4 Mohr's circle for stress

The relations described so far will now be explained in detail with reference to their practical use. The appropriate application of a strain gauge will be made easier and often possible only if the elementary laws described here are taken into consideration prior to the installation and during evaluation of the subsequent measurement results.

Firstly, again consider a plain tension bar, in this case with a rectangular cross-section (Fig 2.1-4) which is loaded with a longitudinal stress σ_y (in this example σ_y corresponds to σ_1 in an uniaxial stressfield with $\sigma_x = \sigma_2 = 0$). If a cut is performed in the plane X-X', the area of the resulting section will be

$$A\phi = \frac{A}{\cos \phi}$$

The stress acting on the section parallel to σ_y and "released" by the cut can be calculated under the assumption that the force $F = A\sigma_y$ is constant for all sections:

$$F = \sigma_y \cdot A = A\phi \cdot \bar{y}$$

$$\bar{y} = \frac{\sigma_y \cdot A}{A\phi} = \sigma_y \cdot \cos \phi \qquad (2.1\text{-}19)$$

Correspondingly, the components of $\bar{y}$, the normal stress σ and the shear stress τ, are

$$\sigma = \bar{y} \cos \phi = \sigma_y \cos^2 \phi = \frac{1}{2} \sigma_y (1 + \cos 2\phi) \qquad (2.1\text{-}20)$$

$$\tau = \bar{y} \sin \phi = \sigma_y \sin \phi \cos \phi = \frac{1}{2} \sigma_y \sin 2\phi \qquad (2.1\text{-}21)$$

After elimination of the angle ϕ, the fundamental equation of Mohr's circle for the uniaxial state of stress is obtained (see Fig 2.1-5)

$$(\sigma - \tfrac{1}{2} \sigma_y)^2 + \tau^2 = (\tfrac{1}{2} \sigma_y)^2 \qquad (2.1\text{-}22)$$

From this circle the normal stress and the shear stress of the uniaxial state of stress can be read for each angle ϕ. It is remarked that the maximum shear strees τ_{max} is related to $\phi = 45^0$ and that $\tau_{max} = \frac{\sigma_y}{2}$

The case presented here is a special case, as $\sigma_x = 0$. It refers to a uniaxial state of stress. Only in a case like this, and then only for the direction in which load σ_y acts, can the formulae (2.1-4) and (2.1-5) be applied. The formulae (2.1-14), (2.1-15) and (2.1-17) (2.1-18) respectively, have to be applied for all other directions and whenever a state of stress other than a uniaxial one exists.

If the plate of Fig 2.1-4 is also loaded with σ_x in addition to σ_y (see Fig 2.1-6), the result is a biaxial state of stress. Analogous to Fig 2.1-4, the stresses

$$\bar{y} = \sigma_y \cdot \cos \phi$$

and

$$\bar{x} = \sigma_x \cos (90^0 - \phi) = \sigma_x \sin \phi$$

are now found in the directions of the axes. From this follows:

$$\sigma = \sigma_x \sin^2\phi + \sigma_y \cos^2\phi = \frac{1}{2}(\sigma_x + \sigma_y) - \frac{1}{2}(\sigma_x - \sigma_y)\cos 2\phi \qquad (2.1\text{-}23)$$

$$\tau = \frac{1}{2}\sigma_y \sin 2\phi - \frac{1}{2}\sigma_x \sin 2\phi = \frac{1}{2}(\sigma_y - \sigma_x)\sin 2\phi \qquad (2.1\text{-}24)$$

Normal stresses and shear stresses in the section are defined by the relations (2.1.-23) and (2.1-24). Now the equation of Mohr's circle is as follows:

$$\left[\sigma - \frac{1}{2}(\sigma_x + \sigma_y)\right]^2 + \tau^2 = \left[\frac{1}{2}(\sigma_y - \sigma_x)\right]^2 \qquad (2.1\text{-}25)$$

Fig 2.1-7 shows Mohr's circle for the biaxial state of stress.

2.1.1.5 Mohr's circle for strain or deformation

A pattern similar to Mohr's circle for stress, where the shear stresses are plotted as a function of normal stresses, is the circle for strain or deformation. The strain ε is plotted on the abscissa, half the angular deformation $\frac{\gamma}{2}$ on the ordinate. Mohr's circle for strain or deformation can be derived from Mohr's circle for stress by using Hooke's laws for the biaxial state of stress. As in Mohr's circle for stress, the intersection points of circle and abscissa indicate the values of the principal strains. Strain and shear deformation can be determined for any direction by means of the deformation circle.

Considering the strains on the tension bar in Fig 2.1-4 $\varepsilon_x = -\mu\varepsilon_y$. The behaviour of strains on the component surface is shown in Fig 2.1-8 for the uniaxial state of stress (polar diagram). Fig 2.1-9 shows the associated deformation circle.

If strain ε_ϕ and shear deformation $\frac{\gamma_\phi}{2}$ are to be determined for any given angle ϕ, the angle 2ϕ has to be plotted in the centre of the deformation circle. The intersection point of leg and circle indicates the quantities of ε_ϕ and $\frac{\gamma_\phi}{2}$

ε_ϕ can also be calculated by means of the relation

$$\varepsilon_\phi = \frac{\varepsilon_x + \varepsilon_y}{2} - \frac{\varepsilon_x - \varepsilon_y}{2}\cos 2\phi \qquad (2.1\text{-}26)$$

resulting from the geometric correlations of the deformation circle. It is the basic relation for evaluation of strain gauge rosette measurements.

2.1.2 Metallic materials under cycling load

According to Section 2.1.1, a material is destroyed if a certain mechanical stress is applied. However, a fracture of the material can also occur at stresses far below the elastic limit if the load is applied several times. A fracture thus obtained is called an endurance fracture or a fatigue fracture.

In practice, fatigue fractures can occur on all machine parts subjected to alternating load (all aircraft components, crankshafts etc).

The area of a fatigue fracture basically comprises two regions:

- the region of the fatigue fracture
- the region of the residual fracture.

The fatigue fracture first consists of one or more small surface cracks which mainly develop in nicks, fillets or surface defects and slowly propagate into the component. Thus, the remaining supporting cross section is consequently reduced until it is no longer able to take up the load applied.

From the relation between residual cross section and original cross section, conclusions can be drawn regarding stress level and number of load cycles. The smaller the residual cross section, the smaller the nominal stress and the larger the number of load cycles.

In the course of time, load (stress) amplitudes of different magnitudes followed by extended periods of rest occur in machine parts. This load distribution produces a line structure in the fatigue fracture area allowing an evaluation of the crack propagation rate. At a continuous loading with uniform load amplitudes, the formation of a line structure does not occur.

2.1.3 Dynamic loading

Up to now the material behaviour has been considered only under the aspect that it can be idealized by a massless spring. In practice, however, this assumption is unacceptable if loads of a higher frequency act on the work. The representation as per Fig 2.1-10, characterizing the structure by means of mere spring behaviour, has to be replaced by a description as per Fig 2.1-11.

The structure has to be considered as a composition of a number of masses coupled via elastic connections. The overall energy impressed into the object is distributed between the spring energy proportional to deflection (potential energy) on the one hand and the mass energy proportional to velocity (kinetic energy) on the other hand, the distribution depending on the frequency of the impressing force. Furthermore, an exchange of energies takes place which is perfect within the so-called natural frequency. Due to the distribution or exchange of energy, e.g. for a beam, fixed at one end, a static linear correlation between the force introduced and the resulting strain distribution over the surface of the specimen no longer exists within the elastic range. Whereas quantity and direction of the load are the dominant factors for the resulting strain when applying fatigue loads, this strain is, in addition, affected decisively by load frequency and resonant behaviour of the specimen in the case of dynamic loading. Coupling of the different structural elements results in local and time varying loads. The body vibrates in defined inherent modes with points of absolute rest (nodes) and maximum deflection (antinodes).

Figs 2.1-12 and 2.1-13 illustrate the first two flexural modes of vibration of a bar supported at both ends. The result is a considerably varying stress distribution which may cause (in the antinodes) high local material loads. This condition, together with the large number of alternating loads resulting from the high frequency can rapidly lead to fatigue phenomena. An example of this is the crack development on aircraft panels caused by engine noise.

2.2 Physical fundamentals of strain gauges

The strain gauge is a versatile measuring device. Effective application however requires knowledge of the laws governing the measuring effect

$$\frac{\Delta R}{R} = \alpha\varepsilon \qquad (2.2\text{-}1)$$

In the following, the basic correlation between changes in the lattice structure of a metal conductor and the elastic behaviour occurring under mechanical loads will be discussed. In order not to complicate the item too much the following derivation is limited to uniaxial stress states only. The electrical characteristics of conductors are covered in Section 2.2.3.

2.2.1 Elasticity of metal conductors

The resistance wire of strain gauges consists of metal alloys (exception: semi-conductor strain gauges, ref Section 2.2.7). The crystal lattice of an alloy is similar to that of an ionic crystal. As the relations of ionic crystals are easy to deal with they will be used to describe mechanical behaviour under load (Fig 2.2-1).

The elements, i.e. atoms, atom groups and ions, of a solid body are retained in their equilibrium position of a three-dimensional crystal lattice by predominantly or exclusively electrical forces and assume regular lattice positions at defined spacings. Position within the lattice arises from the equilibrium between the repulsive effect of the exchange force of the atomic trunks and the electric force of attraction of the metal ions (Coulomb force). Fig 2.2-2a shows the behaviour of the individual forces as dashed curves; the resulting force is indicated by the sum of the two individual forces.

The behaviour of the cumulative forces leads to the physical explanation of Hooke's law, i.e. the proportionality between strain and stress existing for both tension and compression. In Section 2.1, this phenomenon has been dealt with experimentally. The lattice atoms are moved from their equilibrium positions if an external force is acting on the crystal body. Any resulting restoring forces can be illustrated quite vividly by means of Fig 2.2-2. If the curve of forces near the equilibrium position is approximated to point A by means of a tangent (Fig 2.2-2b), proportional restoring forces develop in both load directions (tension and compression). This means that when unloaded atoms return to their original position the crystal body again assumes its initial shape. This phenomenon of a reversible deformation describes the elasticity on which Hooke's law is based.

2.2.2 Thermal expansion of metal conductors

Fig 2.2-2 can also be used to interpret the thermal expansion of a crystalline body. Owing to the thermal effect, harmonic forces act on all atoms causing a vibration of the latter. The excitation forces increase with rising temperature. Thus only small vibration amplitudes occur at low temperatures. As shown in Fig 2.2-2b, the deflection is the same for both displacement directions; the atom vibrates about its equilibrium position.

Fig 2.2-2a shows that this linear correlation between excitation force and deflection is no longer true for higher temperatures. On the contrary, the amplitudes of both displacement directions now differ from each other so that vibrational zero and equilibrium positions no longer coincide. The crystal body's volume has increased. This relationship between temperature and volume explains the coefficient of expansion α_T which is well known in engineering.

2.2.3 Current conduction in a metal conductor

The crystal lattice shown in Fig 2.2-1 consists of positively charged atomic nucleii which are circled by negatively charged electrons on discrete shells. Some of these electrons can move freely within the crystal structure. Therefore, they are called conduction electrons and altogether are defined as electron gas because their behaviour is similar to that of a gas. If an external electrical field is applied, this electron gas starts to move in the direction of the field. The body is electrically conductive. The conductivity χ is defined by the number of free electrons n per unit volume, their elementary charge e_o and their mobility $\bar{u}$, the latter describing the mean electron velocity per unit field intensity with regard to a specific material.

$$\chi = n \cdot e_o \cdot \bar{u} \qquad (2.2\text{-}2)$$

The reciprocal value of χ, ρ, is defined as specific resistance. The resistance of a conductor (e.g. strain gauge) is a function of its length ℓ, its cross section A and its specific resistance ρ.

$$R = \rho \cdot \frac{\ell}{A} \qquad (2.2\text{-}3)$$

2.2.4 Change in resistance of an unsupported wire under tensile and thermal loads.

2.2.4.1 Strain sensitivity

In the following the characteristics of a strain gauge wire will be examined. The effects of the transfer of strain through adhesive and supporting material are covered in Section 2.2.5.

If a wire with a resistance R (equation(2.2-3))is subjected to a strain $\varepsilon = \frac{\Delta \ell}{\ell}$, then

$$\Delta R = \frac{\partial R}{\partial \varepsilon} \Delta \varepsilon \qquad (2.2\text{-}4)$$

applies for small changes in resistance.

The dependence of the relative resistance change $\frac{\Delta R}{R}$ on parameters ρ, ℓ, A (equation (2.2-3)) can be determined by partial differentiation.

$$\left\langle \frac{\Delta R}{R} \right\rangle_{T=\text{const}} = \left(\frac{1}{\rho} \frac{\partial \rho}{\partial \varepsilon} + \frac{1}{\ell} \frac{\partial l}{\partial \varepsilon} - \frac{1}{A} \frac{\partial A}{\partial \varepsilon} \right) \Delta \varepsilon \qquad (2.2\text{-}5)$$

Including the already known correlation (see also Section 2.1.1.1)

$$\frac{1}{A} \frac{\partial A}{\partial \varepsilon} = -2\mu$$

The following applies :

$$\left\langle \frac{\Delta R}{R} \right\rangle_{T=\text{const}} = \Delta \varepsilon \left(\frac{1}{\rho} \frac{\partial \rho}{\partial \varepsilon} + 1 + 2\mu \right) = \Delta \varepsilon \; k_D \qquad (2.2\text{-}6)$$

where k_D is the sensitivity factor of the strain gauge wire, called the gauge factor k_D (Fig 2.2-3). For practical reasons $\Delta\varepsilon$ is normally simply written as ε.

Gauge factor depends on the material of the strain gauge wire and is generally a function of strain. This means that changes in wire resistance are a function of changes in the geometric dimensions and the specific resistance. These characteristics are non-linear. (Fig 2.2-4).

In the elastic range at $\mu \approx 0.3$, the gauge factor k_D assumes a value of about 2 with the typical strain gauge measuring grid alloy constantan. Thus, the proportion resulting from changes in specific resistance is 20%. The effect of specific resistance does not apply to the plastic range as the crystal lattice of the strain gauge wire will not be deformed in this range, but each state of deformation has an identical lattice structure due to a displacement of the lattice planes. Considering the fact that μ in the plastic range assumes the value 0.5, the result is again a gauge factor 2.

Because of the abovementioned non-linearity, only alloys having a gauge factor that is constant within broad ranges of strain are of interest for the manufacture of strain gauges (see Chapter 4). This requirement considerably reduces the number of possible alloys available for strain gauges (Table 2.2-1).

Table 2.2-1: Survey of the most important characteristics of some grid materials for strain gauges (Ref (95))

Alloy Trade Name	Composition in %	Gauge Factor Elastic	Gauge Factor Plastic	Temperature Coefficients of Gauge Factor $\frac{\Delta k}{k}$/100K	Temperature Coefficients of Electrical Resistance αR $10^{-6}K^{-1}$	Coefficient of expansion α_T $10^{-6}K^{-1}$	Specific Resistance ρ, $\mu\Omega \cdot cm$	Remarks
Constantan Advance Eureka	55-60 Cu, 45-40 Ni	2.1	2.0	+1	-20÷+20*	15	49	Low scale resistance
Nichrome V Brightray "C"	80 Ni, 20 Cr	2.2-2.5 *	-2	0÷-2**	60÷100*	15	108	Solid oxide skin; change of crystal structure at 720K; strong effect of cold working
Karma and modifications	74 Ni, 20 Cr (Fe, Al, Cu of different quantities)	2.0-2.3	-2	-1÷-3**	-10÷+10*	13	133	Change of crystal structure at 770K; strong effect of cold working
ISO Elastic (Elinvar)	36 Ni, 8 Cr, 0.5 Mo, Fe (balance)	3.6	2.0	0÷-1**	40	7.2	88	
Platinum Tungsten	8-10W, Pt (balance)	4÷6	-2	-3.5	50÷150*	9	75	Excellent scale resistance stable
Amour alloy "D"	70 Fe, 20 Cr 10 Al	2.2		-1.5	-110*	16	176	Strong effect of heat treatment, corrosion drift partly compensated by change of ρ

* according to cold working or heat treatment

** according to temperature range

2.2.4.2 Temperature sensitivity

According to equation(2.2-5) the dependence of the relative resistance change $\frac{\Delta R}{R}$ is obtained in this case by partial differentiation according to the temperature.

From $$\left\langle \frac{\Delta R}{R} \right\rangle_{\Delta \ell = 0} = \left(\frac{1}{\rho} \cdot \frac{\partial \rho}{\partial T} + \frac{1}{\ell} \cdot \frac{\partial \ell}{\partial T} - \frac{1}{A} \frac{\partial A}{\partial T} \right) \Delta T \qquad (2.2\text{-}7)$$

if α_T = coefficient of thermal expansion

it follows that

$$\left\langle \frac{\Delta R}{R} \right\rangle_{\Delta \ell = 0} = \left(\frac{1}{\rho} \cdot \frac{\partial \rho}{\partial T} - \alpha_T \right) \Delta T \qquad (2.2\text{-}8)$$

The term in parentheses defines the temperature coefficient α_R of a metal conductor which again describes the change in resistance as a function of temperature

$$\left\langle \frac{\Delta R}{R} \right\rangle_{\Delta \ell = 0} = \alpha_R \cdot \Delta T \qquad (2.2\text{-}9)$$

Some numerical values for α_R are stated in Table 2.2-1.

Generally, α_R is a function of the temperature. As the temperature approaches absolute zero, α_R tends towards a limit value; however, at a critical temperature the characteristic of each conductor material suddenly drops to an unmeasureable value ($\rho \to 0$), and the conductor becomes a superconductor.

2.2.5 Strain sensitivity of a bonded strain gauge

The gauge factor k_D of an unsupported conductor material at a uniaxial state of stress has been described in Section 2.2.4.1 (equation (2.2-6)). However, if a strain gauge is applied to a component which is then expanded, a very complex strain/stress state occurs. This results in errors in the transfer of strain from the component via the adhesive and supporting material to the measuring grid. In this case, the strain sensitivity is mainly affected by the shape and characteristics of the measuring grid, the supporting material and the adhesive resulting in a gauge factor k of the bonded strain gauge, which is always smaller than that of an unsupported wire (k_D) i.e. $k < k_D$.

2.2.5.1 A model for illustrating the strain relations in a bonded strain gauge

This chapter describes the conditions on which the geometric dimensioning of a strain gauge is based. Referring to Ref (2) the strain and stress behaviour of the wire strain gauge can be illustrated by a model as shown in Fig 2.2-5.

Assuming that adhesive and supporting material form a homogeneous structure and that the overall modulus of elasticity of the supporting layer TS thus formed is smaller than the modulus of elasticity of the wire (E_D), the transfer of strain is characterized by

- the transfer length ℓ_{BT} and the transfer function $\frac{\varepsilon_{To}}{\varepsilon_B} = f(x)$, respectively indicating the strain behaviour between component B and supporting layer TS, and
- The transfer length ℓ_{TD} and the transfer function $\frac{\varepsilon_O}{\varepsilon_{To}} = f(\xi)$, respectively indicating the introduction of strain from the supporting layer to the measuring grid D. x indicates the linear length of the supporting layer and ξ the linear length of the wire.

The gradual transfer of strain at the ends of supporting layer and grid, respectively, is typical and also explains the differences between grid material and strain gauge sensitivity factors. In Fig 2.2-5, the grid wire sensitivity factor is represented by the area of the rectangle indicated by broken lines, while the strain gauge sensitivity factor is represented by the shaded area.

2.2.5.1.1 Transfer of strain from the component to the supporting layer

Photoelastic tests have shown that the transfer function $\frac{\varepsilon_{To}}{\varepsilon_B} = f(x)$ is based on the effect of the shear stresses τ in the supporting layer. The shear stresses are concentrated at the strain gauge ends and rapidly decrease towards the centre of the strain gauge (Fig 2.2-6b). Thus, only a minor part of the supporting layer, the

transfer length ℓ_{BT}, is involved in the introduction of strain into the measuring grid plane. This means that, contrary to some conceptions encountered in practice, special care has to be taken with regard to perfect adhesion at the boundaries when bonding strain gauges. In Fig 2.2-6c the elements involved are represented by combined spring elements while supporting material and adhesive are symbolized by bending springs and the measuring grid by a tension spring. Fig 2.2-6d shows the resulting stiffness model according to which the transfer function

$$\frac{\epsilon_{To}}{\epsilon_B} = f(x)$$

depends on the overall shear resilience of the supporting layer with the shear modulus (see Section 2.1.1.2).

$$G^* = \frac{E_T^*}{2(1 + \mu_T^*)} \quad \text{(refer equation (2.1-7))}$$

The parameters identified by an asterisk indicate the material constants for the connection resulting from the interaction of adhesive and supporting materials.

The effective modulus of elasticity E_T^* can be approximated from the moduli of elasticity of the supporting material (E_T) and the adhesive (E_K) as well as the associated layer thicknesses ϑ_T and ϑ_K.

Thus

$$E_T^* = \frac{\frac{E_k}{\vartheta k} \cdot \frac{E_T}{\vartheta T}}{\frac{E_k}{\vartheta_k} + \frac{E_T}{\vartheta_T}} (\vartheta_T + \vartheta_k) \qquad (2.2\text{-}10)$$

applies (Ref 2)).

Table 2.2-2 Shear modulus G for various adhesives and overall shear modulus G* for various supporting layers (Ref (3)).

Supporting Material	Shear Modulus G, G*, N/mm^2	Shear Strength N/mm^2
Agol cellulose adhesive	300	5.4
Agol + strain gauge paper	500	4.2
BF2 hot-curing resin adhesive	1000	26.0
BF2 + phenolic resin supporting material	1250	10.8
X 60 adhesive	1580	36.9
X 60 + acrylic resin supporting material	1170	27.5
BC 6035 resin	2600	24.0
BC 6035 + phenolic resin supporting material	2370	23.1

Some typical numerical values for G* and G, respectively, at room temperature are stated in Table 2.2-2.

Fig 2.2-7 shows the associated temperature dependence for some examples.

2.2.5.1.2 Strain transfer from the supporting layer to the measuring wire

When applying the strain gauge, the relations occurring during the transfer of strain from the component to the measuring grid plane can be affected by the adhesive used, the thickness δ_T and the length ℓ_T of the supporting layer, the strain transfer from the supporting layer to the measuring wire is determined by the geometric dimensions of the wire reversal points and by the material characteristics of supporting layer and measuring wire. Both factors are preset by the manufacture of the strain gauge.

Fig 2.2-8 indicates the effect of the wire reversal points and shows, particularly by the development as per Fig 2.2-8b, that not all wire sections of the meander-like measuring wires are in the direction of strain.

Owing to the geometric shape of their reversal points, the section beginnings and ends are expanding less than the component strain ε_B which is assumed to be constant, a biaxial state of stress prevailing in the component or with a uniaxial state of stress due to the effect of transverse contraction, even negative strains (linear compressions) may occur.

Theoretical studies have shown (Ref(3))that the relative transverse strain absorption, i.e. the transverse strain as a function of the strain absorption of the straightened measuring wire in the direction of strain, mainly depends on the measuring length ℓ_M, the radius of the reversal points as well as the relation between moduli of elasticity of wire and supporting layer. The resulting errors will be covered in Chapter 4.

The relation E_D/E_T^* has a decisive effect on the behaviour of $\varepsilon_o/\varepsilon_{To} = f(\xi)$ and thus on gauge factor. For commercial strain gauges the value for E_D/E_T^* at room temperature is about 100. If the plastic supporting layer softens e.g. due to increasing temperature (dE/dT (plastics) >dE/dT (metal), the supporting layer can no longer accurately impress the strain into the measuring wire resulting in a flattening of the transfer function $\varepsilon_o/\varepsilon_{To}$ and thus an increase in the transfer length ℓ_{TD}. This is one of the reasons for the temperature dependence of the gauge factor.

2.2.5.1.3 Conclusions

Important findings for practical utilization are:

- The gauge factor k associated with each strain gauge refers, among other things, to the geometric dimensions of the gauge. A shortening of the supporting material in order to deal with spatial limitations on the component to be tested can result in an overlapping of the transfer function $\varepsilon_{To}/\varepsilon_B$ and $\varepsilon_o/\varepsilon_{To}$ and thus cause a reduction in the gauge factor. It should be noticeable only if a shortened strain gauge is calibrated. The associated expenditure of time and equipment can be avoided if strain gauges of smaller dimensions are used.

- Stiff supporting layers have short transfer lengths ℓ_{BT}. However, it has to be taken into consideration that a large shear modulus G of the adhesive results in a separation of component and adhesive in the case of inadequate adhesion. In the case of an adequate adhesion, the shear stress reaches its peak values at the ends of the supporting layer. Studies on this matter have shown that in the case of strain gauges with brittle supporting material, these shear stress peaks can reach the shear strength of the supporting material and the subsequent destruction of the supporting material results in an uncontrolled separation of the strain gauge from the component. This behaviour becomes very obvious during strain measurements in the cryogenic temperature range if an unfavourable adhesive-supporting material combination is selected.

- The transfer length ℓ_{BT} increases with rising temperature because the shear modulus G and G^*, respectively, diminishes. As in the case of the strain gauge shortening already mentioned, this can also result in an overlapping of the $\varepsilon_{To}/\varepsilon_B$ and $\varepsilon_o/\varepsilon_{To}$ and cause a reduction in the gauge factor.

  At cyrogenic temperatures this phenomenon does not occur.

- If sufficient space is available on the component, strain gauges with large measuring grid lengths are recommended. These enable more reliance to be placed on the gauge factor stated by the manufacturer, a reduction in temperature coefficient, smaller transverse sensitivity and finally a minimum deviation in the linearity of the characteristic curves. (Ref(94)).

2.2.6 Thermal behaviour of a bonded strain gauge under mechanical load

So far the mechanism of a strain gauge wire has been considered under mechanical load (Section 2.2.4.1)or under the effect of temperature (Section 2.2.4.2) alone. This section will explain the behaviour of a bonded strain gauge under combined thermal and mechanical load. In this case the following applies to the change in resistance:

$$\Delta R = \frac{\partial R}{\partial \varepsilon} \Delta \varepsilon + \frac{\partial R}{\partial T} \Delta T \qquad (2.2\text{-}11)$$

Disturbing variables affecting the measuring signal, such as mechanical and mechanical/thermal reactions of the strain gauge, will be neglected (see Section 8.1.3).

If, for example, a tension bar is subjected to load, a stress σ_z will be present in the bar (ε_z) and stress σ_M in the strain gauge (ε_M). An additional increase in temperature results in

$$\varepsilon_z + \alpha_z \Delta T = \varepsilon_M + \alpha_M \Delta T \qquad (2.2\text{-}12)$$

where α_z and α_M are the coefficients of linear expansion for bar and strain gauge respectively.

Thus, the result will be

$$\varepsilon_M = \varepsilon_z + (\alpha_z - \alpha_M) \Delta T \qquad (2.2\text{-}13)$$

If the equations (2.2-6) and (2.2-8) are incorporated into equation (2.2-11), (see also Section 2.2.5) then

$$\frac{\Delta R}{R} = \varepsilon_M \cdot k + \alpha_R \Delta T \qquad (2.2\text{-}14)$$

If the equation(2.2-13)is now incorporated into equation(2.2-14), then

$$\frac{\Delta R}{R} = \varepsilon_z \cdot k + k(\alpha_z - \alpha_M)\Delta T + \alpha_R \Delta T \qquad (2.2\text{-}15)$$

or

$$\frac{\Delta R}{R} = \varepsilon_z \cdot k + [\alpha_R + k(\alpha_z - \alpha_M)] \Delta T \qquad (2.2\text{-}16)$$

Thus a thermal term is superimposed on the mechanical term. The thermal term is composed of the difference between the coefficients of linear expansion of the specimen (α_z) and strain gauge alloy (α_M) and of the resistance temperature coefficient of the strain gauge alloy (α_R). This is also the case when a biaxial state of stress is present in the component surface.

by careful selection of the strain gauge materials it is possible to keep the effect of the second term in equation(2.2-16)very low. In this respect, the manufacturers offer a great variety of so-called adapted temperature coefficients for all important component materials. However, this self-compensation is effective only for a limited temperature range (Fig 2.2-15b). In the case of large temperature changes ΔT (see Chapter 8), it has to be considered also that all parameters stated in equation(2.2-16)are functions of the temperature. By means of correct circuitry however, the effect of the temperature changes can be largely compensated (refer to Section 3.1.1.1).

2.2.7 Semi-conductor strain gauges

Sometimes semi-conductor strain gauges have been used. However, disadvantages have become apparent during their application. As a result, semi-conductor strain gauges are mainly used in the manufacture of transducers where accurate application and subsequent calibration ensure near perfect conditions.

The basic structure of a semi-conductor strain gauge is shown in Fig 2.2-9. Its essential advantage as compared to the metal strain gauge is its higher sensitivity. Many problems typical of strain gauges largely disappear due to the larger output signals. Measurements can often be performed without an amplifier. In addition, the smaller dimensions and the larger variety of resistance values (from $\sim$60Ω up to several kΩ) are important. On the other hand, there are grave disadvantages, non-linearity being the most inconvenient factor apart from the considerable temperature dependence of the resistances and the sensitivity. Their application is only practical when small strains have to be measured. The so-called piezoelectric effect that causes the change in resistance of a semi-conductor and its effect on the application of semi-conductor strain gauges will be discussed later. (Ref(22)).

2.2.7.1 Correlation between electric conductivity and mechanical strain

2.2.7.1.1 p- and n-type conductivity of semi-conductors

A semi-conductor is any material of crystalline structure that is not held together by metallic bonds so that its conductivity is inferior to that of metals.

A typical semi-conductor material is silicon. Its atomic structure shows in the undistorted state an equilibrium between the positive charge of the nucleus and the negative charge of the electrons circling the nucleus. However, the binding of the four electrons circling on the outer shell to the nucleus is not very strong so that there is a tendency to lose an electron even at the slightest increase in energy. This characteristic becomes particularly apparent if positively (such as arsenic) or negatively (such as indium) charged atoms are incorporated in the semi-conductor crystalline structure. (This process is called doping).

The conduction process will now be considered for a case where positively charged atoms are incorporated. If an electric field is applied (supply of energy), electrons separate from the outer shell of the silicon atoms. These negatively charged electrons are "drawn in" by the positive charges of the impurity atoms (acceptors). (Fig 2.2-10). The electrons then move in the opposite direction to the applied field. The process resembles a movement of positive charges (hole conduction) in the direction of the field. The conduction resulting from the positive charge of the impurity atoms is called a p-type conductivity. Unlike metallic conduction where an electron cloud is moving freely and continuously, the conduction of doped semi-conductors is characterized by a discontinuous electron exchange.

If negatively charged impurity atoms (donors) are incorporated in the crystalline formation, they lose their electrons when an electric field is applied. The lost electrons are replaced by electrons from the outer shells of the silicon atom. An n-type conductivity occurs (Fig 2.2-11).

2.2.7.1.2 The piezoelectric effect

Changes in the resistance of metal strain gauges are caused mainly by changes in the conductor volume (see Section 2.2.4). Changes in the resistance of semi-conductor strain gauges are largely based on changes in the movement of the charge of carriers i.e. the change of the specific resistance. This is a result of the piezoelectric effect described below.

As already indicated, the conductivity of semi-conductors will develop only after supply of defined energy quantities, as the electrons are at certain energy levels below the conductivity threshold. These levels shift under load. This shift appears as a change in conductivity and is called the piezoelectric effect.

2.2.7.1.3 Strain sensitivity of a bonded semi-conductor strain gauge

Equation(2.2-6) can be used to interpret the gauge factor of a semi-conductor strain gauge. Unlike metal strain gauges which always have positive gauge factors, the gauge factor of semi-conductor strain gauges can be negative. The value and behaviour of the gauge factor depends on the semi-conductor material used (Ge or Si), the type of conductivity (p-type or n-type), the crystal orientation and the component strain value (Fig 2.2-12 and Fig 2.2-13).

The relation between the change in resistance shown in Fig 2.2-12 and the strain is largely non-linear, The non-linearity generally increases with growing gauge factor as can be seen by the slope of the curve in Fig 2.2-12. For example, a p-type Si strain gauge with a gauge factor 120 shows a non-linearity of about 1% at a strain of 1000 µm/m. The non-linearity of the respective n-type Si strain gauges is larger by a factor of two or three. In order to obtain as large a measuring effect as possible, a large specific resistance and thus a large gauge factor (see Fig 2.2-13) will be selected. Fig 2.2-14, however, shows that the errors caused by temperature change increase with the gauge factor, Thus, the advantage of high sensitivity has to be paid for with the disadvantages of larger errors caused by temperature changes and non-linearity.

The statements of Section 2.2.5 concerning the strain transfers also apply to semi-conductor strain gauges.

2.2.7.1.4 Thermal behaviour of a bonded semi-conductor strain gauge

The thermal behaviour of a semi-conductor strain gauge can also be described by the equation (2.2-16) already stated in Section 2.2-6.

The gauge factor as well as the resistance temperature coefficient α_R of the most commonly known Si strain gauges are positive for p-type Si. A self-compensation of thermal effects would thus be possible only if the coefficient of linear expansion α_{HL} of the strain gauge were larger than the coefficient of linear expansion α_B of the component. Construction materials, however, do not comply with this condition so that a relevant compensation can be obtained only by using appropriate circuitry (see Section 3.1.1.1).

The gauge factor in the case of n-type Si is negative with positive α_R, so that for self-compensation of thermal effects it is necessary that $\alpha_B > \alpha_{HL}$.

It is technically possible to realize self-compensation in this case if the condition

$$\alpha_R = -k \cdot (\alpha_B - \alpha_{HL}) \qquad (2.2\text{-}17)$$

is met by an appropriate setting of the gauge factor.

Fig 2.2-15a finally shows the apparent strains (see Section 8.1.3) of a p-type and an n-type Si strain gauge, each bonded to steel. The compensating effect of the n-type Si strain gauge can be clearly identified.

In consequence, n-type Si is mainly used for semi-conductor strain gauges.

2.2.8 Determination of the gauge factor k

Each strain gauge package contains among other things the following supplier information:

- gauge factor k
- gauge factor variance
- relationship between gauge factor and temperature within a defined temperature range.

A verification of these values can be gained by applying the following calibration method as described in NAS942, ASTME251-86T and VDE/VDI2635 (Refs (31), (26), (28)).

For this purpose several sample strain gauges are bonded on to a bending beam. The bending moment is introduced by defined deformation, not by force. This has the following advantages:

- the bending radius is independent of temperature
- creep effects are negligible
- easier handling because of reduced tendency to oscillate.

Either a triangular beam fixed on one end or a bending beam with constant cross-section being supported at four points is used. By measuring the relative resistance change and calculating the corresponding strain, the gauge factor can be determined by equation (1.2-1).

The major disadvantage of this calibration method is its high sensitivity on:

- variations of beam thickness
- variation in thickness of adhesive

In order to get confident results therefore extreme care must be applied.

References: (2), (3), (22), (61), (62), (76), (81), (83), (84), (94).

3.0 THE MEASUREMENT OF THE RESISTANCE CHANGES OF STRAIN GAUGES

As a strain gauge changes its resistance when strain is applied, it is necessary with respect to the resolution and accuracy of the measurement to carefully select the most appropriate method of recording small resistance changes.

Resistance is a specific quantity; it is the ratio of the fundamental quantities voltage and current:

$$R = \frac{U}{I} \qquad (3.0\text{-}1)$$

In view of this a resistance can be determined only indirectly by means of the fundamental quantities. The simplest measuring circuit is the voltage divider circuit shown in Fig 3.0-1.

With the resistance R known and the constant supply voltage U_s, the relation between U_m and R_x is

$$U_m = \frac{R_x}{R + R_x} U_s \qquad (3.0\text{-}2)$$

If R_x is slightly changed by $\pm\Delta R_x$, then the relation becomes

$$U_m \pm \Delta U_m = \frac{U_s}{R + R_x \pm \Delta R_x} (R_x \pm \Delta R_x) \qquad (3.0\text{-}3)$$

As ΔR_x in case of strain gauge measurements is very small with respect to $(R + \Delta R_x)$ equation (3.0-3) can also be written

$$U_m \pm \Delta U_m = U_S \frac{R_x}{R + R_x} \left(1 \pm \frac{\Delta R_x}{R_x}\right) \tag{3.0-4}$$

According to equation (3.0-4) the total voltage to be measured is composed of the relatively small but interesting component ΔU_m and the many times greater dc voltage portion U_m. As resolution and accuracy of the measurement device are determined by the overall voltage, whereas only ΔU_m needs to be measured, the arrangement as shown in Fig 3.0-1 possesses severe disadvantages.

Because of the big dc voltage portion it is practically impossible to amplify the output voltage in order to get a higher resolution concerning ΔU_m. Any amplification would immediately lead to an overloading of the signal conditioning equipment.

The analysis of equation (3.0-4) has shown that the very simple circuit of Fig 3.0-1 is not useful for static strain measurements. It has been used nevertheless in some cases for dynamic measurements where it is possible to eliminate the influence of the dc voltage portion by means of a capacitive decoupling.

To allow some judgment about the correct usage of this technique in specific cases, the elementary mathematical laws are given below.

For the purpose of a dynamic resistance change Fig 3.0-2 can be replaced by an alternate circuit with the power source

$$U_x = \frac{\Delta R_x}{R + R_x} U_S$$

and the internal resistance

$$R_i = \frac{R \cdot R_x}{R + R_x} \qquad \text{(see Fig 3.0-3)}$$

From this, the measuring voltage results in

$$U_m = \frac{1}{R + R_x} \frac{j\omega R_m C}{1 + j\omega\left(\frac{R \cdot R_x}{R + R_x} + R_m\right)C} \Delta R_x U_S \tag{3.0-5}$$

If, in addition, the following applies

$$R_m >> R$$

$$R_m >> R_x$$

then we have

$$U_m = \frac{1}{R + R_x} \frac{j\omega R_m C}{1 + j\omega R_m C} \Delta R_x U_S \tag{3.0-6}$$

The amplitude behaviour and thus the frequency dependent relation of measured and actual unbalance is described by

$$\frac{U_m}{U_x} = \frac{1}{\sqrt{1 + \left(\frac{1}{\omega R_m C}\right)^2}} \tag{3.0-7}$$

Fig 3.0-4 demonstrates that sufficient accuracy will result only at $\omega C R_m \geq 5$.

Despite its very simple structure this circuit is not used often. Two reasons for this are firstly the fact that in most cases the static unbalance is important and secondly the circuit is very sensitive to interference existing on the supply voltage.

A measuring technique adapted to the requirements has to be independent of the dc voltage as it appears in equation (3.0-4). Fundamentally this leads from the absolute measurement of one voltage to a comparative measurement between two voltages. Thus the voltage drop occurring at the measuring resistor in the unloaded condition is compensated by a reverse voltage. The easiest way of realizing this circuit is paralleling

two voltage dividers. The resulting circuit is the Wheatstone bridge circuit (Fig 1.2-2) Here the measuring voltage U_m is only a function of the unbalance ΔR_2.

The Wheatstone bridge is the predominant measuring circuit for strain gauge measurements. It is therefore necessary to investigate its characteristics in some detail.

3.1 Current and voltage distribution in a Wheatstone bridge

It is not intended to deal with the complete theory of the Wheatstone bridge in this paper. However, as it is of critical importance for the measurement of strains and related quantities such as stresses and loads, the fundamental laws will be investigated. In individual cases it will then be possible to handle a special problem for which otherwise normal simplfications are not applicable.

The measuring circuit of Fig 3.1-1 can be described by the four bridge arm resistances R_i (i=1, 2, 3, 4), the supply voltage U_s including its source resistance R_q, the output resistance R_m and the resulting currents I_o, I_1 and I_2.

According to Kirchhoff's laws the following mesh equations are valid:

$$\begin{aligned} U_s &= (R_3+R_4+R_q)\, I_o - R_3\, I_1 - R_4\, I_2 \\ 0 &= -R_3 I_o + (R_1+R_3+R_m)\, I_1 - R_m\, I_2 \\ 0 &= -R_4 I_o - R_m\, I_1 + (R_2+R_4+R_m)\, I_2 \end{aligned} \qquad (3.1\text{-}1)$$

or in matrix form

$$\{U_s\} = [R]\,\{I\} \qquad (3.1\text{-}2)$$

with the supply voltage vector $\{U_s\}$, reply vector $\{I\}$, and the symmetrical 3 x 3 bridge matrix $[R]$.

$$[R] = \begin{bmatrix} R_3 + R_4 + R_q & -R_3 & -R_4 \\ -R_3 & R_1 + R_3 + R_m & -R_m \\ -R_4 & -R_m & R_2 + R_4 + R_m \end{bmatrix} \qquad (3.1\text{-}3)$$

by solution for $\{I\}$ equation (3.1-2) leads to

$$\{I\} = [R]^{-1}\{U_s\} \qquad (3.1\text{-}4)$$

with regard to the mesh currents.

Now it is possible to determine all other quantities with the equation (3.1-4).

With

$$[R]^{-1} = \frac{1}{\det[R]}\,[\text{adj } R]$$

$$[\text{adj } R] = \begin{bmatrix} (R_1+R_3+R_m)(R_2+R_4+R_m)-R_m^2 & R_3(R_2+R_4+R_m)+R_4R_m & R_4(R_1+R_3+R_m)+R_3R_m \\ R_3(R_2+R_4+R_m)+R_4R_m & (R_3+R_4+R_q)(R_2+R_4+R_m)-R_4^2 & R_m(R_3+R_4+R_q)+R_3R_4 \\ R_4(R_1+R_3+R_m)+R_3R_m & R_m(R_3+R_4+R_q)+R_3R_4 & (R_1+R_3+R_m)(R_3+R_4+R_q)-R_3^2 \end{bmatrix}$$

the loop currents are

$$I_0 = \frac{1}{\det[R]}\,[(R_1+R_3+R_m)(R_2+R_4+R_m) - R_m^2]\,U_s \qquad (3.1\text{-}5)$$

$$I_1 = \frac{1}{\det[R]}\,[R_3(R_2+R_4+R_m) + R_4R_m]\,U_s \qquad (3.1\text{-}6)$$

$$I_2 = \frac{1}{\det[R]}\,[R_4(R_1+R_3+R_m) + R_3R_m]\,U_s \qquad (3.1\text{-}7)$$

det [R] can be written as

$$\det[R] = R_q(R_1+R_3)(R_2+R_4)+R_1R_3(R_2+R_4)+R_2R_4(R_1+R_3) + R_m[R_q(R_1+R_2+R_3+R_4)+(R_1+R_2)(R_3+R_4)]$$

The output voltage is then (see also Fig 3.1-1)

$$U_m = i_m R_m = (I_1 - I_2)\, R_m$$

$$U_m = \frac{1}{\det[R]} (R_2R_3 - R_1R_4)\, R_m U_s \qquad (3.1\text{-}8)$$

Equation (3.1-8) clearly demonstrates the factors decisive for the final result

- power supply voltage U_s
- source resistance R_q
- bridge arm resistances R_i (i=1, 2, 3, 4)
- output resistance R_m

Taking into account a number of technical factors, the correlations can be considerably simplified. It can be generally assumed that the output resistance is very large compared to the bridge arm resistances. On the other hand it is permissible to neglect the supply voltage source resistance R_q for most of the applications. Thus based on the notations as shown in Fig 3.1-1 with

$$R_m \to \infty$$

$$R_q \to 0$$

det [R] can be written

$$\det[R] \approx R_m(R_1 + R_2)(R_3 + R_4)$$

The rapid development of electronics has led to the situation where more and more current controlled bridges are used because it is possible to control more effectively the influence of the lead wires. However, this technique has the disadvantage that the result is given in the dimension of resistance.

The following therefore contains a comparison of the most important fundamental relations for voltage-controlled and current controlled bridges (Ref(23)).

U_s is constant	I_s is constant
$(R_m \to \infty,\ R_q \to 0)$	$(R_m \to \infty,\ R_q \to \infty)$

Bridge output voltage

$$\frac{U_m}{U_s} = \frac{R_2R_3 - R_1R_4}{(R_1+R_2)(R_3+R_4)} \qquad \frac{U_m}{I_s} = R_e \frac{R_2R_3 - R_1R_4}{R_1+R_2+R_3+R_4} \qquad (3.1\text{-}9)$$

Bridge input resistance (resistance between A and D, seen by the power source, see Fig 3.1-1)

$$R_e = \frac{(R_1+R_2)(R_3+R_4)}{R_1+R_2+R_3+R_4} \qquad R_e = \frac{(R_1+R_2)(R_3+R_4)}{R_1+R_2+R_3+R_4} \qquad (3.1\text{-}10)$$

Bridge internal resistance (Resistance between B and C if the bridge is represented by a voltage U_m as source voltage and a corresponding source resistance)

$$R_i = \frac{R_1R_2}{R_1+R_2} + \frac{R_3R_4}{R_3+R_4} \qquad R_i = \frac{(R_1+R_3)(R_2+R_4)}{R_1+R_2+R_3+R_4} \qquad (3.1\text{-}11)$$

Bridge power dissipation

$$N_o = \frac{U_s^2}{R_e} \qquad N_o = I_s^2 R_e \qquad (3.1\text{-}12)$$

Power dissipation per bridge arm

$$N_1 = \frac{R_1}{(R_1+R_2)^2}U_s^2 \qquad N_1 = \left(\frac{R_1+R_2}{R_1+R_2+R_3+R_4}\right)^2 R_1 I_s^2 \qquad (3.1\text{-}13)$$

$$N_2 = \frac{R_2}{(R_1+R_2)^2}U_s^2 \qquad N_2 = \left(\frac{R_1+R_2}{R_1+R_2+R_3+R_4}\right)^2 R_2 I_s^2 \qquad (3.1\text{-}14)$$

$$N_3 = \frac{R_3}{(R_3+R_4)^2}U_s^2 \qquad N_3 = \left(\frac{R_3+R_4}{R_1+R_2+R_3+R_4}\right)^2 R_3 I_s^2 \qquad (3.1\text{-}15)$$

$$N_4 = \frac{R_4}{(R_3+R_4)^2}U_s^2 \qquad N_4 = \left(\frac{R_3+R_4}{R_1+R_2+R_3+R_4}\right)^2 R_4 I_s^2 \qquad (3.1\text{-}16)$$

3.2 Practical application of the Wheatstone bridge

Before going into details with regard to the dependence of the output voltage on the relevant unbalance, some basic characteristics need to be discussed first in the light of equations (3.1-9) to(3.1-16).

3.2.1 Choice of the supply voltage with respect to power dissipation

The bridge has two points of intersection, namely the connections to the power supply line and to the output measuring equipment. The bridge input resistance R_e is a decisive quantity for dimensioning of the bridge supply. According to equation (3.1-9) the measuring signal is proportionally linked with the bridge voltage which is therefore to be stabilized with utmost precision. For this purpose it is necessary to guarantee that the power required is available.

In a normal 120 ohm bridge with a 5 V supply voltage there exists a current of 42 mA and thus a power of 210 mW is dissipated. Owing to the large amount of measurement points which have to be parallel in the individual sections of an aircraft, relatively efficient power supply units are required. Only if this requirement is met may it be assumed as above that the source resistance R_q is negligible.

3.2.2 Choice of the output signal conditioning equipment

The dimensioning of the output signal conditioning equipment is to a large extent influenced by the bridge internal resistance. Normally this equipment consists of a differential amplifier. If the bridge has a voltage source U_m and an internal resistance R_i it can be described in the circuit diagram of Fig 3.2-1.

Assuming a very large amplification factor, it is sufficiently correct to consider the amplifier input current being negligibly low. Based on Fig 3.2-1, the following equation can be derived

$$\frac{U_a}{R_r} = \frac{U_m}{R_g + \frac{R_i}{2}}$$

thus leading to

$$U_a = \frac{R_r}{R_g}\,\frac{1}{1+\frac{R_i}{2R_g}}\,U_m \qquad (3.2\text{-}1)$$

The amplifier output voltage is influenced by the relation of the bridge internal resistance to the amplifier input resistance. The amplification resulting from the external connection $\frac{R_r}{R_g}$ being diminished by the factor $\frac{1}{1+\frac{R_i}{2R_g}}$

This fact has to be considered when adapting the signal conditioning equipment.

3.2.3 Power dissipation in the bridge resistors

The performance quantities N_i (i=1,2,3,4) determine the magnitude of the thermal power converted in the individual bridge resistors. In view of this it has to be taken into account that a reduced size of a strain gauge results in a corresponding increase of the heat transfer resistance. Thus it is possible that an unduly high temperature could develop in the gauge within a short period of time (Ref (4)).

Another point to be considered is the effect on the specimen of the thermal energy transferred. It can happen that materials with poor thermal conductivity will experience locally heated areas which in turn can lead to a change in the material characteristics (e.g. plasticization of plastics).

When selecting the bridge resistance, various performance aspects have to be considered as well. As will be shown later, the sensitivity of the bridge depends directly on the supply voltage (see also equation (3.1-9)). Equations (3.1-12)to(3.2.-16) indicate on the other hand that the thermal power dissipation is a function of the supply voltage squared at constant resistance. Therefore relatively high resistive strain gauges should be applied in critical cases. Then maximum sensitivity can be achieved for a given performance due to the fact that the corresponding relative resistance change of a strain gauge depends only on strain and not on the magnitude of its resistance. Nevertheless, it should be remembered that as a result of equation (3.2-1) the conditions for the determination of the values measured deteriorate with increasing resistance.

The above remarks demonstrate that a number of questions have to be carefully investigated before applying a measuring bridge if errors are to be avoided or minimized.

3.3 Behaviour of the Wheatstone bridge in unbalanced conditions

The behaviour of the bridge in unbalanced conditions is the next point to be discussed. At first, the type of application must be briefly mentioned. Strain gauges are used in aircraft for measuring strains and determination of stresses, forces and moments etc. and, in transducers, for the determination of pressures, accelerations etc. Distinction has to be made between calibrated and uncalibrated systems. Uncalibrated strain gauge bridges, the relation of which to the expected unbalance is known only theoretically, show an accuracy between $\pm 3\%$ and $+5\%$ referred to the full range of the strain. Among other things, the accuracy is influenced by the gauge factor tolerance which depends on the production batch, the transverse sensitivity of the strain gauge, the type and quality of the bonding, the alignment of the strain gauge on the specimen as well as the fluctuation range of the resistance values which also is subject to the manufacturing quality (see Chapter 4). A considerable improvement in the accuracy to values better than $\pm 2\%$ can be achieved if it is possible to carry out a thorough calibration before the actual measurement.

It is important to know these factors when comparing the influences of non-linearities, resulting from the theoretical characteristics of the Wheatstone bridge and the signal conditioning equipment against the overall accuracy of the strain values finally measured. Thanks to the degree of errors occurring in strain gauge measurements, these non-linearities can normally be neglected so that quite clear linear relations result.

Depending upon application, the strain gauge can be configured as quarter, half and full bridges, characterized by 1, 2 or 4 active strain gauges. Fig 3.3-1 shows these types of bridges.

It becomes apparent that it is possible to arrange three different types of half-bridges. For reasons of circuitry however, the arrangement of Fig 3.3-1B is almost exclusively used in practical application. The arrows mark the sign direction of the individual unbalance. With the combination shown in Fig 3.3-1, the maximum sensitivity of the bridge is then achieved. Thus it is necessary to reflect about the most suitable possibility of application and circuitry before the bridge is installed (Ref Chapter 7).

In contrast to the above considerations, the strain is directly incorporated into the equation when calculating the output voltage. For this the relation

$$\frac{\Delta R}{R} = k\varepsilon \qquad \text{is used (see Section 1.2, Fig 1.2-1)}$$

The relations mentioned apply with voltage control. They are compared with the relations referring to current control for some commonly used simplifications.

3.3.1 Quarter active bridge

The following calculations are based on the sign directions of the individual unbalances as shown in Fig 3.3.-1. Regarding a bridge balanced in zero load condition ($R_1R_4 = R_2R_3$) the bridge output voltage U_m can be calculated for an unbalance $+\Delta R_1$ with reference to equation (3.1-9) as follows:

$$\frac{U_m}{U_s} = \frac{R_2R_3-(R_1+\Delta R_1)R_4}{(R_1+\Delta R_1+R_2)(R_3+R_4)} = \frac{R_2R_3-R_1R_4-R_1R_4\frac{\Delta R_1}{R_1}}{(R_1+R_2)(R_3+R_4)+(R_3+R_4)\ \Delta R_1}$$

with $\frac{\Delta R_1}{R_1} = k_1\varepsilon_{11}$ this results into

$$\frac{U_m}{U_s} = -\frac{R_1 R_4}{(R_1+R_2)(R_3+R_4)}\, k_1 \varepsilon_{11}\, \frac{1}{1+\frac{R_1}{R_1+R_2}\, k_1 \varepsilon_{11}} \qquad (3.3\text{-}1)$$

In case of a fully symmetric bridge ($R_1=R_2=R_3=R_4=R$) this equation is reduced to

$$\frac{U_m}{U_s} = -\frac{1}{4}\, k_1 \varepsilon_{11} \frac{1}{1+\frac{1}{2}\, k_1 \varepsilon_{11}} \qquad (3.3\text{-}2)$$

The gauge factor k is approximately 2 for metal strain gauges. Because of the magnitude of the strains occurring in strain gauge technique the non-linear portion can be neglected as shown in Fig 3.3-2. There the non-linearity factor

$$\frac{1}{1+\frac{1}{2}\, k_1 \varepsilon_{11}}$$

is plotted as a function of the strain. Now it is possible to state the linear correlation

$$\frac{U_m}{U_s} = -\frac{1}{4}\, k_1 \varepsilon_{11} \qquad (3.3\text{-}3)$$

This leads to

$$\frac{U_m}{I_s} = -\frac{1}{4}\, R k_1 \varepsilon_{11} \text{ for the current-controlled bridge.} \qquad (3.3\text{-}4)$$

A fact illustrated by both relations is their proportional dependence on the supply. Besides this the current-controlled bridge requires the exact knowledge and uniformity of the bridge resistance.

It is no longer permissible to assume a linear correlation for the semi-conductor gauge due to the considerably higher gauge factor (-100 up to +200) as Fig 3.3-2 also shows. However, a linearization effective at least for small ranges of unbalance can be achieved if the fixed resistances R_2 and R_4 (Fig 3.3-1A) are evenly increased. Fig 3.3-3 indicates which values result for the factor

$$\frac{R_1}{R_1+R_2}\, k = \frac{1}{1+n_1} \qquad \text{where} \quad \left(n_1 = \frac{R_2}{R_1}\right)$$

This is responsible for the non-linearity, when n_1 is increased.

With $n_1 = 9$ an error of 2% results for an unbalance of $10^3\ \frac{\mu m}{m}$. When using this circuit some secondary effects have to be considered:

- the bridge sensitivity decreases
- the bridge internal resistance increases
- the bridge input resistance increases

Before discussing typical characteristics of the half-bridge, some important facts concerning the installation and wiring of quarter-bridges need to be mentioned.

3.3.1.1 Temperature compensation

Different temperatures applied to the constituents of the bridge cause output signals which are not related to load generated strain. One way of suppressing temperature effects often used is the installation of a passive strain gauge (dummy gauge). In Fig 3.3-4 a half-bridge is practically arranged for this case. The compensation gauge is bonded on a non-deforming area of the component to be measured in the direct neighbourhood of the active gauge which is strained by deformation. As it is normally impossible to find a non-deforming area, the gauge is usually bonded on a small sheet of a material corresponding to that of the component. This sheet is attached to the structure as close as possible to the active gauge. It is recommended to use active and dummy gauges from the same batch in order to obtain the same tolerances for the gauge factor and to keep temperature effects as low as possible.

When using an auxiliary sheet, it should be realized that in nearly all cases there are very large differences in the thermal capacity of the sheet and the component and that furthermore the thermal transfer resistance between these two elements is relatively high. In the case of rapid temperature changes it is possible that a deteriorating effect occurs because of temperature differences between component and sheet.

Therefore this application has to be carefully investigated in each individual case.

3.3.1.2 Three-wire method

If only two wires are used for connecting the active gauge to complete the bridge in the case of a quarter-bridge (Fig 3.3-5), large errors can occur. With the wire resistances R_{L1} and R_{L2}

$$\frac{U_m}{U_s} = \frac{k}{4}\,\varepsilon\,\frac{R_1}{R_1+R_{L1}+R_{L2}} \qquad \text{results for the measuring voltage.} \qquad (3.3\text{-}5)$$

Even if it is possible to balance the relatively large bridge asymmetry resulting from the arrangement, the temperature effects in the wires often exert considerable influence even though a self-compensating gauge is used.

In order to avoid these effects a three-wire method (Fig 3.3-6) is used for the quarter-bridge circuit if the effects cannot be compensated by means of a passive gauge in the manner described above.

In this circuit R_{L1} and R_{L2} are located in adjacent bridge arms and their influences compensate each other if the arms are of identical length, i.e. installed parallel. R_{L3} is located in the high-resistive closed output circuit and its influence is thus negligible.

3.3.2 Half-active bridge

Mainly due to reasons of wire routing, the arrangement of Fig 3.3-1B is normally used when applying half active bridges. Furthermore, the measuring quantities of the individual circuits differ only slightly against the bridge described below.

However, it has to be stated that an arrangement according to Fig 3.3-1C can be advantageous too when using semi-conductor gauges e.g. in transducers. In the case of complementary resistances occurring in the relevant longitudinal arms being considerably higher than the active gauges, the arrangement looks very much like an arm-controlled current supply which will be discussed later.

Applying equation (3.1-9) to the arrangement of Fig 3.3-1B leads for a bridge balanced in zero load condition ($R_1R_4=R_2R_3$) to

$$\frac{U_m}{U_s} = \frac{(R_2-\Delta R_2)R_3-(R_1+\Delta R_1)R_4}{(R_1+R_2+\Delta R_1-\Delta R_2)(R_3+R_4)}$$

Introducing

$$\frac{\Delta R_1}{R_1} = k_1\varepsilon_{11} \text{ and } \frac{\Delta R_2}{R_2} = k_2\varepsilon_{22}$$

results to

$$\frac{U_m}{U_s} = -\frac{R_1R_4(k_1\varepsilon_{11}+k_2\varepsilon_{22})}{(R_1+R_2)(R_3+R_4)\left(1+\frac{R_1}{R_1+R_2}k_1\varepsilon_{11}-\frac{R_2}{R_1+R_2}k_2\varepsilon_{22}\right)} \qquad (3.3\text{-}6)$$

In most cases fully symmetrical bridges and identical gauge factors will be applied. Then equation (3.3-6) reads:

$$\frac{U_m}{U_s} = -\frac{k}{4}\,\frac{\varepsilon_{11}+\varepsilon_{22}}{1+\frac{k}{2}(\varepsilon_{11}-\varepsilon_{22})} \qquad (3.3\text{-}7)$$

Normally the gauges are installed in such a way that $\varepsilon_{11}=\varepsilon_{22}=\varepsilon$ (refer to Section 7.12).

In this case the result is

$$\frac{U_m}{U_s} = -\frac{k}{2}\,\varepsilon \qquad (3.3\text{-}8)$$

Under the assumptions laid down above, the half active bridge with regard to linearity shows considerably better characteristics as compared to the quarter active bridge. In addition it is more sensitive by a factor of 2 for the cases discussed.

The output voltage of the current controlled bridge results in

$$\frac{U_m}{I_s} = -\frac{R}{2} k\varepsilon \qquad (3.3\text{-}9)$$

3.3.3 Full active bridge

Based on equation (3.1-9) the output voltage with the bridge balanced in zero load condition ($R_1R_4=R_2R_3$) is

$$\frac{U_m}{U_s} = -\frac{R_1R_4}{(R_1+R_2)(R_3+R_4)} \cdot \frac{k_1\varepsilon_{11}+k_2\varepsilon_{22}+k_3\varepsilon_{33}+k_4\varepsilon_{44}}{1+\frac{R_1}{R_1+R_2}k_1\varepsilon_{11}-\frac{R_2}{R_1+R_2}k_1\varepsilon_{22}-\frac{R_3}{R_3+R_4}k_3\varepsilon_{33}+\frac{R_4}{R_3+R_4}k_4\varepsilon_{44}} \qquad (3.3\text{-}10)$$

Equation (3.3-10) is again based on the signal directions of Fig 3.3-1E. As only small unbalances are considered, the products and powers of unbalances are neglected.

In case of a fully symmetric bridge ($R_1=R_2=R_3=R_4=R$) with identical gauge factors and an appropriate installation of the gauges (see Section 7.12) that leads to

$$\varepsilon_{11}=\varepsilon_{22}=\varepsilon_{33}=\varepsilon_{44}=\varepsilon$$

the following equation results:

$$\frac{U_m}{U_s} = -k\varepsilon \qquad (3.3\text{-}11)$$

and for the current-controlled bridge

$$\frac{U_m}{I_s} = -Rk\varepsilon$$

Thus under the assumptions laid down above the full active bridge possesses the highest degree of sensitivity among all bridge types discussed.

3.4 Bridge balancing and compensation

Different techniques are used to get defined starting conditions at the beginning of a measurement. They can be categorized into direct and indirect methods. Direct methods are based on balancing resistors which form a part of the bridge itself and by adjustment lead to a zero bridge output signal. Indirect methods are based on the compensation of the bridge output voltage by means of electronic or computing networks outside the bridge circuit.

3.4.1 Bridge balancing

The most common balancing circuit is the shunt bridge (Fig 3.4-1). The efficiency of this network can be calculated by replacing the star-shaped circuit by a corresponding triangular circuit (Fig 3.4-2), thus leading to

$$R_a = R_o \frac{1+2p-x^2}{1+x} \qquad (3.4\text{-}1)$$

$$R_b = R_o \frac{1+2p-x^2}{1-x} \qquad (3.4\text{-}2)$$

$$R_c = R_o \frac{1+2p-x^2}{p} \qquad (3.4\text{-}3)$$

R_c occurs only as a supply voltage loading and does not influence the bridge behaviour. R_a and R_b, however, appear as parallel resistors for R_3 and R_4.

The following criteria do apply to the selection of R_o and p:

- the maximum zero unbalance shall be compensated by adjusting x to ± 1
- the values of R_a and R_b shall not change the bridge sensitivity compared to a non-shunted bridge; their influence shall be negligible
- the compensation performance shall be as linear as possible
- the power supply shall be loaded as low and continuous as possible by R_c

Using the power supply load requirement the elementary conditions can be formulated

$$R_o >> R_e \qquad (R_e = \text{bridge input resistance})$$

$$p > 1$$

The performance of the circuit shall be discussed on the basis of its main use as a generator of defined calibration signals. This method is always applied when it is not sufficient to simply connect known resistors in parallel.

Another main field of application is the compensation of zero load bridge unbalances.

Using equation(3.1-9)and assuming $R_1=R_2=R_3=R_4=R$ it follows

$$\frac{U_m}{U_s} = \frac{1}{4}\left(\frac{\Delta R_3^*}{R_3^*} - \frac{\Delta R_4^*}{R_4^*}\right) \qquad \begin{matrix}(^* \text{ indicates } R_3 \| R_a \text{ and } R_4 \| R_b) \\ R_3 \simeq R_3^* \qquad R_4 \simeq R_4^*\end{matrix} \tag{3.4-4}$$

Under the assumptions laid down above, equation(3.4-4)can be written

$$\frac{U_m}{U_s} = \frac{1}{4R}\left(\Delta R_3^* - \Delta R_4^*\right)$$

ΔR_3^* and ΔR_4^* can be calculated as follows

$$\Delta R_3^* = R_3^* - R_{3(x=0)}^* = R\left(\frac{1+2p-x^2}{\frac{R}{R_o}(1+x)+1+2p-x^2} - \frac{1+2p}{2(\frac{R}{R_o}+p)}\right)$$

$$\Delta R_4^* = R_4^* - R_{4(x=0)}^* = R\left(\frac{1+2p-x^2}{\frac{R}{R_o}(1-x)+1+2p-x^2} - \frac{1+2p}{2(\frac{R}{R_o}+p)}\right)$$

This leads to

$$\frac{U_m}{U_s} = -\frac{1}{2}\,\frac{(1+2p-x^2)\,\frac{R}{R_o}\,x}{(\frac{R}{R_o}+1+2p-x^2)^2 - (\frac{R}{R_o}x)^2}$$

$$\frac{U_m}{U_s} = -\frac{1}{2}\,\frac{R}{R_o}\,x\,\frac{1}{1+2p}\,\frac{1-\frac{x^2}{1+2p}}{(\frac{R}{R_o(1+2p)}+1-\frac{x^2}{1+2p})^2 - \frac{R^2x^2}{R_o^2(1+2p)^2}} \tag{3.4-5}$$

Taking into account

$$\frac{R}{R_o(1+2p)} << 1 - \frac{x}{1+2p}$$

$$\frac{R^2x^2}{R_o^2(1+2p)^2} \to 0$$

the relation between U_m and x can be described with good accuracy

$$\frac{U_m}{U_s} = -\frac{1}{2}\,\frac{R}{R_o}\,\frac{x}{1+2p} \tag{3.4-6}$$

Thus under the above assumption the bridge unbalance is directly proportional to the displacement x. When used for calibration therefore defined signals can be generated.

The counterpart of the shunt bridge is the use of compensatory balancing as shown in Fig 3.4-3. Based on a servo loop the bridge output voltage is always zero-balanced.

The relationship between the displacement x and the strain shall be calculated for a quarter bridge as an example by using equation (3.1-9)

$$R_2(R_3+\frac{R_o}{2}(1-x)+\Delta R_3)-R_1(R_4+\frac{R_o}{2}(1+x))=0 \qquad (3.4\text{-}7)$$

Introducing $R_1=R_2=R_3=R_4=R$ and $\frac{\Delta R_3}{R_3}=k\varepsilon$ leads to

$$x=\frac{R}{R_o}k\varepsilon \qquad (3.4\text{-}8)$$

The displacement x is directly proportional to the unbalance. In addition to being independent of the supply voltage, owing to the complexity and the low dynamics caused by the motor, the use of this arrangement is nevertheless limited to exceptional cases.

3.4.2 Compensation

Besides the use of direct methods, indirect compensation is often used. This can be done by analogue or digital techniques using either analogue amplifiers to add a compensating voltage to the bridge output voltage or when using digital computers which can store the zero load condition in the core for later calculation of the unbalance in the case of multi-channel equipment.

3.5 Bridge power supply

Voltage or current-controlled bridges are mostly used for the applications considered in this report. In addition, it is possible to have an a.c. voltage supply and a bridge with separate current-fed arms. Some general aspects of the power supply will now be explained in a comprehensive form.

3.5.1 Voltage control

A voltage-controlled bridge is shown in Fig 3.5-1. The handicap of this arrangement can be realized at first glance. The voltage actually applied to the bridge, as compared with U_o, is reduced by the voltage drop at the resistances $\frac{R}{2}$ of the leads.

Since there is a proportional relationship between the output and the supply voltage, with the exception of the self-balancing bridge, (see equation (3.1-8))short leads with a low resistance should be used.

These difficulties, which must be balanced against the advantage of a fairly simple circuit, can be eliminated by connecting a sensing line. This line serves to determine the actual bridge voltage which is then readjusted to the required value by means of a control circuit (six-wire circuit, Fig 3.5-2).

A variant of this circuit is often used in aircraft. In this case power supply support points are provided with said sensing lines. The lead wires between these support points and the surrounding bridges are then so short that their influence is negligible.

3.5.2 Current control

If the uncertainties of voltage control are to be avoided, current control can be used. However, circuit arrangements are now more complex. Each bridge needs a separate supply and the measured signal is proportionally influenced by the bridge resistance.

3.5.3 Separate-arm-controlled current supply

The separate-arm-controlled current supply as shown in Fig 3.5-3 is used in particular in multi-point measuring techniques. This bridge is marked by absolute linearity. A disadvantage is again the dependence of the output signal on the magnitude of the arm resistance.

3.5.4 A.C. voltage supply

In the case of static long-term measurements requiring a good amplifier drift behaviour, almost exclusive use is made of the carrier frequency method (Fig 3.5-4) with the bridge being supplied with an a.c. voltage.

This circuit has a band-pass characteristic. Its transmission frequency range is determined by the magnitude of the carrier frequency f_T and the band width B of the band-pass filter. These characteristics ensure a particularly low interference susceptibility. Thermoelectric voltages, amplifier drifts, mains disturbances as well as high-frequency interferences (excess noise etc) have no effect. By using phase-selective demodulation and subsequent filtering a d.c. voltage signal U is obtained which is largely free from interference. However, the magnitude of the carrier frequency is normally limited by cable capacity. Therefore, this circuit is only used for the determination of dynamic measurements in exceptional cases.

References: (21), (25), (26), (34).

3.6 Immunity from electrical and magnetic disturbances

In conclusion, some elementary aspects regarding the circuit technique to be applied will be dealt with. Observance of these aspects will considerably improve immunity from disturbance. The immunity from disturbance of the measuring chain described depends, in the first line, on the type of grounding and on the connection of the individual elements of the measuring chain. Two basic influences have to be taken into consideration:

3.6.1 Common-mode voltages

In the case of a power supply connected according to Fig 3.6-1, both inputs of the measuring amplifier have the same potential relative to ground. Although, theoretically, there should not be a measurable signal, a voltage which is dependent on the amplifier quality (common-mode suppression), is built up at the amplifier output. For the circuit shown in Fig 3.6-1 the common-mode voltage amounts to $\frac{U_s}{2}$.

In the case of common-mode suppression of 60 db and if U_s = 5 V the apparent measuring voltage is:

$$U_{m\ c.m.} = \frac{2.5V}{1000} = 2.5\ mV$$

Taking a maximum measuring range of 10 mV, which applies to quite a lot of bridges, this would correspond to an unacceptable measurement error of 25%.

This effect can be mitigated by a balance-to-earth supply (Fig 3.6-2). In this case with symmetrical bridge resistors, the common-mode voltage disappears completely in the balanced condition.

3.6.2 Electrical and magnetic disturbances

Interfering voltages may be induced in the leads and measuring grids by electrical and magnetic disturbances (Fig 3.6-3). This influence can be substantially reduced when the individual cables are twisted and shielded. Twisting is the only practicable protection against magnetic disturbances, whilst shielding suppresses the influence of electrical disturbances.

References: (23), (24), (25), (34), (58), (89), (90).

3.7 Filtering

In practical applicationsof the Wheatstone bridge in strain gauge measurements it is often helpful and advantageous to use filtering techniques in the signal conditioning stage to improve the result.

When the static portion within the signal is of main interest, but this part is submerged by a big noise level, a low pass filter can be used to improve the signal/noise ratio. If on the contrary, the dynamic portion of the signal is of interest but is practically hidden within a big dc part, decoupling can be achieved by introducing a high-pass filter. Most often a band pass filter is applied which allows concentration on the interesting frequency range.

In any case, when evaluating the resulting signals, the filter characteristics have to be taken into account with respect to amplitude and phase response in order to avoid errors.

4.0 ERROR ESTIMATION FOR STRAIN GAUGES WITH METALLIC MEASURING GRIDS

The advantages of strain gauges are simple handling, high adaptability to the various measuring tasks, suitability for static and dynamic loads up to the highest structural frequencies prevailing.

In general, gauge factor tolerance, linearity and hysteresis, response to temperature change, time/temperature creep behaviour, fatigue behaviour, insulation defects and others are considered to determine the accuracy of a strain gauge measurment. This shows that a simple strain gauge (Fig 1.2-1) is actually a very complex system when applied and that the resulting total accuracy of measurement depends not only on the strain gauge itself but also on the properties of the adhesive, the component under test, the protective materials and the bridge circuits (Chapter 3). Thus change in any one of these elements produces a change in the measurement characteristics.

4.1 Resistance tolerances of strain gauges

Most strain gauges are manufactured with nominal resistances of 120Ω to 600Ω. The question of optimum resistance value can be answered only if the entire measuring arrangement (supply voltage, lead resistances etc) is taken into consideration (Chapter 3). During manufacture, however, certain tolerances of the resistance nominal value cannot be

avoided. Criteria for this are the basic material, the metal heat, mechanical and thermal treatment and others. Strain gauges manufactured in the same production process form a so-called batch. Basically, strain gauges connected together in one bridge should have very close resistance values in order to avoid extensive balancing. This is usually achieved when the strain gauges are from the same batch. Balancing may not be necessary however if, at a given resistance tolerance band and using a computer, the initial bridge unbalance is taken into consideration. (This is particularly cost-effective in the case of a large number of measuring points.)

Foil strain gauges normally have a tolerance of ±0.5% of the nominal resistance but the same tolerances can also be obtained with wire strain gauges by using selection procedures.

Only the resistance of the applied strain gauge can be used as a reference value when measuring the resistance, as pre-stressing of the strain gauge conductor cannot always be avoided due to the setting of the adhesive.

According to VDE/VDI 2635 (Ref(28)) the resistance of the bonded strain gauge at room temperature and the resistance at delivery must not differ by more than 0.2%.

4.2 Gauge factor k

4.2.1 Gauge factor tolerances

The gauge factor is the most important parameter of a strain gauge (equation(2.2-6)). It indicates the correlation between the strain of the component and the resulting resistance variation.

The gauge factor is determined on a calibration beam having a constant flexural moment and a transverse contraction $\mu = 0.3$. As the gauge factor can only be determined for a bonded strain gauge, it can only be defined with characteristic tolerance ranges obtained by continuous sampling. In general the sample is approximately 1% of the batch according to type and repeatability of the manufacturing process. The tolerance of the gauge factor directly affects the measurement accuracy. Normally, foil strain gauges show better characteristics in the rolling direction than in the perpendicular direction (Ref(27)). This naturally results in smaller tolerance ranges and furthermore in different gauge factors for the various legs of a strain gauge rosette, for example.

The strain gauge measuring grid in the supporting material is generally in a triaxial state of stress caused by a shrinking of the supporting material during curing as well as changes in volume of the supporting material caused by humidity and temperature variations. During strain measurements the strain to be measured is superimposed on this state of stress and it is unevenly distributed over the entire grid length so that the yield point may be locally exceeded. The result is that large deviations of the gauge factor against those given by the manufacturer may occur even with exactly the same conductor material. According to Ref(27), this uncertainty can amount to several percent. This shows that the gauge factor obviously depends on the bonding conditions. Only a strain gauge bonded by means of a hot-setting adhesive is within the tolerances of ±0.5% stated by the manufacturer.

Furthermore, abnormal changes of the gauge factor can occur after several load and temperature cycles although the strain gauge shows no defect. Therefore, it is necessary to ensure that strain gauges are stored under nearly constant climatic conditions prior to their application to avoid possible faulty measurements.

The temperature dependence of the gauge factor at high temperature is covered by Chapter 8. A constantan grid type strain gauge used mainly in the lower temperature range shows a gauge factor increase of $\sim$ +0.6% per 100K.

4.2.2 Transverse strain sensitivity t

Each strain gauge not only responds to deformations in the direction of its longitudinal axis with the gauge factor k_ℓ but also to those perpendicular to its longitudinal axis with the gauge factor k_t

$$t = k_t/k_\ell \qquad (4.2\text{-}1)$$

As already mentioned in Section 4.2.1, this effect has been taken into consideration as the gauge factor is determined on a bending calibration beam with a transverse strain ratio of $\sim$ 0.3 that shows no shearing.

During measurements on a biaxial stress field however, transverse strains deviating from the relation $\varepsilon_{transverse}/\varepsilon_{longitudinal} \sim -0.3$ may well affect the result (Section 2.2).

The transverse strain sensitivity (t) is kept low by means of narrow flat-grid winding in the case of wire-grid strain gauges and by means of enlarged end points in the case of foil-grid strain gauges. To a small extent it also depends on the adhesive and on the measuring grid supporting material. Generally, however, the transverse strain sensitivity (t) can be assumed to be below 1%. (Ref(18)).

4.3 Errors caused by hysteresis and non-linearity

If a component is loaded and subsequently unloaded, the same loads can result in different stresses. The effect causing these errors is called hysteresis.

The deviation of the relative resistance change $\Delta R/R$ from the straight line $k\varepsilon_B$ based on the gauge factor also causes errors called non-linearity. As this deviation is the result of a mechanical hysteresis in the strain gauge, it is difficult to separate the two error sources from each other.

Non-linearity errors caused by the circuitry will be neglected at this point (Chapter 3).

According to Fig 4.3-1, non-linearity and hysteresis can occur for various reasons:

- plastics (plastic supporting materials and adhesives) do not always act according to Hooke's law (Fig 4.3-1a);
- according to Fig 4.3-1b, structural changes as well as geometric variations in the plastic deformation range of the measuring grid material can also occur and result in permanent changes in resistance.

A strain range up to approx 10000 µm/m is of interest for strain gauge measurements during flight. It can be assumed that the non-linearity and hysteresis error will be $\leq \pm 1\%$ after the first loading if good adhesives and strain gauges are used. After completion of the first load cycle, in most cases this error will hardly exceed ±0.1%.

4.4 Maximum static elasticity of strain gauges

The maximum elasticity of a strain gauge is that strain at which the strain indication deviates by more than 10% from the straight line defined in Section 4.3. It depends on the grid geometry, the material characteristics of grid, supporting material and adhesive as well as on the ambient conditions (temperature, humidity and component surface). At room temperature, most flat-grid wire and foil strain gauges with grid lengths of 10 mm endure strains up to ±20000 to ±40000 µm/m. Shorter strain gauges with measuring grid lengths of $\leq$6 mm can be strained up to approx ±10000 to ±20000 µm/m. Precise data on this subject is difficult to obtain.

4.5 Creep effects

If a strain gauge is strained for a sufficient period of time, relaxation phenomena can occur in the supporting material resulting in an enlarged transfer zone at the measuring grid ends (Section 2.2)

The forces counteracting the restoring force of the strained measuring grid can partly relax. This slowly developing process is called "creeping". Creeping is stimulated by temperature increases, thus it is time and temperature dependent. Numerous other parameters also affect the creep phenomena. So, for example, long strain gauges are less susceptible to creeping than short ones due to the small share of the transfer zones (Fig 2.2-6) in the overall measuring grid length. A favourable configuration of the measuring-grid reversal points as well as the selection of the thinnest possible supporting material foils also reduce creeping.

The creep behaviour of applications is extensively illustrated by so-called time-temperature creep diagrams (Fig 4.5-1) which show lines of similar relative creeping for a certain application as a function of time and temperature.

Thus a user must try to apply a highly creep-resistant combination for measurements extending over a prolonged period of time.

4.6 The temperature coefficient of a strain gauge

According to Section 2.2.6, the temperature coefficient α_T of a bonded strain gauge is composed of the parameters k, α_R, α_Z and α_M, which are all a function of temperature.

By special pre-treatment of the strain gauge grid material, such as work-hardening and heat treatment, α_R in particular can be predetermined by the manufacturer so that the strain gauge bonded on a certain component will have an extremely small α_T (µm/m/K) (Fig 2.2-14). Normally information on α_T is supplied with each strain gauge. In practice, circuitry compensation methods are used in addition so that these errors are compensated for twice and can normally be neglected (Section 3.3.1.1 and 7.12).

4.7 Fatigue strength of a strain gauge

A strain gauge can be loaded several times up to the limit of its maximum elasticity. The number of allowable repetitions depends on the materials used for the strain gauge, on the strain amplitude and on the type of loading. As in the case with other materials, the measuring grid and the strain gauge connecting parts also show material fatigue. Fatigue failure initially appears as zero drift and finally as a fatigue fracture.

According to Ref(30),the fatigue strength diagram shown in Fig 4.7-1 can be considered as typical for high-quality universal strain gauges. This figure shows the zero drift and failure zones as a function of the alternating strain amplitude and the number of load cycles.

4.8 Effects of the thickness of the adhesive layer

It is pointed out in other chapters of this report that a strain gauge can only measure surface strains (except in plastics or building materials). Owing to the thickness of the adhesive layer a strain gauge subjected to flexural load measures a slightly larger strain than the actual component strain. This is due to the distance of the measuring grid from the component surface. The usual thickness x of the adhesive layer varies from ~10 µm up to 40 µm, according to the adhesive used. The errors for components of various thicknesses h can be calculated and the result of the measurement can be corrected according to the relation

$$\varepsilon = \varepsilon_m \frac{1}{1+\frac{2x}{h}} \qquad (4.8\text{-}1)$$

where ε_m = strain measured and ε = component strain.

This does not take account of stiffening effects (see Section 4.10).

4.9 Angular errors during application of the strain gauge

In order to avoid angular errors it is necessary to carefully adjust the strain gauge in the direction of the strain to be measured. Otherwise the result for a uniaxial state of stress has to be corrected using the relation

$$\varepsilon_x = \frac{\varepsilon_\alpha}{\cos^2\alpha} \qquad (4.9\text{-}1)$$

ε_x is the component strain to be measured in the x direction and ε_α is the strain measured in direction α (see Section 7.1.5.2 for references to rosettes).

4.10 The stiffening effect

A bonded strain gauge stiffens the material to be measured. This stiffening cannot be neglected in the case of thin specimens. Its effect depends on the cross sectional area and the moduli of elasticity (Ref (31). In the case of normal application, a mean modulus of elasticity between 5000 and 10000 N/mm^2 can be assumed for adhesive, supporting material and strain gauge. For a 1 mm thick aluminium sheet, for example, the error then amounts to about 2%. Equation (4.10-1) can be used for a rough estimate in case of tensile loads or compressive loads:

$$F(\%) = \frac{E_G \cdot \vartheta_G}{E_B \cdot \vartheta_B} \cdot 100 \qquad (4.10\text{-}1)$$

where ϑ_G = thickness of strain gauge and adhesive

and ϑ_B = thickness of base material

4.11 Insulation resistance effect

The insulation resistance of a strain gauge may be reduced by environmental effects (humidity, oil, dust etc), resulting in an uncontrolled adulteration of the measured values. Variations in the insulation resistance during the measuring process are a particularly important source of errors.

The insulation resistance of a bonded strain gauge including leads should exceed 1000 MΩ. To ensure this value even during long-term measurements, the measurement point must be adequately covered (see Section 6.6).

A detailed description of this effect on accuracy is given in Section 8.1.3.

4.12 Averaging effect of the strain gauge over the entire measuring grid area

The output signal of a strain gauge is determined by the strain behaviour below the measuring grid; the measured results always represent the mean value of the local strain distribution. Thus an accurate strain measurement can only be performed by using a point-like strain gauge. But it is practically impossible to manufacture such small strain gauges.

Thus, a reliable measurement requires some knowledge of the strain gradient which must be very small over the entire measuring grid area.

Fig 4.12-1 and Fig 7.2-1 show the basic correlation between the measuring grid length and the measured strain ε_m of a notched bar which has a highly inhomogeneous strain distribution with regard to the strain indicated.

4.13 Estimation of the total errors

The accuracy of strain measurements with strain gauges is limited by the properties described above but can be improved by calibration in some cases. For this reason, a total error of approximately ±5% has to be expected under normal conditions. In addition, special ambient conditions require an individual error investigation. Errors of approximately ±2% can be expected in the case of calibrated measuring points.

References: (18),(26),(27),(28),(29),(30),(31),(52),(64),(66),(67),(68),(72),(77),(83),(86).

5.0 TYPES OF STRAIN GAUGES

5.1 Strain gauge configuration

The multitude of known strain gauges can be classified into two main groups: strain gauges with supporting materials and free-grid strain gauges. For most practical applications, strain gauges with their measuring grids firmly attached to an electrically insulating material or embedded in a supporting material are used. Only the terminals emerge from this supporting material. Fig 1.1-1 shows the basic configuration of these strain gauges. The many possible variations of this basic type will be described in the following sections.

As indicated by its name, the free-grid strain gauge (Fig 8.1-1) consists of the measuring grid only which is normally attached to a secondary supporting material. This is removed from the measuring grid during installation. Installation of a free-grid strain gauge is difficult because of the frailty of the thin conductor material. They are generally used only in temperature ranges where common supporting materials cannot be used and when the use of special application techniques can be justified. Apart from type and shape, the measuring grid size has to be taken into consideration when selecting a strain gauge (see Fig 5.2-1).

5.2 Grid types and shapes

There are several hundred different strain gauge configurations which, however, can all be assigned to one of the five basic types shown in Fig 5.2-1.

5.2.1 Wire-grid strain gauge

The wire-grid strain gauge is the most commonly used strain gauge, the measuring grid consisting in this case of a drawn wire (measuring grid materials have been described in Section 2.2) which is arranged meander-like on the supporting material by means of a jig. Thicker lugs consisting mainly of copper alloys are soldered or welded to the ends of the very thin measuring wire. Then another supporting layer is placed on the wire, lugs and supporting material and subsequently cured at elevated temperature.

The bend at the reversal points of this type of strain gauge have an adverse effect as part of the active grid is located crosswise to the measuring direction so that transverse strains are included in the measuring signal.

In the case of a uniaxial state of stress however, this error will have no effect if the Poisson's ratio of the material to be tested and the material on which the strain gauge factor was determined comply with each other. As the Poisson's ratios of commonly used metallic materials do not differ very much from each other, the transverse sensitivity can generally be neglected in this case.

Other conditions prevail in the case of a biaxial state of stress and with plastics, particular fibre-reinforced plastics (see Section 7.13). There, considerable errors may occur if the transverse sensitivity of a strain gauge is neglected.

This error source is not important for strain gauges in transducers since it is removed by calibration.

5.2.2 Flat-coil gauges

The flat-coil strain gauges (Fig 5.2-1B) are less important. In this case the measuring wire is wound around an intermediate supporting material. A major disadvantage of this strain gauge is its considerable thickness which may introduce errors in the measurement strains in thin components (refer to Section 4.10).

5.2.3 Cross-bridge gauges

The cross-bridge strain gauge (Fig 5.2-1C) is hardly used any more but will be described here for reasons of completeness. In this case, single wires are laid parallel to each other and are subsequently connected by relatively thick cross bridges. The numerous soldered joints, however, have an adverse effect. The advantage of this type is its low transverse sensitivity and good strain response in the active measuring wires.

5.2.4 Metal-foil gauges

The metal-foil gauges (Fig 5.2-1D) are of increasing importance. During manufacture, the metal foil is attached to the supporting material, then the desired grid shape is printed on the foil with acid-resistant paint. The grid shape can also be applied photochemically by coating the metal foil with a light-sensitive medium and then exposing it, as required. The bare metal areas are then removed by etching in an acid bath so that the desired grid is retained. By this method any desired grid shape and size can be produced which is a great advantage. In particular, any desired rosette shape can be obtained with considerable accuracy. Another advantage of this strain gauge is its small thickness (<25 µm) allowing it to be used on very thin components. In early types a disadvantage was the low fatigue strength of the metal foil strain gauges (due to strain and current peaks on poorly etched conductor paths). Fortunately this disadvantage has largely been eliminated by improving the manufacturing process. Metal-foil strain gauges are already equivalent to the conventional wire strain gauges as far as their dynamic range is concerned. Another advantage of the metal-foil gauge type is the better heat dissipation from the measuring grid via the supporting material to the adhesive and component. It can thus be subjected to a higher current than a wire strain gauge of the same size.

Unlike the wire strain gauge which only shows positive transverse sensitivity values, metal foil strain gauges can have a positive or a negative value according to the design. The description in Section 2.2.5.1 of the wire strain gauge also applies in this case.

5.2.5 Strain gauges with metal supporting materials

Apart from the free-grid strain gauge which can be designed either as a wire or a metal-foil strain gauge, strain gauges with metal supporting materials (Fig 5.2-1E) are used mainly in cases of high temperatures. For this type of strain gauge, the manufacturer uses high-temperature adhesives to bond the measuring grid to a metal lamina which will be spot-welded to the component to be measured.

Another type has the measuring wire isolated and embedded in a metal tube which again is attached to a weldable lamina.

5.3 Supporing materials and their configuration

The transfer of strain from the component to the strain gauge is determined by the following properties of the supporting material:

- adhesive power
- modulus of elasticity
- electrical insulation
- hygroscopic behaviour
- thermal conductivity
- thermal strength
- creep strength
- elasticity
- fatigue strength
- aging resistance
- temperature dependence of all properties

The supporting material is used to transfer the strain from the component to the measuring grid as efficiently and accurately as possible. It must therefore be properly bonded to the component. This requires an adhesive that adheres well not only to the component but also to the supporting material (Section 2.2.5.1).

Another pre-requisite is the smallest possible thickness of the supporting material. An excessively thick supporting material causes stiffening in thin components and thus leads to errors in the measured values (refer to Section 4.10). The minimum radius of curvature of the strain gauge is considerably affected by the thickness of the supporting material. Thus only a very thin strain gauge can be used if a small radius of curvature or a small wall thickness is concerned. Component stiffening and the minimum radius of curvature are, of course, also affected by the modulus of elasticity of the supporting material. An increased modulus of elasticity results in a growing stiffening and a decreased flexibility so that the smallest possible modulus of elasticity is desirable. However if the modulus of elasticity becomes too small, the supporting material (generally plastics) can no longer transfer the strain from the component (generally metal) to the metallic measuring grid. So here, too, a compromise has to be found when selecting the supporting material.

In order to ensure an adequate electrical insulation even with extremely thin supporting material foils (see Section 4.11 and Section 8.1.3), the material must be an efficient insulator. Insulation is affected by the ambient humidity, therefore a good supporting material must not be hygroscopic.

The supporting material should also be as good a thermal conductor as possible. On the one hand, the heating of the measuring grid caused by the supply voltage must be efficiently dissipated and on the other, the temperature of the strain gauge should be as close as possible to that of the component in order to avoid measuring errors in the case of considerable ambient temperature variations.

The supporting material should not creep under load in order to avoid measuring errors in particular during static long-term measurements. Furthermore, it should also be able to endure high strains (> 10000µm/m) without being damaged and should have an adequate dynamic strength. The values for maximum elasticity and dynamic strength of the supporting material should be higher than the values of the same quantities of the measuring grid material in order to take full advantage of the measuring grid properties.

The supporting material should retain the properties previously described with the greatest possible stability for as large a temperature range as possible from cyrogenic up to the highest temperatures.

None of the materials so far used meets the stated maximum requirements. Some of the materials, however, are particularly suitable for specific fields of application. Thus it has to be determined in each case which of the available strain gauges is best suited to meet the specified requirements.

The characteristics of some of the more commonly used strain gauge types are stated below to facilitiate decision making.

5.3.1 Strain gauges with paper supporting material

Paper supporting materials are not used to any extent today. The paper supporting materials impregnated with acrylic or epoxy resin were hygroscopic so that their application was limited to a very small temperature range (150 to 350 K).

5.3.2 Strain gauges with epoxy or phenolic resin supporting material

Supporting materials using epoxy or phenolic resin bases were developed. Most of their properties have been considerably improved (temperature range 70 to 400 K), but they have now been replaced to a large extent by more advanced supporting materials. Today strain gauges on an epoxy or phenolic resin supporting materials are manufactured only for some specific fields of application. Examples are highly vibration-resistant wire strain gauges on phenolic resin bases and metal-foil strain gauges on an epoxy resin base. These are commercially available and particularly recommended for the manufacture of transducers. However, these types require special application methods so that in spite of their good characteristics their use in normal fields of application is not recommended.

5.3.3 Strain gauges with polyimide-foil supporting material

Today, metal-foil strain gauges on a polyimide-foil basis are almost the only ones recommended for standard measurements. They are available in many sizes, shapes and with different resistances. They are flexible and easy to apply. The special advantages of this supporting material are its extended thermal field of application, its relatively large flexibility, its improved hygroscopic behaviour and its easy application.

5.3.4 Strain gauges with glass-fibre-reinforced supporting material

Strain gauges with glass-fibre-reinforced epoxy, phenolic or polyimide resin supporting materials are recommended for very accurate measurements or measurements under severe environmental conditions (such as elevated temperature). However, the application of these strain gauges requires an increased effort if their improved properties are to be utilized.

5.3.5 Strain gauges for large strains

Wire strain gauges on a cellulose basis and metal-foil strain gauges on polyimide-foil basis are available for measuring very large strains. These specially treated strain gauges can be used to measure strains up to 100000 µm/m or 200000 µm/m. Table 5.3-1 shows some typical parameters for various strain gauge groups. The values stated are approximate values that may differ considerably for the individual manufacturers.

The latest manufacturers data and, if necessary, consultory services should be requested if the application of strain gauges is planned as this paper cannot deal in detail with special problems associated with installation.

Table 5.3-1: Typical properties of some strain gauge groups

Type of strain gauge	Measuring grid material	Measuring grid lengths (mm)	Resistance (Ω)	Overall thickness (μm)	Max elasticity (cm/m)	Cauge Factor k	Available shapes	Fields of application
1. Wire strain gauge								
a) on paper basis impregnated with acrylic resin	Constantan	2-70	60,120 300,350 500,600	100-150	2-5	2	uniaxial strain gauge, bi-,triaxial rosettes	Normal measurements without special conditions
b) on a phenolic resin basis	Constantan	2-150	120,300 350,500 600	120-170	2-5	2	uniaxial strain gauge bi-, triaxial rosettes	As above
c) on a phenolic resin basis	Y-3 or Y-9 (special alloy)	6-20	120-600	130-160	0.5-0.7	2	uniaxial strain gauge	Highly vibration-resistant strain gauge for dynamic measurements.
2. Metal-foil strain gauge								
a) on a polyimide foil basis	Constantan	0.2-100	120,350	20-60	2-20	2	uniaxial strain gauge, bi-, triaxial,membrane rosettes, chains	All normal measurements; this group offers largest variety of types.
b) on glass-fibre polyimide basis	Stabiloy	0.8-6	120,350	20-60	2	2	uniaxial strain gauge	Special measurements in high and low temperature ranges
c) on glass-fibre phenolic resin basis	Constantan	0.6-10	120,350	50-80	2	2	uniaxial strain gauge biaxial rosettes	Precision measurements, manufacture of transducers
d) on a phenolic resin basis	Constantan	0.8-23	120,300 600	50-100	1-2	2	uniaxial strain gauge bi-,triaxial rosettes	Normal measurements
e) on an epoxy basis	Constantan	1-60	120,350 1000	40-60	2-4	2	uniaxial strain gauge bi-,triaxial rosettes	Normal measurements
f) various strain gauges on an epoxy and glass fibre-epoxy basis	Constantan Isoelastic Karma Armour - D Nichrome-V	0.5-25	120,350 500, 1000	50-100	0.5-5	depending on the measuring grid material	uniaxial strain gauge bi-,triaxial rosettes	Precision measurements, manufacture of transducers, hi high and low temperature ranges
g) various free-grid strain gauges with wire or metal foil measuring grid	Isoelastic Karma Armour - D Nichrome-V Pt-W alloy 1200 Alloy 800	3-13	120,350 500	-	0.5-1		uniaxial strain gauge	Measurements in high and low temperature ranges

5.4 Vapour-deposited strain gauges

The new technology of vapour-depositing strain gauges is of increasing importance, at least for the manufactureof transducers. In this case, the gauge area of the transducer is first provided with an insulating layer. Subsequently, the measuring grid is vapour-deposited over a mask particularly adapted to the absorptivity required. This method results in a considerably simpler application process since the relatively complicated bonding procedure is not required.

On the other hand, the procedure is only suitable for large scale production as a relatively large amount of tooling is necessary. Furthermore, its use other than for the manufacture of transducers is impracticable because gauge factor variations lead to the need for calibration.

Reference: (71)

6.0 APPLICATION OF STRAIN GAUGES TO STATIC AND DYNAMIC SHORT AND LONG TERM MEASUREMENTS UNDER NORMAL CONDITIONS

6.1 Preliminary remarks

6.1.1 Technical boundary conditions

First let us define the normal conditions under which a strain gauge is used in aircraft flight test. The temperatures prevailing on an aircraft are between 350 K on the ground (solar influence) and approximately 200 K during flight at high altitudes. Stagnation-point and friction temperatures (which may exceed 475 K on aircraft flying at high speeds) as well as temperatures found close to the engine will be neglected for the time being. Chapter 8 describes the strain gauge technique used under these specific conditions of application.

Furthermore, there are various complicating environmental conditions such as high air humidity, condensed water, icing etc. A special effort is required during the installation of strain gauges in order to obtain reliable measuring results under the conditions described.

As with other bonding techniques, the most important pre-requisite for the bonding of strain gauges is extreme cleanliness. Even the slightest traces of contamination, in particular of grease and oil, will prevent the attainment of an efficient bond. If the areas to be bonded are insufficiently cleaned, faulty measurements can be expected. The resulting costs for reinstallation, recalibration etc may considerably exceed the originally estimated installation expenditure. Quite often, reinstallation is not possible (e.g. in the case of closed wing boxes).

Engineering work is also required to determine the most favourable positions of the strain gauges for a certain measurement.

No difficulties are encountered if the strains at critical cross sections only have to be determined. The measurement of forces on control linkages that can be replaced at any time without major difficulties, is no particular problem.

However, the accomplishment of flight load measurements on the structure (refer to Section 7.14) requires very accurate planning in order to determine the most favourable measuring positions.

The available space, in a thin tail profile for instance, has to be considered too if possible. New passages in the supporting structure should not be provided for connecting cables access.

All of these boundary problems have to be settled prior to the application of the strain gauges.

6.1.2 Organizational boundary conditions

Nearly all flight load measuring points have to be installed inside the structure, thus impeding direct access after completion of assembly. Strain gauge installation has therefore to be included in the production process. This requires exact coordination between test department and production to ensure the furnishing of material and the assignment of installation personnel. The fact that several years may pass from installation to calibration or measurement also has to be considered. From the above it follows that major projects require the early preparation of a time and material schedule.

The numerical system required to identify the measuring points will be neglected for the time being as it is almost always predetermined by the general measuring point system.

In spite of the briefness of the statements included in this chapter, the extreme importance of the organization with regard to a perfect and cost-effective performance of the installation work must be clearly emphasized at this point.

6.2 Material selection

The material most suitable for the various applications has to be selected from the numerous materials available taking into consideration the abovementioned technical boundary conditions. In this connection, a number of factors have to be considered:

Selection of the strain gauge manufacturer:

- the manufacturer has to have sufficiently large stock of required strain gauge types and shapes;
- he must have the necessary adhesives, protective materials and pretreatment media;
- the nearest branch or agency of the manufacturer should not be too far away; at least it should be located in the same country;
- delivery times should not be too long, even for somewhat unusual types;
- the price should be within reasonable limits;
- apart from the values stated in the data sheets, the manufacturer should also describe the test procedures which were used to determine the values.

Selection of the materials:

- selection of strain gauge materials (measuring grid and supporting material) to suit the ambient conditions to be expected and providing the required accuracy;
- selection of adhesives, pretreatment media, protective and other secondary materials;
- determination of the minimum size (Ref 4) for the selected strain gauge resistance and the selected supply voltage;
- determination of thermal compensation coefficients;
- selection of the necessary strain gauge shapes (uniaxial strain gauge, $0^{\circ}/90^{\circ}$ - or $\pm 45^{\circ}$ - rosettes, triaxial rosettes).

Each individual user of strain gauges will, of course, attach a different importance to the stated selection criteria.

For the frequent user having to perform not only flight tests but also static and dynamic ground tests, it is advisable, taking account of the required number of strain gauges, to have a sufficiently large stock of special strain gauges available. He will then be more independent and flexible so that neither the variety of types of the individual manufacturers nor the delivery times will be a decisive factor.

Moreover, it is advisable to order the required secondary materials such as adhesives, pretreatment media and protective materials, from different manufacturers. Based on our own experience and by means of comparative tests regularly performed with new materials entering the market, it is always possible to use the most suitable secondary material in each case.

Less frequent users who for example have to perform only routine flight tests, must be sure that the manufacturer can readily and quickly supply certain special strain gauges; for only then will the user be able to treat new measuring requirements with adequate promptness.

In this case, all secondary materials available from one manufacturer should be preferred in order not to waste time and money on lengthy preliminary tests. Furthermore, each manufacturer will be ready to give assistance, if necessary, which will be facilitated by small geographical distances.

The price of the individual strain gauges is less important for both users as it will not exceed 10% of the entire installation and calibration costs. Thus, using the least expensive strain gauge would be of only minor consequence to the total price even in the case of large quantities.

However, the selection of suitable adhesives, protective materials and pretreatment media will have a considerably larger effect on the total price. These media can affect the work time required which contributes considerably (~80%) to the installation costs.

The selection of hot-setting adhesive with a lengthy and complicated curing cycle, for example, would result in high installation costs. If, however, a cold-setting adhesive is selected that is simple to work, the costs are considerably lower.

This reflection on costs, however, should not result in the selection of the simplest and least expensive adhesive particularly when the quality is very much inferior to that of hot-setting adhesive. The costs possibly arising due to reinstallation and recalibration have already been mentioned. As in many other respects, here too a reasonable compromise has to be found.

Some boundary conditions remain to be considered; however, they can only be approximated as they largely depend on the conditions of application such as purpose and method of application, time available, access to the bonding areas and last but not least the component materials.

First, the strain gauges must endure the expected application temperatures. When selecting the measuring grid material it has to be determined whether accurate results are expected at the assumed maximum temperatures or whether measurements are to be performed at normal temperatures only. Constantan measuring grids, for example, can be heated up to 450 K, but accurate results cannot be expected at these temperatures due to structural changes (refer to Chapter 8).

It is recommended that a small safety margin be included in order to avoid possible destruction of measuring points in case of over-temperatures.

Table 6.2-1 shows the acceptable thermal limits for some of the strain gauge families. However, when planning their use it is recommended that the manufacturers be consulted.

The same applies to the dynamic load capacity of strain gauges which, however, is not important for conventional materials. Increased attention has to be paid to this fact only if high-strength steels or titanium alloys are to be loaded to a value just below their load capacity.

In general, strain gauges and adhesives need not be resistant to chemical attack. Appropriate materials have to be used to protect them against these influences (see Section 6.6) if injurious chemicals are present.

The minimum size of the strain gauge is determined by the supply voltage selected, the resistance selected and the thermal conductivity of the material to be tested (refer to Section 3.2.1 and Ref (4)).

The thermal compensation coefficients of strain gauges and component should match. However, in particular cases strain gauges actually designated for another material can also be used in order to avoid a profusion of types. For example, a strain gauge with α_T = 23 µm/m/K (Al) should not be installed on a titanium component (α_T = 9 µm/m/K). However, a strain gauge designated for steel (α_T = 12 µm/m/K) can well be used for titanium. Special care must also be taken that within a single full-bridge (only here is this method permissible at all) strain gauges from only one package are used in order to avoid excessive dependence of the zero point on the temperature.

Table 6.2-1: Acceptable temperature ranges for strain gauges

Supporting material	Temperature limits (K)		
	Lower limit	Upper limit for sustained loading	Upper limit for short-term loading
Paper impregnated with acrylic resin	70	350	370
Phenolic resin	70	420	470
Phenolic resin-glass fibre	70	500	520
Polyimide	70	450	480
Polyimide-glass fibre	4	600	650
Epoxy resin	70	400	450
Epoxy resin-glass fibre	4	550	650
Asbestos	100	670	700

The values refer to the supporting materials; the limits for the measuring grid materials are stated in Table 2.2-1 and those for the adhesives in Table 6.4-1.

The selection of the strain gauge types will differ considerably from one user to the other. If a strain gauge is to be used only once, a simple strain gauge will probably be selected in order to keep the variety of types and thus the storing costs as low as possible. The $0^{\circ}/90^{\circ}$ - or the $\pm 45^{\circ}$ - rosettes required can also be formed by single strain gauges. The angle errors occurring are compensated by subsequent calibration. (Ref(7)).

6.3 Pretreatment of bonding areas

As already mentioned, extreme cleanliness is required if successful measurements with strain gauges are to be performed. Thus the bonding areas have to be thoroughly cleaned and prepared for the selected type of adhesive. After precleaning, two cleaning phases are generally required (mechanical and chemical cleaning) which may, however, overlap.

6.3.1 Precleaning

First, all coarse contamination and surface treatment media, such as varnish, grease, rust etc, have to be removed. This can be effected mechanically by means of abrasion, polishing with emery, sand blasting etc or chemically by means of solvents or pickling media; in the latter case the compatibility of adhesive and pickling medium has to be proved by preliminary tests. The very active pickling media might penetrate into porous materials from where they are difficult to remove and may affect the properties of the adhesive. Furthermore, irregularities of the bonding surfaces should be removed if possible.

6.3.2 Mechanical pretreatment

Subsequent to the removal of surface contamination, the bonding areas have to be thoroughly degreased by means of lint-free tissue (Kleenex, Kimwipes etc) impregnated with an adequate solvent such as MEK (methyl-ethyl-ketone), freon, chlorotene or equivalent. The tissue has to be changed frequently until it no longer shows any colouration. Care has to be taken that a first large, then steadily decreasing area is cleaned thus avoiding new contamination and grease particles being transferred to the bonding surface from the periphery.

Subsequent to cleaning the bonding surface should again be roughened uniformly with circular grinding movements using emery paper or cloth (grain 250 to 400). Then degreasing as described above is repeated.

Anodized and clad Al components should be handled with care as they are generally very sensitive to notches. Deep scratches and nicks have to be avoided by all means. However, care has to be taken that the oxide layer is completely removed.

6.3.3 Chemical pretreatment

In addition and subsequent to the work described above, chemical pretreatment is possible to remove even the smallest remaining contamination and oxide layers. For this purpose, a slightly acid medium (metal conditioner) has proved useful.
It is best applied to the bonding surface with circular movements by means of wet-type emery paper, grain 250-400 held by tweezers, if possible.

After having removed the conditioner with a piece of tissue, the surface has to be treated with a neutralizer as most adhesives do not or poorly adhere to acid surfaces. Neutralizing should be repeated several times to obtain a perfect bonding surface.

The strain gauge should be bonded as soon as possible following the pretreatments described above to avoid reoxidation of the surface. After treatment the bonding surface should, of course, not be touched again.

It is also useful to treat the bonding surface of the strain gauge with a neutralizer right before bonding.

In general, the pretreatment procedure described here can be used at any time. However, it is possible that the manufacturer of the strain gauges and adhesives prescribes a procedure differing in detail from the one described. The instructions and remarks of the manufacturer should be complied with.

6.4 Adhesives

The adhesive is of decisive importance. It must be able to transfer the strain from the component to the strain gauge in the best possible way within the entire temperature range. It may neither creep nor should it lose its adhesion even after several years. Its insulation resistance should be as high as possible.

6.4.1 Cold-setting adhesives

Adhesives curing at room temperature generally do not wholly meet the above stated conditions. As a rule, they are less age-resistant than hot-setting adhesives and their load-capacity is slightly lower. However, they are well suited for flight measurements if used with special care.

A considerable number of adhesives are offered. Most of them can be assigned to one of the groups mentioned in Table 6.4-1.

Table 6.4-1: Survey of some groups of adhesives

Type of adhesive	Temperature range (K)	Elasticity (cm/m)	Curing time (h)
1) Cold-setting adhesives			
a) acrylic resins	70-350	2-3	0.3-0.5
b) cyanoacrylates	100-370	2-5	0.1-0.25
c) epoxy resins	4-400	1-3	8-16
2) Hot-setting adhesives			
a) epoxy resins	4-650	1-2	4-8
b) phenolic resins	20-450	1-2	6-8
c) polyimide resins	10-650	1-2	5-8
d) ceramic adhesives	10-1300	0.5-1	4-8

6.4.1.1 Acrylic resin adhesives

Acrylic resin adhesives are usually two-component adhesives, their temperature limits ranging between 70K and 350K. At lower temperatures the adhesive becomes very brittle. If the temperature exceeds 370K, it softens and creep phenomena, i.e. zero shift, occurs. At temperatures exceeding 420K the adhesive is destroyed. If temperatures from 350K to 420K only occur when no load is applied, static loadings and measurements can be resumed as soon as the temperature has fallen below the 350K limit.

Acrylic resin adhesives are fast-setting. The pot-life for temperatures from 290 to 295K is 1 to 2 minutes so that dynamic measurements can be initiated after 10 to 15 minutes and static measurements after 20 to 30 minutes. Low temperatures retard while higher temperatures accelerate the curing.

For flight measurements acrylic resin adhesives should be used only for short-term measurements. As they are very hygroscopic, the strain gauges should be adequately protected after bonding (see Section 6.6).

This type of adhesive is most suitable for the fastening of (light) cables, as well as for deformation and acceleration pick-ups.

6.4.1.2 Cyanoacrylates

Cyanoacrylates are fast-setting single-component adhesives. Polymerization is initiated by humidity. Temperatures from 290 to 295K and an atmospheric humidity from 40 to 70% have proved to be the most favourable conditions. Curing at low temperature or low humidity requires considerable time. At more than 80% humidity shock hardening takes place and prevents the formation of good adhesive joints.

If the limits indicated (290 to 295K, 40 to 70% relative humidity) are observed, dynamic measurements can be initiated 10 minutes after bonding and static measurements 15 minutes after bonding.

Cyanoacrylates give good results and can also be used for dynamic flight measurements over extended periods.

The various adhesives available on the market differ from each other only as far as their setting time is concerned. An accelerator is required for some cyanoacrylate adhesives, but for some applications the use of an accelerator will result in shock hardening or embrittlement and thus insufficient bonding.

6.4.1.3 Other adhesives

Apart from the adhesives described above, there are a few other cold-setting adhesives based mostly on epoxy resin. These adhesives can be used for static measurements from 4K to 400K by making proper selection from different manufacturers and types.

Further adhesives are offered for large strains. The temperature limits for these adhesives are 70K and 340K respectively.

All of these adhesives require a curing time of up to 24 hours at room temperature, the strain gauges having to be applied with a pressure of 5 to 20 N/cm^2.

At higher curing temperatures the curing times are reduced and bonding quality is considerably increased.

The authors obtained excellent results with an araldite resin system from CIBA, the AV 138 + HV 998 types. The curing time at room temperature is about 8 hours and the strain gauge should be applied with a pressure of 5 to 40 N/cm^2 (higher contact pressured result in thinner bonding layers). At higher temperatures a considerable reduction in curing time can be achieved; at 350K it is approximately 30 minutes, at 370K it is only 10 to 15 minutes.

The adhesive was loaded within a range of 20K to 420K. In the unloaded condition the adhesive withstood thermal loads up to 470K without noticeable deterioration of its bonding properties. It can be used for long term flight measurements as well as for the manufacture of transducers.

6.4.2 Hot-setting adhesives

Hot-setting adhesives can be used within the entire temperature range from 4K to 1300K; however very few of the types will reach the maximum temperature.

Hot-setting adhesives can also be used for normal temperature ranges if the bonding has to meet particularly stringent requirements.

The availability of hot-setting adhesives is quite extensive so that only a selected number is described in some detail. They can also be classified into various groups of adhesive systems.

6.4.2.1 Epoxy resins

Apart from the cold or hot-setting adhesives described in Section 6.4.1.3, a number of epoxy systems are offered which can only be artificially cured. The types offered by different manufacturers can be used for the temperature range 4K to 650K.

Some types (solvent-diluted single component types) have to be pre-dried at room temperature or elevated temperatures at about 320K.

Curing temperatures are between 400K and 480K, depending on the type. Some adhesives require different temperature cycles during curing, some require additional ageing after bonding.

The curing time is up to eight hours at different temperature levels.

The contact pressure applied during bonding amounts to 5 to 100 N/cm^2 depending on type.

A proper selection and comparison of different types is recommended.

6.4.2.2 Phenolic resins

One of the few adhesives in this group has to be cured for two hours at 400K applying a minimum pressure of 150 N/cm^2. No contact pressure is required for ageing.

6.4.2.3 Polyimide resins

This type of adhesive can be used for static measurements from 4K to 600K and for dynamic measurements up to 670K. Due to the complex curing procedure its use is limited almost exclusively to the manufacture of transducers.

6.4.2.4 Ceramic adhesives

This group again comprises a very large number of adhesives. Ceramic adhesives are preferred for free-grid strain gauges manufactured from high-temperature resistant alloys. But ceramic adhesives can also be used in connection with strain gauges having asbestos supporting materials (Japanese manufacturer). The application technique for free-grid strain gauges with ceramic adhesives is described in some detail in Chapter 8.

However, all ceramic adhesives should be used for flight measurements only if extreme conditions prevail. The very difficult application of free-grid strain gauges and the high curing temperatures require installation conditions which can practically only be achieved in laboratories.

Ceramic cements can be used for high temperature measurements up to 1250K.

6.4.2.5 Special procedures

Flame-spraying is a special application procedure. In this case the free-wire measuring grid is embedded in Al_2O_3which is sprayed on to the measuring object and strain gauge at very high temperatures.

Another special procedure concerns the welding of strain gauges. The measuring grids are bonded to a metal lamina by means of a ceramic adhesive and the metal lamina is spot-welded to the measuring object.

The special procedures are less useful for flight measurements than the ceramic adhesives. They should be used only at temperatures that cannot be endured by other strain gauges and adhesives (refer Chapter 8).

6.5 Wiring technique

The connection of the extremely thin strain gauge lugs to the relatively thick lead wire should normally be effected via a solder terminal bonded in front of the strain gauge.

Special attention should be paid to the connection from the strain gauge to the solder terminal. The lug should never be connected to the solder terminal under mechanical stress as a fatigue fracture of the lug will rapidly occur in the case of dynamic loading. The risk of a premature fatigue fracture can be reduced by a small bend in the lug (Fig 6.5-1).

Another procedure is recommended for the strain gauges which are provided with pre-tinned connecting points (diameter ∿0.3 mm). Here the lead should first be stripped over a length of 15 mm. Now one or two of the single wires will be bent away from the lead; the remaining wires are cut short to a length of ∿2 mm and soldered to the solder terminals. The remaining long wires are bent in a bow to the connecting point where they are soldered by means of a special soldering iron (Fig 6.5-2). Thus a connection is made which can endure even extreme dynamic loads.

Strain gauges offered with integrated solder terminals are an exception. Here the solder terminals are permanently attached to the strain gauge. The transition from the thin measuring-grid cross section to the thick connecting cross section is such that it can resist even high dynamic loads.

All strain gauge manufacturers incorporate solder terminals of various sizes and arrangements, including those for rosettes, in their delivery programmes.

Care must be taken that the solder terminals are not affected by maximum temperatures occurring during application and that they can be bonded in a single step with the adhesive selected for the strain gauges.

Furthermore, the melting point of the solder used should be higher than the maximum working temperature in order to avoid a separation of the solder joint.

Special connecting techniques described in detail in Chapter 8 have to be used for high temperature measurements.

Teflon or kapton-insulated leads are recommended as connecting wires for flight measurements. They resist temperatures ranging from 4 K to 530 K (teflon) and to 600 K (kapton). The wires should be shielded and twisted to avoid interference. Stranded wires should be given preference to solid wires due to their better flexibility.

Three or four core cables are used according to the type of bridge applied (semi or full bridges).

PVC-insulated wires should not be used for flight measurements. They are far more sensitive to fuels and hydraulic oils than teflon or kapton and are less age resistant.

For high temperature ranges, only glass-fibre insulated wires and strips should be used.

Up to approximately 520 K, tin-plated or silver-plated Cu is used as a conductor material. Strips of Cr-Ni alloy can be used in the high temperature range but up to 750 K nickel-plated Cu conductors are also stable.

6.6 Protective materials

The protection of strain gauges against environmental conditions is of great importance. Fuel and hydraulic oils used in an aircraft as well as their vapours detrimentally affect strain gauges and adhesives. Condensed water and ice change the insulation resistance thus altering the measured result. Measuring cables and terminals are mechanically loaded due to vibration.

Precautions against all these adverse effects have to be taken as far as possible by using an adequate protective material.

Various protective materials such as microcrystalline wax, vaseline, greases etc that are easy to work can be used for ground tests if only small temperature deviations from room temperature are likely to be encountered.

In the case of higher temperatures between 220K and 420K, cement-like self-adherent media or certain types of solvent-diluted natural rubber can be used. Combinations of the media stated can also be used.

The combination of some types of cement with Al foil has also proved quite successful for ground tests. Subsequent to bonding and connection of a strain gauge, the latter is covered by a layer of cement. Then the Al foil is placed and pressed on to the self-adherent cement.

However, none of the procedures stated is suitable for long-term flight measurement. In this case, silicone resins should be used. Only resins that contain no acid solvents may be used to ensure they have no corrosive effect on the contact surface.

As with other media, the strain gauge, soldering terminals, connecting cables and a certain area surrounding the strain gauge have to be thoroughly cleaned prior to applying a primer coat to the measuring point.

Teflon cables, moreover, have to be prepared for bonding by means of an etchant.

After curing of the primer, the silicone resin can be applied to the measuring point. Under the influence of air humidity, the resin is cured forming a rubber-like mass which is resistant to various solvents, water and mechanical loads.

Other methods have to be used for measurements in fuel tanks or under the influence of SKYDROL. The silicone resins suggested swell if affected by fuel or SKYDROL thus destroying wiring and strain gauge. Furthermore the primers will be dissolved.

Even another protective layer on top of the silicone resin will be ineffective. Small fuel quantities can diffuse through nearly all resins and any riveted joint. The swelling of the silicone layer results in a destruction of the upper protective layer and thus a destruction of the measuring point.

The period between installation and destruction is very large and may extend over several years. For this reason, preliminary tests are very time-consuming if they are to give accurate information on the quality of the protection. Preliminary tests covering only a few months do not give sufficient evidence.

Tank sealing media can be used as protective materials. These media are resistant to fuel and do not swell. It is essential that strain gauges and adhesives are not affected either by the cured or by the uncured protective material. Furthermore, strain gauges and adhesives should not be affected even by small fuel quantities.

Similar requirements apply to measuring points having contact with SKYDROL. Here too silicone should not be used. However, the fuel-resistant materials suggested above are not resistant to SKYDROL either. They have to be protected by an additional layer of NYCOTE protective coating type 7-11 or PN1005 of PRC. The first protective layer has to be completely covered by this additional layer with sufficient overlapping the latter at the edges.

6.7 General instructions

The handling of strain gauges during application has been covered in detail in the references (manufacturers documents). Nevertheless, the basic facts will be described again at this point.

The best positioning accuracy can be obtained by securing the strain gauge to the bonding surface with adhesive tape such as scotch tape, subsequent to its preparation (degreasing and neutralizing). It is advisable to fix the solder terminal to the same adhesive tape.

Now it is possible to accurately position the strain gauge on the measuring point without having to touch the former and to fix it provisionally by means of the scotch tape. The adhesive tape can be removed from the component as often as necessary to correct the strain gauge alignment until the proper position has been found.

Then one side of the adhesive tape is again detached and the strain gauge/adhesive tape combination folded back in a longitudinal direction so that the bonding surfaces of strain gauge and soldering terminal are turned upwards. Using the relevant instructions, the strain gauge and/or bonding surface are then coated with adhesive whereupon the adhesive tape with strain gauge and soldering terminal is folded down and pressed on to the bonding surface. During the subsequent curing operation, the adhesive tape prevents slipping of the strain gauge.

In the case of fast-setting adhesives, it is sufficient to press the strain gauge with the thumb for some minutes to the bonding surfaces. It is recommended first to exert pressure on the centre of the strain gauge and then to press out excessive adhesive from below the strain gauge by rolling the thumb along the gauge. It is advisable to use teflon foil placed above the adhesive tape as an intermediate layer.

If longer curing periods are required, the strain gauge has to be held by G clamps, spring clips, weight-loading or similar devices. In the case of artificial curing it has to be ensured that the contact pressure is neither too low nor too high even at elevated temperatures. In this case, the use of G clamps is excluded.

In order to obtain a uniform loading, the strain gauge should be covered with a rubber cushion above which a metal plate is placed. After the adhesive has been cured, the clamping devices and adhesive tapes can be removed.

Prior to connecting the measuring cables, visual inspections as well as measurements of the strain gauge resistance and of the insulation resistance should be performed. After connection to a sensitive measuring device (strain gauge measuring bridge) even the bonding can be tested by simple means. The measured value is recorded, then an eraser is pressed on to the measuring grid and the value read again. In the case of large deviations it has to be assumed that an air bubble is enclosed below the strain gauge. If so, the strain gauge has to be removed and a new one applied.

The example given in Chapter 9 illustrates how several strain gauges can be applied at the same time if slow curing adhesives are used. In the case of fast-setting adhesives however this procedure cannot be used.

Care has to be taken when marking the measuring position. A hard pencil or even a scriber should not be used in order not to damage the surface (notch effect). If strain gauges are to be bonded to sheet metal in positions exactly facing each other (Section 7.12), the dimension should be referred to the component edges etc. If this is impossible (e.g. in the case of riveted joints), a pointed magnet on one side and a thin steel needle or small steel ball on the other side of the sheet metal can be used to obtain exact reference lines.

Strain gauges for long-term measurements should not be installed too close to rivet holes. The irregular strain distributions prevailing in this case may result in a local excessive loading of the measuring grid. Furthermore, small quantities of water and fuel may penetrate through the rivet holes to the strain gauge and destroy the measuring point. Here even the best and most expensive protecting procedures will be ineffective as no rivet can be considered absolutely leakproof.

If measurements are performed in fuel tanks, the voltage supply of the strain gauge should include a power limitation. If individual measuring bridges are damaged in spite of efficient insulation and protection (visual inspection of the measuring points in the tank is seldom possible and then only under adverse conditions), it is possible that in certain cases short circuits and thus sparking will occur leading to the danger of explosions if the tanks are empty (saturated air/fuel mixture). This can be prevented by a properly adjusted power limitation. (Refs (4),(7)).

7.0 STRAIN GAUGES FOR SPECIAL APPLICATION

The previous chapters have only dealt with descriptions of the function and application of uniaxial strain gauges. Quite often, however, it is impossible to obtain a sufficiently accurate measurement of the strain or stress conditions prevailing on a component by means of uniaxial strain gauges. Special measures have to be taken to determine, process and interpret the values to be measured properly. The various possibilities are described in the following sections.

7.1 Measurement of multi-axial strain conditions and the determination of mechanical stress conditions

In the case of multi-axially stressed components the measurement of strain in only one direction is inadequate. Generally, the principal stresses and thus the magnitude and direction of the maximum shear stress have to be determined for these components. It is, of course, impossible to measure a triaxial state of strain in metallic components by means of strain gauges as this state only occurs within the component whereas strain gauges can only measure surface strains. So the triaxial state will be neglected in the following as it is not consistent with experimental stress analyses. It should be pointed out, however, that according to equation(2.1-16)(Section 2.1.1.4) a third calculable strain component occurs at a biaxial state of stress.

Fortunately, the biaxial state of stress on the component surface is easy to determine. For this purpose, strain gauge rosettes of various configurations and types are available. They consist of two or three individual strain gauges arranged on a common supporting material with various relative orientations. The function of these individual strain gauges complies with the information given earlier, the difference consisting solely in the assessment of the importance of the relations between the individual strains.

Each user can, of course, produce his own rosettes by the application of two or three single strain gauges. However, commercial rosettes should always be given preference to self-made rosettes. The angles between the individual grids have to be exactly observed and the individual grids should be as close to each other as possible to obtain a sufficiently accurate measurement especially in areas with large strain gradients.

The price difference (e.g. a triaxial rosette is typically 1.5 times as expensive as three single strain gauges) is offset by the reduced effort required in bonding the rosettes. Generally, three steps are required for three single strain gauges whereas the rosettes are applied in one step. In addition, the angle between individual gauges must be accurately determined while in the triaxial rosette these are already fixed and defined.

7.1.1 Triaxial rosettes

In general, it can be assumed that the principal strain directions are only known for a few components. Thus, for example, control linkages are only loaded with tensile or compressive forces so that in this case a uniaxial state of stress with known principal directions prevails. Torque shafts and to some extent also wing and tail spar webs are only shear-stressed by torsional moments and shearing forces respectively. Also in this case the principal directions are known. Most other component surfaces however always show biaxial states of stress with unknown principal directions. The determination of the principal strains by magnitude and direction can be performed by means of the triaxial rosettes already mentioned of which two different configurations are considered here: the $0^{\circ}/45^{\circ}/90^{\circ}$ rosette and the $0^{\circ}/60^{\circ}/120^{\circ}$ rosette (see Fig 7.1-1).

Both rosettes function according to the same principle. The strains in three known directions are measured and from this the principal stresses are calculated by magnitude and direction.

Both types of rosettes show the same absolute result, neither being superior to the other. Manual evaluation of the 0/45/90 rosette outputs requires slightly less effort than for the 0/60/120 rosette. However with modern computer data reduction, this superiority is relatively unimportant.

It is, of course, possible to determine the principal stresses by magnitude and direction from any combination of angles. However, the derivation of a general calculating method would exceed the scope of this report. Therefore, only the two types already mentioned will be considered in the following discussions.

For this evaluation of rosettes the following definitions are used:

- the three rosette legs are identified by 'a', 'b' and 'c';
- the 'sense of rotation' of the legs is positive in a mathematical sense (counter-clockwise) as per type A (Fig 7.1-1) for the 0/45/90 rosette and type D for the 0/60/120 rosette.
- Types B and C correspond to type A as only the direction but not the sense (sign) of the strain measured depends on the measuring grid arrangement. The same applies to types E to G which are variations of type D;
- the location of the largest principal stress σ_1, with regard to the rosette leg a is defined by angle α, the sense of rotation, starting from a, is also positive in a mathematical sense

  α may be defined by $0^{\circ} \leq \alpha < 180^{\circ}$

These definitions are extremely important for the assessment of rosettes. Accurate measured results with the formulae developed below can be expected only if the definitions are carefully observed. If slightly different formulae are stated in the referenced literature this only means that different definitions have been used. The respective relations apply if the definitions indicated are observed. Furthermore, this analysis is also referenced again to the relations prevailing at a biaxial state of stress (Mohr's circle for stress and deformation, Section 2.1.1.4, 2.1.1.5).

As the evaluation of both types of rosette is based on the laws described by Mohr, it is extremely important to understand these laws.

While the mathematical analysis of the biaxial state of stress has been described in Section 2.2.1.4 taking the principal stress directions as a basis, the following consideration is made under the aspect of experimental stress analysis where the directions of the individual strain gauges serve as reference systems. Then the actual direction of the principal stresses has to be determined from the measured outputs of the three individual strain gauges.

It appears necessary to deal with this derivation in some detail to illustrate that the origin of these correlations (which are very important for practical applications) are independent of a mere tabulation. For in practice serious errors repeatedly occur caused by a lack of knowledge and wrong application of the boundary conditions.

7.1.1.1. $0^{\circ}/45^{\circ}/90^{\circ}$ rosettes

The formulae required for the assessment of rosettes can be derived from the relations of the deformation circle. As defined above, the strain ε_a is measured for the reference direction 'a'($\alpha = 0^{\circ}$), strain ε_b is measured at 45° (mathematically positive rotation) and strain ε_c at 90°, subsequent to the application of rosettes.

The following derivation is used to determine the direction α as well as the values of the principal strains and principal stresses from the measured quantities.

Fig 7.1-2 shows a $0^{\circ}/45^{\circ}/90^{\circ}$ rosette; the associated deformation circle for assumed values of ε_a, ε_b and ε_c is also shown.

Fig 7.1-2 illustrates that

$$\varepsilon_a = m + r\cdot\cos 2\alpha = \frac{\varepsilon_1+\varepsilon_2}{2} + \frac{\varepsilon_1-\varepsilon_2}{2} \cos 2\alpha \qquad (7.1\text{-}1)$$

$$\varepsilon_b = m + r\cdot\sin 2\alpha = \frac{\varepsilon_1+\varepsilon_2}{2} + \frac{\varepsilon_1-\varepsilon_2}{2} \sin 2\alpha \qquad (7.1\text{-}2)$$

$$\varepsilon_c = m - r\cdot\cos 2\alpha = \frac{\varepsilon_1+\varepsilon_2}{2} - \frac{\varepsilon_1-\varepsilon_2}{2} \cos 2\alpha \qquad (7.1\text{-}3$$

where

$$m = \frac{\varepsilon_1+\varepsilon_2}{2} = \frac{\varepsilon_a+\varepsilon_c}{2} \qquad (7.1\text{-}4)$$

is the ε-coordinate of the centre of the circle and

$$r = \frac{\varepsilon_1-\varepsilon_2}{2} = \sqrt{\frac{(\varepsilon_a-\varepsilon_b)^2+(\varepsilon_b-\varepsilon_c)^2}{2}} \qquad (7.1\text{-}5)$$

is the radius of the circle.

Now it is possible to determine the reference angle. From equation (7.1-2) it follows that

$$r\cdot\sin 2\alpha = \varepsilon_b - m = \varepsilon_b - \frac{\varepsilon_a+\varepsilon_c}{2} \qquad (7.1\text{-}6)$$

and (7.1-1) results in

$$r\cdot\cos 2\alpha = \varepsilon_a - m = \varepsilon_a - \frac{\varepsilon_a+\varepsilon_c}{2} \qquad (7.1\text{-}7)$$

After dividing equation(7.1-7)by equation(7.1-6)using the relation $\frac{\sin\alpha}{\cos\alpha} = \tan\alpha$

it follows that

$$\tan 2\alpha = \frac{\varepsilon_b-m}{\varepsilon_a-m} = \frac{\varepsilon_b - \frac{\varepsilon_a+\varepsilon_c}{2}}{\varepsilon_a - \frac{\varepsilon_a+\varepsilon_c}{2}} \qquad (7.1\text{-}8)$$

or

$$\tan 2\alpha = \frac{2\,\varepsilon_b - (\varepsilon_a+\varepsilon_c)}{\varepsilon_a - \varepsilon_c} \qquad (7.1\text{-}9)$$

Angle α is thus

$$\alpha = \frac{1}{2} \arctan \frac{2\,\varepsilon_b - (\varepsilon_a+\varepsilon_c)}{\varepsilon_a - \varepsilon_c} \qquad (7.1\text{-}10)$$

giving the location of the largest principal strain ε_1 with regard to leg "a" of the rosette. As ε_2 is always acting perpendicular to ε_1, the location of the smallest principal strain ε_2 is determined too.

As defined above, however, the reference angle α may become $0^\circ \leq \alpha < 180^\circ$ which means that formula (7.1-10) is not yet definite. For a definite determination of α the signs for numerator and denominator must be considered for the quotient which is an argument of the tangent.

$$\alpha = \frac{1}{2} \arctan \frac{Z}{N} \qquad (7.1\text{-}11)$$

$$Z = 2\,\varepsilon_b - (\varepsilon_a + \varepsilon_c) \qquad (7.1\text{-}12)$$

$$N = \varepsilon_a - \varepsilon_c \qquad (7.1\text{-}13)$$

Table 7.1-1 shows the assignment of the different sign variations to angle α which is thus definitely determined. Now the directions of ε_1 and ε_2 determined by reference angle α can be added to Fig 7.1-2 according to the above definition.

Table 7.1-1: Assignment of the signs of numerator Z and denominator N (formulae (7.1-11) and (7.1-51)) to reference angle α.

Z	≥ 0	> 0	≤ 0	< 0
N	> 0	≤ 0	< 0	≥ 0
2α	$0 \leq 2\alpha < 90^\circ$	$90^\circ \leq 2\alpha < 180^\circ$	$180^\circ \leq 2\alpha < 270^\circ$	$270^\circ \leq 2\alpha < 360^\circ$
α	$\frac{1}{2}\arctan\left\|\frac{Z}{N}\right\|$	$\frac{\pi}{2} - \frac{1}{2}\arctan\left\|\frac{Z}{N}\right\|$	$\frac{\pi}{2} + \frac{1}{2}\arctan\left\|\frac{Z}{N}\right\|$	$\pi - \frac{1}{2}\arctan\left\|\frac{Z}{N}\right\|$
α	$0 \leq \alpha < 45^\circ$	$45^\circ \leq \alpha < 90^\circ$	$90^\circ \leq \alpha < 135^\circ$	$135^\circ \leq \alpha < 180^\circ$

The parameters ε_1 and ε_2 are determined from the relevant directions. According to Fig 7.1-2

$$\varepsilon_1 = m + r \text{ and } \varepsilon_2 = m - r \tag{7.1-14}$$

From (7.1-1) it follows that

$$r = \frac{\varepsilon_a - m}{\cos 2\alpha} \tag{7.1-15}$$

If this equation is substituted in (7.1-14) then

$$\varepsilon_1 = m + \frac{\varepsilon_a - m}{\cos 2\alpha} \text{ and } \varepsilon_2 = m - \frac{\varepsilon_a - m}{\cos 2\alpha} \tag{7.1-16}$$

After substitution of (7.1-4) the relations for the principal strains are

$$\varepsilon_1 = \frac{\varepsilon_a + \varepsilon_c}{2} + \frac{\varepsilon_a - \varepsilon_c}{\cos 2\alpha} \text{ and } \varepsilon_2 = \frac{\varepsilon_a + \varepsilon_c}{2} - \frac{\varepsilon_a - \varepsilon_c}{\cos 2\alpha} \tag{7.1-17}$$

A second approach is also possible. It yields the same results for ε_1 and ε_2; however, the function of angles $\cos 2\alpha$ has been eliminated permitting the calculation of ε_1 and ε_2 even with $\alpha = 45^\circ$ and $\alpha = 135^\circ$. ($\cos 2\alpha = \cos 90^\circ = \cos 270^\circ = 0$)

(7.1-14) is again taken as a basis.

From (7.1-2) it follows that

$$\sin 2\alpha = \frac{\varepsilon_b - m}{r} \tag{7.1-18}$$

and using the auxiliary equation

$$\cos 2\alpha = \sqrt{1 - \sin^2 2\alpha}$$

this results in

$$\cos 2\alpha = \sqrt{1 - \left(\frac{\varepsilon_b - m}{r}\right)^2} \tag{7.1-19}$$

If this equation is substituted in (7.1-1) then

$$\varepsilon_a = m + \sqrt{r^2 - (\varepsilon_b - m)^2} \tag{7.1-20}$$

and after substitution of (7.1-4) the radius of the circle for strain will be

$$r = \frac{1}{\sqrt{2}} \sqrt{(\varepsilon_a - \varepsilon_b)^2 + (\varepsilon_b - \varepsilon_c)^2} \tag{7.1-21}$$

If (7.1-21) and (7.1-4) are substituted in (7.1-14), the principal strains are as follows

$$\varepsilon_1 = \frac{\varepsilon_a + \varepsilon_c}{2} + \frac{1}{\sqrt{2}} \sqrt{(\varepsilon_a - \varepsilon_b)^2 + (\varepsilon_b - \varepsilon_c)^2}$$

$$\varepsilon_2 = \frac{\varepsilon_a + \varepsilon_c}{2} - \frac{1}{\sqrt{2}} \sqrt{(\varepsilon_a - \varepsilon_b)^2 + (\varepsilon_b - \varepsilon_c)^2} \qquad (7.1\text{-}22)$$

The principal strains of the plane strain state and the directions are found in equations (7.1-10), (7.1-17) and (7.1-22). Now only the principal stresses remain to be determined.

As the principal strains and their directions are known and as the directions of principal strains and principal stresses are identical, Hooke's law can be used to determine the principal stresses:

$$\sigma_1 = \frac{E}{1-\mu^2} (\varepsilon_1 + \mu\varepsilon_2) \qquad (7.1\text{-}23)$$

$$\sigma^2 = \frac{E}{1-\mu^2} (\varepsilon_2 - \mu\varepsilon_1) \qquad (7.1\text{-}24)$$

Substituting (7.1-17) in (7.1-23) and in (7.1-24) results in the following relation

$$\sigma_{1,2} = E \left[\frac{\varepsilon_a + \varepsilon_c}{2(1-\mu)} \pm \frac{\varepsilon_a - \varepsilon_c}{2(1+\mu)\cos 2\alpha} \right] \qquad (+ \text{ for } \sigma_1, - \text{ for } \sigma_2) \qquad (7.1\text{-}25)$$

If the result (7.1-22) is substituted in (7.1-23) and (7.1-24), then the relations for the principal stresses are

$$\sigma_{1,2} = \frac{E(\varepsilon_a + \varepsilon_c)}{2(1-\mu)} \pm \frac{E}{\sqrt{2}\,(1+\mu)} \sqrt{(\varepsilon_a - \varepsilon_b)^2 + (\varepsilon_b - \varepsilon_c)^2} \qquad (7.1\text{-}26)$$

(+ for σ_1, - for σ_2)

Furthermore, the diameter of Mohr's circle for deformation corresponds to the maximum shear deformation

$$2r = \gamma_{1,2} = \gamma \max \qquad (7.1\text{-}27)$$

$$r = \frac{\gamma_{1,2}}{2} \qquad (7.1\text{-}28)$$

If (7.1-15) is substituted in (7.1-27) then

$$\gamma_{1,2} = 2 \frac{\varepsilon_a - m}{\cos 2\alpha} \qquad (7.1\text{-}29)$$

Inclusion of (7.1-4) results in

$$\gamma_{1,2} = \frac{\varepsilon_a - \varepsilon_c}{\cos 2\alpha} \qquad (7.1\text{-}30)$$

If (7.1-21) is applied, (7.1-27) will change to

$$\gamma_{1,2} = \sqrt{2} \sqrt{(\varepsilon_a - \varepsilon_b)^2 + (\varepsilon_b - \varepsilon_c)^2} \qquad (7.1\text{-}31)$$

Considering (2.1-6) and (2.1-7) the maximum shear stress from (7.1-30) will be

$$\tau_{max} = E \frac{\varepsilon_a - \varepsilon_c}{2(1+\mu)\cos 2\alpha} = \frac{\sigma_1 - \sigma_2}{2} \qquad (7.1\text{-}32)$$

or from (7.1-31)

$$\tau_{max} = \frac{E}{\sqrt{2}\,(1+\mu)} \sqrt{(\varepsilon_a - \varepsilon_b)^2 + (\varepsilon_b - \varepsilon_c)^2} \qquad (7.1\text{-}33)$$

This comprises the derivations for the $0^o/45^o/90^o$ rosette. The most important formulae have been summarized in Table 7.1-2.

References: (8), (12).

7.1.1.2 $0^o/60^o/120^o$ rosettes

As in the case of the $0^o/45^o/90^o$ rosette, here too the necessary formulae can be derived from the geometric relations of Mohr's circle for deformation. As defined above, Strain ε_a is measured in the direction 'a' ($\alpha = 0^o$), strain ε_b at 60^o (mathematically positive rotation) in direction 'b' and ε_c at 120^o in direction 'c'.

Figure 7.1-3 shows $0^o/60^o/120^o$ rosette and the applicable circle of strain for the assumed measured values of ε_a, ε_b and ε_c.

Figure 7.1-3 illustrates that:

$$\varepsilon_a = m + r\cos 2\alpha = \frac{\varepsilon_1+\varepsilon_2}{2} + \frac{\varepsilon_1-\varepsilon_2}{2}\cos 2\alpha \qquad (7.1\text{-}34)$$

$$\varepsilon_b = m + r\cos(120^o-2\alpha) = \frac{\varepsilon_1+\varepsilon_2}{2} + \frac{\varepsilon_1-\varepsilon_2}{2}\cos(120^o-2\alpha) \qquad (7.1\text{-}35)$$

$$\varepsilon_c = m + r\cos(240^o-2\alpha) = \frac{\varepsilon_1+\varepsilon_2}{2} + \frac{\varepsilon_1-\varepsilon_2}{2}\cos(240^o-2\alpha) \qquad (7.1\text{-}36)$$

Furthermore

$$m = \frac{\varepsilon_a+\varepsilon_b+\varepsilon_c}{3} = \frac{\varepsilon_1+\varepsilon_2}{2} \qquad (7.1\text{-}37)$$

These are the basic equations from which the relation for the reference angle can be derived.

Using the auxiliary equation

$$\cos(\alpha-\beta) = \cos\alpha\cos\beta + \sin\alpha\sin\beta \qquad (7.1\text{-}38)$$

then (7.1-35) is

$$\varepsilon_b = m + r(\cos 120^o\cos 2\alpha + \sin 120^o \sin 2\alpha) \qquad (7.1\text{-}39)$$

and (7.1-36) is

$$\varepsilon_c = m - r(\cos 60^o\cos 2\alpha + \sin 60^o \sin 2\alpha) \qquad (7.1\text{-}40)$$

Using the additional auxiliary relations

$$\sin 2\alpha = \frac{\tan 2\alpha}{\sqrt{1+\tan^2 2\alpha}} \qquad (7.1\text{-}41)$$

and

$$\cos 2\alpha = \frac{1}{\sqrt{1+\tan^2 2\alpha}} \qquad (7.1\text{-}42)$$

then the relations (7.1-34) to (7.1-36) are

$$\varepsilon_a = m + \frac{r}{\sqrt{1+\tan^2 2\alpha}} \qquad (7.1\text{-}43)$$

$$\varepsilon_b = m - \frac{r}{2\sqrt{1+\tan^2 2\alpha}}(1 - \sqrt{3}\tan 2\alpha) \qquad (7.1\text{-}44)$$

$$\varepsilon_c = m - \frac{r}{2\sqrt{1+\tan^2 2\alpha}}(1 + \sqrt{3}\tan 2\alpha) \qquad (7.1\text{-}45)$$

Equations(7.1-44) and (7.1-45) will be

$$r = \frac{2(m-\varepsilon_b)\sqrt{1+\tan^2 2\alpha}}{1 - \sqrt{3}\tan 2\alpha} \qquad (7.1\text{-}46)$$

$$r = \frac{2(m-\varepsilon_c)\sqrt{1+\tan^2 2\alpha}}{1 + \sqrt{3}\tan 2\alpha} \qquad (7.1\text{-}47)$$

Equating (7.1-46) and (7.1-47) results in

$$\frac{m-\varepsilon_b}{1-\sqrt{3}\tan 2\alpha} = \frac{m-\varepsilon_c}{1+\sqrt{3}\tan 2\alpha} \qquad (7.1\text{-}48)$$

and, after having substituted (7.1-37), the relation for the reference angle α is

$$\tan 2\alpha = \frac{\sqrt{3}\,(\varepsilon_b-\varepsilon_c)}{2\,\varepsilon_a-\varepsilon_b-\varepsilon_c} \tag{7.1-49}$$

hence

$$\alpha = \frac{1}{2}\,\text{arc tan}\,\frac{\sqrt{3}\,(\varepsilon_b-\varepsilon_c)}{2\,\varepsilon_a-\varepsilon_b-\varepsilon_c} \tag{7.1-50}$$

Its magnitude having to be determined from (7.1-50) analogous to the $0^o/45^o/90^o$ rosette - by considering the signs of numerator A and denominator N:

$$\alpha = \frac{1}{2}\,\text{arc tan}\,\frac{Z}{N} \tag{7.1-51}$$

$$Z = \sqrt{3}\;\;(\varepsilon_b - \varepsilon_c) \tag{7.1-52}$$

$$N = 2\varepsilon_a - \varepsilon_b - \varepsilon_c \tag{7.1-53}$$

For this purpose Table 7.1-1 should be used which applies not only to the $0^o/45^o/90^o$ rosette but also to the $0^o/60^o/120^o$ rosette.

After having determined α, the principal directions 1 and 2 can be entered into Fig 7.1-3 taking into consideration the above stated definitions; direction 1 should be entered at an angle α, (proceeding from a mathematically positive rotation), direction 2 at $\alpha + 90^o$.

Now the principal strains ε_1 and ε_2 can be determined. Fig 7.1-3 shows that

$$\varepsilon_1 = m + r,\;\; \varepsilon_2 = m - r \tag{7.1-54}$$

From (7.1-34) it follows that

$$r = \frac{\varepsilon_a - m}{\cos 2\alpha} \tag{7.1-55}$$

If this term is substituted in (7.1-54) then

$$\varepsilon_1 = m + \frac{\varepsilon_a - m}{\cos 2\alpha}\,,\quad \varepsilon_2 = m - \frac{\varepsilon_a - m}{\cos 2\alpha} \tag{7.1-56}$$

After substitution of (7.1-37), the relations for the principal strains are

$$\varepsilon_{1,2} = \frac{\varepsilon_a + \varepsilon_b + \varepsilon_c}{3} \pm \frac{2\varepsilon_a - \varepsilon_b - \varepsilon_c}{3\cos 2\alpha}\,; \qquad (+ \text{ for } \varepsilon_1,\;\; - \text{ for } \varepsilon_2) \tag{7.1-57}$$

Here, too, a second approach will be adopted which evades the function of angles cos 2α so that a calculation is possible even at $\alpha = 45^o$ and $\alpha = 135^o$.

From (7.1-34) it follows that

$$r = (\varepsilon_a - m)\;\sqrt{1 + \tan^2 2\alpha} \tag{7.1-58}$$

If (7.1-49) is substituted, then

$$r = \sqrt{(\varepsilon_a - m)^2 + \frac{1}{3}(\varepsilon_b - \varepsilon_c)^2} \tag{7.1-59}$$

and if (7.1-37) is substituted the relation for the radius of the circle of strain is

$$r = \sqrt{\frac{(2\varepsilon_a - \varepsilon_b - \varepsilon_c)^2}{9} + \frac{1}{3}\,(\varepsilon_b - \varepsilon_c)^2} \tag{7.1-60}$$

$$= \frac{2}{3}\sqrt{\varepsilon_a^{\,2} + \varepsilon_b^{\,2} + \varepsilon_c^{\,2} - \varepsilon_a\varepsilon_b - \varepsilon_a\varepsilon_c - \varepsilon_b\varepsilon_c}$$

If (7.1-37) and (7.1-60) are substituted in (7.1-54), then

$$\varepsilon_{1,2} = \frac{\varepsilon_a + \varepsilon_b + \varepsilon_c}{3} \pm \frac{2}{3}\sqrt{\varepsilon_a^{\,2} + \varepsilon_b^{\,2} + \varepsilon_c^{\,2} - \varepsilon_a\varepsilon_b - \varepsilon_a\varepsilon_c - \varepsilon_b\varepsilon_c} \tag{7.1-61}$$

(+ for ε_1, - for ε_2)

These are the formulae for the determination of the principal strains. Now the formulae (7.1-57) or (7.1-61) can be substituted in the equations of Hooke's law (7.1-23) and (7.1-24) resulting in the formulae of the principal stresses.

From (7.1-57) it follows that

$$\sigma_{1,2} = E\left[\frac{\varepsilon_a + \varepsilon_b + \varepsilon_c}{3(1-\mu)} \pm \frac{2\varepsilon_a - \varepsilon_b - \varepsilon_c}{3(1+\mu)\cos 2\alpha}\right]; \qquad (+ \text{ for } \sigma_1, \; - \text{ for } \sigma_2) \qquad (7.1\text{-}62)$$

then (7.1-61) is

$$\sigma_{1,2} = \frac{E}{1-\mu}\,\frac{\varepsilon_a + \varepsilon_b + \varepsilon_c}{3} \pm \frac{2E}{3(1+\mu)}\sqrt{\varepsilon_a^2 + \varepsilon_b^2 + \varepsilon_c^2 - \varepsilon_a\varepsilon_b - \varepsilon_a\varepsilon_c - \varepsilon_b\varepsilon_c} \qquad (7.1\text{-}63)$$

As already described in Section 7.1.1.1, the diameter of Mohr's circle for deformation, 2 r, is equal to the maximum shear deformation. Formulae (7.1-27) and (7.1-28) apply.

Having substituted (7.1-55) in (7.1-27) then

$$\gamma_{1,2} = 2\,\frac{\varepsilon_a - m}{\cos 2\alpha} \qquad (7.1\text{-}64)$$

and having substituted (7.1-37) then

$$\gamma_{1,2} = \frac{2}{3}\,\frac{2\varepsilon_a - \varepsilon_b - \varepsilon_c}{\cos 2\alpha} \qquad (7.1\text{-}65)$$

Substituting (7.1-60) in (7.1-27) results in

$$\gamma_{1,2} = \frac{4}{3}\sqrt{\varepsilon_a^2 + \varepsilon_b^2 + \varepsilon_c^2 - \varepsilon_a\varepsilon_b - \varepsilon_a\varepsilon_c - \varepsilon_b\varepsilon_c} \qquad (7.1\text{-}66)$$

Using (2.1-6) and (2.1-7) the maximum shear stress from (7.1-29) will be

$$\tau_{max} = E\,\frac{2\varepsilon_a - \varepsilon_b - \varepsilon_c}{3(1+\mu)\cos 2\alpha} = \frac{\sigma_1 + \sigma_2}{2} \qquad (7.1\text{-}67)$$

or from (7.1-66)

$$\tau_{max} = \frac{2E}{3(1+\mu)}\sqrt{\varepsilon_a^2 + \varepsilon_b^2 + \varepsilon_c^2 - \varepsilon_a\varepsilon_b - \varepsilon_a\varepsilon_c - \varepsilon_b\varepsilon_c} \qquad (7.1\text{-}68)$$

Thus the derivations for the $0^\circ/60^\circ/120^\circ$ rosette are also defined. The most important formulae for this type of rosette have been summarized in Table 7.1-2).
References:(8),(12)

7.1.2 Biaxial rosettes

If the directions of the principal stresses of a component are known, then the magnitude of the principal stresses and the maximum shear stress can be determined by means of biaxial rosettes (90° rosettes). The directions of the principal stresses might be seen from the component type or from the type of load; they can also be determined for example by means of preliminary tests using brittle varnish (refer to Section 1.3).

In this case a 90° rosette is applied so that one strain gauge 'a' is parallel to the direction of the largest principal stress and one strain gauge 'c' is parallel to the direction of the smallest principal stress (90° from 'a'). The reference angle α of Section 7.1.1.1 is now 0°. With this strain gauge combination the strains ε_a and ε_o are the same as the strains ε_1 and ε_2.

Thus the formulae of Hooke's law for the plane state of stress (7.1-23) and (7.1-24) can be directly applied to determine the magnitude of the principal stresses.

Fig 7.1-4A to C, shows various types of biaxial rosettes.

The determination of the shear deformation is also quite simple since the diameter of the circle of strain, 2r, is equal to the maximum shear deformation,

$$\gamma_{1,2} = 2r = \varepsilon_a - \varepsilon_c = \varepsilon_1 - \varepsilon_2 \qquad (7.1\text{-}69)$$

Thus the maximum shear stress can be calculated by means of the formulae (2.1-6) and (2.1-7)

$$\tau_{max} = E\,\frac{\varepsilon_a - \varepsilon_c}{2(1+\mu)} \qquad (7.1\text{-}70)$$

Reference: (8).

Table 7.1-2: Summary of the most important evaluation formulae for triaxial rosettes (refer definitions on page 46).

Parameter	$0^C/45^O/90^O$ rosette	$0^O/60^O/120^O$ rosette
Reference angle α	$\alpha = \frac{1}{2} \arctan \frac{2\varepsilon_b-(\varepsilon_a+\varepsilon_c)}{\varepsilon_a-\varepsilon_c}$ (7.1-10) See also Table 7.1-1	$\alpha = \frac{1}{2} \arctan \frac{\sqrt{3}(\varepsilon_b-\varepsilon_c)}{2\varepsilon_a-\varepsilon_b-\varepsilon_c}$ (7.1-50) See also Table 7.1-1
Principal strains $\varepsilon_1, \varepsilon_2$	$\varepsilon_{1,2} = \frac{\varepsilon_a+\varepsilon_c}{2} \pm \frac{\varepsilon_a-\varepsilon_c}{2\cos 2\alpha}$ (7.1-17) $\varepsilon_{1,2} = \frac{\varepsilon_a+\varepsilon_c}{2} \pm \frac{1}{\sqrt{2}}\sqrt{(\varepsilon_a-\varepsilon_b)^2+(\varepsilon_b-\varepsilon_c)^2}$ (7.1-22)	$\varepsilon_{1,2} = \frac{\varepsilon_a+\varepsilon_b+\varepsilon_c}{3} \pm \frac{2\varepsilon_a-\varepsilon_b-\varepsilon_c}{3\cos 2\alpha}$ (7.1-57) $\varepsilon_{1,2} = \frac{\varepsilon_a+\varepsilon_b+\varepsilon_c}{3} \pm \frac{2}{3}\sqrt{\varepsilon_a^2+\varepsilon_b^2+\varepsilon_c^2-\varepsilon_a\varepsilon_b-\varepsilon_a\varepsilon_c-\varepsilon_b\varepsilon_c}$ (7.1-61)
Principal stresses $\sigma_{1,2}$	$\sigma_{1,2} = E\left(\frac{\varepsilon_a+\varepsilon_c}{2(1-\mu)} \pm \frac{\varepsilon_a-\varepsilon_c}{2(1+\mu)\cos 2\alpha}\right)$ (7.1-25) $\sigma_{1,2} = E\,\frac{\varepsilon_a+\varepsilon_c}{2(1-\mu)} \pm \frac{E}{\sqrt{2}(1+\mu)}\sqrt{(\varepsilon_a-\varepsilon_b)^2+(\varepsilon_b-\varepsilon_c)^2}$ (7.1-26)	$\sigma_{1,2} = E\left[\frac{\varepsilon_a+\varepsilon_b+\varepsilon_c}{3(1-\mu)} \pm \frac{2\varepsilon_a-\varepsilon_b-\varepsilon_c}{3(1-\mu)\cos 2\alpha}\right]$ (7.1-62) $\sigma_{1,2} = E\,\frac{\varepsilon_a+\varepsilon_b+\varepsilon_c}{3(1-\mu)} \pm \frac{2}{3}\frac{E}{1+\mu}\sqrt{\varepsilon_a^2+\varepsilon_b^2+\varepsilon_c^2-\varepsilon_a\varepsilon_b-\varepsilon_a\varepsilon_c-\varepsilon_b\varepsilon_c}$ (7.1-63)
Maximum shear deformation $\gamma_{1,2} = \gamma_{max}$	$\gamma_{1,2} = \frac{\varepsilon_a-\varepsilon_c}{\cos 2\alpha}$ (7.1-30) $\gamma_{1,2} = \sqrt{2}\sqrt{(\varepsilon_a-\varepsilon_b)^2+(\varepsilon_b-\varepsilon_c)^2}$ (7.1-31)	$\gamma_{1,2} = \frac{2}{3}\frac{2\varepsilon_a-\varepsilon_b-\varepsilon_c}{\cos 2\alpha}$ (7.1-65) $\gamma_{1,2} = \frac{4}{3}\sqrt{\varepsilon_a^2+\varepsilon_b^2+\varepsilon_c^2-\varepsilon_a\varepsilon_b-\varepsilon_a\varepsilon_c-\varepsilon_b\varepsilon_c}$ (7.1-66)
Maximum shear stress $\tau_{1,2} = \tau_{max}$	$\tau_{max} = E\,\frac{\varepsilon_a-\varepsilon_c}{2(1+\mu)\cos 2\alpha}$ (7.1-32) $\tau_{max} = \frac{E}{\sqrt{2}(1+\mu)}\sqrt{(\varepsilon_a-\varepsilon_b)^2+(\varepsilon_b-\varepsilon_c)^2}$ (7.1-33)	$\tau_{max} = E\,\frac{2\varepsilon_a-\varepsilon_b-\varepsilon_c}{3(1+\mu)\cos 2\alpha}$ (7.1-67) $\tau_{max} = \frac{2}{3}\frac{E}{(1+\mu)}\sqrt{\varepsilon_a^2+\varepsilon_b^2+\varepsilon_c^2-\varepsilon_a\varepsilon_b-\varepsilon_a\varepsilon_c-\varepsilon_b\varepsilon_c}$ (7.1-68)

7.1.3 Shear stress measurements with 90° rosettes

Section 7.1.2 describes the evaluation of biaxial rosettes if stresses and shear stresses are to be determined. In that case both rosette legs had to be considered as independent strain pick-ups. Sometimes, however, only the shear stress is important, for instance on wing and tail spar webs that can be considered, in a sense, as pure shear panels.

Now, a strain gauge cannot be used for the direct measurement of shear deformation as it only responds to normal strains but not to shear deformation. On the other hand, there exists a defined correlation between shear deformation and normal strain due to the laws of elasticity.

It is therefore possible to obtain a signal directly proportional to the shear stress by proper interconnection of two or four strain gauges in one Wheatstone bridge. Referring to Section 7.1.2, the attempt must be made to measure the term $(\varepsilon_a - \varepsilon_c)$ in formula (7.1-70) directly. This is possible by interconnecting the strain gauges 'a' and 'c' of a 90 rosette to a semi-bridge as shown in Fig 7.1-5A. Then the bridge output voltage u_m is directly proportional to the term $(\varepsilon_a - \varepsilon_c)$ so that

$$\tau_{a,c} = E \frac{U_m \cdot C}{2(1+\mu)} = G \cdot U_m \cdot C = G \cdot \gamma \qquad (7.1\text{-}71)$$

with $U_m \cdot C = \varepsilon_a - \varepsilon_c$

If $\varepsilon_a = \varepsilon_1$ and $\varepsilon_b = \varepsilon_2$, then $\tau_{a,c} = \tau_{max}$

The measured signal and thus the sensitivity is doubled if a "shear rosette" or "full-bridge rosette" according to Fig 7.1-4D is used and if the four strain gauges of this rosette are interconnected to a full-bridge as per Fig 7.1-5B. Here, the measuring voltage corresponds to the term

$$\tau_{a,c} = E \cdot \frac{U_m \cdot C}{4(1+\mu)} = \frac{1}{2} G \cdot U_m \cdot C = \frac{1}{2} G \cdot \gamma \qquad (7.1\text{-}72)$$

where

$$U_m \cdot C = \varepsilon_a - \varepsilon_b + \varepsilon_c - \varepsilon_d$$

If $\varepsilon_a = \varepsilon_c = \varepsilon_1$ and $\varepsilon_b = \varepsilon_d = \varepsilon_2$, then $\tau_{a,c} = \tau_{max}$

Reference: (16).

7.1.4 Boundary conditions for the application of rosettes

The formulae stated in Sections 7.1.1 to 7.1.3 only apply to a homogeneous isotropic material (equal modulus of elasticity and equal transverse contraction in any direction) and only in the range of Hooke's law. These formulae cannot be used either for plastic materials or for anisotropic, inhomogeneous materials such as fibre-reinforced materials (refer to Section 7.13). In the latter case, other complex considerations are generally necessary for the determination of principal strains and stresses.

7.1.5 Error estimations for measurements with strain gauge rosettes

Even if all instructions given until now are carefully observed, considerable errors may occur during measurements with strain gauge rosettes. Three main groups can be distinguished:

- insufficient knowledge of the material constants
- orientation errors (also mounting errors)
- systematic errors

Their effect on the measured result will be explained below, proceeding in each case from the occurrence of a single error. In addition the different errors can occur simultaneously and cause large total errors.

7.1.5.1 Errors of material constants

The constants stated in the material standards are generally used to calculate the principal stresses. However, the values actually occurring may deviate considerably from the standard values.

Differences up to +5% can be observed in Young's modulus of elasticity. According to Table 7.1-2, they have a proportional effect on the measurement. In the case of rolled sheet metals in particular the moduli of elasticity can differ considerably from each other in rolling direction and perpendicular to the same, thus also causing errors in the measured result. In this case even the required isotropy mentioned above is no

longer met.

If accurate measurements are required it is recommended that the material constants of specimens taken from the work piece should be determined.

Inaccuracies in Poisson's ratio have only little effect (Ref (32)) which can be seen at once from their occurrence in the equations summarized in Table 7.1-2. In consequence, no detailed description will be given here.

7.1.5.2 Orientation errors

Errors in the orientation of the rosettes may result in large errors in the final result. Basically, this concerns of course the biaxial rosette for which the knowledge of the principal directions and the accurate arrangement of the measuring grids in these directions is very important.

The magnitude of an error for the biaxial rosette depends on two factors: the deviation of the measuring grid from the principal directions and the ratio of the two principal stresses

$$R_\sigma = \frac{\sigma_1}{\sigma_2} \qquad (7.1\text{-}73)$$

The determination of the shear stress τ_{max} is affected only by the deviation from the principal directions.

According to Ref (33), the extent of the errors occurring at various stresses can be calculated by means of the following relations

$$n_{\sigma_1} = \frac{1-R_\sigma}{2R_\sigma} (1-\cos 2\beta)\ 100\ \{\%\} \qquad (7.1\text{-}74)$$

$$n_{\sigma_2} = \frac{R_\sigma-1}{2} (1-\cos 2\beta)\ 100\ \{\%\} \qquad (7.1\text{-}75)$$

$$n_{\tau\ max} = -(1-\cos 2\beta)\ 100\ \{\%\} \qquad (7.1\text{-}76)$$

where β is the deviation of the measuring grids from the principal directions.

An exhaustive derivation of the formulae will not be given at this point; it can be taken from the references if necessary.

However, some special cases will be studied in detail.

If $\sigma_1 = \sigma_2$ (hollow sphere under internal pressure), then $R_\sigma = 1$. In this case, no directional errors can be observed and shear stress does not occur.

A thin-walled hollow cylinder has an internal pressure load $\sigma_1 = 2\sigma_2$, i.e. $R_\sigma = 2$. The relevant errors are shown in Fig 7.1-6.

On a pure shear panel $\sigma_1 = -\sigma_2$, thus $R_\sigma = -1$ which results in the errors $n_{\sigma_1} = n_{\sigma_2} = n_{\tau_{max}}$; they correspond to the representation of $n_{\tau_{max}}$ given in Fig 7.1-6.

In the case of uniaxial states of stress ($\sigma_2 = 0$), a faulty arrangement results in finite values for σ_2, i.e. for these stresses errors of unlimited relative extent are possible. It can generally be said that with $R_{\sigma\to\infty}$ (approximation to the uniaxial state of stress) the relative error of σ_2 also approaches infinity.

As the single strain gauge yields a mean value of the strain underneath the active part of the measuring grid (refer to Section 4.12 and 7.2), even triaxial rosettes can show considerable arrangement errors if these rosettes are applied on areas with large strain gradients. If the rosettes used are too large, the measuring grids may cover areas of different strain conditions. The resulting inaccuracies, however, are difficult to assess as they largely depend on local conditions.

Even if rosettes with measuring grids arranged one upon the other are used as shown in Fig 7.1-1c and g, a considerable reduction of these errors can hardly be expected since additional limitations have to be accepted. In this case only very low supply voltages should be used as otherwise the measuring grids would heat one another up. Furthermore, flexural loads may adulterate the measured result as the distance of the individual measuring grids from the work piece surface and thus the flexures differ. Finally, stiffening effects have to be taken into consideration in particular with thin sheet metals (see Section 4.10).

Reference (33).

7.1.5.3 Systematic errors

Systematic errors concerning measurements with single strain gauges have been dealt with in detail in Chapter 4. However, at this point some additional remarks, in particular on the effects of error propagation, have to be made in view of the special characteristics of the rosette.

Sections 7.1.1 to 7.1.3 indicate that the principal strains $\varepsilon_{1,2}$ and the reference angle α depend on the strains $\varepsilon_{a,b,c}$ measured. This clearly shows that the errors made during measurement of strains affect the accuracy of $\varepsilon_{1,2}$ and α and thus of $\sigma_{1,2}$.

Reference (32) proves that the standard deviations of the principal strains $S\varepsilon_1$ and $S\varepsilon_2$ for the $0^\circ/60^\circ/120^\circ$ rosette are equal to the standard deviation S_ε of the measuring values $\varepsilon_{a,b,c}$ (assuming that $S\varepsilon = S\varepsilon_a = S\varepsilon_b = S\varepsilon_c$). The standard deviation of angle α is thus

$$S_\alpha = \sqrt{\frac{2}{3}} \frac{S_\varepsilon}{\varepsilon_1 - \varepsilon_2} \tag{7.1-77}$$

The relations of the $0^\circ/45^\circ/90^\circ$ rosette are somewhat more complicated

$$S\varepsilon_1 = S_\varepsilon \sqrt{1 + \sin 2\alpha(\sin 2\alpha - 1)} \tag{7.1-78}$$

$$S\varepsilon_2 = S_\varepsilon \sqrt{1 + \sin 2\alpha(\sin 2\alpha + 1)} \tag{7.1-79}$$

$$S_\alpha = \frac{S_\varepsilon}{\varepsilon_1 - \varepsilon_2} \sqrt{\frac{1}{2} + \cos^2 2\alpha} \tag{7.1-80}$$

Unlike the $0^\circ/60^\circ/120^\circ$ rosette, the standard deviations $S_{\varepsilon_{1,2}}$ now depend not only on S_ε but also on the angle of reference α. Table 7.1-3 shows by means of a numerical example that S_{ε_1} or S_{ε_2} may assume values up to 1.73 S_ε depending on the magnitude of α.

In general, S_α is unimportant as the uncertainty during geometrical measurements of installed rosettes is usually larger.

Very similar conditions to those for $S_{\varepsilon_{1,2}}$ apply for error effects with regard to the principal stresses $S\sigma_{1,2}$.

The statements will be explained by an example. If a relative uncertainty

$$f_\sigma = \frac{S_\sigma}{\sigma} \; 100\% \tag{7.1-81}$$

is introduced where

S = standard deviation

σ = actual stress

and if the following is assumed for calculation

$\varepsilon_1 = 1000 \frac{\mu m}{m}$, ($\varepsilon_2$ results from the type of the state of stress)

$S_\varepsilon = S_{\varepsilon a} = S_{\varepsilon b} = S_{\varepsilon c} = \pm 10 \frac{\mu m}{m}$

$E = 210{,}000 \text{ N/mm}^2$

$\mu = 0.30$

then the values given in Table 7.1-3 apply.

This shows that the $0^\circ/60^\circ/120^\circ$ rosette usually offers a greater measuring reliability than the $0^\circ/45^\circ/90^\circ$ rosette. However, if the principal directions and the exact arrangement are known, even the $0^\circ/45^\circ/90^\circ$ rosette may yield favourable results.

If errors resulting from inaccuracies of the modulus of elasticity are considered, the differences between both types of rosettes become less important for the final results.

Moreover, the transverse sensitivity of the single strain gauges is important in the case of a multi-axial state of stress. In general, it is relatively small; however, it may cause considerable relative errors in the result of the smaller one of the two principal stresses if it is not corrected.

Table 7.1-3: Standard deviations S of the principal strains $\varepsilon_{1,2}$ and the principal stresses $\sigma_{1,2}$ as well as relative uncertainty f for various states of stresses.

			$0^o/45^o/90^o$ rosette (the values depend on α)	$0^o/60^o/120^o$ rosette (the values are independent of α)
S_{ε_1}	(μm/m)		8.7 - 17.3	10
S_{ε_2}	(μm/m)		10 - 17.3	10
S_{σ_1}	(N/mm^2)		2.2 - 4.0	2.4
S_{σ_1}	(N/mm^2)		2.4 - 4.0	2.4
At $\sigma_1 = -\sigma_2$	f_{σ_1}	(%)	1.36 - 2.51	1.49
(shear panel)	f_{σ_2}	(%)	1.49 - 2.51	1.49
At $\sigma_1 = 2\sigma_2$	f_{σ_1}	(%)	0.89 - 1.64	0.97
(tank wall)	f_{σ_2}	(%)	1.94 - 3.30	1.94
At $\sigma_2 = 0$	f_{σ_1}	(%)	1.05 - 1.93	1.14
(uniaxial state of stress)	f_{σ_2}	(%)	$\to \infty$	$\to \infty$
At $\sigma_1 = \sigma_2$	f_{σ_1}	(%)	0.73 - 1.35	0.80
(ball)	f_{σ_2}	(%)	0.87 - 0.96	0.80

Assumptions:
ε_1 = 1000 μm/m
S_ε = 10 μm/m
E = 210,000 N/mm^2
μ = 0.30

Usually, the transverse sensitivity on the strain gauge data sheet is identified by k_t given in %. It represents the relationship between the gauge factor crosswise to the grid direction k_t ($k_{transverse}$) and the gauge factor in grid direction k_ℓ (k_{axial})

$$q = \frac{\frac{\Delta R}{R}}{\frac{\varepsilon_t}{\frac{\Delta R}{R}}} = \frac{k_t}{k_\ell} \qquad (7.1\text{-}82)$$

Owing to the insignificant difference, k_ℓ and k can be equated as

$$k_\ell = \frac{k}{1-\mu q} \qquad (7.1\text{-}83)$$

applies.

If the transverse sensitivity is q = 2% and if $\mu = 0.3$, the difference amounts to only 0.6%, this corresponds to the uncertainty of the gauge factor itself.

The error acting on the strain due to the transverse sensitivity of the single strain gauge results from the relation

$$n_\varepsilon = \frac{q(\frac{\varepsilon_t}{\varepsilon_\ell} + \mu)}{1 - \mu q} \qquad (7.1\text{-}84)$$

or if using the simplified equation stated under (7.1-83)

$$n_\varepsilon = q \frac{\varepsilon_t}{\varepsilon_\ell} \qquad (7.1\text{-}85)$$

It is now possible to eliminate the effects of the transverse sensitivity by calculation. Table 7.1-4 shows the corresponding relations for biaxial rosettes.

The relations for triaxial rosettes are much more complicated. Therefore, the indication of corrective formulae for $\varepsilon_{a,b,c}$ is dispensed with, especially since in this case the individual types of rosettes have to be treated differently.

The conditions are again less complex if it can be assumed that all single strain gauges have approximately the same transverse sensitivity. In this case, the correction can be effected even after determination of the principal strains by means of the relations of Table 7.1-4 applicable for both types of rosettes.

References:(5), (18), (33), (52), (66), (82).

7.2 Measurement of strain behaviour by means of strain gauge chains

On panels with high strain gradients, the maximum strain is difficult to assess by single strain gauges as the point of maximum strain is generally not accurately known. When applying a strain gauge with large grid length, ε_{max} is covered by the gauge; however, the mean strain measured can be far below ε_{max} by the averaging effect resulting from this length (strain gauge "A" in Fig 7.2-1; refer also to Section 4.12).

When using strain gauges with small grid lengths it is very likely that measurements are taken at points far away from ε_{max} caused by a faulty application of the gauge (strain gauge "B" in Fig 7.2-1).

Strain gauge chains are most suitable for the measurement of the strain gradients and ε_{max}. In that case, several single strain gauges with accurately defined grid distances are arranged on a common supporting material. It is now quite easy to determine location and magnitude of ε_{max} from the individual measured values (Fig 7.2-1, strain gauge $C_{1,2...}$).

The manufacturers of strain gauges offer quite a number of different strain-gauge chain configurations. Fig 7.2-2 shows a selection of these types.

The measuring grid sizes available on the market range from 0.5 x 0.6 mm to 4 x 4 mm; the spacing, i.e. the distance between the individual measuring grid centres, ranges from 0.8 to 4 mm.

Table 7.1-4: Corrective formulae for consideration of the transverse sensitivities of single strain gauges of rosettes

Biaxial rosettes (equal transverse sensitivity of both strain gauges)

$$\varepsilon_1 = \varepsilon_a = (1-\mu_o q)(\varepsilon_a' - q\varepsilon_c') \approx \varepsilon_a' - q\varepsilon_c' \qquad (7.1\text{-}86)$$

$$\varepsilon_2 = \varepsilon_c = (1-\mu_o q)(\varepsilon_c' - q\varepsilon_a') \approx \varepsilon_c' - q\varepsilon_a' \qquad (7.1\text{-}87)$$

$$\gamma = (\varepsilon_1' - \varepsilon_2')\, C_j = (\varepsilon_1' - \varepsilon_2')\, \frac{1-\mu_o q}{1-q} \qquad (7.1\text{-}88)$$

Biaxial rosettes (different transverse sensitivity of both strain gauges)

$$\varepsilon_1 = \varepsilon_a = \frac{\varepsilon_a'(1-\mu_o q_a) - q_a \varepsilon_c'(1-\mu_o q_c)}{1-q_a q_c} \qquad (7.1\text{-}89)$$

$$\varepsilon_2 = \varepsilon_c = \frac{\varepsilon_c'(1-\mu_o q_c) - q_c \varepsilon_a'(1-\mu_o q_a)}{1-q_a q_c} \qquad (7.1\text{-}90)$$

Triaxial rosettes (equal transverse sensitivity of the three strain gauges)

$$\varepsilon_1 = (\varepsilon_1' - q\varepsilon_2')\, \frac{1-\mu_o q}{1-q^2} \qquad (7.1\text{-}91)$$

$$\varepsilon_2 = (\varepsilon_2' - q\varepsilon_1')\, \frac{1-\mu_o q}{1-q^2} \qquad (7.1\text{-}92)$$

(ε_a', ε_c' = values measured)

(ε_1', ε_2' = uncorrected principal strains calculated from $\varepsilon_{a,b,c}$)

Measurements can be performed either in the direction of the chain or perpendicular to the direction of the chain or alternately in both directions, the latter measurement comprising a chain of biaxial rosettes.

Apart from that there are $0^o/60^o/120^o$ rosette chains with measuring grid sizes of 1.2 x 1.2 mm and a spacing of 4 mm.

Generally, a chain consists of 10 single strain gauges but larger chains are also known.

A rosette chain, however, never comprises more than 5 rosettes (i.e. 15 single strain gauges) on one piece of supporting material.

The types of arrangements for connections are numerous. In most cases they are arranged symmetrically on both sides of the chain, sometimes using a common connection. However, there are chains having all connections on one side.

Reference (74).

7.3 Strain gauges for flexural strain measurements

If flexural strains are to be measured on a component, strain gauges are generally applied to both sides of the component. If this is impossible for spatial reasons, the flexural strain can be measured on one side only by bonding two strain gauges at a specified distance one above the other. Such combinations of strain gauges arranged one above the other is available on the market (Flexa-Gages).

If the exact distances between the strain gauges and the component thickness are known, the component strain on the side opposite the strain gauge can be determined assuming a linear strain distribution over the entire cross section (Fig 7.3-1).

However, using this procedure requires some compromises. First of all, there is the effect of the relation of the component thickness to the thickness of the intermediate supporting layer. On the one hand, the distance between the two measuring grids relative to the component thickness should be very large if the effect of errors in the determination of the measuring grid distance is to be small. On the other hand, the intermediate supporting layer should be very thin to keep stiffening effects low. Furthermore, the effect of the modulus of elasticity of the intermediate supporting layer has to be taken into consideration. If E is too large, a noticeable stiffening of the component occurs even with relatively thin intermediate supporting layers. If E is too small, transfer of the strain to the upper strain gauge is insufficient resulting again in deficiencies(see also Section 4.10).

Intermediate supporting layer materials with a modulus of elasticity from 5000 to 15000 N/mm^2 have proved most suitable; in the case of Al and Ti, E=10000 N/mm^2 should not be exceeded because of component stiffening.

The thickness of the intermediate supporting layer should be about 25% to 50% of the component thickness. Only if it is possible to accurately determine the distance between the two measuring grids can smaller intermediate supporting layer thicknesses below 10% of the component thickness be used.

The appropriate length of the intermediate supporting layer depends on the thickness of the layer. Studies with a "Pertinax" intermediate supporting layer($E \sim 15000\ N/mm^2$) have shown that the strain is completely transferred to the upper strain gauge only after a length corresponding to 15 to 20 times the intermediate supporting layer thickness. Thus the overall length of the intermediate supporting layer should not be less than 30 to 40 times the thickness.

These requirements largely limit the applicability of this procedure.

At component thicknesses below 1 mm the procedure is generally not applicable because of excessive inaccuracy. On the other hand, the intermediate supporting layer length will become very large for the abovestated reasons at component thicknesses exceeding 10 mm.

Pre-fabricated flexural strain gauges (Flexa-Gages) cannot be used on curved components due to pre-stress on supporting material and strain gauge.

Finally, it must be mentioned that this procedure is limited to uniaxial strain gauges or strain gauge chains. Rosettes cannot be used due to poor connecting conditions.

If the procedure is used for panels with high strain gradients, measuring errors have to be expected in view of the extended strain introduction distances.

7.4 Strain gauges for membrane stress measurements

It is quite difficult to determine membrane stresses with the strain gauges described up to now. However, membrane rosettes developed especially for this purpose are well suited for the assessment of specific stress and strain relations (Fig 7.4-1).

Membrane rosettes are almost exclusively used for the manufacture of transducers, (e.g. pressure pick-ups, load pick-ups); but a brief description of them will follow for reasons of completeness.

Mostly, membrane rosettes are designed as full-bridge rosettes (Fig 7.4-2A). Four active strain gauges are arranged on a common supporting material, two of them are located in the centre of the membrane. They only record the positive circular strain. The other two strain gauges at the membrane edge record the negative radial strain. This arrangement makes it possible to obtain a large bridge output signal and this a high sensitivity transducer.

There are also quarter-bridge membrane rosettes (spiral-type rosettes, Fig 7.4-2B) recording only strain at the centre of the membrane.

Owing to the special strain conditions, both types of rosettes are always designed for a specific membrane diameter which can only be varied within small tolerances (±5%).

Commercial rosettes are available with membrane diameters from 5 to ∿32 mm.

References: (6), (17)

7.5 Strain gauges for the determination of residual stresses

In many components residual stresses are produced by working processes such as forging, rolling, milling, sawing, welding etc. In general, residual stresses can be determined only by means of radiography (Ref (B4)) or by destruction of the component. Both procedures can hardly be used for flight measuring techniques. Nevertheless, the second procedure will be briefly described.

Mathar's drill-hole procedure is the one most frequently used. Here a drill-hole rosette, a $0^{\circ}/45^{\circ}/90^{\circ}$ rosette or a special type of $0^{\circ}/60^{\circ}/120^{\circ}$ rosette(Fig 7.5-1) is first applied to a point where the residual stress state is to be measured. In the case of sheet metals and plates it is advisable to apply such rosettes to both sides exactly opposite each other. The residual stresses are partly set free by a hole drilled in the centre of the rosette. Now the residual stresses can be determined according to magnitude and direction from the measured values from the three rosette legs by means of special relations (Ref (9)).

Differences in the measured values of the two rosettes located opposite each other indicate flexural residual stresses.

If, by gradual spot-drilling of the specimen, the strains are determined as a function of the drill-hole depth, it is possible to define the residual stress distribution approximately over the entire specimen thickness.

However, it is impossible to eliminate the residual stresses completely by means of the drill-hole procedure. If a segment is cut from this specimen, the stresses are completely eliminated in this part. The residual stresses can thus be fully determined by applying a rosette prior to cutting and using conventional rosette evaluation methods. The larger hole diameter required is an essential disadvantage in using this procedure compared with the drill-hole procedure.

Other known procedures (boring-bending procedure etc) differ from the above stated approaches only by their method of eliminating the residual stresses. Thus they need not be described here.

References: (9), (59), (85).

7.6 Stress gauges

The preceding chapters deal with strain gauges that can be used for strain measurements. The stresses can then be determined from the strains by means of the procedure described.

Sometimes, however, only the stress (not the strain) in a certain direction is of interest. For this purpose, stress gauges are available. Stress gauges are strain gauges with a special grid configuration.

For a strain gauge the resistance change is proportional to a strain change parallel to the gauge. For a stress gauge the resistance change is proportional to a stress change parallel to the gauge. There are two types of stress gauges: The T-type and the V-type.

The performance of the T-type is based on the relation

$$\sigma_x = \frac{E}{1-\mu^2}\,(\varepsilon_x + \mu\varepsilon_y) \qquad (7.6\text{-}1)$$

Fig 7.6-1 shows this type of gauge. The measured signal is produced, in each case, by adding the strain in measuring direction ε_x and the μ-fold transverse strain $\mu\varepsilon_y$.

Using the configuration shown in Fig 7.6-1A, this is arranged by the different nominal resistances of the two measuring grids. The value of the stress is then obtained by a corresponding weighting (multiplication) of the output signal with E or $\frac{E}{1-\mu^2}$ (according to the information on the data sheet).

The compliance of the transverse strain ratios for stress gauges with the material to be measured is a pre-requisite for appropriate application. The gauges are thus designed for defined values of μ. Remaining differences can be balanced by the parallel connection of a resistor to one of the two measuring grids (Ref (69)).

The performance of the V-type is based on the relation

$$\sigma_x = \frac{E}{2(1-\mu)}\,(\varepsilon_\psi + \varepsilon_{-\psi}) \qquad (7.6\text{-}2)$$

under the condition that $\cos 2\psi = (1-\mu)(1+\mu)$.

Fig 7.6-1, B shows this type of gauge. In Fig 7.6-1, C is similar but composed of two strain gauges.

The gauge shown in Fig 7.6-1D is still more versatile. In this case it is unimportant whether two single strain gauges are applied at an angle of 90° or whether a biaxial rosette is used. The arrangement is adjusted to the material transverse strain ratio by parallel connection of the resistor R_q to the crosswise bonded strain gauge. The value of R_q is calculated from the equation

$$R_q = \frac{\mu \cdot R_{DMS}}{1-\mu} \qquad (7.6\text{-}3)$$

By rearranging the parallel resistor R_q from the transverse to the longitudinal strain gauge, the stress in transverse direction can also be determined by means of this same strain gauge configuration.

References: (69), (87), (B14).

7.7 Measurement of material fatigue

The resistance of each strain gauge changes under load. The change in resistance per load cycle grows with increasing load and strain amplitude until fracture of the the measuring grid, the connections or in the component itself occurs after a certain number of load cycles.

The effect of the increase in resistance is utilized in the fatigue life gauge to obtain direct information on aging. It has proved a versatile instrument for experimental studies. However, fundamental knowledge and extreme care are necessary when this gauge is used and the measured results are interpreted, in order to avoid misinterpretation.

The configuration of the fatigue life gauge is similar to that of a strain gauge. It also consists of a measuring grid embedded in a supporting layer. However, its functioning differs considerably from that of a strain gauge.

The change in resistance of the strain gauge is proportional to the strain at the measuring point. After unloading it reassumes its original value of resistance whereas the fatigue life gauge retains a residual unbalance. This residual unbalance increases with a growing number of load cycles, i.e. the fatigue life gauge "stores" all load cycles occurring from the time of its installation. Thus, the change in resistance measured against the original value is a measure not only for the number of load cycles to which it was exposed but also for the strain level to which it has been subjected. This behaviour suggests two different possible applications for fatigue life gauges.

The fatigue life gauge can be used as a load cycle counter if certain boundary conditions are met. Although mechanical counters have a considerably higher accuracy than the fatigue life gauge, the latter is often better and easier to install. However, a prerequisite for its use is that the same strain level is reached with each load cycle and that the extent of the strain is known.

From the above it follows that the strain amplitude can be concluded from the change in resistance of the fatigue life gauge if the number of load cycles is known and the amplitude is constant. This method of application is particularly suitable for the measurement of rotating shafts in which case it is possible to dispense with slip-rings or telemetry systems.

The fatigue life gauge can also be used to assess variations in the amplitude levels under dynamic load. A gauge installed for this purpose on a structure shows a certain resistance behaviour depending on the number of load cycles for constant load amplitudes. If this amplitude now changes after a number of cycles, e.g. due to a fatigue fracture occurring in the proximity, this is indicated by a change in the slope of the resistance curve which can be used to identify the damage.

If varying load amplitudes occur, the mean load level can be determined by means of comparative measurements. This is demonstrated by Ref (48), using results obtained on four aircraft of the same type. These results show that the two aircraft which were in an aerobatics squadron were subjected to considerably higher loads than two similar aircraft used as training aircraft. The measurements further show that the load depends on the respective position of the aircraft during formation flight.

Similar comments apply to its use for comparative measurements on components of different configurations being subjected to the same load spectra. In this case, the fatigue life gauge applied to the best part shows the least change in resistance.

However, the main purpose for the application of a fatigue life gauge is to obtain a reliable indication with regard to "fatigue" or the remaining life until surface cracks appear. This requires, first of all, the determination of critical points on a structure. Furthermore, comparative measurements have to be performed with regard to the strains occurring at these points by using test bars of the same material. Only then is a useful statement on the remaining life possible.

Furthermore, it has to be considered that a certain strain level is required for the optimum application of a fatigue life gauge. Very often it is therefore necessary

to resort to strain multipliers (refer to Section 7.12).

These multipliers must also be used if materials with very low fatigue strength are to be measured.

Up to this point, the possible application of single fatigue life gauges has been described. For various purposes, accurate preliminary tests and comparative measurements are absolutely necessary. In addition, certain boundary conditions with regard to load amplitudes and the number of load cycles have to be met in most cases. However, the field of application can be considerably enlarged by combining several fatigue life gauges.

Reference (5) shows how a combination of three fatigue life gauges with different strain sensitivity can be used for the measurement of random strain distributions. However, evaluation requires extensive computer programmes. The measuring results published confirm the excellent applicability of this procedure.

Reference (35) uses another approach. In this case two fatigue life gauges with different sensitivities (varying changes in resistance at equal strain amplitudes and load cycle numbers) are combined. With this arrangement relatively accurate statements of the remaining life of the test specimen can also be made.

As already indicated, quite useful results are obtained with the two last-mentioned procedures even without extensive preliminary tests; however, the accuracy of the statements can be considerably increased by preliminary and comparative tests.

References: (4), (15), (19), (20),(32), (35),(48).

7.8 Measurement of crack propagation

Like the fatigue life gauge, the crack propagation gauge is not used for strain measurements although it, too, is related to the strain gauge.

The crack propagation gauge is used to assess the propagation rate of a detected crack as a function of time and number of load cycles, respectively. In certain cases of application, such as with test bars, the gauge permits the determination not only of the time at which the crack occurs but also of its location. However, this requires the connection of special recording electronics.

Like the strain gauge, the crack propagation gauge is also embedded in a supporting material, but unlike the strain gauge, its measuring grid consists of several adjacent, parallel-connected resistance paths. If a crack propagates under a gauge, the resistance paths are broken one after the other. The result is a gradual increase of the total resistance. As the distances between the resistance paths are exactly known, it is not difficult to determine the location of the crack and its propagation rate.

Crack propagation gauges with distances of 0.25, 0.5 and 2.0 mm between the paths are available on the market with the number of paths amounting to 10 or 20. If connected as recommended by the manufacturer, the total resistance will be between 2.5 and 50Ω according to the number of paths broken.

7.9 Measurement of large strains

Strains up to about 25000 µm/m can be measured with normal strain gauges. Special strain gauges and adhesives are available for strains up to 200 000 µm/m. When the signals from these gauges are evaluated, the non-linearity of the bridges has to be taken into consideration (see Chapter 3) unless other procedures are applied to determine changes in resistance.

Strain transformers have to be used (see Section 7.11) if the above-stated difficulties are to be avoided; the strain transformers reduce the actual strains to smaller strains for measuring purposes.

References: (68), (72), (77).

7.10 Special procedures for strain gauge application

In previous chapters it has always been assumed that the strain gauge has been applied to the measuring object by means of an adhesive. However, special procedures have also been used which permit application without adhesive and these should be mentioned.

7.10.1 Self-adherent strain gauges

A self-adherent strain gauge has been specially developed for measurements on components with highly polished surfaces. In this case, the adhesion of thin elastomers is used to transfer the strain (Ref (36)). However, in practice this method has not been very successful because reliability is not good.

7.10.2 Pressure application of strain gauges

A procedure has also been developed to apply strain gauges by means of pressure. The strain gauge rosettes were applied to the measured object (plexiglass) using a special rubber cushion and a pressure of about 150 N/cm^2. Comparative measurements with rosettes applied by bonding showed excellent agreement in the measured values. The reproducibility was also excellent. The relatively great force and the space required for the rubber cushion during measurements are a disadvantage.

A particularly suitable field of application is indicated in another paper describing the pressure application of strain gauges in drill-holes by means of a pressure hose (ref (37)).

The advantage of the pressure application method is that the strain gauges or rosettes can be used again at another location after each measurement. However, care has to be taken that the gauges are not excessively loaded as permanent deformations in the gauges must be avoided.

References: (37), (42).

7.11 Strain transformers

Special strain gauges are available for the measurement of large strains; semi-conductor strain gauges can be used for an accurate measurement of even the smallest strains. The difficulties encountered with strain gauges with regard to their temperature sensitivity and/or their non-linear behaviour can be avoided by using strain transformers. With these devices, strain can be transferred to an area where it can easily be measured with standard measuring instruments.

The application of normal strain gauges sometimes results in considerable errors caused solely by the stiffening effect of the metal measuring grids if these gauges are used for the measurement of large strains (> 50 000 µm/m) on materials with a small modulus of elasticity (rubber, plastics). These and other difficulties can be avoided by using strain transformers for large strains as shown in Fig 7.11-1A. In this case the longitudinal strain ε_1 of the component is transformed into a flexural strain. The transformation ratio of the pick-up can be determined by an appropriate selection of the bow dimensions. It is also possible to reduce the stiffening effect to a minimum by using a very thin sheet metal strip as the bow.

The laws concerning the design of the bow and the determination of the transformation ratio are included in Ref (11). However, it is recommended that the transformation ratio on each bow should be determined experimentally.

Very often, even the smallest strains have to be measured with great accuracy. In this case, inductive or other displacement transducers can be used for large gauge lengths. They cause a minimum stiffening on the component. Still it is possible to sense small strains. Cases of application, in particular in connection with fatigue life gauges, have become known (refer Section 7.7).

Fig 7.11-1B to C show the basic and simultaneously the oldest types of transformers actually known. The component strain occurring between the bonded surfaces is transferred via the bonding surface to the intermediate supporting layer, the actual transformer. By providing limited gauge lengths with reduced cross section, increased strains occur which can be measured with strain gauges (punched end in the case of B, central cross-section reduction in the case of C).

Amplification coefficients of 2 to 3 can be obtained with these types. However, they can be used only on very thick components due to the considerable stiffening effect.

Smaller stiffening effects and larger amplification coefficients (2 to 10) are obtained with the transformer shown in Fig 7.11-1D developed by Hawker-Siddeley. In this case, the strain gauge and fatigue life gauge, respectively, are bonded on to the slots of the intermediate supporting layer. In order to avoid destruction of the pick-up caused by local excessive load, the strain gauge should only be applied to the transformer together with an intermediate layer ($\sim$0.1 mm) of kapton or a similar material.

A rigid connection exists between the two bonding surfaces of the types described up to this point so that the forces to be transferred are relatively large. The only rigid connection of the type shown in Fig 7.11-1E and F (developed by Micro-Measurement) is the strain gauge itself which means that the stiffening effects are very small. Furthermore, effective amplification coefficients can be set more accurately than with other types.

The strain gauge has been provided with a silicone-rubber layer to avoid buckling of the strain gauge under pressure load. Amplification coefficients up to 25 can be obtained with these configurations.

References: (11), (53), (88).

7.12 Geometrical arrangement and electrical interconnection to realize special measuring effects

Earlier chapters have only dealt with uniaxial strain gauges or the combination of uniaxial strain gauges into rosettes. It has been assumed that the measured signals, from say three rosette legs, are measured with three separate bridges; then the principal directions strains and stresses are calculated.

If the principal directions are approximately known, it is also possible to obtain special measuring effects by combining several strain gauges and interconnecting them in a Wheatstone bridge. This possibility has already been mentioned in Chapter 3 and in Section 7.1.3 it has been used for shear measurements.

Table 7.12-1 shows a number of different interconnection possibilities. The strain gauge arrangement on a component, the interconnection in a Wheatstone bridge and the sensitivities or bridge factors are given. The formulae indicate the strain on the component surface. In the following, the various bridge interconnections will be described in detail; however, the effects of cable resistances etc will be neglected. The relevant corrections are explained in Chapter 3 and can be applied here by analogy.

- Bridge 1 in Table 7.12-1 shows a simple quarter-bridge. It is obvious that the strain gauge reads not only under tensile or compressive load but also under the action of a flexural moment. A strain gauge not temperature-compensated will also show an apparent strain ε_S in the case of temperature variations. But even a strain gauge which has been compensated for temperature changes will yield a small signal resulting from inaccuracies in compensation; this aspect, however, will not be taken into consideration at this point.

- In bridge 2, the fixed resistor (R_{22}) is replaced by a temperature compensation strain gauge. The temperature sensitivity observed is caused by the differences between the temperature variation curves of the two strain gauges. It is generally very small if both strain gauges are from one package or at least from the same manufacturing batch. The sensitivity in the table is equal to zero and will be neglected in the following (refer to Section 3.3.1.1).

- In bridge 3, the compensation strain gauge is applied to the component where it picks up the transverse strain and amplifies the output signal.

- In bridges 4 and 5, two strain gauges each are arranged opposite each other on the component. A compensation of the portion from the longitudinal load (bridge 4) on the one hand and the portion from the flexure (bridge 5) on the other is possible by different arrangements of the strain gauges in the two bridges. It has to be noted that bridge 5 again shows temperature sensitivity.

- Bridge 6 is a combination of two-half-bridges according to bridge 3. In this case, the sensitivities are doubled not only for longitudinal loads but also for flexural moments.

- Bridge 7 is a combination of two half-bridges according to bridge 2. However, here the effect of the flexural moment is compensated.

- Bridge 8 is the bending bridge with the highest sensitivity. All effects resulting from longitudinal loads, torsional moments and temperature variations have been compensated by adequate circuitry.

- Bridges 9, 10 and 11 show the same strain gauge arrangement on the component; various effects are obtained by different interconnections. In bridge 9 only longitudinal loads and in br dges 10 and 11, only flexural moments are effective. Various sensitivities are obtained by different interconnections of bridges 10 and 11.

- Bridge 12 is a special type. Here, four strain gauges are interconnected in a half-bridge.

- Bridges 13, 14 and 15 are torque measuring bridges with various strain gauge arrangements. Sensitivities and compensating effects are the same for all three bridges.

- The bridges 16 and 17, representing shearing force bridges, are similar to those mentioned immediately above.

Only very few bridge interconnections are of importance for flight measurement techniques.

Bridge 9 is almost exclusively used for tensile/compressive load measurements on control linkages or turnbuckles as in this case all effects resulting from possible flexural loads, temperature variations etc are compensated and this bridge shows a high sensitivity.

One of the bridges 13, 14 or 15 can be used for rotating shafts.

Various bridges are used for structural measurement.

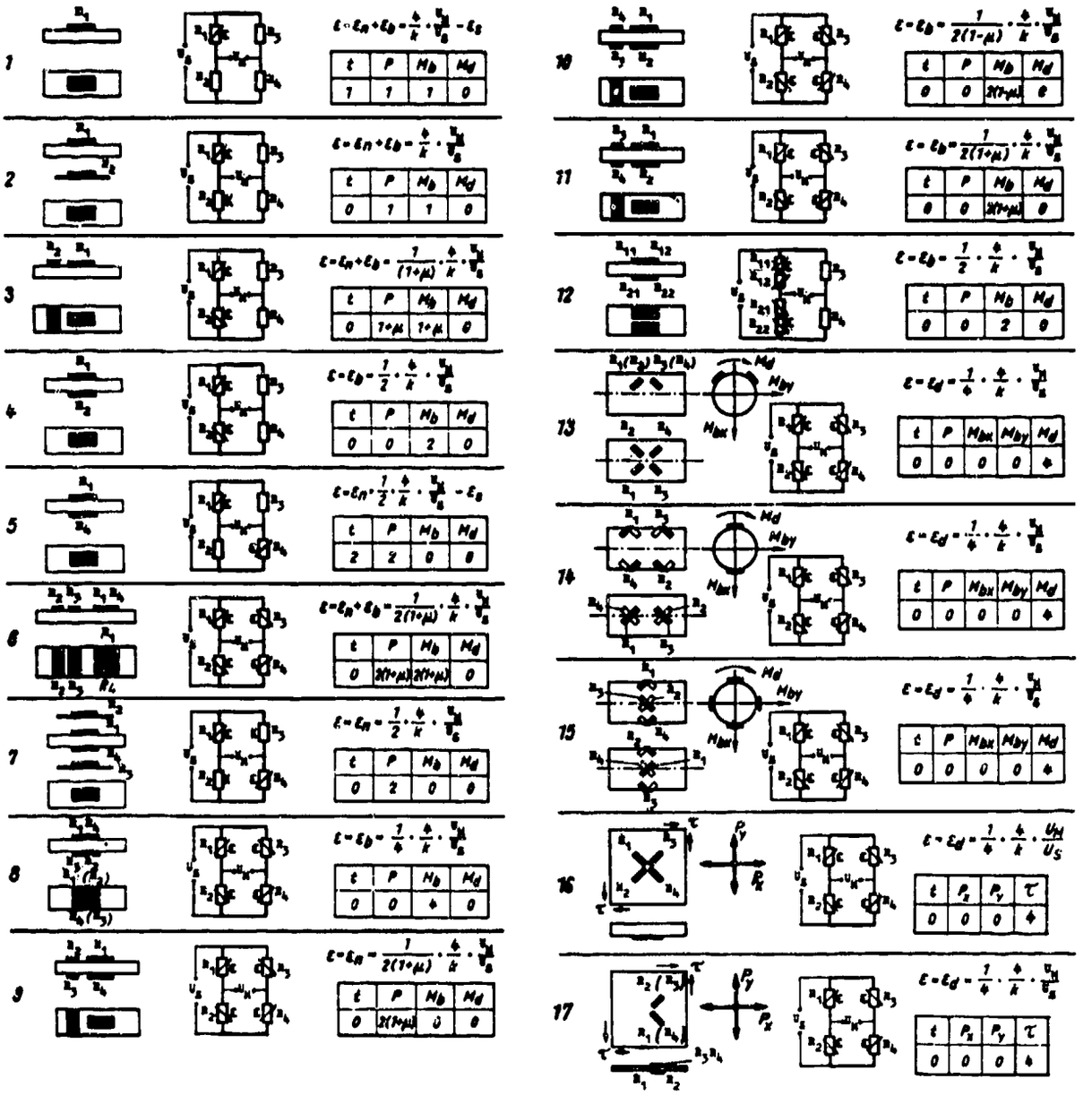

	t	P	M_b	M_d
1	1	1	1	0
2	0	1	1	0
3	0	1+μ	1+μ	0
4	0	0	2	0
5	2	2	0	0
6	0	2(1+μ)	2(1+μ)	0
7	0	2	0	0
8	0	0	4	0
9	0	2(1+μ)	0	0
10	0	0	2(1+μ)	0
11	0	0	2(1+μ)	0
12	0	0	2	0

	t	P	M_{bx}	M_{by}	M_d
13	0	0	0	0	4
14	0	0	0	0	4
15	0	0	0	0	4

	t	P_x	P_y	τ
16	0	0	0	4
17	0	0	0	4

t - temperature change
P - longitudinal force
M_b - bending moment
M_d - torque
k - gauge factor
ε - strain
ε_b - bending strain
ε_n - normal (longitudinal) strain
ε_s - appearent strain
U_S - supply voltage
U_M - bridge output voltage

Table 7.12-1 Interconnection of strain gauges to obtain special measuring effects

Bridges 16 or 17 are used for shearing force measurements on spar webs. Here it has to be noted that the relatively thin metal web on high wing spars (with thick wing profiles) may buckle even under small loads. In such cases it is necessary to use bridge 17 provided that the strain gauges and the $\pm 45^{\circ}$ rosettes, respectively are located if possible exactly opposite each other on the metal web. Only then are the effects of buckling on the results compensated.

Similar comments apply to torque measuring bridges that can be applied either to the skin or even better to spar webs. In the example given in Chapter 9, the torque measuring bridges were positioned on the skin for spatial reasons.

Bridge 11 is almost exclusively used for flexural moment measurements on spar caps or even on stringers (one half bridge each on the wing profile upper and lower surface). Although it is less sensitive than bridge 8, its temperature behaviour is more favourable (the temperature induced output of bridge 8 is only zero if the same temperature variations occur at R_1 and R_3 or R_2 and R_4).

The interconnection possibilities indicated above are only a small selection of the most important ones. Quite a number of other possibilities, even with 8, 12 or 16 strain gauges, can be applied; they are reserved for very specific purposes.

The description of these special bridges would exceed the scope of this report.

Reference: (69).

7.13 Measurement of strains on and in fibre-reinforced components

Fibre-reinforced materials are of increasing importance for the aerospace industry. Their high stiffness and strength values as well as their low specific weight and in particular the ability to orient the fibres such that their strength values coincide with highly-stressed directions offer considerable advantages.

The application of strain gauges on these materials is generally not difficult. Almost any known adhesive is well suited for bonding the strain gauges on to the filler (mostly epoxy resin). They can also be embedded into the material without affecting the strength behaviour or the component thickness. This is impossible with other materials, as is well known. For this purpose, connecting cables are soldered to the strain gauge prior to its application. The strain gauge is now placed between the fibre layers together with its connecting cables without using a special adhesive; the filler resin is then cured (Ref (40)).

No special measuring problems will occur with regard to components that can be calibrated if their low thermal conductivity against metals is taken into consideration. In this case, larger measuring grids or smaller supply voltages should generally be applied. (Ref (4)).

However, considerable difficulties may occur if principal strains or mechanical stresses are to be determined from the measured strains.

Fibre-reinforced materials are inhomogeneous and anisotropic. Each of the directions has other elastic parameters (moduli of elasticity and transverse contraction ratios) so that even the determination of strains has to be performed with great care.

Transverse contraction ratios can vary between 0.2 and 0.85 depending on the fibre direction and the degree of filling. Thus the transverse sensitivity of the strain gauge may introduce considerable errors at these extreme values. A correction of the errors is recommended whenever the elasticity parameters and the transverse sensitivity of the strain gauge are known.

The moduli of elasticity show a similarly large spread. The values of two test bars of boron-fibre epoxy with different fibre layers and directions are stated as an example:

1) 9 layers with the directions

   $2 \times 0^{\circ}$, $\pm 45^{\circ}$, 90°, $\pm 45^{\circ}$, $2 \times 0^{\circ}$

2) 8 layers with the directions $4 \times (\pm 45^{\circ})$

	(1)	(2)
E_0°	114,000 N/mm^2	19,000 N/mm^2
E_{90}°	52,000 N/mm^2	19,000 N/mm^2
μ	0.42	0.85
G	28,000 N/mm^2	-

The values for the moduli of elasticity show that it is impossible to calculate a mechanical stress from the strain values measured unless the fibre layers and the degree of filling are known and the elasticity parameters have been determined by means of test bars.

But even after having determined the parameters they should not be taken for granted as these parameters cannot be considered constants according to Ref (41). The values also depend on the configuration of the specimen.

References: (4), (34), (40), (70).

7.14 Interconnection of strain gauge bridges for the measurement of defined load elements (structural measurements)

Mechanical loads can be completely described by three orthogonal forces (longitudinal, transverse and vertical direction) and three orthogonal moments (moments around the longitudinal, transverse and vertical axis). (Fig 7.14-1).

In general, however, the individual elements occur simultaneously and it is then impossible to distinguish them from each other. A strain gauge bridge installed anywhere on the wing, for example, responds to any of the load types mentioned above. Its output signal does not permit an individual determination of the portions of the elementary loads.

For the specific application on flight test Skopinski (Ref (38)) was the first to develop a procedure that can be used to obtain the required separation into orthogonal forces and moments by means of an adequate interconnection of strain gauge bridges. By concentrating on the component's bending moment, torsion moment and shear force, he simplified the task of application. The examples of applications that became known in practice through flight testing show quite useful results although the effort concerning installation, calibration and calculation is considerable. Its realization is not possible without the use of digital computers.

In the following, the basic laws from which the Skopinski equations can be easily derived are explained in order to judge the efficiency of these methods and to give some information about the effort implied in their usage. For direct application further studies of the corresponding references are necessary.

7.14.1 Basic mathematical relations

The output voltage of a strain gauge installed at random on a multi-dimensionally stressed component is a function of the load applied

$$u = f(L) \tag{7.14-1}$$

The following set up applies

$$u = a_{11}P_x + a_{12}P_y + a_{13}P_z + a_{14}M_x + a_{15}M_y + a_{16}M_z + a_{17}P_xP_y + \ldots \tag{7.14-2}$$
$$+ a_{1j}P_x^u\, P_y^v\, P_z^w\, M_x^r\, M_y^s\, M_z^t$$

when taking into account the individual load elements.

In this case, it has to be borne in mind that even within the validity of Hooke's law the non-linear terms have to be considered (being introduced by geometrical characteristics of the structure).

Considering j load elements for j bridges installed, the following system of equations results

$$\begin{aligned} u_1 &= a_{11}P_x + a_{12}P_y + \ldots + a_{1j}P_x^u\, P_y^v\, P_z^w\, M_x^r\, M_y^s\, M_z^t \\ u_2 &= a_{21}P_x + a_{22}P_y + \ldots + a_{2j}P_x^u\, P_y^v\, P_z^w\, M_x^r\, M_y^s\, M_z^t \\ u_j &= a_{j1}P_x + a_{j2}P_y + \ldots + a_{jj}P_x^u\, P_y^v\, P_z^w\, M_x^r\, M_y^s\, M_z^t \end{aligned} \tag{7.14-3}$$

or, if a matrix notation is used,

$$\begin{Bmatrix} u_1 \\ u_2 \\ \vdots \\ u_j \end{Bmatrix} = \begin{bmatrix} a_{11} & a_{12} & \cdots & a_{1j} \\ a_{21} & a_{22} & \cdots & a_{2j} \\ \vdots & \vdots & & \vdots \\ a_{j1} & a_{j2} & & a_{jj} \end{bmatrix} \begin{Bmatrix} P_x \\ P_y \\ \vdots \\ P_x^u\, P_y^v\, P_z^w\, M_x^r\, M_y^s\, M_t^t \end{Bmatrix} \tag{7.14-4}$$

or

$$\{u\} = [a]\ \{L\} \tag{7.14-5}$$

In equations (7.14-3) to (7.14-5) the output signals of the bridges involved are described by means of a linear combination of the load vector elements involved. It is very easy to determine this load vector if the determinant of the square coefficient matrix is not singular, i.e. no linear relationship exists between the coefficients of the individual bridges.

$$\begin{aligned} &\det [a] \neq 0 \\ &\{L\} = [b] \quad \{e\} \\ &[b] = [a]^{-1} \end{aligned} \tag{7.14-6}$$

In accordance with equation (7.14-6) the individual load elements can be determined by adding the bridge signals weighted with the corresponding factors of the [b] matrix. This requires, however, the experimental determination of the [b] matrix by pre-test calibration. The calibration procedure can be seen from the following calculation.

Only the pure forces and moments of the load vector elements are important. This results in a new, limited system of equations.

$$\begin{Bmatrix} P_x \\ P_y \\ P_z \\ M_x \\ M_y \\ M_z \end{Bmatrix} = \begin{bmatrix} b_{11} & b_{12} - - - b_{1j} \\ b_{21} & b_{22} - - - b_{2j} \\ | & | \quad\quad | \\ | & | \quad\quad | \\ | & | \quad\quad | \\ | & | \quad\quad | \\ | & | \quad\quad | \\ b_{61} & b_{62} - - - b_{6j} \end{bmatrix} \begin{Bmatrix} u_1 \\ u_2 \\ | \\ | \\ | \\ | \\ u_j \end{Bmatrix} \tag{7.14-7}$$

or with {L'} as reduced load vector

$$\{L'\} = [b'] \quad \{u\} \tag{7.14-8}$$

where [b'] is the 6 x j coefficient matrix.

The determination of the first line coefficients of the [b'] matrix is given below as an example:

$$P_x = \{b_{11} \quad b_{12} - - - - - - b_{1j}\} \begin{Bmatrix} u_1 \\ u_2 \\ | \\ | \\ | \\ u_j \end{Bmatrix} \tag{7.14-9}$$

or, after transposition,

$$P_x = \{u_1 \quad u_2 - - - - - - u_j\} \begin{Bmatrix} b_{11} \\ b_{12} \\ | \\ | \\ | \\ b_{1j} \end{Bmatrix} \tag{7.14-10}$$

The application of j calibration loads at various positions results in the following (these loads are marked by an asterisk):

$$\begin{Bmatrix} P_{x1}^* \\ P_{x2}^* \\ \\ \\ P_{xj}^* \end{Bmatrix} = \begin{bmatrix} u_{11} & u_{12} - - - - u_{1j} \\ u_{21} & u_{22} - - - - u_{2j} \\ | & | \quad\quad | \\ | & | \quad\quad | \\ | & | \quad\quad | \\ u_{j1} & u_{j2} - - - - u_{jj} \end{bmatrix} \begin{Bmatrix} b_{11} \\ b_{12} \\ \\ \\ b_{1j} \end{Bmatrix} \qquad (7.14\text{-}11)$$

$$\{P_x^*\} = [u] \quad \{b_1^*\} \qquad (7.14\text{-}12)$$

where $\{b_1^*\}$ e column vector of the coefficients b_{1i} ($i = 1, 2, \ldots, j$) yielded by transpositi the first line of the coefficient matrix $[b']$.

This results in the following equation for the coefficients to be determined

$$\{b_1^*\} = [u]^{-1} \quad \{P_x^*\} \qquad (7.14\text{-}13)$$

It is, by no means, common practice to install six bridges per force element but rather to attempt to reduce their number as far as possible. This requires the use of additional mathematical techniques, in particular from the field of statistics. This will not be discussed at this point as these procedures have been described in detail in the references.

References: (38), (39).

7.14.2 Calibration process

After balancing of the bridges, defined loads are introduced into the object in various steps at accurately fixed points to determine the matrix elements of equation (7.14-11). Assuming that Hooke's law applies, non-linearities are caused only by component geometry so that due to the use of unchanged introduction points, there is a linear relation between bridge voltage and introduced load.

$$u = k_o \quad P_x^*$$

where the inclination k_o is determined by the most favourable straight line to be drawn through the measuring points of the individual load steps. Subsequent standardisation to the unit load is advisable for practical application purposes.

7.14.3 Interconnection of bridges

Interconnection of bridges can be effected either electronically or by resistors. The advantage of interconnection by means of analogue computer circuits (addition via operational amplifiers) is that it can be done with a relatively small number of bridges as these can be used in various combinations due to decoupling by the amplifiers. However, in this case each bridge must be provided with its own amplifiers. Therefore, individual bridges are generally interconnected via resistors. As this method implies an interaction of the interconnected bridges, each bridge can be used only once. Therefore, several bridges have to be installed.

If the internal resistance is the same for all interconnected bridges, which is mostly the case, the connective resistor R_{ii} (Fig 7.14-2) can be calculated from the relation

$$R_{ii} = \left(\frac{b_{11}}{b_{1i}} - 1\right) R \qquad (7.14\text{-}14)$$

where b_{11} is the largest coefficient of the interconnection.

All adjacent bridges are connected via the connective resistors R_{ii} to the neutral arm of the bridge associated with this coefficient. The resistors may assume values from a few ohms to several kilo-ohms.

Sensitivity and linearity of the new combination are generally checked by recalibration during which a combined load is introduced into the structure.

Furthermore, occasional calibrations for inspection purposes are recommended. They can easily be performed by applying a defined load to a given point (e.g. by attaching a weight).

The method of direct interconnection of strain gauge bridges may be replaced by multi-channel recording and later digital computing if appropriate. It has to be mentioned nevertheless that if on-line display for test reasons is necessary during flight, as in the example in Chapter 9, this method is not economically applicable today.

References: (36), (38), (39).

7.15 High-frequency strain measurements

Strain gauges can also be used to measure shockwaves and high-frequency vibrations. The detectable degree of slope and frequency range, respectively, are limited by the gauge length.

Fig 7.15-1 illustrates the change in resistance of the strain gauge at the impact of a shockwave. The shock front, assumed to be vertical, moves with a velocity c. Then, a period

$$t = \frac{L}{c} \qquad (7.15\text{-}1)$$

will elapse before this front passes over the gauge. The actual height of the wave will be indicated only after the end of the gauge has been reached by the wave as the strain gauge only measures the mean value of the various strains occurring over its length. Owing to the linear expansion of the strain gauge, the slope of the wave front seems to have been diminished, an effect that grows with increasing lengths. Thus, strain gauges used for the measurement of steep slopes have to be as short as possible.

However, the behaviour of strain gauges during high frequency vibration measurements is more important for flight testing purposes. In special cases, frequencies up to 5 kHz have to be measured in case of sonic loads.

Here, too, the strain gauge length is the restrictive factor. We must always ensure that this length is small relative to the wave length of the vibration. If this requirement is not met, the value indicated by the gauge will again be too small due to the averaging effect; no indication at all will take place if the two values coincide. Thus the actual boundary frequency that can be measured by a strain gauge also depends on the velocity of sound in the material to be measured. The boundary frequency of steel/aluminium ($c \sim 4700$ m/sec) for a given relation between wave and gauge lengths is stated in Table 7.15-1 if a specific error is acceptable.

The references describe applications up to frequencies of 44 kHz so that in this connection no problems may be expected for flight measurements.

References: (21), (54), (55), (56), (57).

Table 7.15-1: Boundary frequencies for strain measurements according to Ref (54).

Wave length/Gauge length	Boundary frequency 1/sec	Error %
22.2	40,000	1
9.9	80,000	5
6.59	120,000	10
4.0	240,000	30

7.16 Strain gauges of excessive lengths

Strain gauges with grid lengths up to ~10 mm, in certain cases even up to ~20 mm, are used for tests on metal components.

Although commercial strain gauges with excessive lengths up to 150 mm can be used here for certain special measurements they are, first of all, intended for application in the building industry such as measurements on concrete components. In this case the averaging effect (see Section 4.12) of the strain gauge is intentionally used.

7.17 Interferometric strain gauges

Now that an economic coherent light source is available in the form of the laser, tests to utilize optical strain gauges have been reported (Ref (86) Fig 7.17 1). In this case, transparent materials of minor stiffness are used and applied to the specimen like strain gauges. However, a bonding is effected only at the gauge ends.

The interference pattern results from the overlapping of the rays reflected from the external and internal surfaces of the strain gauge if the latter is exposed to rays emitted from a laser via a beam splitting mirror as shown in Fig 7.17-1. The distance of the interference lines depends on the optical thickness of the gauge. Under load this thickness and thus the interference pattern changes. Conclusions with regard to the strain can be drawn from recordings of these changes.

Reference: (86).

References for Chapter 7:

(5), (6), (8), (9), (11), (12), (13), (14), (15), (16), (17), (18), (19), (20), (32), (33), (34), (35), (36), (37), (38), (39), (40), (42), (48), (53), (54), (55), (56), (57), (68), (69), (74), (87), (88).

8.0 USE OF STRAIN GAUGES UNDER EXTREME ENVIRONMENTAL CONDITIONS

In the preceding chapters, the strain gauge was described as a versatile means for determining component surface strains. It was assumed that the measurements were not performed at extreme temperatures, in magnetic fields, in nuclear radiation or under vacuum conditions.

For a long time, however, measurements by means of strain gauges have also been performed under extreme environmental conditions. For instance on hot parts of missile combustion chambers or on components partly located in the engine exhaust stream.

The purpose of this chapter is to give a survey of the possibilities and limits of the strain gauge technique under extreme environmental conditions. Temperature is the most important of these conditions and will thus be treated more thoroughly in this text.

8.1 Use at extreme temperatures

In the lower temperature range (200 to 450K) the measuring grid material used is mainly constantan (Section 6.2). In the case of higher temperatures, up to 1000K, however, constantan has to be replaced by more stable alloys because of its low scale resistance and structural changes. These include, for example, modified Ni Cr alloys (Nichrome V, Karma, Nimonic 90), Fe Cr Ni alloys (Elinvar, Iso-Elastic), Fe Cr Al and Pt W alloys. The large number of alloys used indicates that an ideal grid material has not been found so far. Table 2.2-1 summarizes the most commonly used strain gauge alloys. The table makes clear that the alloys used do not all possess the ideal characteristics. The alloys with a low resistance temperature coefficient, for example, show high drift rates and even metallurgic transformations; on the other hand, the stablest alloys have very high temperature coefficients α_R and unfavourable gauge factors.

8.1.1 Technical configurations of strain gauges for extreme temperature and their attachment to the component

- Typical strain gauge configurations are shown in Fig 8.1-1. The configuration commonly used for room temperature is shown in Fig 8.1-1a. The measuring grid with the necessary leads is embedded in a plastic supporting material. The thin sheets thus obtained are bonded to the component to be examined, using organic adhesives. The applicability of organic materials is limited to the temperature range from 20K to 450K; within this range they are quite reliable. The restriction with regard to higher temperatures is caused by the decrease in the strength of these materials, which prevents a complete transfer of the component strains to the grid (Section 2.2.5.1). In addition, decomposition and combustion of supporting materials and adhesives leads to destruction of the strain gauge within a short period of time.

- Inorganic adhesives are used for temperatures exceeding 450K. Strain gauges for such applications are delivered on removable plastic supporting materials (Figs 8.1-1b and c). In principle, the strain gauge, with the grid facing the component, is placed on the measuring surface which has been electrically insulated by a thin coat of adhesive. Part of the measuring grid is exposed by removing the plastic supporting material and ceramic adhesives are applied to it. The adhesives used are available in the form of aqueous solutions and are applied by means of a hair brush. When the surface of the adhesive coat has dried, another part of the grid can be exposed and bonded until the grid has been completely attached to the component. Subsequently, the adhesive is cured in accordance with manufacturers' specifications.

  The grid of the strain gauge shown in Fig 8.1-1b can also be transferred by applying a technique, called flame-spraying (Fig 8.1-2). The adhesive for these so-called "window gauges" consists of aluminium or zinc oxide. Aluminium or zinc oxide bars are held in the flame of an acetylene oxygen burner. At the bar end, the oxide material melts, and the liquified small drops are sprayed on to the appropriate surface by means of compressed air. One of the distinct advantages of the flame-spraying technique is that high temperature

cures are not required in order to achieve high temperature operating capability. This feature is especially significant when bonding gauges to large structures that cannot easily be brought to cure temperature.

- An important advance towards a simplification of attachment is represented by the weldable strain gauges (Fig 8.1-1d). In the case of these gauges the measuring grid is bonded to a thin steel plate during the manufacturing process. The measurement elements thus obtained are attached to the component by spot-welding (Fig 8.1-3). Caution should be exercised in the use of weldable gauges on titanium structures because of the effect on the fatigue life of the structure (Ref (96)).

8.1.2 Influences of lead-wire resistances

At room temperature the lead resistance can usually be neglected or corrected for since it does not change very much (copper leads, constant temperature). If, however, strain gauges are used at extreme temperatures, the leads used should consist of the same high-temperature alloys used for the measuring grids in order to prevent thermal stresses and because of the better resistance to corrosion. In view of the high specific resistance of these materials (Ni Cr strips), the lead resistance cannot be neglected. Furthermore, local temperature variations can occur along the leads so that special attention must be paid to the influence of the lead resistance on zero drift and sensitivity of the bridge (refer to Section 3.3).

If twisted leads or closely spaced parallel leads of the same length are used, there is no zero drift and the apparent strains (refer Section 8.1.3) become nil. In general it is impossible to perform a correction with regard to sensitivity under the marginal conditions specified above. In practice, therefore, lead influences should be kept as small as possible.

8.1.3 Apparent strains

Changes in the resistance of a strain gauge which are not caused by strains related to stresses caused by mechanical loads lead to false indications called apparent strains. Causes for such changes in resistance are:

Temperature effects

- changes in the wire resistance as a result of temperature variations;
- strains as a result of different linear expansion coefficients of measuring wire and component
- changes in the insulation resistance.

Time effects

- corrosion of the measuring grid
- structural changes
- creep effects

Mathematical coverage of the temperature effects mentioned is provided in Section 2.2.6, equation (2.2-16). This equation shows that the strain gauge quality is mainly determined by the expression

$$\frac{1}{K}\,\alpha_R + \alpha_B - \alpha_{DMS}$$

The parameters α_R and α_{DMS} for the measuring grid materials used are summarized in Table 2.2-1.

The table shows that temperature coefficients α_R of 50µm/m/K are easily reached by various alloys. In order to be able to measure strains of, for instance, 1000 µm/m with an almost 100% accuracy, the temperature must be constant even in fractions of degrees (Figs 8.1-4 to 6). This requirement is seldom met in practice. Therefore compensation procedures, as described in Section 3.3.1.1, must be applied. In principle these procedures offset at least the disturbing thermal portion. But these procedures, making use of circuit possibilities, are only fully effective in the case of strain measurements at constant temperatures since in this case the bridge can be balanced at the appropriate test temperature.

In the case of strain measurements at variable temperatures balancing is only possible at room temperature. These so-called thermal stress measurements are difficult to achieve even with current techniques and if these methods are applied, concessions must be made in measuring accuracy expected since the individual strain gauges interconnected in the bridge will always have a different resistance temperature coefficient α_R. The magnitude of the resultant false signal, which is also called an effect of residual temperature, can be gathered from Figs 8.1-4 to 8.1-6 for the three most important measuring grid materials Pt W, Nichrome V and modified Karma.

Too low and inconstant insulation resistances, caused by humidity or temperature variations, also result in apparent strains. The insulation resistance R_{is} acts as a shunt resistance relative to the strain gauge (Fig 8.1-7).

If the insulation resistance R_{is} decreases by $-\Delta R_{is}$, the overall resistance change is

$$\frac{R(R_{is} - \Delta R_{is})}{R + R_{is} - \Delta R_{is}} - \frac{R \cdot R_{is}}{R+R_{is}} \approx - \frac{R\Delta R_{is}}{R+R_{is}}$$

The relative resistance change is then

$$\frac{-R\Delta R_{is}}{R+R_{is}} \Big/ \frac{R \cdot R_{is}}{R+R_{is}} = - \frac{\Delta R_{is}}{R_{is}}$$

The following equation results for the apparent strain:

$$\varepsilon_s = - \frac{1}{k} \frac{\Delta R_{is}}{R_{is}} \qquad (8.1\text{-}1)$$

Fig 8.1-8 shows the change of the insulation resistance of ceramic adhesives. Their upper temperature limit is a result of ionization processes and depends on the purity grade of the bonding agent. Measurements up to approximately 1000K can be performed using strain gauges bonded with ceramic adhesives. In this case, apparent strain due to changes in the insulation resistance are hardly existent.

In the case of high temperatures, the measuring grid corrosion is a source of time-dependent apparent strains. On the one hand, the electrical resistance is continuously increased by the reduction of the conductor cross-section, i.e. a gradually increasing strain is simulated. On the other hand it is possible that the alloy composition and thus the specific resistance is changed by selective corrosion owing to different corrosion rates of the individual alloy components.

The corrosion is not only a result of the air oxygen and other gaseous corrosive materials but can to a large extent also be attributed to the adhesives. Especially before setting the latter can be extremely corrosive. The corrosion rate is also influenced by varying humidity at temperatures below 370K (some adhesives are hygroscopic).

As a result of plastic deformation by stretching or rolling the metallurgic condition of the measuring grid wires and foils is not stable at high temperatures. It is true that it seems to be "frozen" at low temperatures, but it leads to noticeable drift phenomena at higher temperatures.

In addition, quite a number of the measuring grid alloys, such as the Ni-Cr alloys, show structural changes in certain temperature ranges. These changes within the elementary cells of the crystals, which occur when the characteristic temperature ranges are exceeded, result in considerable changes in the wire resistance. These, in turn, lead to marked drift phenomena. The overall temperature range of a strain gauge alloy is thus limited mainly by corrosion and structural changes. The drift rate for Karma, Nichrome V and Pt W alloys, expressed in µm/m/min, is plotted as a function of the temperature in Fig 8.1-9. The relevant limit temperatures can be taken from this figure.

In the cryogenic temperature range down to 20K, drift phenomena of the type mentioned above have not been observed on the alloy "modified Karma" which is commonly used for this temperature range.

In the case of loaded strain gauges, another cause for time-dependent apparent strains can be mentioned, the so-called "creeping". Creeping is a gradual yielding of adhesive and supporting material under the restoring force of the stretched measuring wire. In the case of high temperature measurements with ceramic adhesives and measurements in the cryogenic temperature range with organic adhesives (epoxy resin) this effect is hardly noticeable or is at least unimportant in comparison with the other time effects.

Due to the non-disappearing mean modulus of elasticity of the strain gauge components, the application of a strain gauge leads to a local stiffening of the component and thus to a disturbance of the stress behaviour in the area of the strain gauge measuring points.

In the case of different linear longitudinal expansion coefficients of the component and the strain gauge a deformation of the component, similar to a bi-metal effect, might also occur and result in further considerable errors in measurement (Ref (B11)). The effects mentioned are, of course, particularly obvious in the case of thin components ($\leq$ 1 mm). In the high-temperature range, with the use of ceramic adhesives or metal supporting materials, but also at cryogenic temperatures they should not be disregarded.

The magnitude of the individual apparent strains can be assessed for the marginal test conditions only by the user himself. The values given in Tables 8.1-1 and 8.1-2 can be taken as a calculation basis.

8.1.4 Dependence of the gauge factor k on temperature

The gauge (strain sensitivity) factor k of a strain gauge is a function of the temperature (see Section 2.2.4.1, equation (2.2-6)).

The temperature coefficient of k can be calculated from this equation.

It has not yet been definitely determined which term of the sum causes the gauge factor change. Ref (43) assumes that the quantity $\frac{1}{\rho}\frac{\partial \rho}{\partial \varepsilon}$ is practically independent of the temperature, so that $\frac{1}{k}\frac{\partial k}{\partial T}$ is determined only by the temperature behaviour of the transverse contraction ration μ; whereas Ref (44) is of the opinion that $\frac{1}{k}\frac{\partial k}{\partial T}$ is determined by the first term of the sum.

Table 8.1-1: Linear expansion coefficient α of various strain gauge grid materials and component materials between room temperature 293K and temperature according to Ref (43), (45). For further information see Ref (B9).

Temperature	Constantan	Nichrome V	Karma	Nimonic 90	X12 CrNi 188	AlZnMg1
K	$<\alpha> 10^{6}/K$					
20		9	9.5		-	16.9
100	-	11.3	11.9	-	-	21.7
293	-	-	-	-	-	-
373	15.2	13.4	13.6	11.3	17.7	-
473	14.9	13.2	13.4	12.4	18.0	-
573	15.0	13.3	13.4	13.1	18.2	-
673	15.2	13.5	13.6	13.6	18.6	-
773	-	13.9	13.9	14.1	19.0	-
873	-	-	-	14.7	19.2	-
973	-	-	-	15.2	-	-
1073	-	-	-	16.0	-	-

According to Section 2.2.5.1 changes in the material properties of wire and supporting material must also be expected.

Fig 8.1-10 shows the temperature dependence of k for four alloys. It can be seen that substantial changes of k must be expected at higher temperatures. However, it can be assumed that the gauge factor has good repeatability.

Fig 8.1-11 shows the gauge factor charge of modified Karma in the cryogenic temperature range. The zone of spread of the gauge factor change for tensile and compressive stresses is also indicated. The gauge factor change is repeatable in this range as well.

8.1.5 Hysteresis: maximum static strain

In the high-temperature range, a hysteresis exceeding the normal limits can be observed only in the case of weldable strain gauges with metal supporting material. Fig 8.1-12 shows the maximum deviation for a weldable strain gauge at load cycles of 1000 µm/m referenced to the unloaded component, at a constant test temperature. It can be seen that a permanent hysteresis has to be expected for weldable strain gauges. This permanent hysteresis can be caused by a plastic deformation of the welding points, as described in Section 2.2.5.1.

According to VDE/VDI 2635 (Ref (28)), by definition the maximum permissible static strain is reached when there is a 10% deviation between indicated and actual strain. In the case of welded strain gauges and strain gauges attached by means of ceramic adhesives the maximum permissible strains are about 5000 µm/m. In the cryogenic range, at 20K, measurements with strains of 3500 µm/m were successfully completed (Ref (45)).

Table 8.1-2: Linear expansion coefficient α and modulus of elasticity of various adhesives according to Ref (43) and (45) between room temperature 293K and temperature T.

Adhesive	Al-Pl		Al-PBX		Rokide A		Epoxy resin Av138+HV998	
Temperature K	<α> 10^{-6}/K	<E> N/mm²	<α> 10^{-6}/K	<E> N/mm²	<α> 10^{-6}/K	<E> N/mm²	<α> 10^{-6}/K	<E> N/mm²
20	-	-	-	-	-	-	30	6,000
100	-	-	-	-	-	-	36.4	5,800
293	-	-	-	-	-	-	-	3,100
373	7.4	10,000	10.4	5,500	-	43,000	-	-
473	8.8	9,800	11.5	5,500	-	-	-	-
573	9.8	9,300	12.3	5,500	5.3	-	-	-
673	10.8	9,000	13.0	5,500	-	-	-	-
773	12.3	9,000	13.9	5,800	-	-	-	-
873	18.0	14,000	15.7	11,000	6.6	-	-	-
973	16.5	12,000	15.2	6,500	-	-	-	-
1073	15.0	1,000	15.0	3,000	7.0	-	-	-

8.1.6 Summary of the most important temperature characteristics

In order to be able to assess the limits and possibilities of static strains at extreme temperatures, the most important influence factors are summarized in Table 8.1-3. But this data can only be regarded as nominal values since all characteristics can be influenced by the mechanical background of the grid, i.e. by the degree of cold working.

The strain gauge characteristics are set to certain values by the manufacturer by cold working and subsequent artificial aging at defined temperatures. The different statements often found in the referenced literature at least do not discount the suspicion that the "cultivation" of characteristics can hardly be reproduced to an adequate degree.

8.2 Use under hydrostatic pressure

The problems involved in using strain gauges under hydrostatic pressure are not so much related to the technical configuration of the strain gauges as to the field of application techniques. Bubble-free layers of adhesive are indispensable. It is recommended that a substantially higher contact pressure than specified by the strain gauge manufacturer for normal applications be used.

Flat grid strain gauges show a linear-dependent zero point indication in the order of 5 to 10 µm/m for each 1000 N/cm² in the range up to 5000 N/cm².

All attempts to clearly determine the behaviour of strain gauges under very high pressures have failed. But it can be said that the influences are in any case unimportant, if not negligible. Measurements by Ref (46) show a certain dependence of the gauge factor on the pressure applied. According to Ref (46), the gauge factor changes by approx 0.4% per 10000 N/cm².

Reference: (46).

8.3 Use under nuclear radiation

Among the measuring grid materials used for strain gauges, only the Constantan and Pt W alloys have proved to be stable under nuclear radiation. Nichrome V and semi-conductor materials are subject to major resistance changes. Phenolic resin has the best resistance of all plastics of the measuring grid supporting materials and adhesives. In addition, the ceramic bonding agent based on aluminium oxide (flame spraying, see Section 8.1.1 and Fig 8.1-2) has also stood the test. More detailed information cannot be given since the measured results are influenced by the dose of radiation as well as by the radiation type. It is recommended that this information be obtained from test measurements under actual operating conditions.

Reference: (47).

Table 8.1-3: Characteristics of typical strain gauge systems at extreme temperatures

Grid material Supporting material Application technique	Modified Karma Epoxy glass fibre Bonding with e.g. AV 138 + HV 998	Nichrome V Steel Weldable	Pt W Free grid Flame spraying
Application time	two hours		
Recommended temperature range 293 K to	20 K	670 K	770 K
Apparent strain in µm/m (k=2) for steel 1.49.74.9 aluminium AlZnMg1	- ≙60	460 -	62100 -
Zero point uncertainty in µm/m (k=2) for measurements below variable temperature	≤ ± 100	≤ ± 75	≤ ± 250
Zero point drift in µm/m (k=2) for a measuring time of 60 min	≤ ± 10		
Creeping in µm/m (k=2) for a measuring time of 60 min.	≤ ± 10		
Linearity and hysteresis for a component strain of: ε_{max} = 1000 µm/m in µm/m (k=2) 1st loading 2nd loading ε_{max} = 3000 µm/m in µm/m (k=2) 1st loading	≤ ±40 (permanent)	≤ +70 ≤ +25 (permanent)	
Gauge factor change and spread in % between 293 K and the recommended temperature range	+3.5 ±0.5	-8.5 ±2.5	-14 ±2.5

8.4 Use in magnetic fields

Strain gauges with constantan measuring grids have proved useful in extremely strong magnetic fields. Ref (51) contains a report about studies on strain gauges in the constant magnetic field of a proton accelerator with flux densities of up to 20 kilogauss/cm^2. No effects of the magnetic field were observed on strain gauges with constantan and Pt W measuring grids. Strain gauges with isoelastic measuring grids, on the contrary, showed considerable zero drift displacements. Therefore they must not be used in magnetic fields.

Caution is also required in the case of alternating magnetic fields since inductive voltages might occur in the strain gauge.

Reference: (51).

8.5 Use of strain gauges under vacuum conditions

The problems encountered in using strain gauges under vacuum conditions are primarily related to the field of application techniques.

In order to prevent air bubbles in the adhesive layer the contact pressure selected for bonding should be higher than for applications under normal conditions since air bubbles might lead to destruction of the measuring point. Care should also be taken in selecting the necessary protective materials. A glass fibre mat impregnated with epoxy resin (contact pressure approx 10 N/cm^2) has proved quite useful for applications up to about 10^{-7} torr. (Ref (45)).

The use of strain gauges under maximum vacuum conditions ($<10^{-7}$ torr) creates many more problems since the degassing rates (torr litre/sec cm^2) of the plastic materials used for the strain gauge measuring point are very high. This might lead to problems with respect to the final pressure required. Ref (49) contains some data on the degassing rates of various plastic materials.

References for Chapter 8:

(B10), (B11), (4), (8), (43), (44), (45), (46), (47), (49), (50), (51), (60), (63), (65), (72), (78), (79), (80), (91), (92), (93), (95), (96), (97), (98), (99).

9.0 INSTRUMENTATION OF TWO VAK 191 B AIRCRAFT WITH FLIGHT LOAD MEASURING SYSTEMS

The preceding chapters have shown the diversity of the spectrum of factors which must be taken into consideration when using strain gauges. The interaction of all factors involved contributes also to a large extent to the success of a measurement. It is very difficult to describe this aspect in the abstract. It seems to be useful, therefore, to conclude with an example.

For this purpose, the instrumentation of the VAK 191 B VTOL aircraft built by VFW-Fokker with strain gauge systems is described in some detail.

From 1968 to 1970 the VAK 191 B prototypes were manufactured. Two aircraft, V1 and V2, were to be provided with flight load measuring systems during manufacture (see Section 7.14).

The following measuring sections were planned for each aircraft:

- 4 measuring sections in the wing (2 port and 2 starboard)
- 2 measuring sections in the horizontal tail (1 port and 1 starboard)
- 1 measuring section in the vertical tail
- 1 measuring section in the rear fuselage
- a number of measuring points on the landing gears and flight controls.

A requirement of approximately 2000 single strain gauges (or correspondingly smaller quantities of biaxial rosettes), including certain reserve quantities, was estimated for the two aircraft.

9.1 Selection of components

In this connection, the following constructive and application-specific aspects had to be taken into consideration:

- Wing design:

  Torsion box with 4 main and intermediate spars, upper and lower skins riveted, all components milled, very thin wing profile.

- Horizontal tail design:

  Torsion box with 4 spars and riveted skin panels, centre box (within the fuselage) in two-spar construction, milled from block.

- Vertical tail design:

  Torsion box with 3 spars and riveted skin panels.

- Operating speeds:

  Hover flight up to high subsonic speed at high altitudes. During hovering, hot bleed air was tapped from the engines and led through the wing box to the wing tip via pipes for control purposes. The temperatures in the vicinity of the bleed lines reached approximately 470K, but the hovering time was limited to a few minutes.

The basic characteristics of strain gauge and adhesives needed were determined from the following conditions:

- The design data and the statements in the NACA Report (Ref (38)) led to the conclusion that up to 6 full-bridges had to be interconnected. This resulted in the strain gauge resistance of R = 600Ω (it was necessary that the total resistance of the interconnected bridges was not too small).

- Since measurements in the aircraft were to be carried out on aluminium components only the temperature coefficient was fixed at

  $\alpha_t \approx 23$ µm/m/K

- A measuring grid length of 6 mm was selected but on account of production problems encountered by the manufacturer a strain gauge with a 7 mm measuring grid length was used.

- According to specifications, a maximum temperature of 470K was expected but no measurements were planned during hovering (it is only during hovering that this high temperature is reached). From this it followed that all components had to withstand these temperatures but that it was not absolutely necessary for strain gauge and adhesive to be capable of performing at these temperatures. Nevertheless, the temperature limit of the strain gauge selected amounted to about 500K for static measurements. It was the HBM type 7/600 LB 13, a metal foil strain gauge with constantan measuring grid and phenolic resin supporting material. It was not intended to use $0^{\circ}/90^{\circ}$ or $\pm 45^{\circ}$ rosettes; all configurations required were to be built up from single strain gauges.

- The adhesive selected was the epoxy resin system AV138 + HV998 (refer to Section 6.4.1.3). On account of the simple handling (cold setting) and its fairly good properties this adhesive promised the most favourable results with respect to temperature resistance and installation effort.

- The solder support points to be used with the strain gauge adhesive were also purchased from HBM, but partly also from BUDD. A solder with a melting point of 520K was selected for the soldering joints.

- Teflon-insulated 3 or 4-core shielded cables (cross-section 3 or 4 x AWG26 ~ 0.14 mm^2) with silver-plated copper conductors were selected as connecting cables.

- For protective purposes, the silicone resin Elastosil 33 with the primer FD manufactured by Wacker was chosen.

- Auxiliary material such as emery paper and cloth with different grain sizes, MEK, various tools etc was also provided.

All the components had been in use at VFW-Fokker for an extended period so that an excellent team which was fully familiar with the installation technique was available.

9.2 Installation technique

The installation technique will be described by taking measuring section 1 (Fig 9.2-1), the inboard section on the port wing, as an example.

9.2.1 Location of strain gauges

All strain gauges, their cabling and their protective covers had to be installed in the wing box before one of the skins (in this case the upper skin) was riveted, i.e. before the torsion box was closed.

All spars were designed as U sections, but the strain gauges for the bending bridges could not be placed on the U section legs since, as far as possible, damage during riveting had to be avoided. Furthermore, in the case of strain gauges being bonded between rivets, the strain gauge is mostly positioned relatively close to the next rivet. This can increase unreliability since practically no rivet can be made water-tight.

For the reasons mentioned above, the strain gauges for the bending bridges were thus positioned on the spar webs, relatively far away from the rivet holes and the riveting tools. The decrease in sensitivity, as compared with other arrangements, was accepted.

The shearing force bridges were placed on the spar webs between the strain gauges of the bending bridges.

The torsion bridges were attached to the inner surfaces of the skins, one torsion bridge between two spars.

The exact position of the strain gauges on the spars and skin panels is shown in Figs 9.2-2 to 9.2-8.

It should be noted that all bridges were duplicated in order to provide for an adequate selection with respect to the interconnection of the bridges according to Ref (38). Furthermore, some reserve bridges had to be available.

9.2.2 Installation of the strain gauge bridges

For reasons of schedule, manufacture had to proceed very quickly. This, together with the fact that all strain gauges on the spar web were located quite close to each other, necessitated the following installation procedure:

- Full-scale drawings of the measuring position were prepared on the basis of drafts or the object itself;
- All strain gauges and soldering support points planned for the respective position, including the appropriate measuring point numbers, were included in these drawings. The connecting wires for the individual bridges were also drawn to scale in the applicable colours;
- Self-adherent tape (sufficiently wide Scotchtape) was then stretched out over the drawings with the adherent side facing upwards. The completely prepared strain gauges and soldering support points were then attached to it in accordance with the drawings.
- Parallel to these operations, the bonding surface of the object was prepared for the bonding process. In addition, the rubber cushions for applying pressure on the strain gauges as well as the clamping devices were adapted to the area concerned.
- After completion of the preparatory work described above, the adhesive components could now be weighed, mixed and applied to the strain gauges. The tape with the strain gauges and soldering support points, all of them coated with adhesive, was placed on the appropriate surface of the structure and fixed by means of clamping devices. The clamping devices were removed after 8 hours at the earliest but in most cases not before the next day in order to ensure proper setting of the adhesive.
- It was possible to prepare the wiring on the basis of the full-scale drawing. The individual wires were cut to the correct length, stripped, tin-plated and then bent to the proper shape in accordance with the drawing.
- After removal of the clamping devices, the adhesive tape and excess adhesive, all strain gauges were individually checked for resistance and insulation resistance. Subsequently, the strain gauge lugs were soldered and the resistance measurements repeated. Afterwards the completely prepared connecting wires were soldered to form the full-bridges, and the measuring cable was connected. The unbalance and insulation were measured.
- When all the measured values were within the permissible tolerance range, the entire measuring points were thoroughly cleaned, degreased and coated with FD primer. When the primer had dried, the silicone resin was applied.

The bridges were considered acceptable unless the unbalance exceeded a value of approximately ±1000 με. In a few exceptional cases, ±1500 με had to be accepted as well for reasons of time. A minimum insulation resistance value of 1000 MΩ was required; but generally the insulation resistance was about 10^5 MΩ.

The values measured after the individual operations were entered on forms specially developed for this purpose in order to permit the detection of changes at any time.

After completion of the bridges the torsion box was closed and riveted. During the subsequent control measurements, only one of approximately 300 full-bridges installed in the two aircraft showed a major unbalance indicating a defect in one of the strain gauges or in the wiring.

9.2.3 Installation time requirements

Although the team was fully familiar with the installation technique from the very beginning, individual steps of the procedure could continuously be improved and refined in the course of work. When installation work was commenced, 13 working hours were required for each full-bridge. During the final phase the same operation did not take more than 8 hours.

9.3 Calibration

After completion of the strain gauge system, the aircraft was finally assembled and equipped. Calibration work was not performed until approximately two years after installation of the strain gauge bridges, in June 1972.

The check measurements prior to calibration revealed only slight changes in the measured values. Most of them, however, could be attributed to reasons connected with the assembly techniques used. The output signals picked up during calibration were also acceptable. There were no significant non-linearities or zero drifts so

that, with the exception of the bridge already mentioned, all bridges were available for interconnection.

The calibration technique will not be dealt with in this section. It is described in some detail in Section 7.14.

The interconnection of measuring section 1 will be described as an example.

Using a large-capacity computer system, the best combinations among the existing bridges were selected by means of a computer program developed by VFW-Fokker.

- For the shearing force measuring system, a shearing force bridge of spar 1 was used as the main bridge. The shearing force bridges of spars 3 and 4 which were weakened as specified in the program [illegible] were added. In order to keep the signal undisturbed by other influences, a bending bridge of spar 2 and a torsion measuring bridge of spar 1 were also connected.

- The measuring system for bending moments comprised four bridges. The main bridge was a bending bridge of spar 3. Added to this were two shearing force bridges of spars 1 and 3 as well as one torsion measuring bridge of spar 1.

- The torsion measuring system had to be composed of six bridges. A bending bridge of spar 2 proved to be the most favourable solution for the main bridge. The arrangement was completed by a shearing force bridge of spar 1, a bending bridge of spar 4 and three torsion bridges of spars 2, 3 and 4.

The interconnection of all other measuring sections was similar.

From the 24 bridges installed, 15 were selected for combinations, so that 9 bridges were still available if any of the bridges should fail. However, it must be expected that much more complicated interconnections could be required in the case of a new combination.

9.4 Results

Flight tests were started subsequent to calibration. All measuring points connected to the measuring systems provided satisfactory measured values.

A control measurement of zero drifts and insulation resistances at the time of flight testing resumption in July 1974 did not reveal any important changes in the measured values for the measuring points checked.

REFERENCES

Books

(B1) Hütte I, Theoretische Grundlagen. 28. Auflage, Akademischer Verein Hütte, e.V., Verlag Wilhelm Ernst & Sohn, Berlin 1955.

(B2) Dubbel, Taschenbuch fur den Maschinenbau. Sass, F. und Bouchet, Ch. Springer Verlag Berlin, Göttingen, Heidelberg, 1958.

(B3) Neubert, H K P, "Strain Gauge Kinds and Uses", Macmillan, London, Melbourne, Toronto, 1967.

(B4) Rohrbach, Chr., Handbuch für elektrisches Messen mechanischer Größen VDI-Verlag, Düsseldorf, 1967.

(B5) Merz, Ludwig, Grundkurs der Meßtechnik, Teil II, Das elektrische Messen nichtelektrischer Größen. Verlag R. Oldenbourg München und Wien.

(B6) Haug, Albert, Elektronisches Messen mechanischer Größen. C.Hanser-Verlag München 1969.

(B7) Szabo, Istvan, Einführung in die Technische Mechanik. Springer-Verlag Berlin, Göttingen, Heidelberg, 1959.

(B8) Drever, Georg, Drillinder, Egon, Festigkeitslehre und Elastizitätslehre. VEB-Fachbuchverlag, Leipzig 1964.

(B9) Kohlrausch F., Praktische Physik, Band III-Tafeln. Herausgeber Günter Lautz, Rolf Taubert, Verlag B. G. Teubner, Stuttgart.

(B10) Flügge, S., Handbuch der Physik, Band 6, Elastizität und Plastizitat. Springer-Verlag 1958.

(B11) Analysis of bi-metal thermostats. Optical Soc. Amer. and Rev. Sci. Instruments 11 (1925), Nr 3, S 233

(B12) Zienkiewicz, Holister, Stress Analysis, Kap 11. Verlag J Wiley 1965.

(B13) Timoshenko S and Goodier J N: Theory of Elasticity, McGraw-Hill Book Company Inc, New York.

(B14) Dally I and Riley F: Experimental Stress Analysis, McGraw-Hill Book Company Inc, New York

(B15) Perry C C and Lissner H R: The Strain Gauge Primer, McGraw-Hill Book Company Inc, New York.

Reports and publications

(1) Tadeusz M. Drzewiecki, Fluidic Strain Gauge Concepts. HDL-TR-1571, Harry Diamond Laboratories, Washington DC 20438.

(2) Rohrbach, Chr., Czaika, N., Deutung des Mechanismus des Dehmungsceßstreifens und seiner wichtigsten Eigenschaften an Hand eines Modells. Materialprüfung, Bd.1, 1959, Heft 4, Seite 121-131.

(3) Hönisch G, Der Einfluß der Dehnüngsubertragung zwischen Bauteil und Meßdraht auf den k-Faktor von Dehnungsmeßstreifen. Maschinenbautechnik, Bd 15, 1966 Heft 2 und 3, Seite 61-68, 133-136.

(4) MM. Lochham/München, Optimale elektrische Speisung von Dehnungsmeßstreifen. Tech note TN-127.

(5) Nagy, Istvan, Betrachtungen über die Meßunsicherheit bei det Bestimmung des ebenen Verzerrungszustandes mittels DMS-Rosetten. HBM, Meßtechnische Briefe, 1, 1973.

(6) Birkenfeld, Willi, Die praktische Anwendung von Membran-rosetten. HBM, Darmstadt, Meßtechnische Briefe, 2, 1967.

(7) Hoffmann, Karl, Hinweise zur Auswahl von Dehnungsmeßstreifen und DMS-Klebstoffen. HBM, Darmstadt, Meßtechnische Briefe, 1, 1965.

(8) Keil, Stefar, Analyse ebener Spannungszustände mit Hilfe von Dehnunemeßstreifen. HBM, Darmstadt, Meßtechnische Briefe, 1 und 2, 1972.

(9) Birkenfeld, Willi, Messung von Eigenspannungen mittels Dehnungsmeßstreifen. HBM, Darmstadt, Meßtechnische Briefe, 3, 1968.

(10) Tschierschke, Peter, Messung der behinderten Wärmedehnung bei Temperaturen bis zu 650°C. HBM, Darmstadt, Meßtechnische Briefe, 3, 1968.

(11) Kautsch, Rudi, Einfacher Dehnungstransformator für die Messung großer Dehnungen. HBM, Darmstadt, Meßtechnische Briefe, 3, 1968.

(12) HBM, Darmstadt, Grafisches Auswerteverfahren von Messungen mit rechtwinkligen 0°/45°/90° - Rosetten. Meßtechnische Briefe, 1, 1967.

(13) Birdenfeld, Willi, Grafisches Auswerteverfahren von Messungen mit gleichwinkligen 0°/120°/240° - DMS-Rosetten. HBM, Darmstadt, Meßtechnische Briefe, 1, 1968.

(14) Grünenberg, Reginald E, Messung von Materialermüdung mit Hilfe von Widerstandssensoren. MM, Lochham/München, Juni 1968.

(15) Narendra J. Sheth, Stephen L Bussa, Nelson M Mercer, Determination of Accumulated Structural Loads from S/N Gauge Resistance Measurements. International Automotive Engineering Congress, Detroit, Michigan, Jan 8-12 1973, 730139.

(16) Perry C C, Plane-shear Measurement with Strain Gauge Vishay Micro-Measurements, Tech note TN131, May 1969.

(17) MM, Lochham/München, Design considerations for diaphragm pressure transducers. Tech note TN129, August 1968.

(18) MM, Lochham/München, Errors due to transverse sensitivity in strain gauges. Tech Note TN137.

(19) S/N Fatigue Life Gauge, Vishay Micro-Measurements, Product Bulletin PB 103.

(20) Dorsey J, Engineering Concepts in Fatigue Life Gauge Use, Vishay Micro-Measurements, Application Note AN127.

(21) Glaskovskii B A, Strain and Deformation Measurements, certain problems of the calculation and selection of the carrier frequency in pulse strain gauge, Measurement Techniques, 1968, H12, A.1643-1645.

(22) Reznicek Ivan, Halbleiterdehnmeßsteifen in der Praxis Der Elektroniker, 6, 192, S.261-269.

(23) Becker, Herbert, Die Gleichstrombrücke als Meßwertumformer, ATM, Blatt J910 Teil I, J910-6, Teil II, J910-7, Teil III, J910-8, 1966.

(24) Siebert, Joachim, Widerstandsmeßbrücke mit schnellem elektronischen Selbstabgleich, ATM, J 913-2, 1972.

(25) Grave, H F, Zur Dynamischen Messung nichtelektrischer Größen, Elektro-Anzeigen, 26. Jg. 1973, Teil I, Nr. 6, S. 96-99, Teil II, Nr 7, S.127-129.

(26) ASTM Designation: E251-67 (8.9.1967) Standard Method of Test for Performance Characteristics of Bonded Resistance Strain Gauges in 1968 Book of ASTM Standards, Part 31.

(27) Andreae, Götz, Zur Genauigkeit von Dehnungsmeßstreifen, Materialprüfung 12, 1970, Nr 3. S. 87-92.

(28) VDE/VDI 2635 (Entwurf), Dehnungsmeßstreifen mit metallischem Mesgitter, Kenngrößen und Prüfbedingungen, März 1972

(29) Rohrbach, Chr, Czaika, N, Das Kriechen von Dehnungsmerstreifen als rheologisches Problem, Materialprüfung 2 (1960), Nr 3, S 98-105.

(30) Rohrbach, Chr, Czaika N, Über das Dauerschwingverhalten von Dehnungsmerstreifen Materialprüfung 3 (1961), Nr 4, S. 125-136.

(31) National Aerospace Standard (NAS), Strain Gauges, Bonded Resistance, NAS 942 Aerospace Industries Association of America, Inc.

(32) S/N Fatigue Life Gauges, Applications/Manual, 2nd edition April 1969, Vishay Micromeasurements

(33) Errors due to misalignment of strain gauges, MM, TN-138.

(34) Wilson J D, The Heating Effect of Strain Gauges on Araldite Models, Strain 8, 1972, Apr, S.74-75.

(35) Kowalski H C, Eine neue Methode zur Bestimmung von Dauerermüdungsbrüchen, Zwei-Element-Ermüdungs-Streifen, ISA Trarsactions, 11, 1972, 4, S.358-368

(61) Bretsch J, Halbleiter-Dehnungsmeßsteifen, ATM, J135, 2974, Teil I:J 135-28, S 57-60, Teil II:J 135-29, S 71-74.

(62) Irrgang B, Mechanoelektrisch e Halbleiterwandler, msr 15, 1972, H 8, S 283-287.

(63) Wnuk St P, Progress in High Temperature and Radiation Resistant Strain Gauge Development, Experimental Mechanics 5, 1965, 5, S 27A-33A.

(64) Onnen F H, Kriecherscheinungen bei Dehnungsmeßstreifen als Folge der mechanischen Spannungen in der Klebstoffschicht, Feinwerktechnik 72, 1968, 9, S 409-413.

(65) Wolf H, Schlichtung, H.D, Zur Messung statischer Beanspruchungen großer Bauteile bei hohen Temperaturen mit Dehnungsmeßstreifen, ATM, V132-23, 1967, S 261-266.

(66) K-Faktor und Dauerschwingverhalten von 90°- Rosetten, MM, TN-D 01.

(67) Dauerschwingverhalten von Dehnungsmeßstreifen, MM, TN-130.

(68) Andreae G, Über das Verhalten von Dehnungsmeßstreifen bei großen Dehnungen, Meterialprüfung 13 (1971), Nr 4, S 117-123.

(69) Dehnungsmeßstreifen, Schaltungsmethodik mit mehreren DMS, Elektronik 1967, Teil 1, Arbeitsblatt 19, H. 9, Teil 2, Arbeitsblatt 19, H.10.

(70) Sullivan T L, Chamis C C, Some Important Aspects in Testing High-Modulus Fibre Composite Tubes Designed for Multiaxial Loading, NASA TM 58045, 1972.

(71) Anzalone B, Verständnis und Anwendung von Dehnungsmeßstreifen, Instruments and Control Systems I, Teil I:CS 45, 1972, 12, S 55-56 (Meßfühler) Teil II:CS 46, 1973, 1, S 60-62 (Träger), Teil III:CS 46, 1973, 2, S 70-71 (Leitungscrähte)

(72) Bertode R, High-Temperature High-Elongation Resistance Strain Gauges, Journal of Strain Analysis, Vol 4, Nr 3, 1969, S 228-235.

(73) Chernyshev V M, Methods of Measuring Non-linear Deformations, Ind. Laboratory 37, 1971, Nr 3, S 435-437.

(74) Hörnig, R, Ausmessung det Dehnungsverteilung in den Gebieter örtlich stark veränderlichen Spannungen mit Ketten-Dehnmeßstreifen, MTZ 27/10, S 420-421.

(75) Hooper J A, The Theory and Design of Photoelastic Load Gauges Incoporating Glass Element Transducers, Int. Journal of Rock Mechanics and Mining Sciences 9, 1972, 3, S 363-401.

(76) Kharitonov G M, Khitrova O M, Errors due to Non-stationary Thermal Conditions in the Measurement of Static Strain Semiconductor Resistance Strain Gauges. Teplovye Napriazheniia v Elementakh Konstruksii, 1971, 11, S 204-208.

(77) Krempel E, Evaluation of High-Elongation Foil Strain Gauges for Measuring Cyclic Plastic Strain, Experimental Mechanics 8, 1968,8, S 19-26.

(78) Lemcoe M M, Errors in High-Temperature Strain Measurements, Experimental Mechanics 8, 1968, 2, S 19N-26N.

(79) Lemon T L H, Measurements of Static Strain on Titanium under Rapid Heating, Strain 7, 1971, Apr, S 66-73.

(80) Lemcoe M M, Accuracy of Strain Measurements at Elevated Temperatures with Electric Resistance Strain Gauges, ASTM STP, 1970, 467, S 12-34.

(81) Mason W P, Forst J J, Tornillo L M, Recent Developments in Semiconductor Strain Transducers, ISA Preprint Nr: 15-NY60, S 1-8, Instrument Automation Conference 1960.

(82) Millward H R, Higginson F D, A Printed Technique for Use with Strain Gauge Rosettes, Strain 4, 1965, Oct, S 33-34.

(83) Onnen R, Fritz H, Über die Bestimmung der mechanischen Spannungen bei Dehnungsmeßstreifen und ihren Einfluß auf die Meßgenauigkeit, Feinwerktechnik, 70, 1966, 10, S 466-474.

(84) Palfreyman R D, Trugman L A, Semiconductor Strain Gauge Application for Flight Control Systems, IEEE Transactions on Industrial Electronics and Control Instrumentation 19, 1972, May, S 56-61.

(85) Peiter A, Vergleichbare Röntgen [illegible] zur Eigenspannungmessung, Schweizer Archiv 37, 1971, Dez S [illegible]

(86) Akhemtzyanov M K, Strain Measurem[illegible] [illegible]terferometric Strain Gauges, Industrial Laboratory 35, 1969, [illegible]5.

(87) Hehn K H, Schulz W, Brückenschaltungen [illegible] unmittelbaren Messung der Material-spannung HBM-MTB 2/66.

(88) Kautsch R, Dehungstranformatoren bei a[illegible] groß[illegible] oder zu kleinen -Werten, ATM J 135-26, Feb 1970.

(89) Nydegger K, Fehlerquellen beim Messen mit Dehnungsmeßstriefen und ihre Beseitigung, Teil I: ATM J 135-21, Juni 1966, Teil II:ATM J 135-22, Nov 1967, Teil III:ATM J 135-25, Dez 1967.

(90) Haug A, Brückenschaltungen für Dehnmeßstreifen und ihr Abgleich, Teil I: ATM J 135-23, Sept 1967,Teil II: ATM J 135-24, Oct 1967, Teil III: ATM J 135-27, März 1970.

(91) Telinde C, Behaviour of Strain Gauges and Temperature Sensors at Low Temperatures, Instrument Society of America, 22nd Annual ISA Conference, Sept 11-14, 1967, Chicago, Illinois. Preprint No P21-2-PHYMMID-67.

(92) Telinde, J C, Strain Gauges in Cryogenic Environement, McDonald-Douglas Paper 5099, Oct 1968.

(93) Telinde J C, Investigation of Strain Gauges at Cryogenic Temperatures, McDonald-Douglas Paper 3835, Nov 1966.

(94) Stehlin P, Dehnungsverteilung in und um Dehnungsmeßstreifen, Journal of Strain and Analysis 7, 1972, H 3, S 228-235.

(95) Knublauch E, Über die Messung einiger Eigenschaften von Hochtemperature-Dehnungsmeßstreifen und ihre Deutung, Math. Nat. Fak, FU Berlin, Dez 1966.

(96) Wilson, Earl I, Installation and Testing of Strain Gauges for High-Temperature Aircraft Applications, NASA Flight Research Center, Edwards, Calif.

(97) Wilson, Earl I, Use of Strain Gauges for Measurement of Flight Loads in a High Temperature Environment, Instrument Society of America, 68-555, 1968.

(98) Wilson, Earl I, Strain Gauge Installation on the YF-12 Aircraft, NASA Flight Research Center, Edwards, Calif.

(99) Wilson, Earl I, and Egger, Richard L: Design and Operation of a 1500°F Thermal-Null Strain Gauge, NASA Flight Research Center, Edwards, Calif.

(100) Harting D, Evaluation of a Capacitive Strain Measuring System for Use to 1500°F, Proceedings of the 21st Int. Instrumentation Symposium, Philadelphia, May 1975.

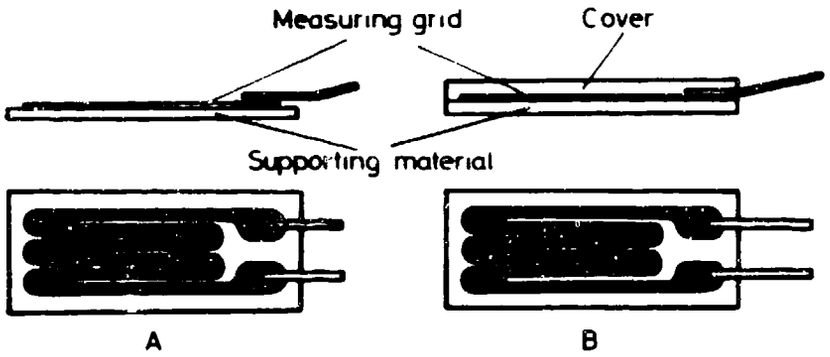

Fig. 1.2 - 1: Basic structure of a strain gauge
A Uncovered measuring grid
B Covered measuring grid

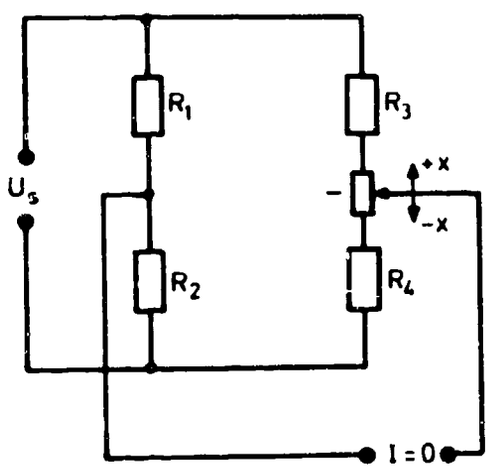

Fig. 1.2 - 2: Wheatstone bridge (balancing method)

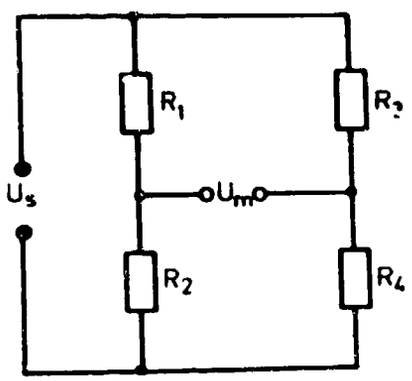

Fig. 1.2 - 3: Wheatstone bridge (diagonal voltage method)

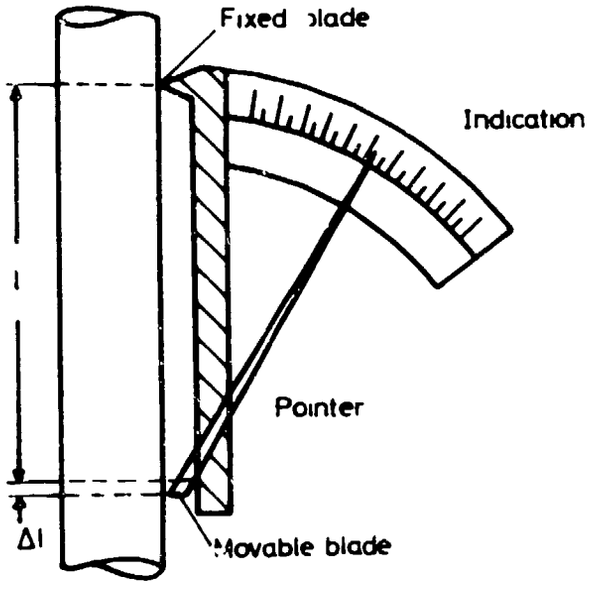

Fig. 1.3 - 1: Mechanical extensometer (B3)

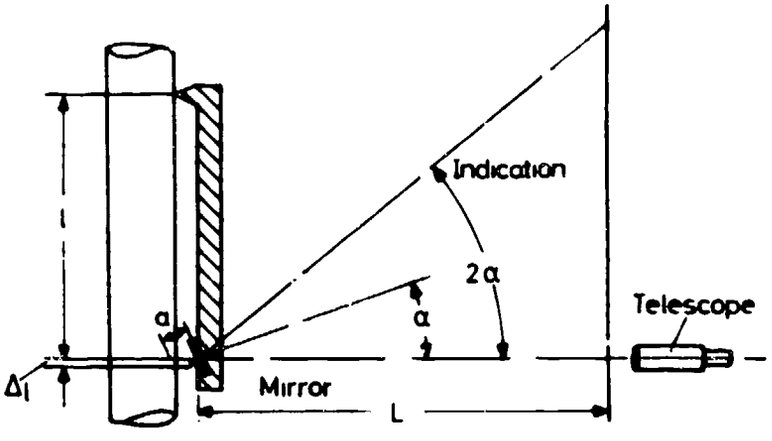

Fig. 1.3 - 2: Martens' extensometer (B3)

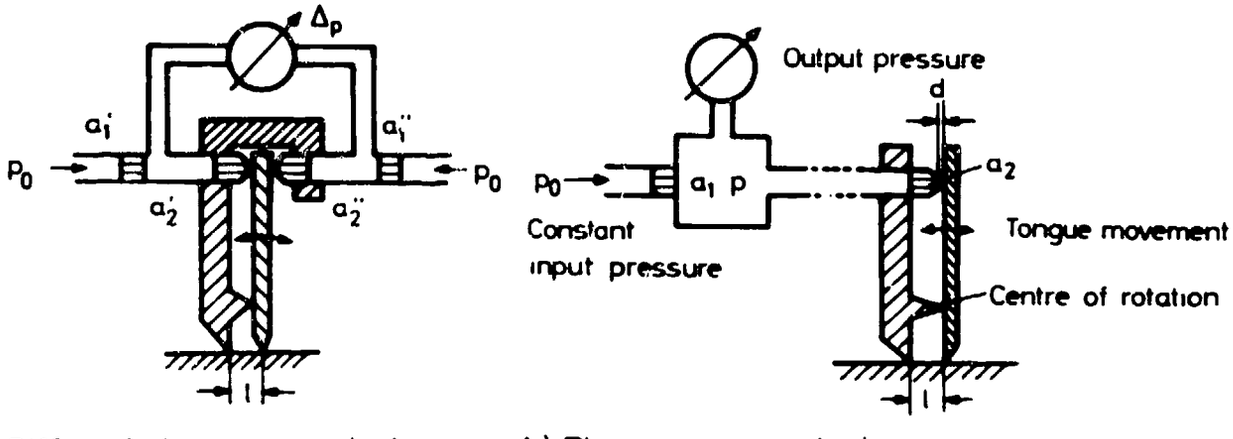

Fig. 1.3 - 3: Pneumatic transducer (B3)

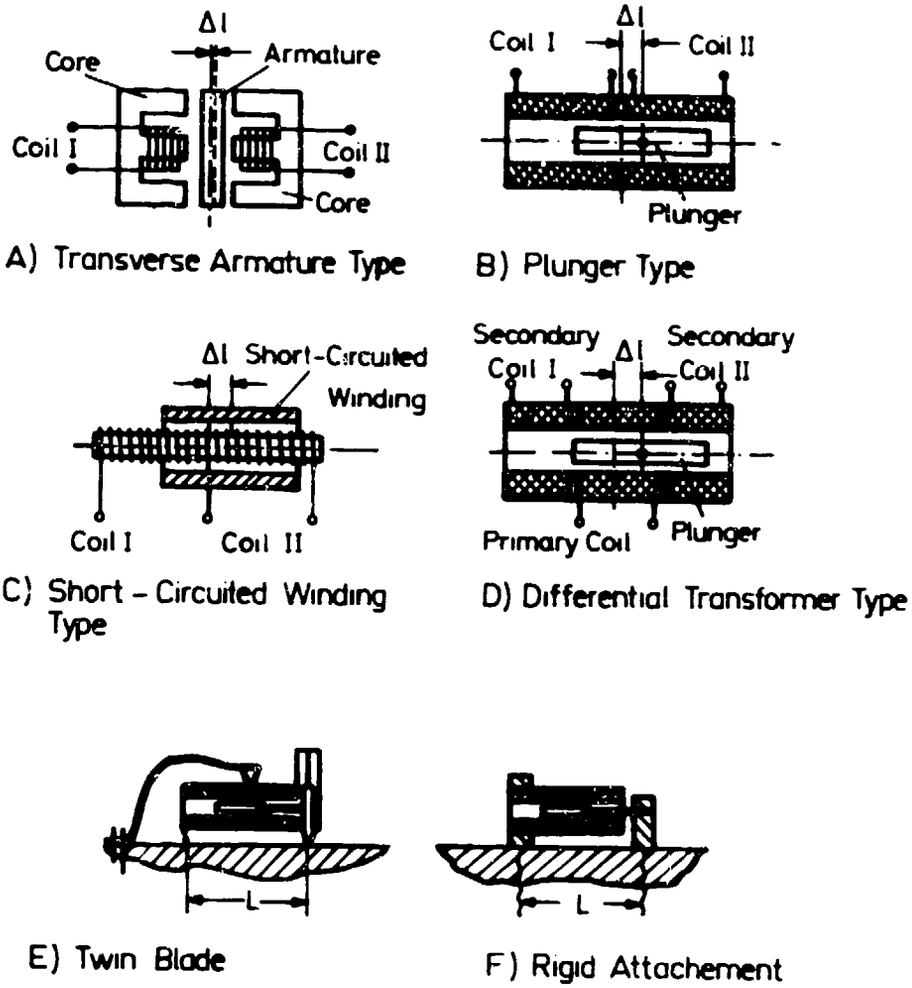

Fig. 1.3 - 4: Inductance transducer (B3)(B4)

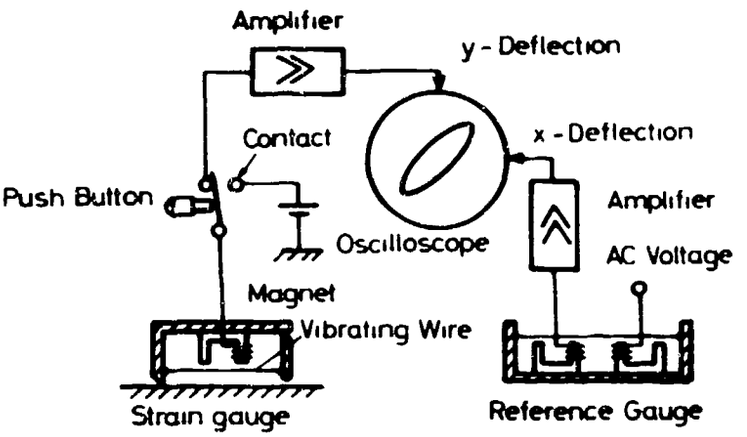

Fig. 1.3 - 5: Vibrating-wire transducer (B3)

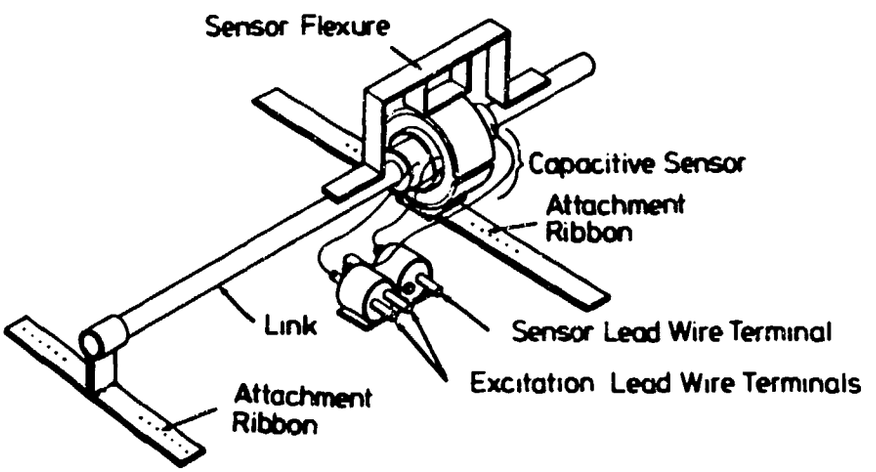

Fig. 1.3 - 6: Basic structure of a capacitive transducer.

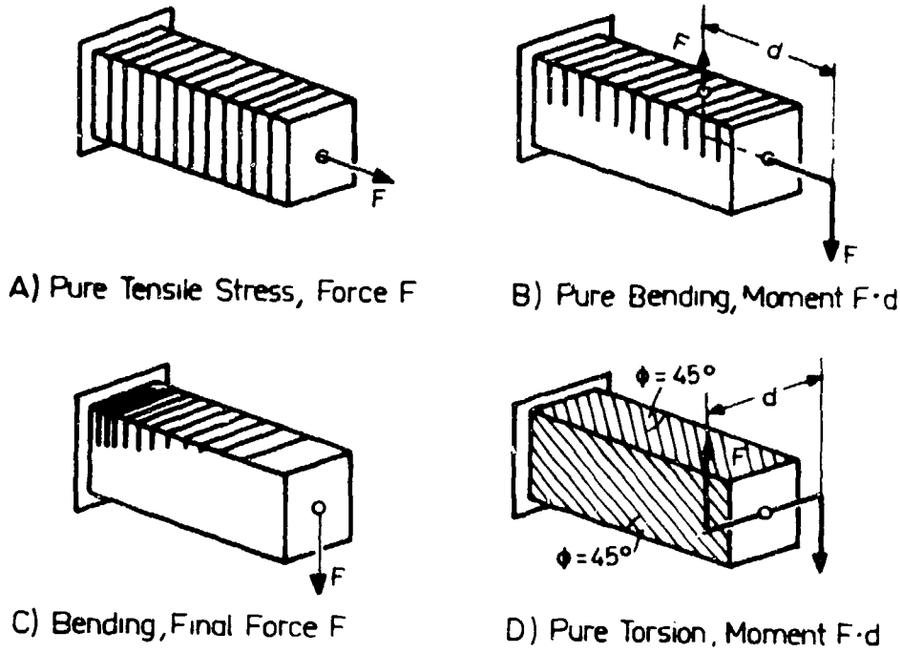

Fig. 1.3 - 7: Brittle lacquer method
typical crack pattern in a bar under elementary stresses

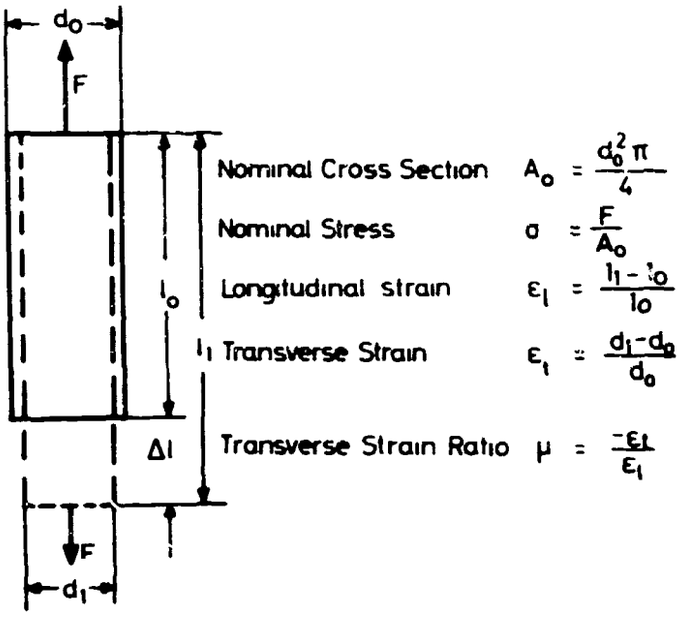

Fig. 2.1 - 1: Circular bar under tension load

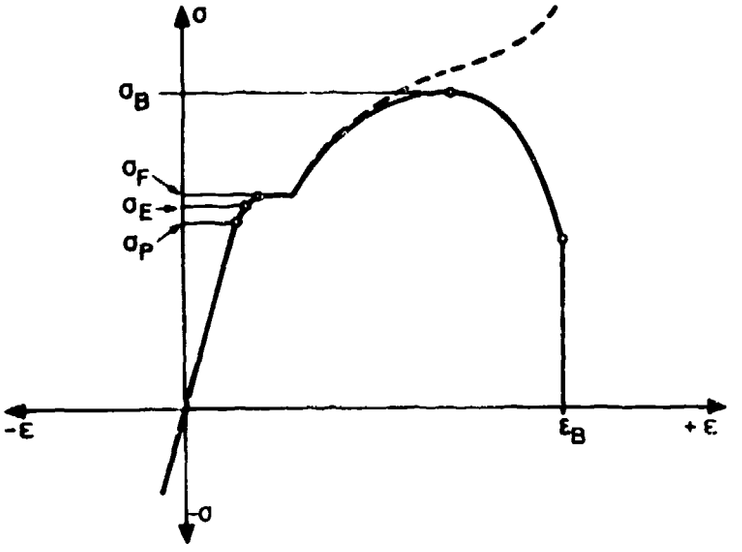

Fig. 2.1 - 2: Schematic σ - ε - diagram for mild steel

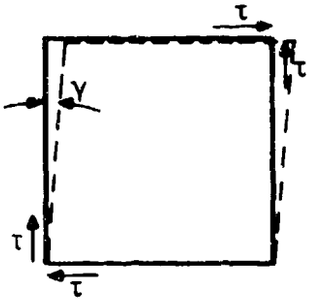

Fig. 2.1 - 3: Element of a shear-stressed panel

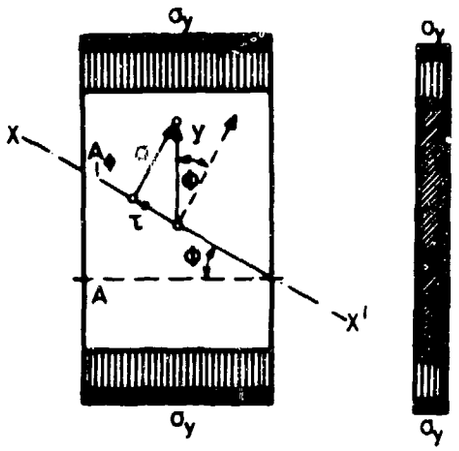

Fig. 2.1 - 4: Uniaxially stressed plate (B7)

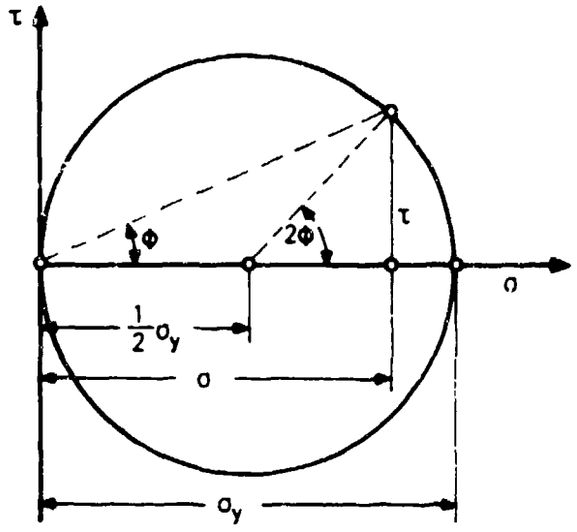

Fig. 2.1 - 5: Mohr's circle for the uniaxial state of stress

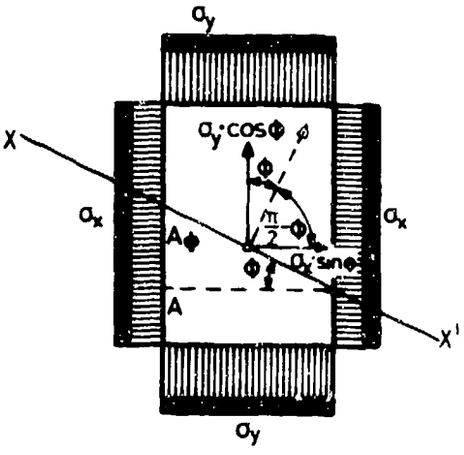

Fig. 2.1 - 6: Biaxially stressed plate (B7)

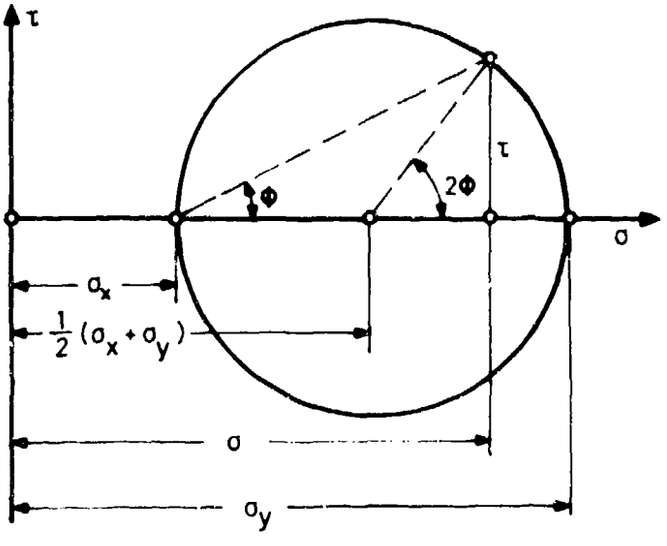

Fig. 2.1 - 7: Mohr's circle for the biaxial state of stress

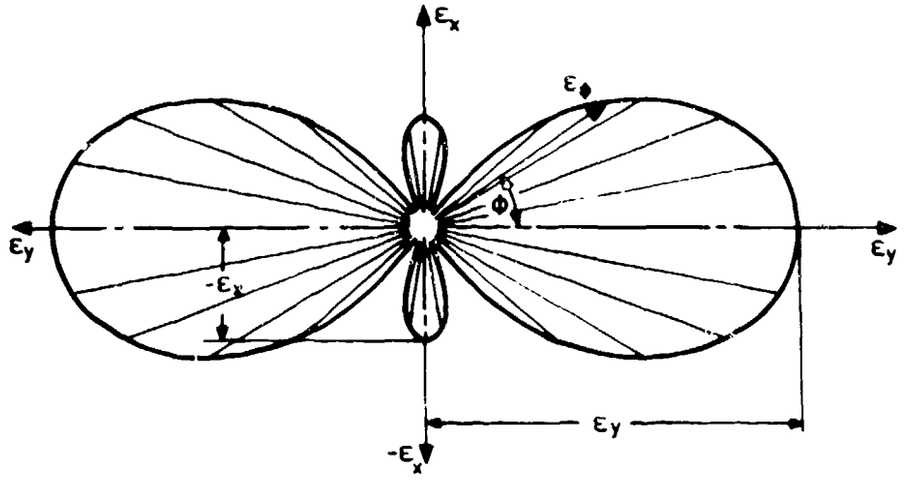

Fig. 2.1 - 8: Planar state of deformation of the uniaxial state of stress

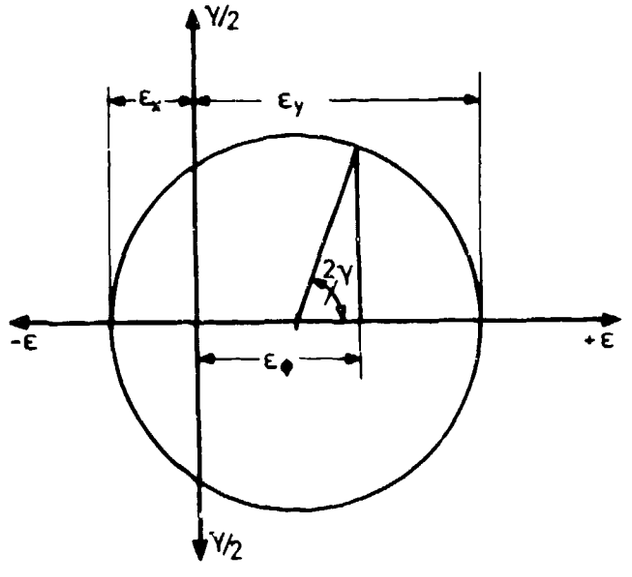

Fig. 2.1 - 9: Mohr's circle for deformation
applicable to the condition shown in Fig. 2.1 - 8

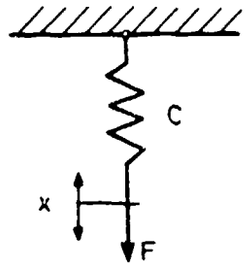

Fig. 2.1 - 10: Spring system

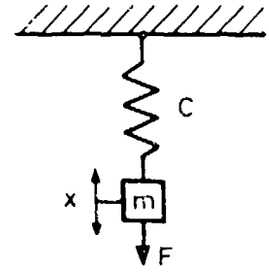

Fig. 2.1 - 11: Spring/mass system

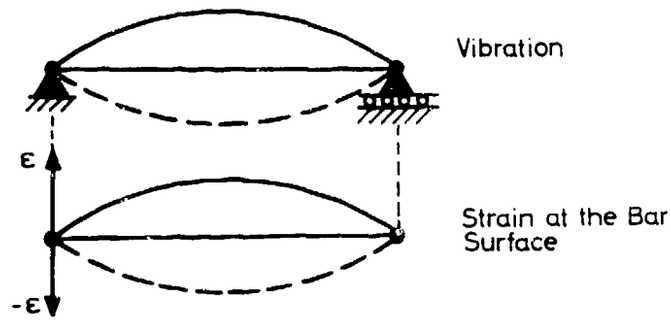

Fig. 2.1 - 12: Simple two-node vibration (bar supported at both ends)

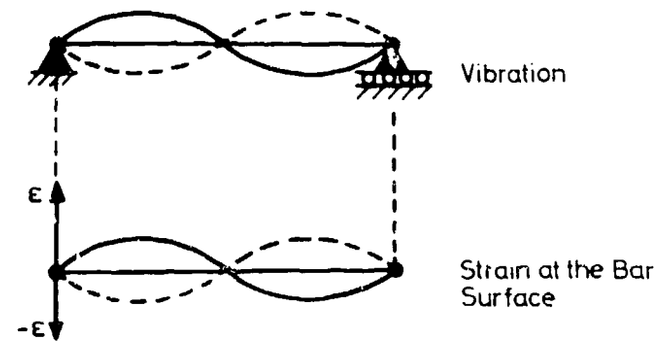

Fig. 2.1 - 13: Three-node vibration (bar supported at both ends)

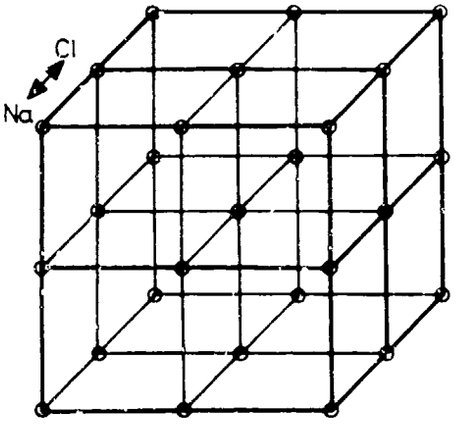

Fig. 2.2 - 1: Crystal lattice (elementary lattice cell) of the ionic crystal NaCl

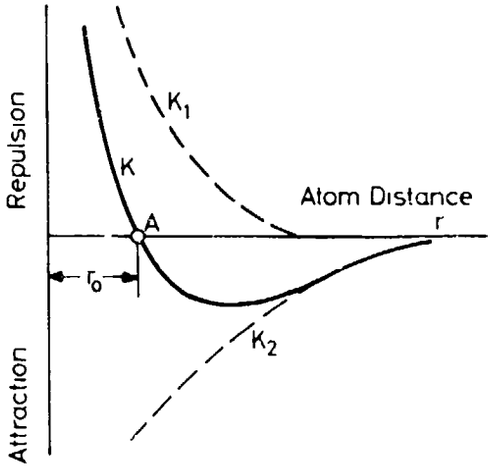

Fig. 2.2 -2a: Forces of attraction and repulsion in a solid body
r = distance between two atoms
r_o = equilibrium distance

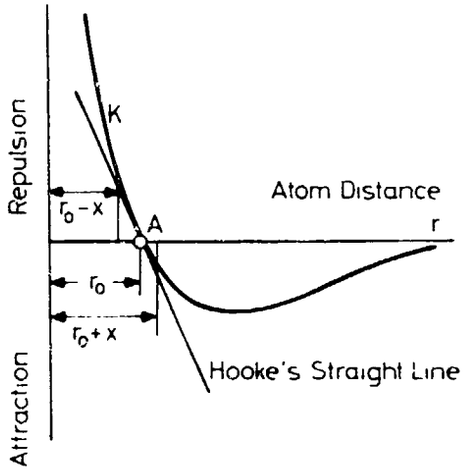

Fig. 2.2 - 2b: Cumulative force near equilibrium position
± x = change caused by thermal and/or mechanical deformation

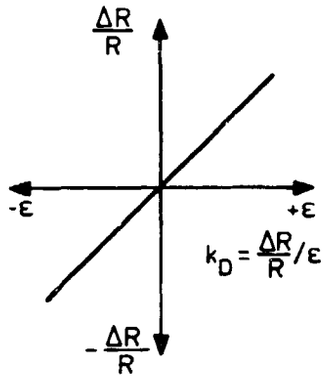

Fig. 2.2 - 3: Definition of the gauge factor k_D for metal conductors

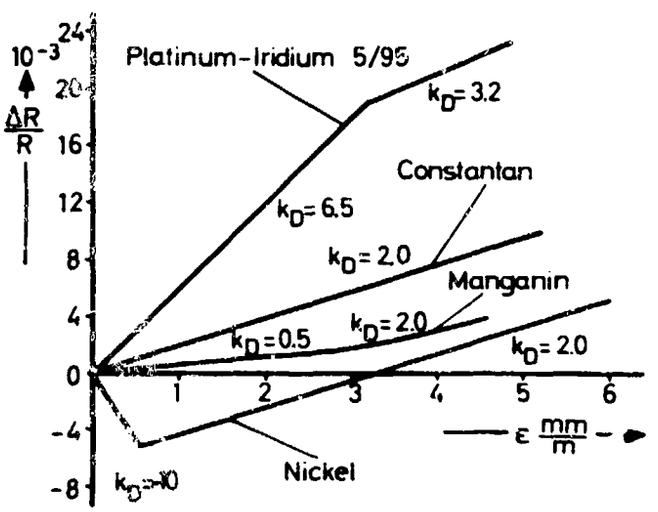

Fig. 2.2 - 4: Resistance versus strain characteristics of unsupported metal conductors

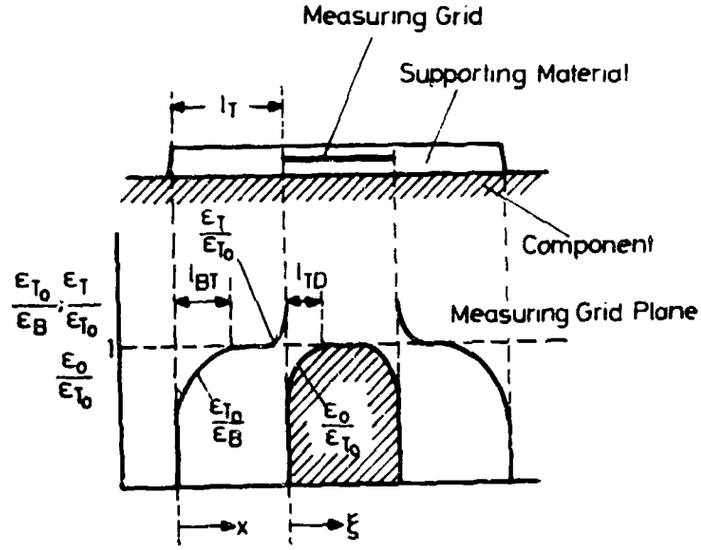

Fig. 2.2 - 5: Basic strain behaviour in a bonded strain gauge

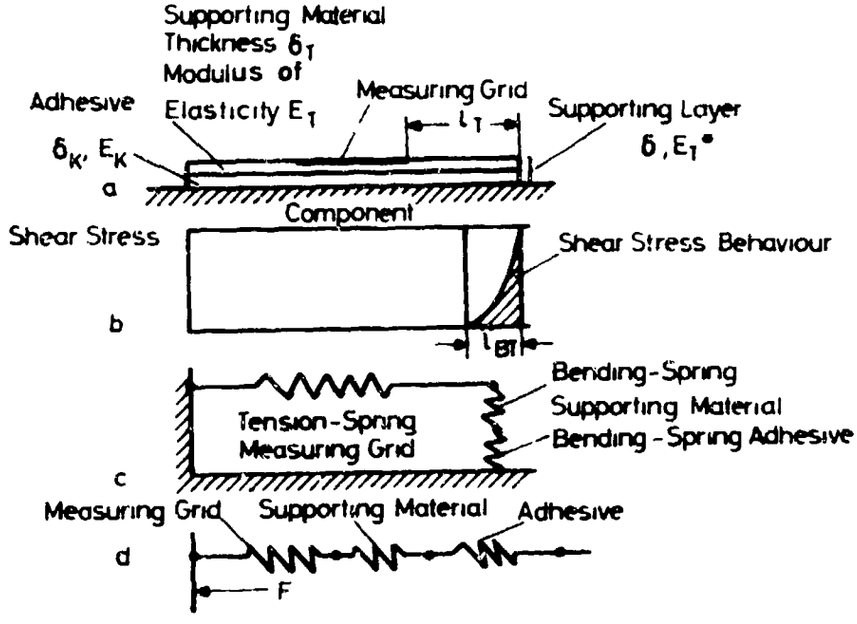

Fig. 2.2 - 6a/d: Model conception of the action of a strain gauge according to Rohrbach and Czaika (2)

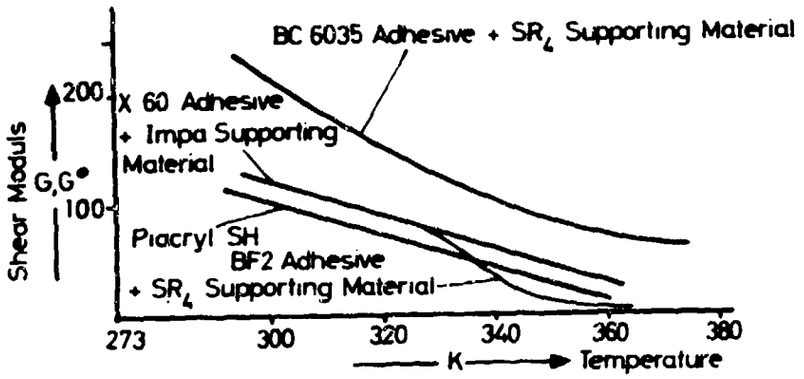

Fig. 2.2 - 7: Shear modulus of supporting layers as a function of the temperature according to /3/

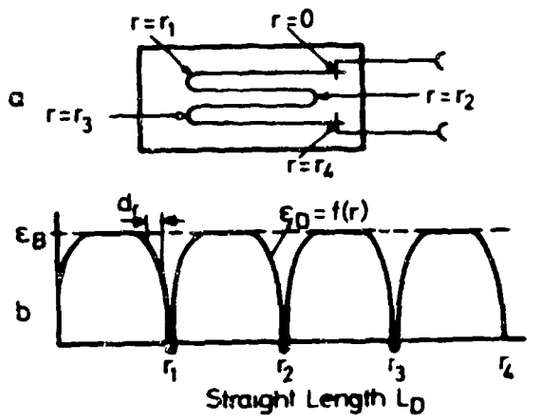

Fig. 2.2 - 8a: Measuring wire in meander-like arrangement

Fig. 2.2 - 8b: Strain behaviour in a straightened measuring grid

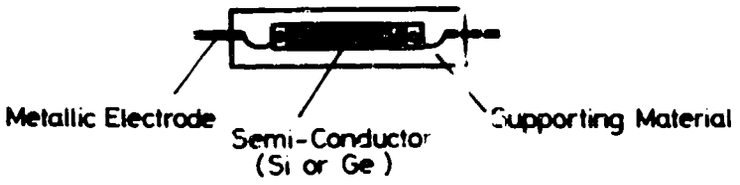

Fig. 2.2 - 9: Basi structure of a semi-conductor strain gauge

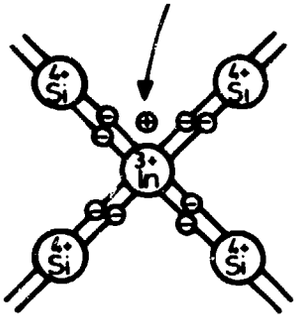

Fig. 2.2 - 10: Impurity conduction in a p-type semi-conductor

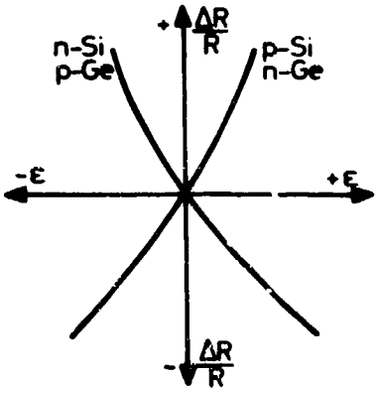

Fig. 2.2 - 12: Examples of gauge factor variations in semi-conductor strain gauges

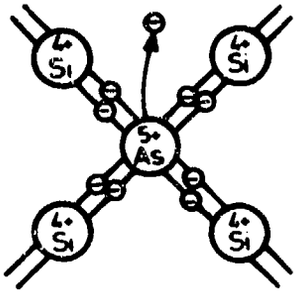

Fig. 2.2 - 11: Impurity conduction in a n-type semi-conductor

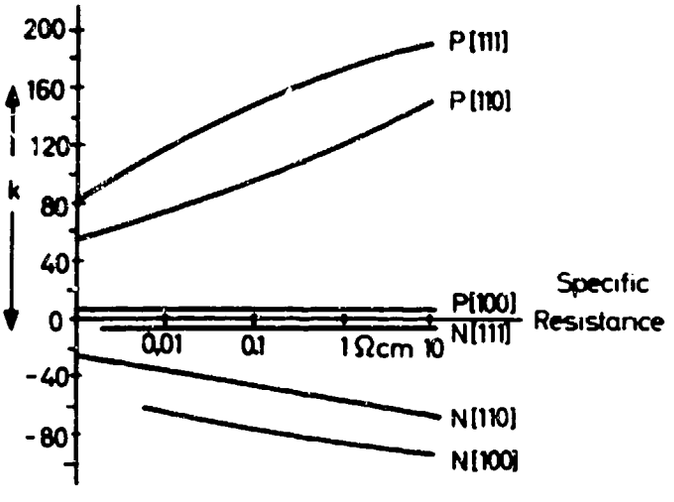

Fig. 2.2 - 13: Gauge factor of a semi-conductor strain gauge as a function of specific resistance, doping and crystal orientation

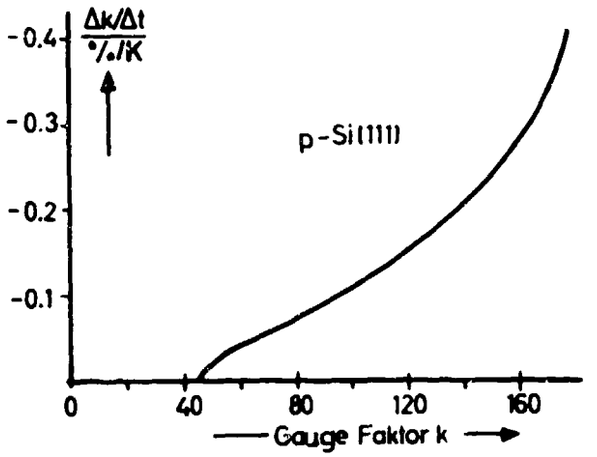

Fig. 2.2 - 14: Temperature dependence of the gauge factor of a semi-conductor strain gauge

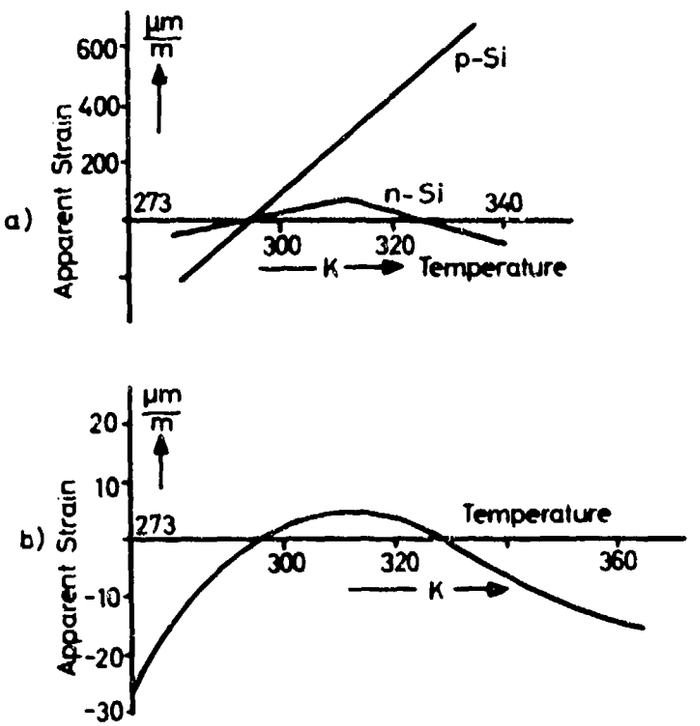

Fig. 2.2 - 15a: Self-compensating effect of a p-type and n-type Si semi-conductor strain gauge on steel

Fig. 2.2 - 15b: Self-compensating effect of a metal strain gauge on steel

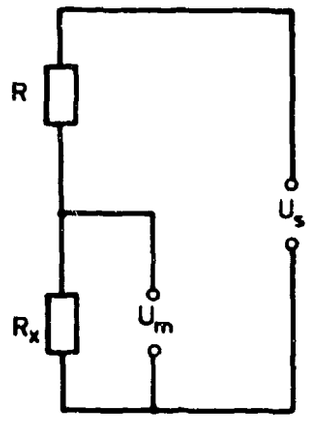

Fig. 3.0 - 1: Voltage divider circuit

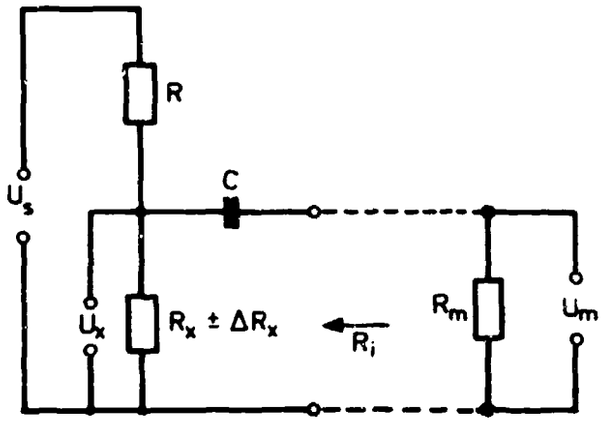

Fig. 3.0 - 2: Voltage divider circuit for measuring alternating signals

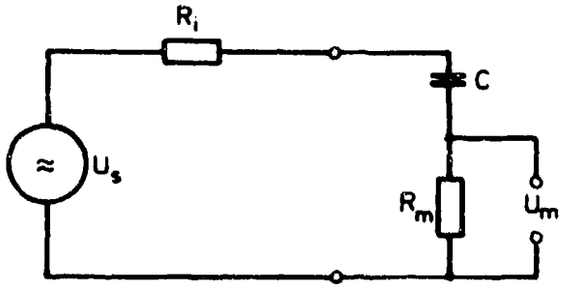

Fig. 3.0 - 3: Alternate circuit diagram for Fig. 3-2

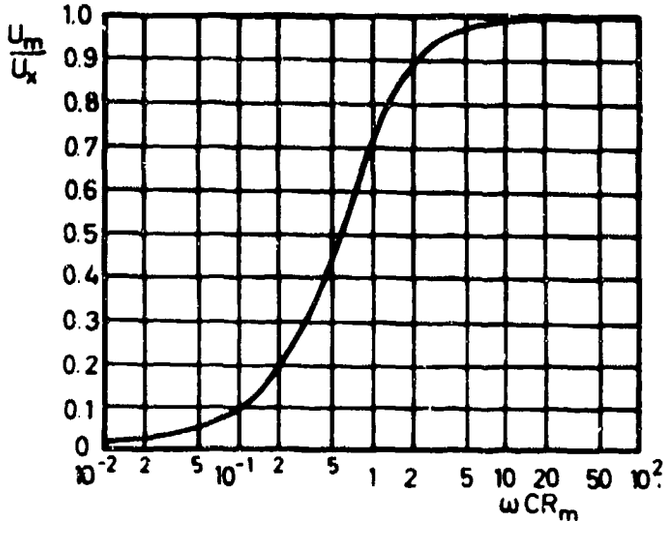

Fig. 3.0 - 4: Frequency dependent measuring voltage curve applicable in the case of the utilization of a voltage divider circuit for alternating loads ($\omega = 2\pi f$) (83) (see circuit in Fig. 3-2)

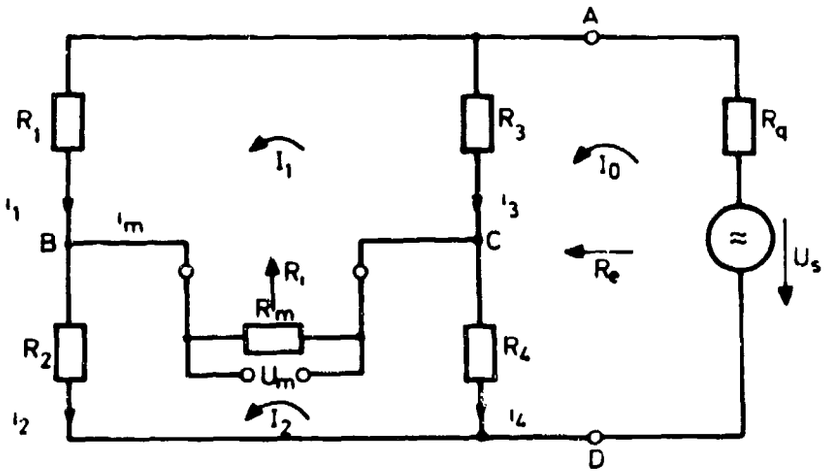

Fig. 3.1 - 1: Current and voltage distribution in the Wheatstone bridge

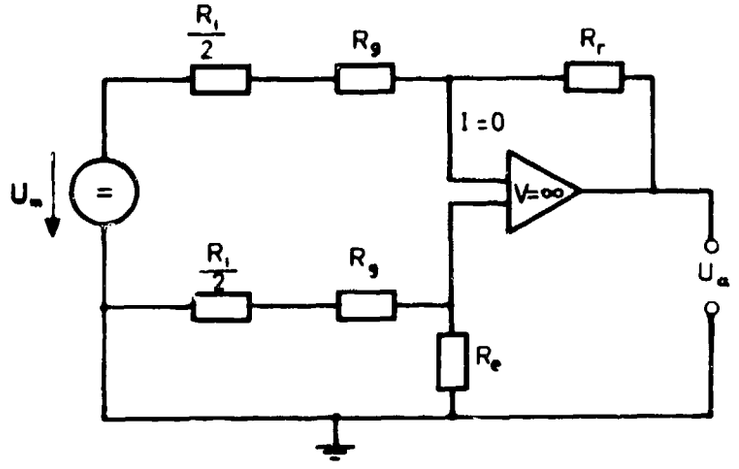

Fig. 3.2 - 1: Alternate circuit diagram for a Wheatstone bridge

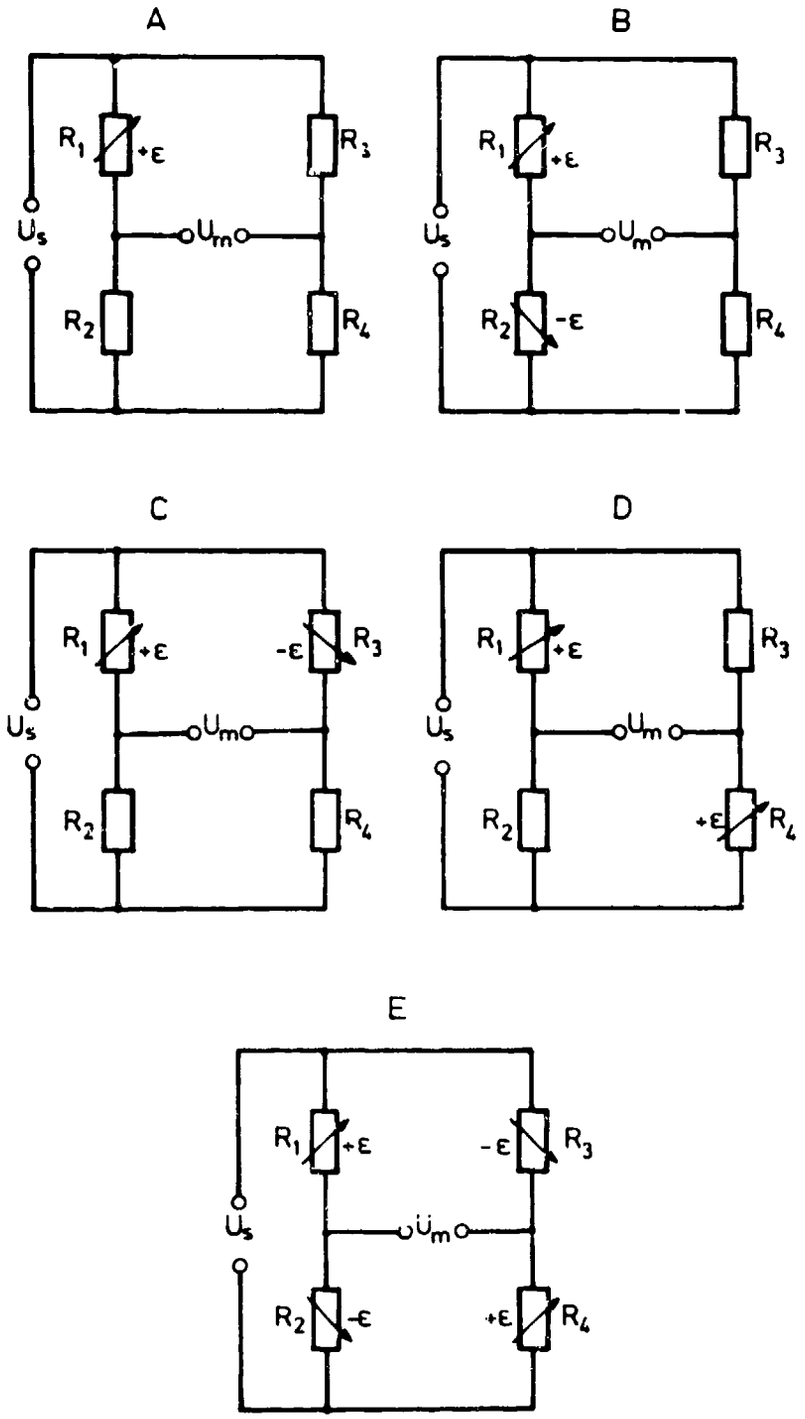

Fig. 3.3 - 1: Various bridge arrangements

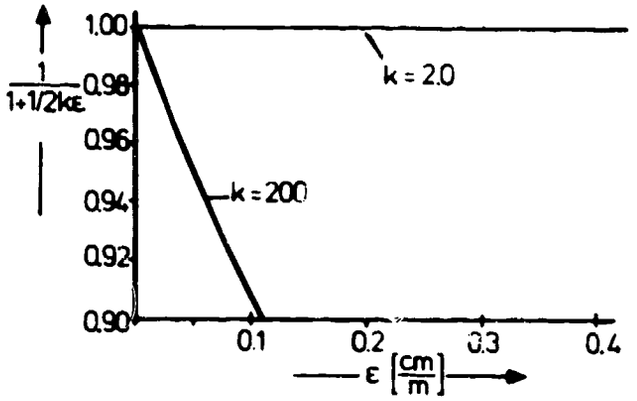

Fig. 3.3 - 2: Non-linearity factor of a quarter-active-bridge

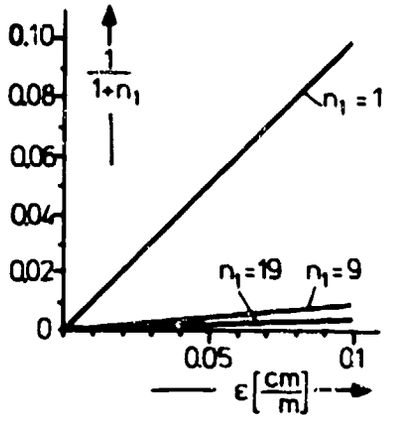

Fig. 3.3 - 3: Dependence of the non-linearity factor on the resistance ratio

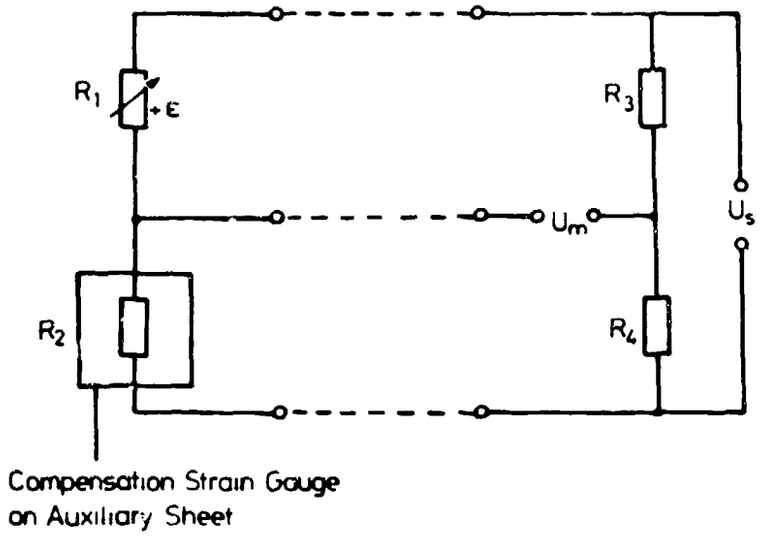

Fig. 3.3 - 4: Quarter-active-bridge temperature-compensated by a passive strain gauge

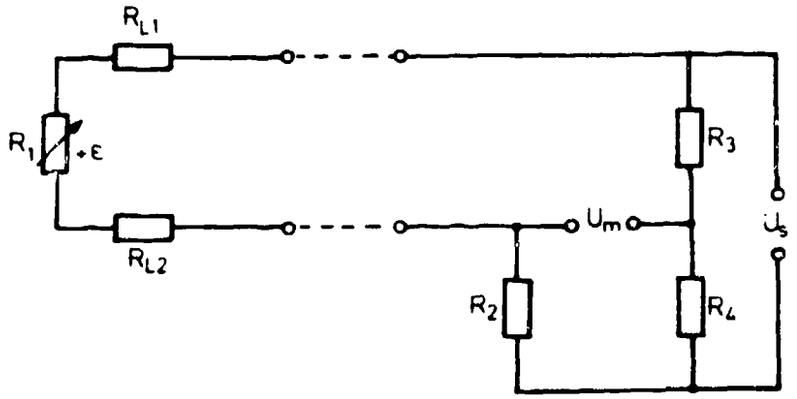

Fig. 3.3 - 5: Lead wire resistances in a simple quarter-active-bridge

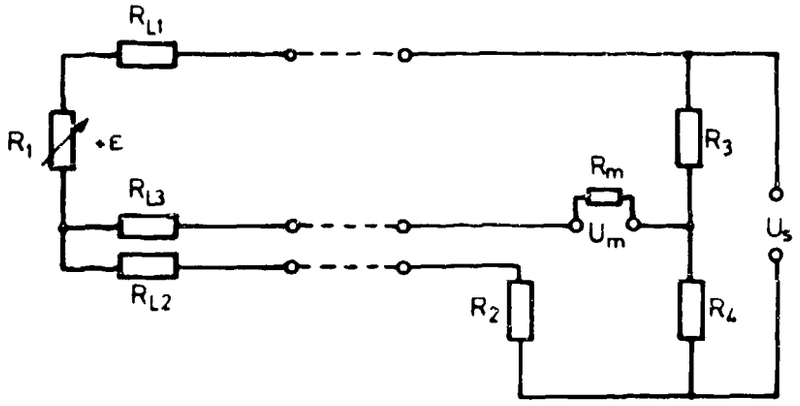

Fig. 3.3 - 6: Quarter-active-bridge with a three-wire circuit

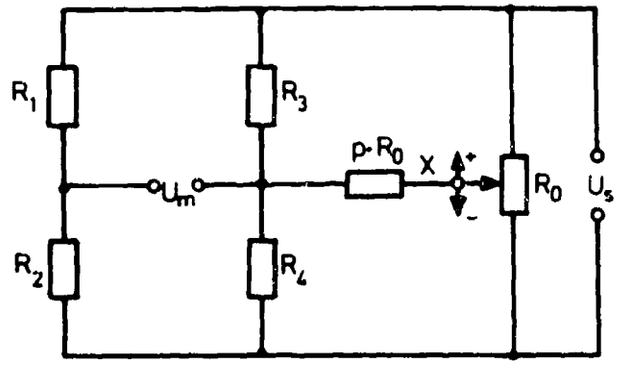

Fig. 3.4 - 1: Bridge balancing by a shunt bridge

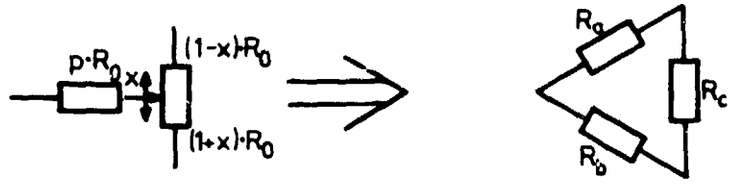

Fig. 3.4 - 2: Equivalent representation of the shunt bridge shown in Fig. 3.4 -1

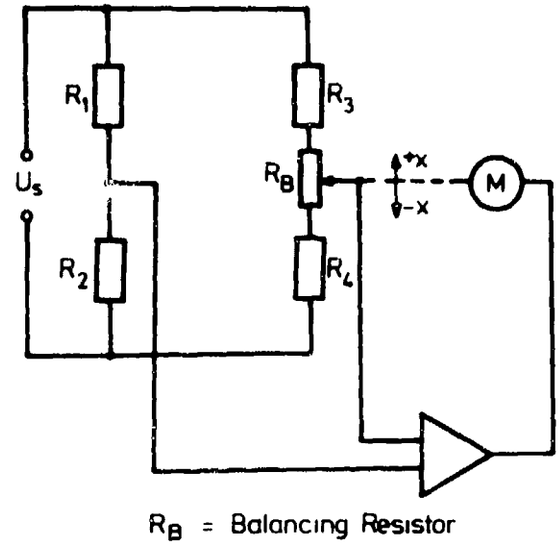

Fig. 3.4 - 3: Compensation by balancing resistor

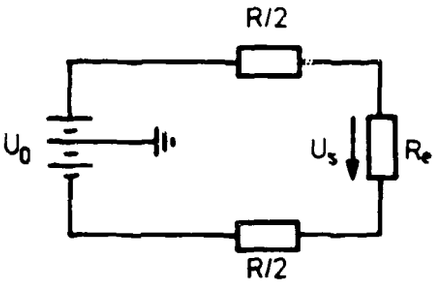

Fig. 3.5 - 1: Voltage-controlled bridge

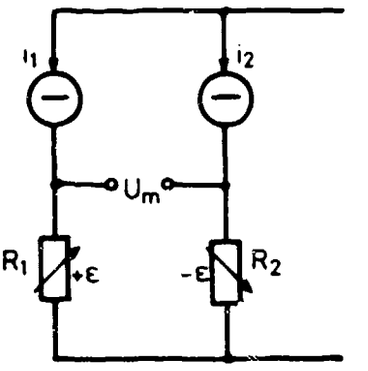

Fig. 3.5 - 3: Separate-arm-controlled current supply

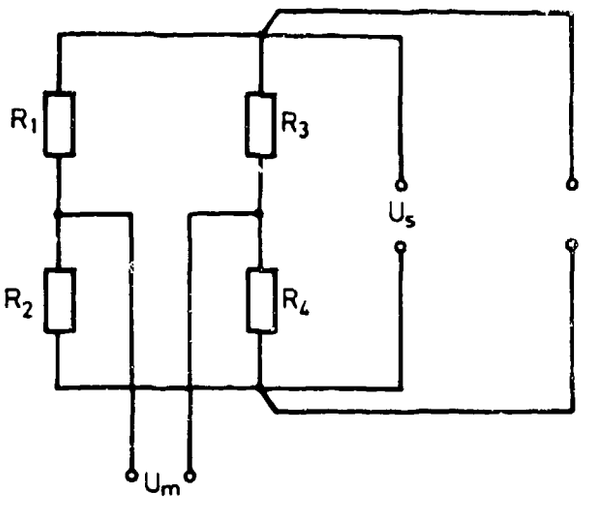

Fig. 3.5 - 2: Six-wire circuit for a voltage-controlled bridge

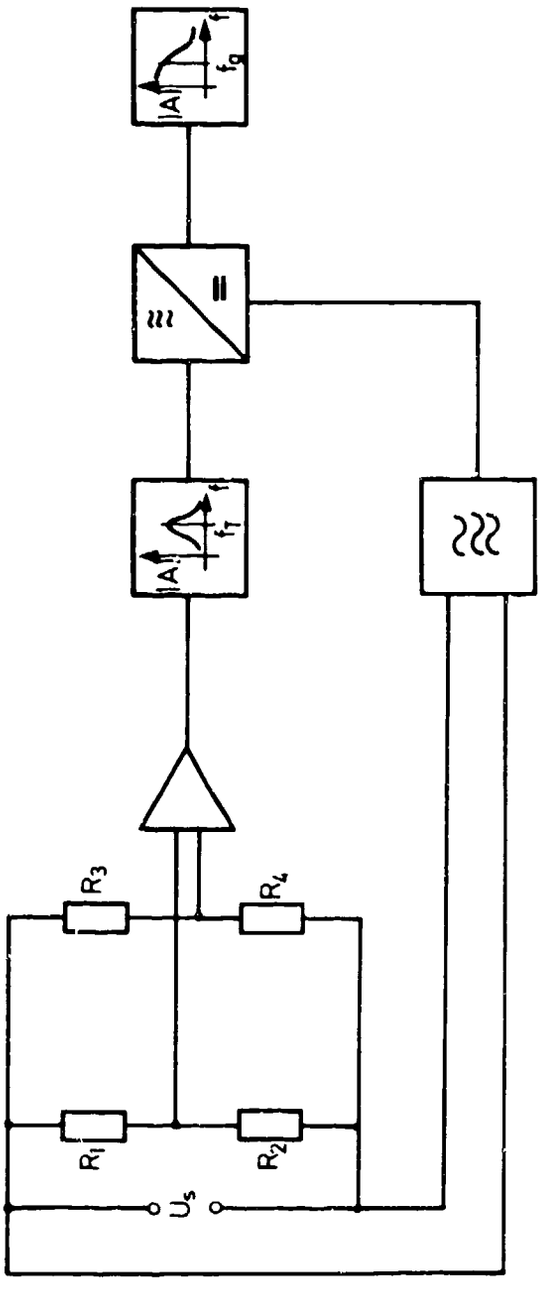

Fig. 3.5 - 4: AC voltage supply

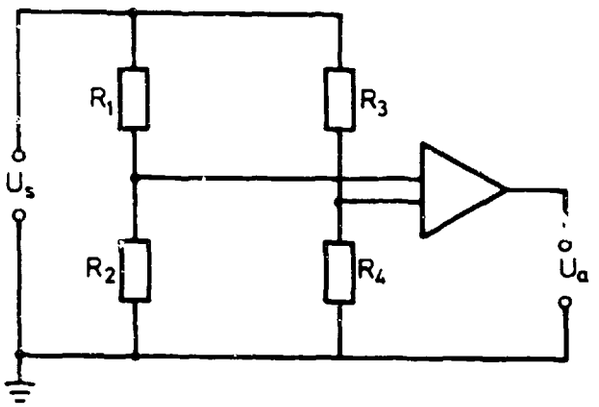

Fig. 3.6 - 1: Measuring arrangement with a large common-mode voltage

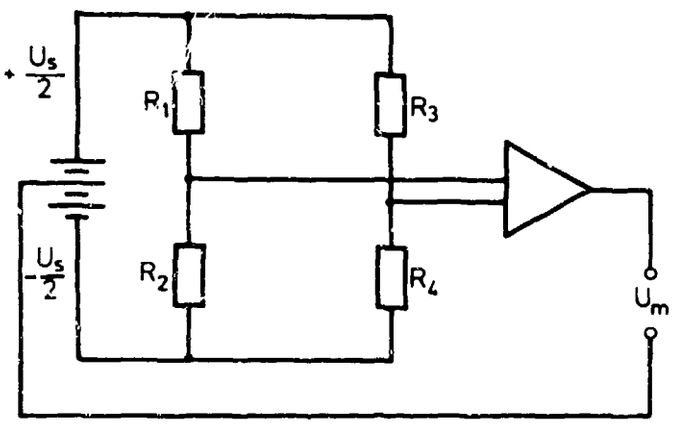

Fig. 3.6 - 2: Earth-symmetrical bridge

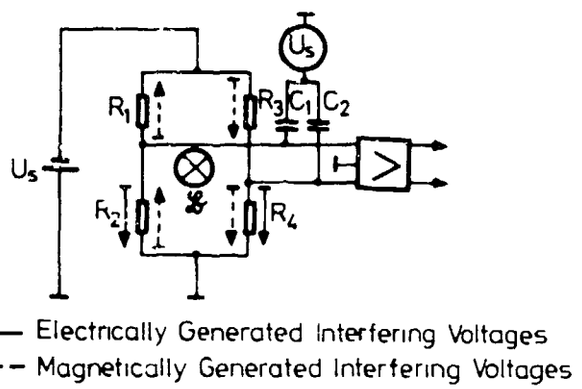

Fig. 3.6 - 3: Influence of electrical and magnetic interference fields on measuring bridges in the case of an asymetrical supply (B4)

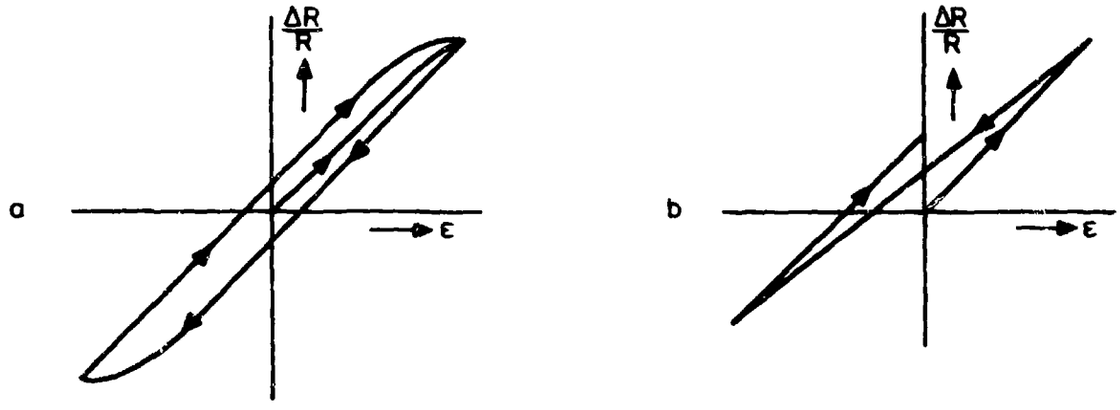

Fig. 4.3 - 1: Mechanical hysteresis of strain gauges

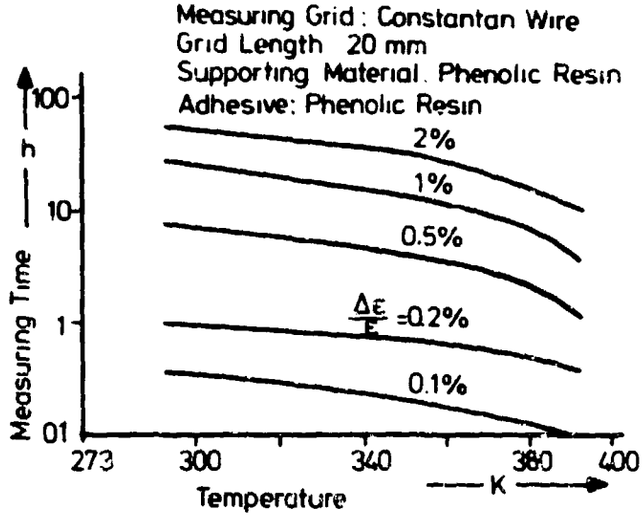

Fig. 4.5 - 1: Time-temperature creep diagram

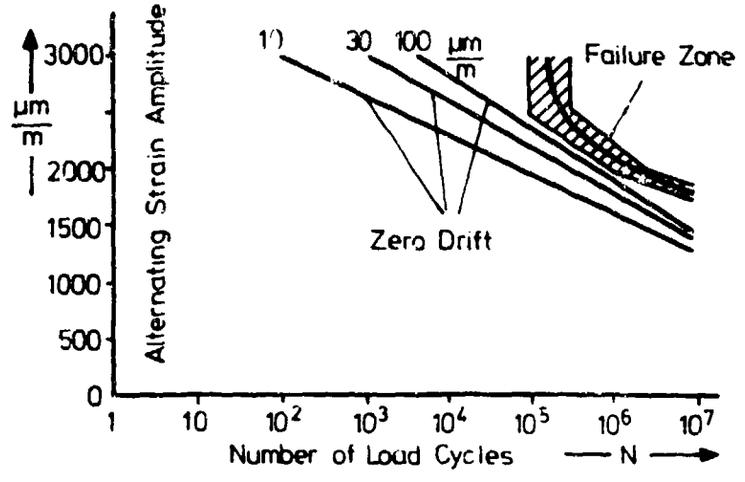

Fig. 4.7 - 1: Fatigue strength diagram
Zero drift and failure zone of modern foil strain gauges as a function of the number of load cycles and the alternating strain amplitude

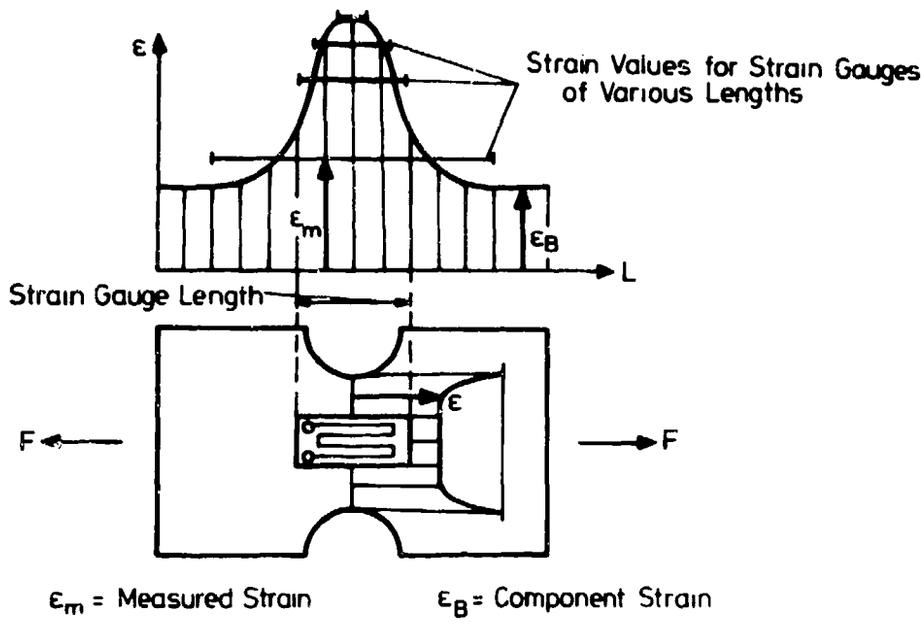

Fig. 4.12 - 1: Basic correlation between the measuring grid length of a strain gauge and the measuring value illustrated by the notched bar test

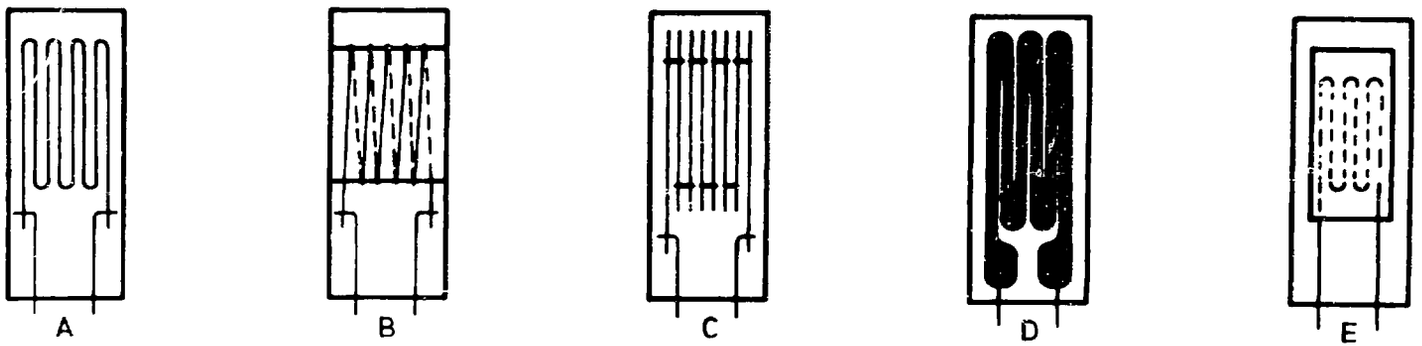

Fig. 5.2 - 1: Basic types of strain gauges

A Flat-grid
B Flat-coil
C Cross-bridge
D Metal-foil
E Strain gauge with metal supporting material

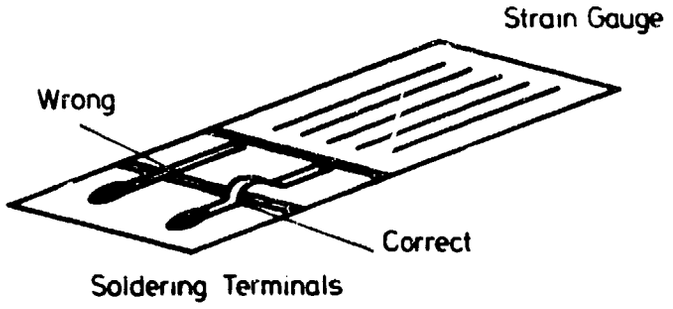

Fig. 6.5 - 1: Connection technique for strain gauges (general)

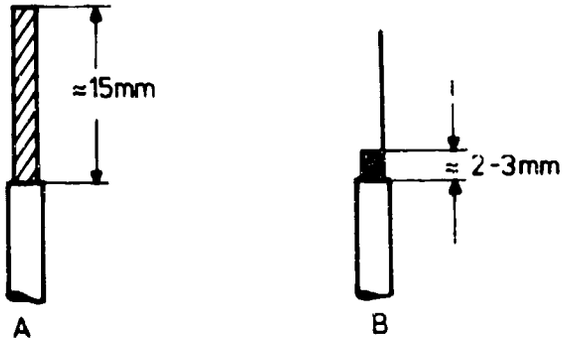

lead stripped over long length

all single wires but one cut short

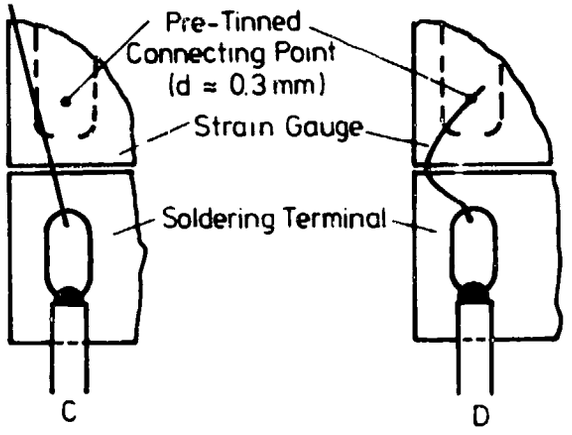

prepared lead soldered to the soldering terminal

single wire bent and soldered to the pre-tinned connecting point

Fig. 6.5 - 2: Connection technique for strain gauges (recommended by the manufacturer)

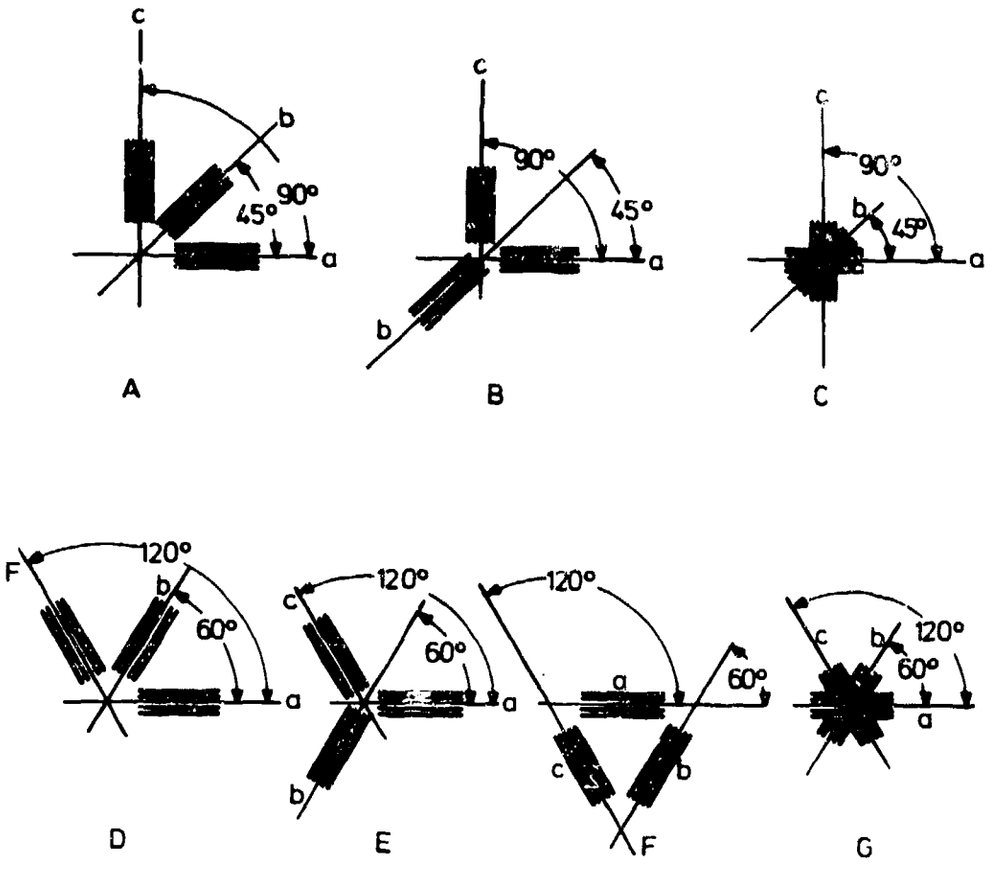

Fig. 7.1 - 1: Various types of triaxial rosettes

A to C $0^{\circ}/45^{\circ}/90^{\circ}$ rosettes
D to G $0^{\circ}/60^{\circ}/120^{\circ}$ rosettes

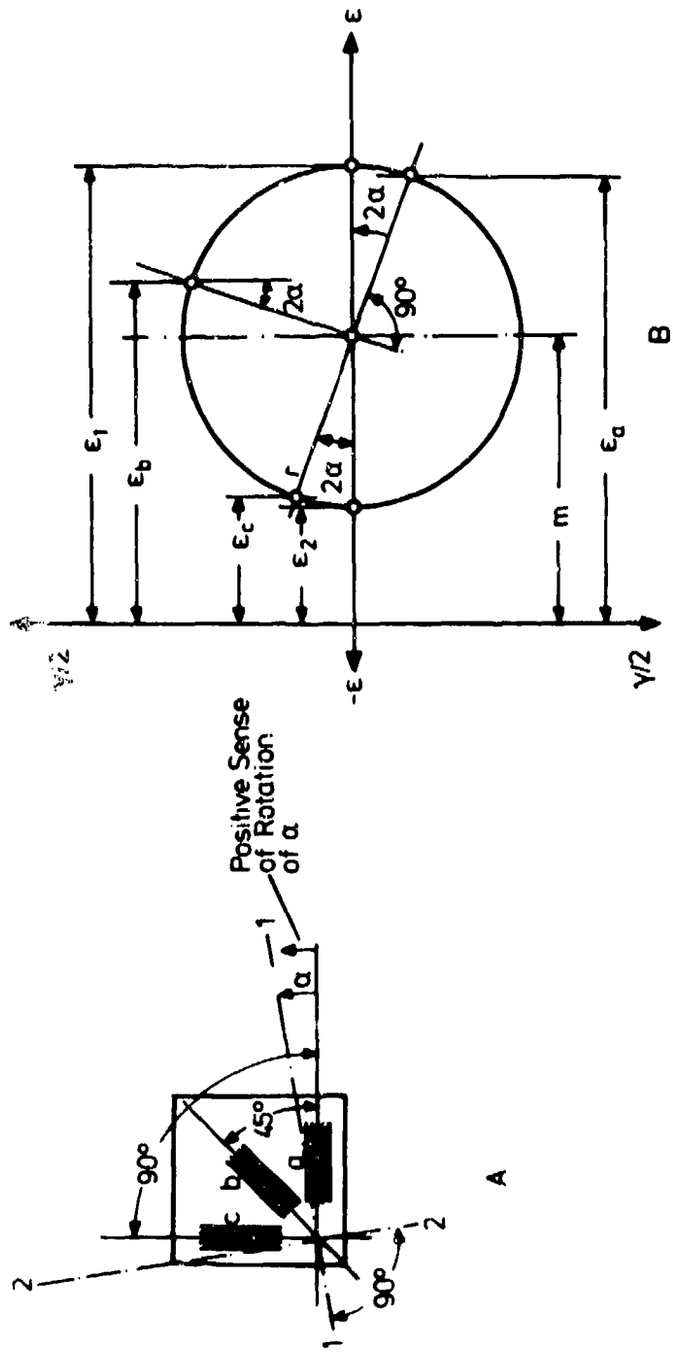

Fig. 7.1-2: $0^{\circ}/45^{\circ}/90^{\circ}$ rosette

A: rosette with measuring directions a,b,c; direction $\hat{a}=0^{\circ}$ and principal directions 1,2 the locations of which are determined from the circle of strain

B: circle of strain for measured values $\varepsilon_a, \varepsilon_b, \varepsilon_c$ and the resulting values $\varepsilon_1, \varepsilon_2$ and α

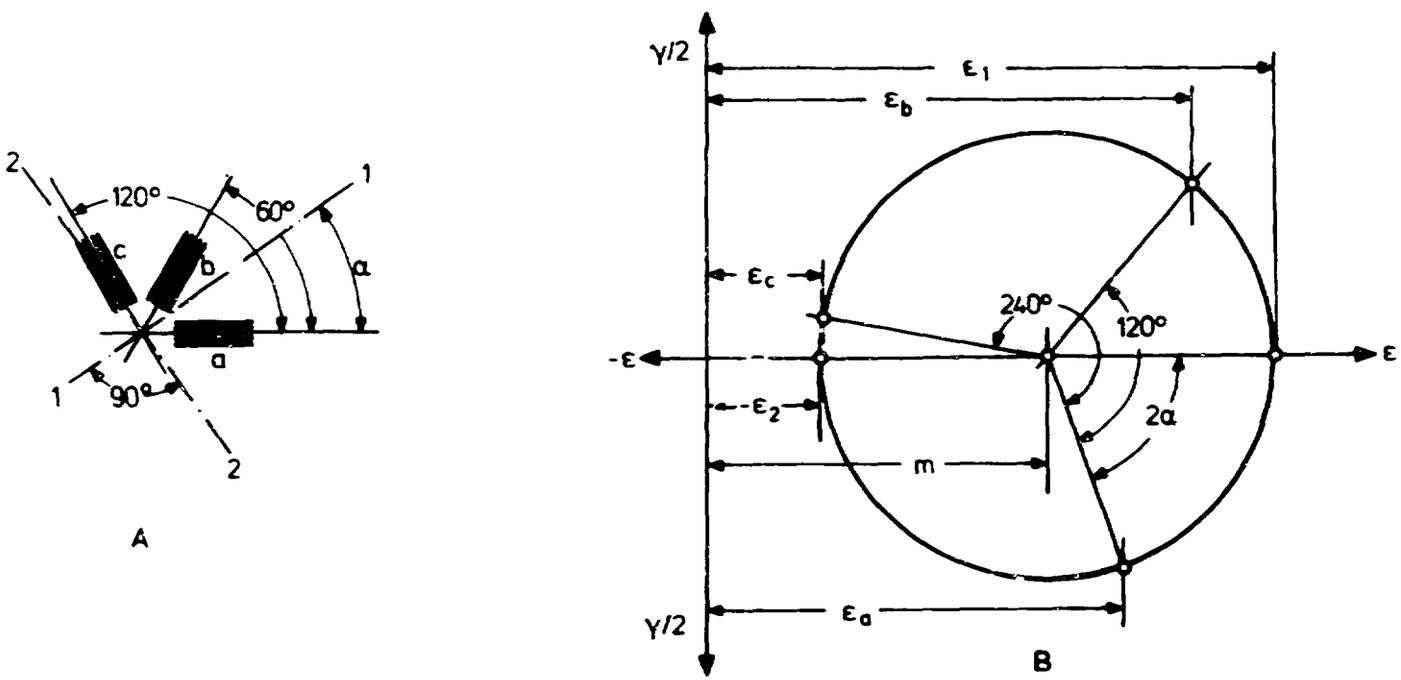

Fig. 7.1-3: 0^0 / 60^0 / 120^0 rosette

A: rosette with measuring directions a,b,c; direction $\hat{a}=0^0$ and principal directions 1,2

B: circle of strain for measured values $\epsilon_a, \epsilon_b, \epsilon_c$

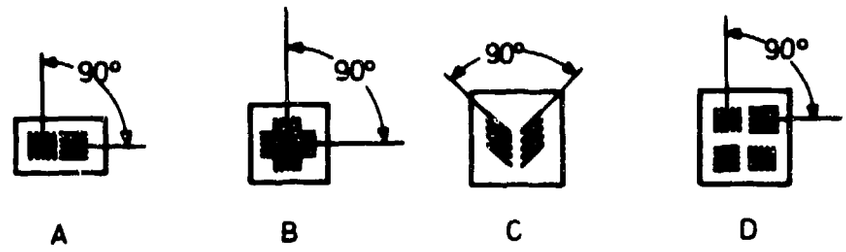

Fig. 7.1 - 4: 90° rosette
A, B normal type
C type for shear measurements
D full bridge type

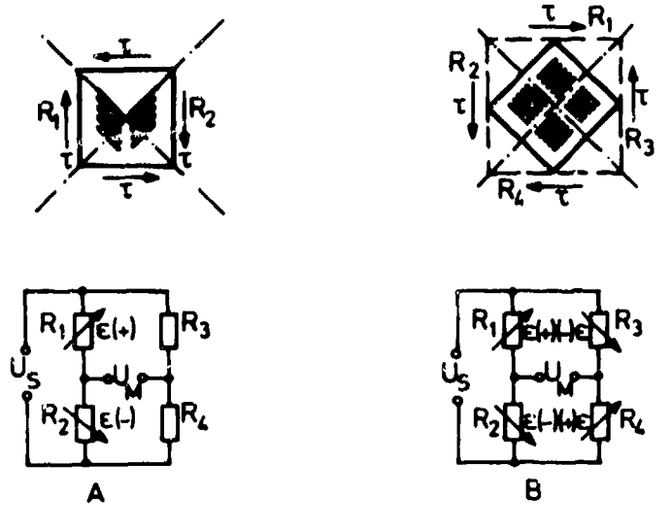

$$(\varepsilon_{11} - \varepsilon_{22}) \triangleq U_M \qquad (\varepsilon_{11} - \varepsilon_{22} - \varepsilon_{33} + \varepsilon_{44}) \triangleq U_M$$

$$\tau_{max} = E \frac{\varepsilon_{11} - \varepsilon_{22}}{2(1+\mu)} \qquad \tau_{max} = E \frac{\varepsilon_{11} - \varepsilon_{22} - \varepsilon_{33} + \varepsilon_{44}}{4(1+\mu)}$$

Fig. 7.1 - 5: Shear measurements with 90° rosette

A semi-bridge
B full-bridge

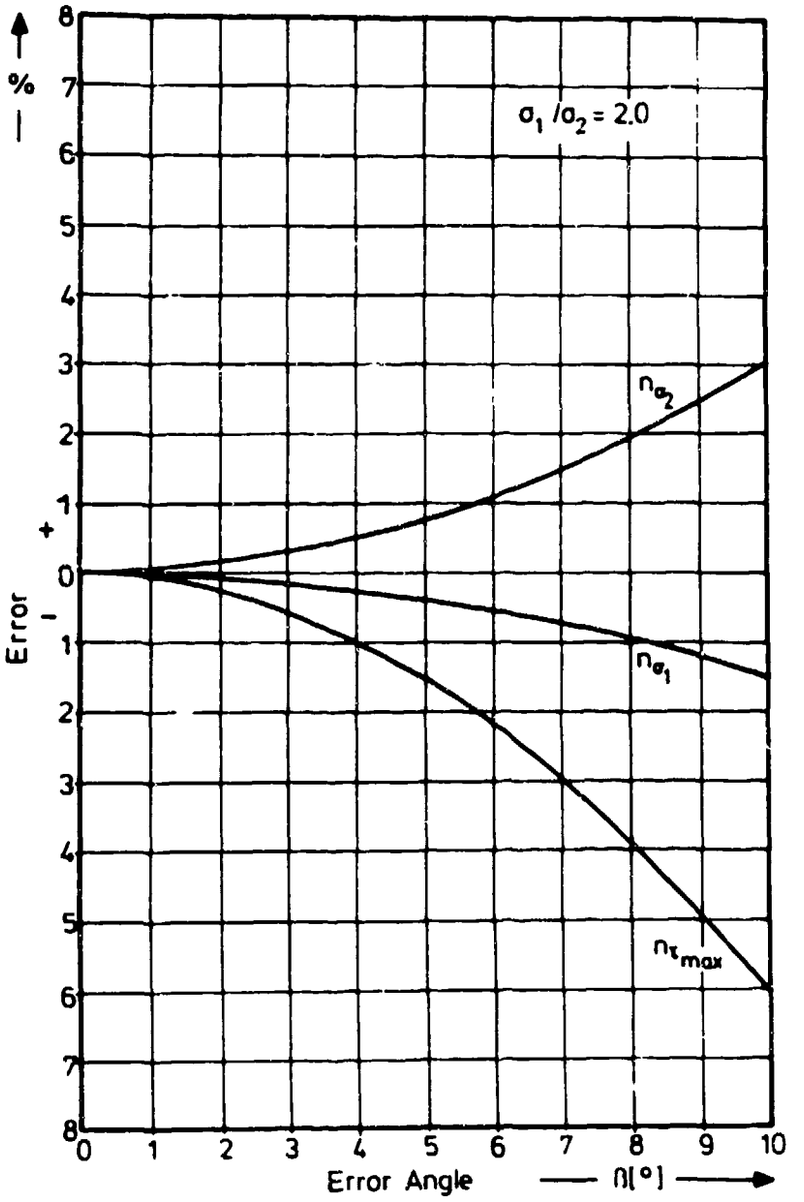

Fig. 7.1 - 6: Errors occuring during determination of stress due to orientation errors caused during strain gauge installation for $\sigma_1/\sigma_2 = 2$ (33)

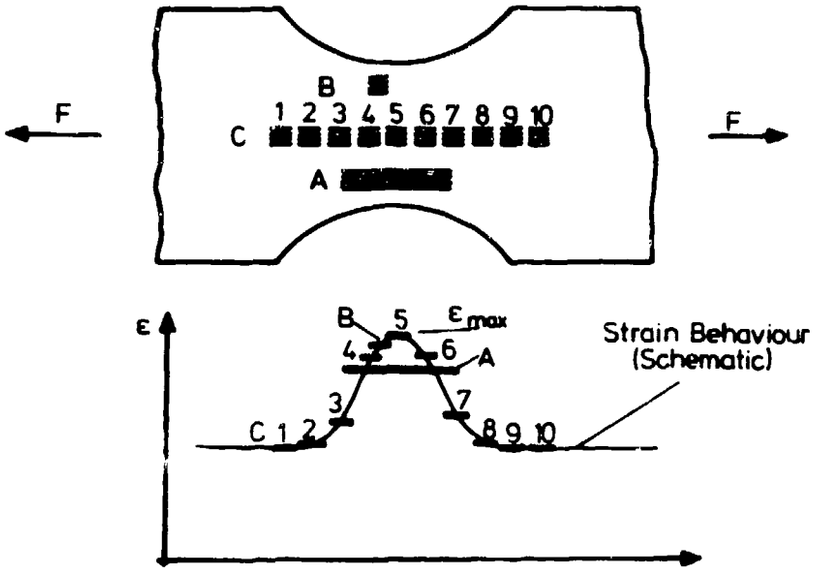

Fig. 7.2 - 1: Measurement of strain behaviour and strain maxima by means of strain gauge chains
Strain gauge A: measuring grid too long
Strain gauge B: not accurately positioned at ε_{max}
Strain gauge C_{1-10}: strain gauge chain

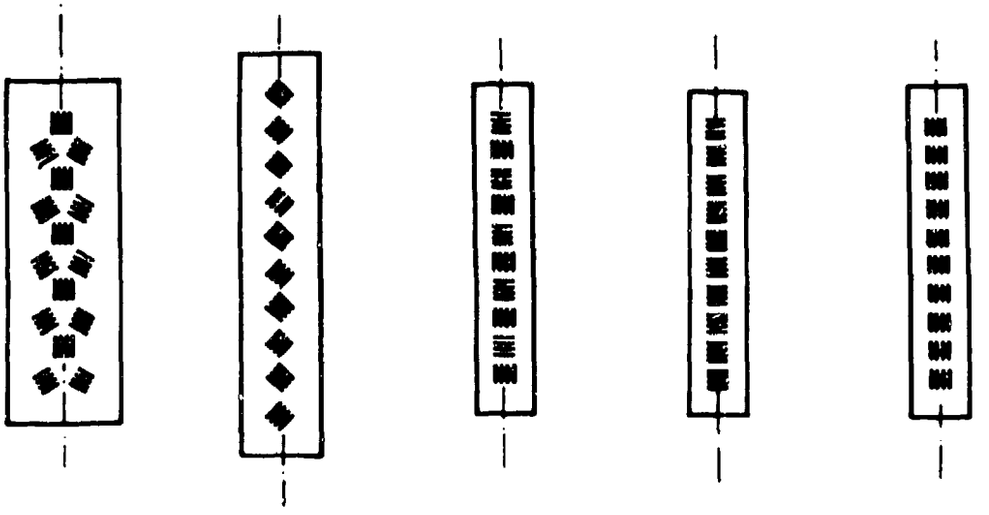

Fig. 7.2 - 2: Various types of strain gauge chains

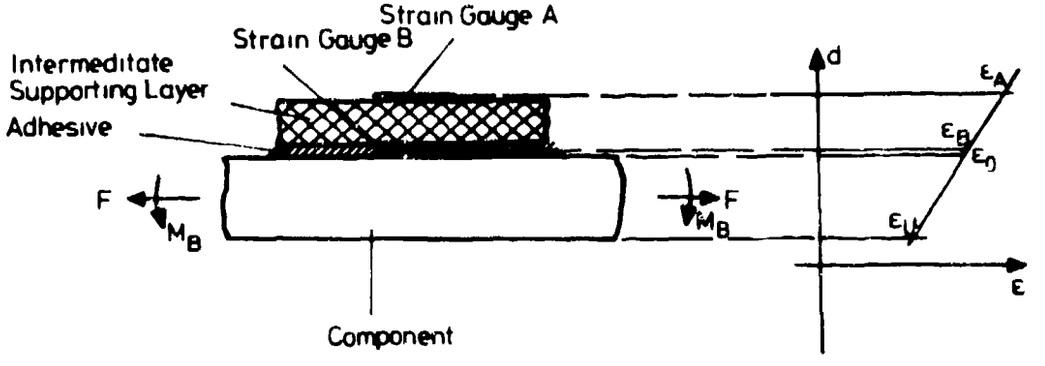

Fig. 7.3 - 1: Flexural strain measurements

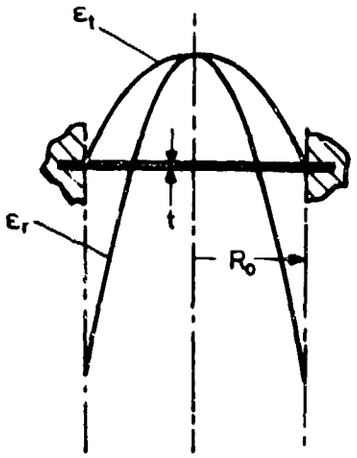

Fig. 7.4 - 1: Strain conditions on pressure-loaded clamped membranes /17/

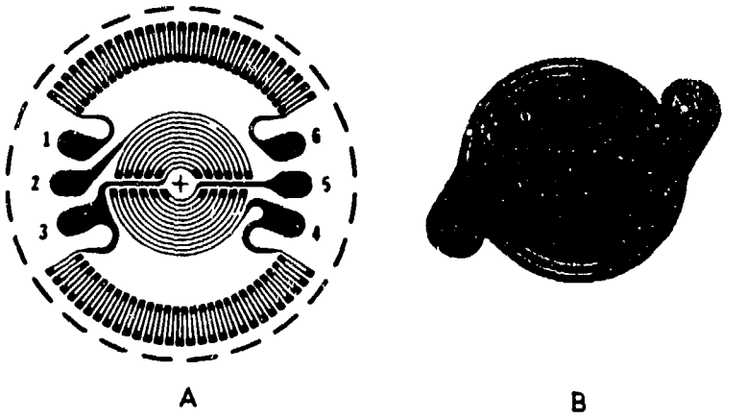

Fig. 7.4 - 2: Membrane rosette types
A full bridge
B quarter bridge

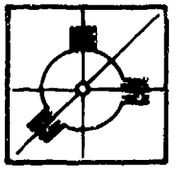

Fig. 7.5 - 1: Rosette for residual stress measurements according to the drill-hole procedure

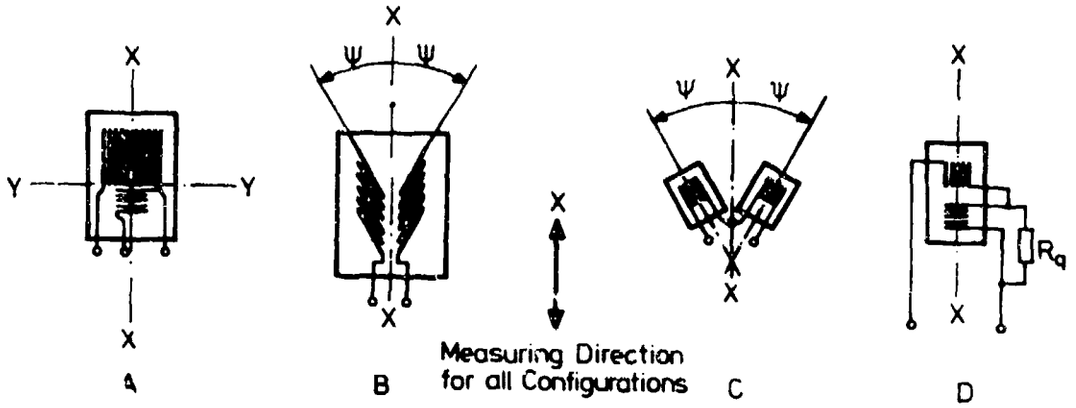

Fig. 7.6 - 1: Stress gauge types

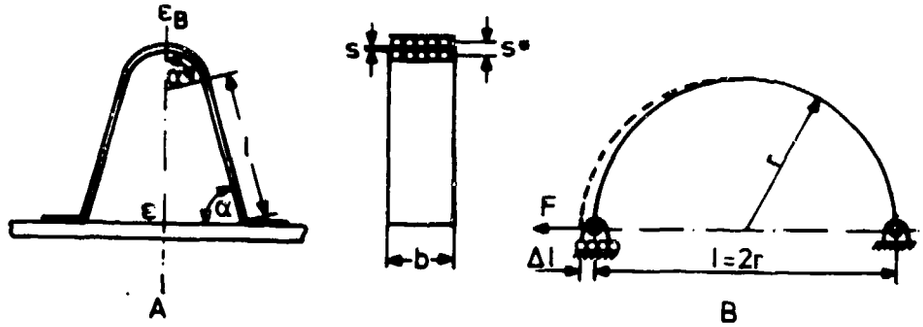

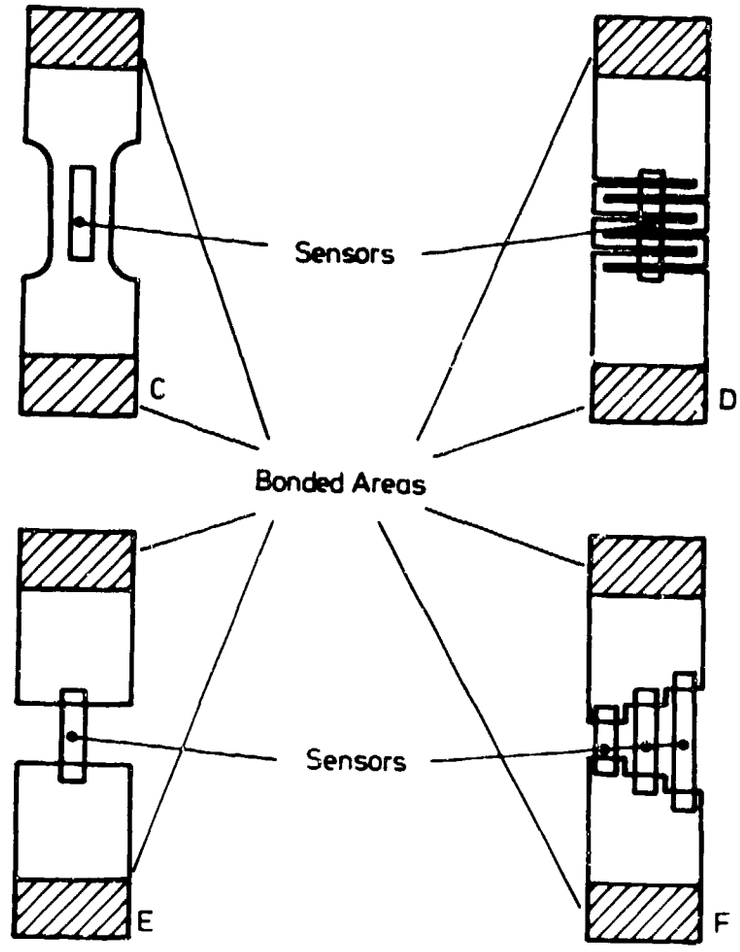

Fig. 7.11 - 1: Strain transformers
A,B strain transformers for excessively large strains
C,D,E,F strain transformers for excessively small strains

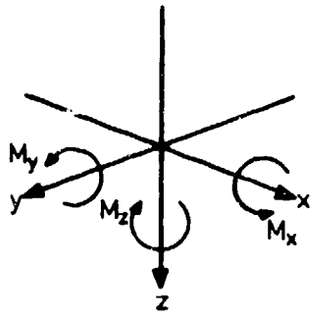

Fig. 7.14 - 1: Coordinate system for forces and moments as used in chapter 7.14

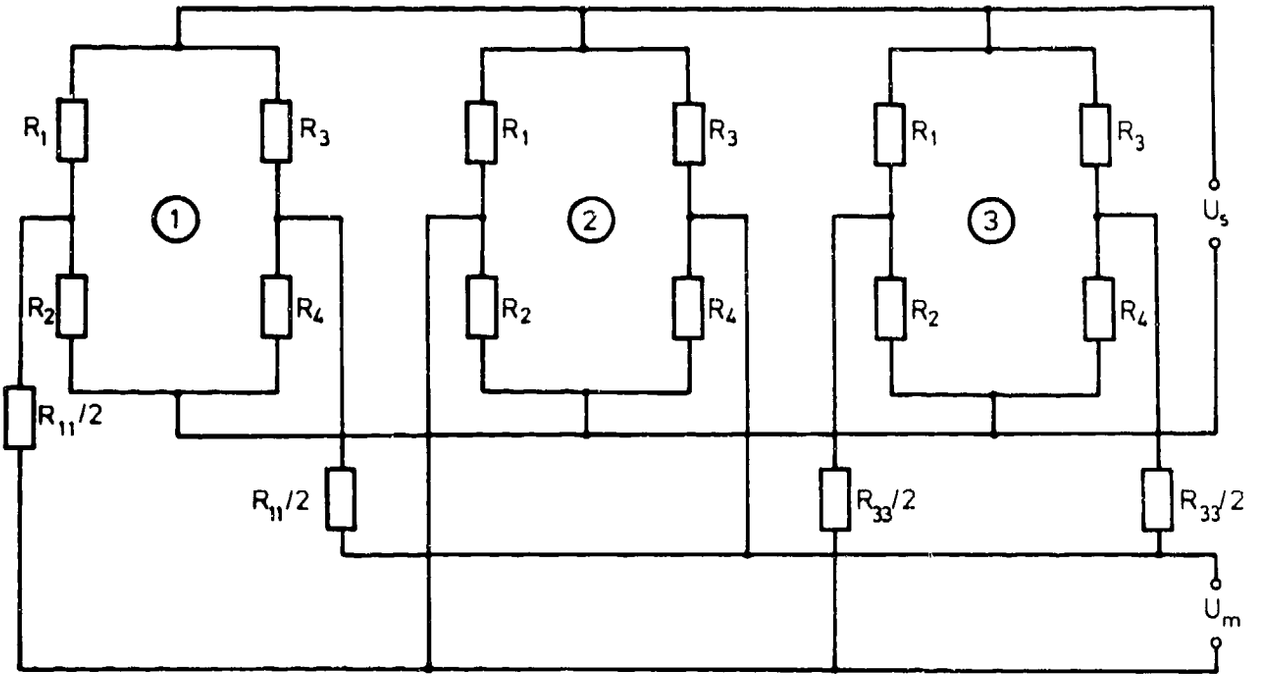

Fig. 7.14 - 2: Bridge interconnections

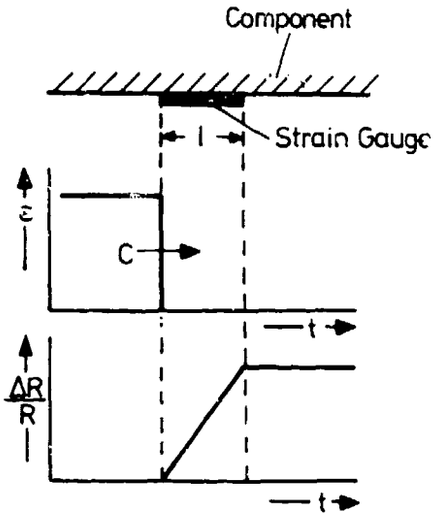

Fig. 7.15 - 1: Strain gauge indication during passage of a shockwave

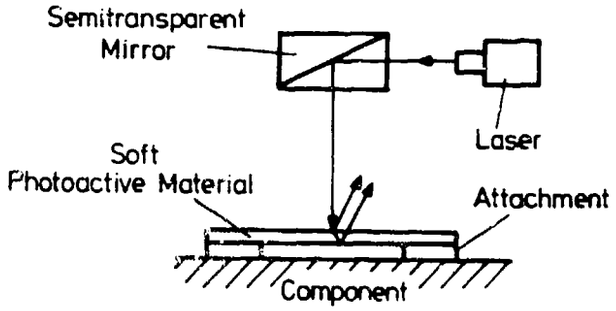

Fig. 7.17 - 1: Principle of the interferometric strain gauge

Normal Configuration

a

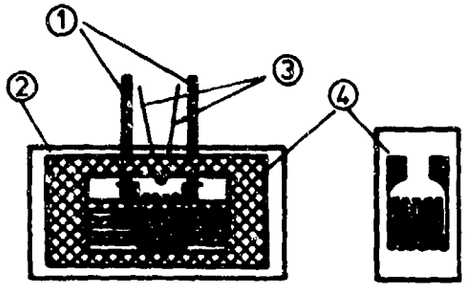

HT Strain Gauge with Removable Plastic Supporting Materials

① Connecting Leads
② Protective Foil
③ Thermocouple
④ Supplementary Supporting Material

b c

Weldable HT Strain Gauges

x x x x Welding Points

Single Gauge Half - Bridge

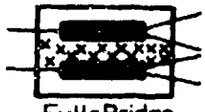

Full - Bridge

d

Fig. 8.1 - 1: High temperature strain gauge configurations

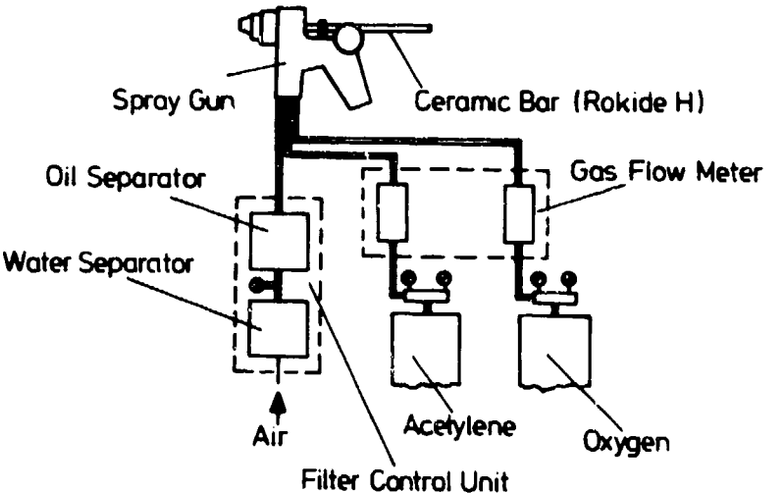

Fig. 8.1 - 2: Flame spraying device for application of free-grid strain gauges

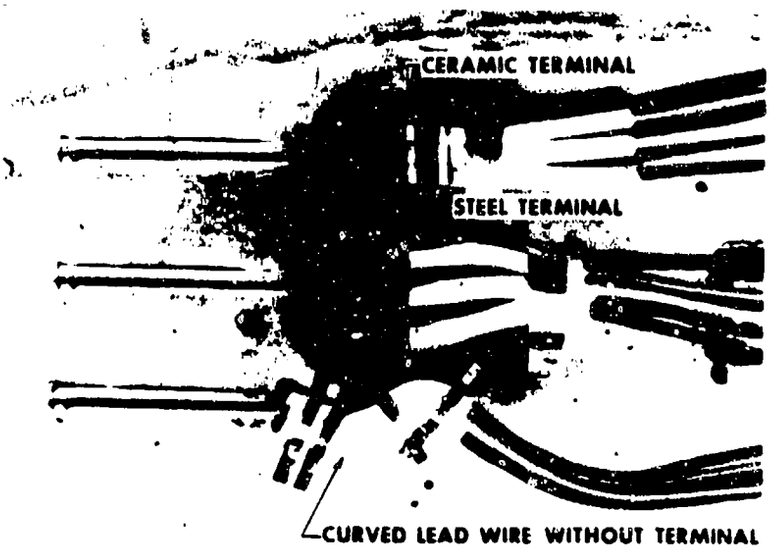

Fig. 8.1 - 3: Application and connection of weldable strain gauges (96)

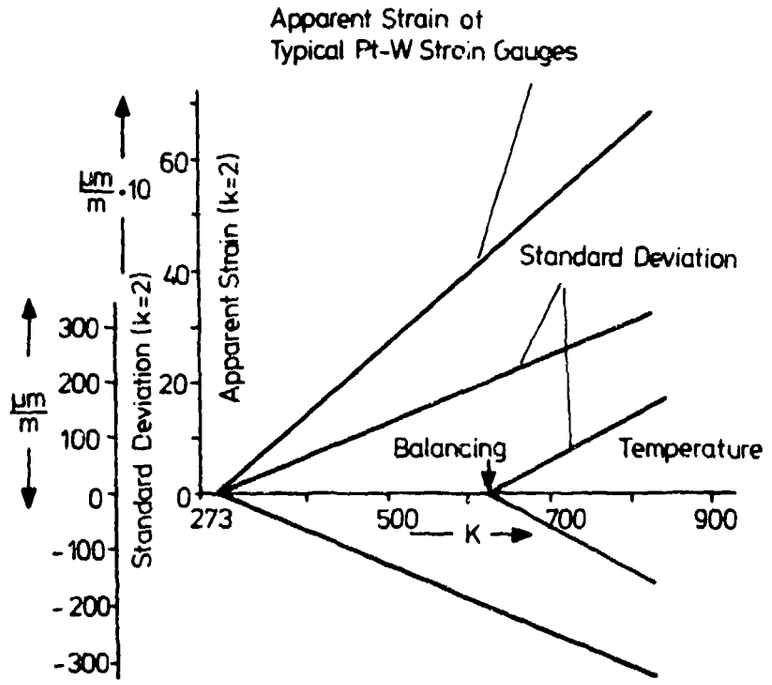

Fig. 8.1 - 4: Apparent strain (k=2) of typical Pt-W strain gauges applied to Co Cr Ni steel by flame spraying and their standard deviation, referenced to the mean value, as a function of temperature

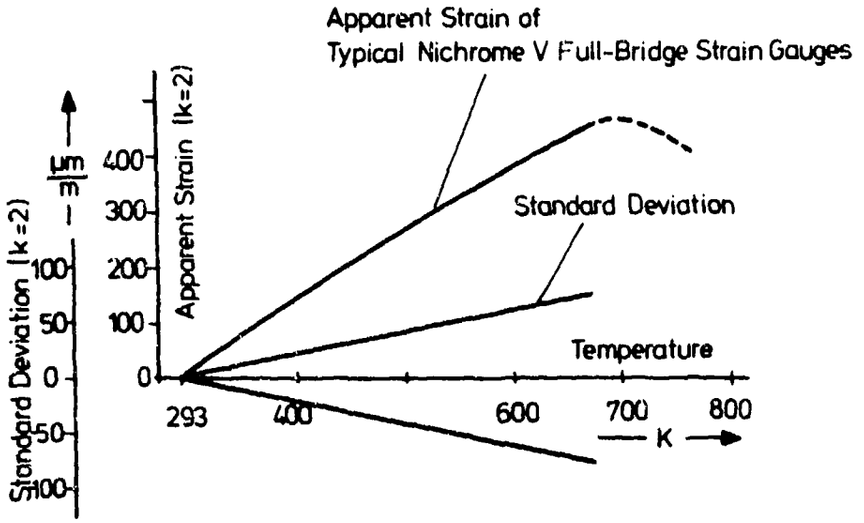

Fig. 8.1 - 5: Apparent strain (k=2) of typical weldable strain gauges on Co Cr Ni steel and their standard deviation, referenced to the mean value, as a function of temperature

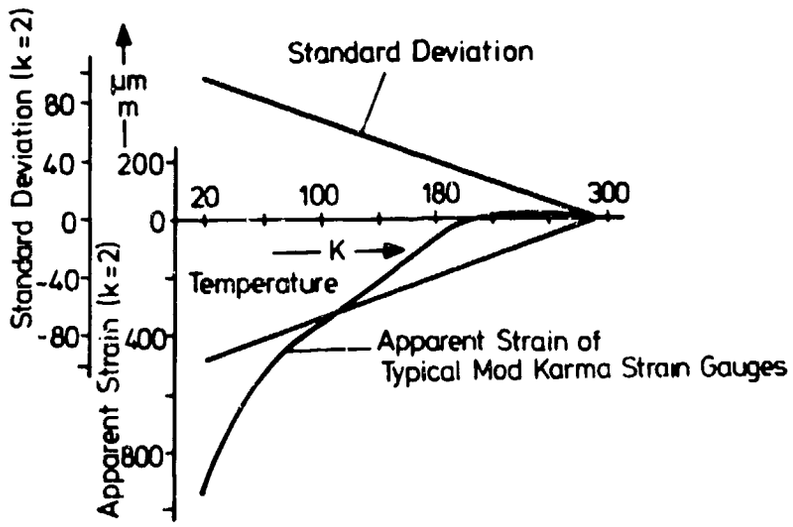

Fig. 8.1 - 6: Apparent strain (k=2) of typical modified Karma foil strain gauges on Al Zn Mg 1 and their standard deviation, referenced to the mean value, as a function of temperature

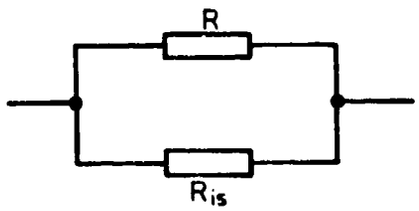

Fig. 8.1 - 7: Strain gauge insulation resistance

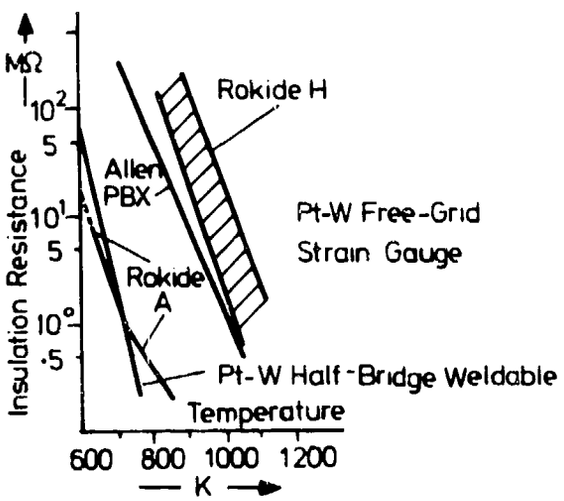

Fig. 8.1 - 8: Insulation resistance of high-temperature adhesives as a function of temperature

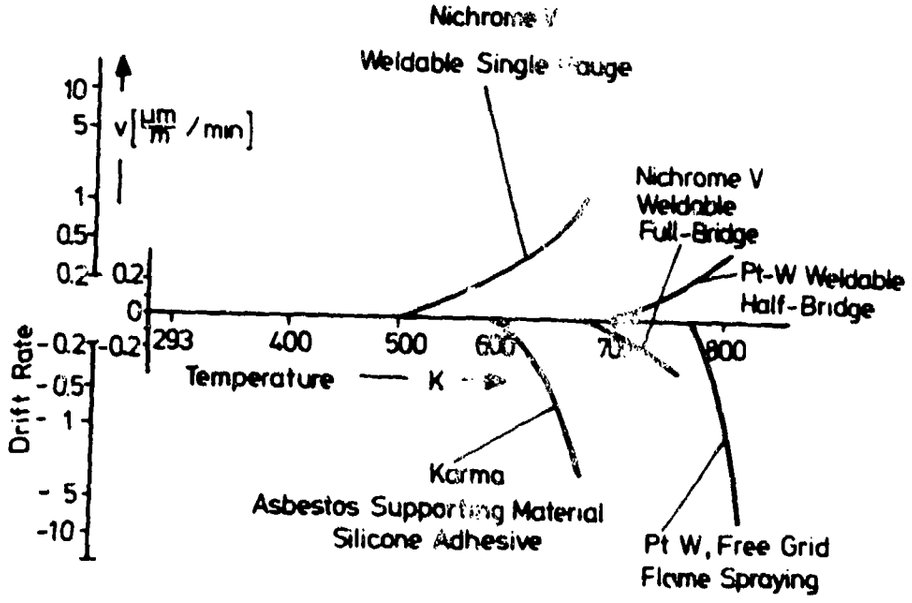

Fig. 8.1 - 9: Drift rates of various high temperature strain gauges

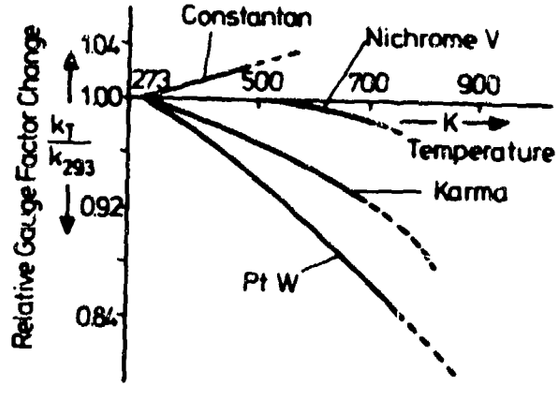

Fig. 8.1 - 10: Relative gauge factor change of various strain gauge grid materials as a function of temperature

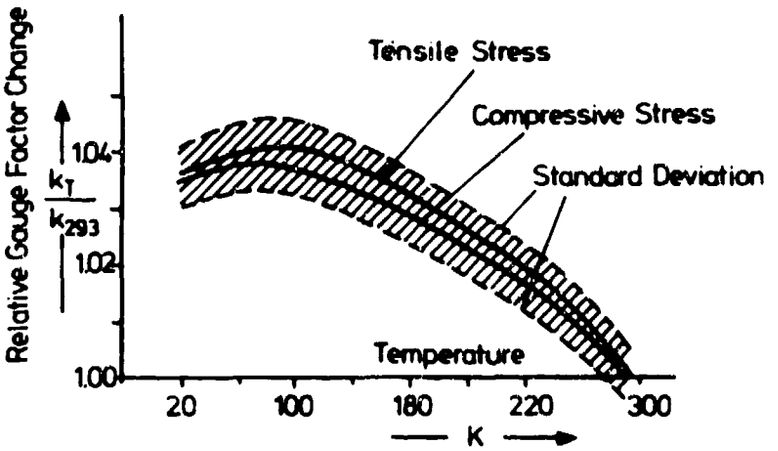

Fig. 8.1 - 11: Relative gauge factor change of typical modified Karma foil strain gauges on Al Zn Mg 1 as a function of temperature

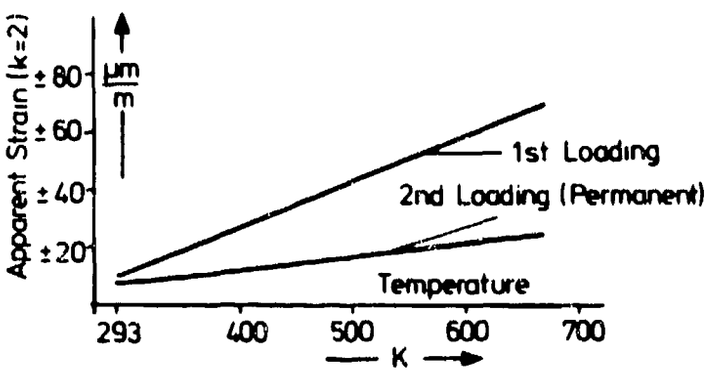

Fig. 8.1 - 12: Hysteresis of typical full-bridge strain gauges on CoCrNi steel as a function of temperature

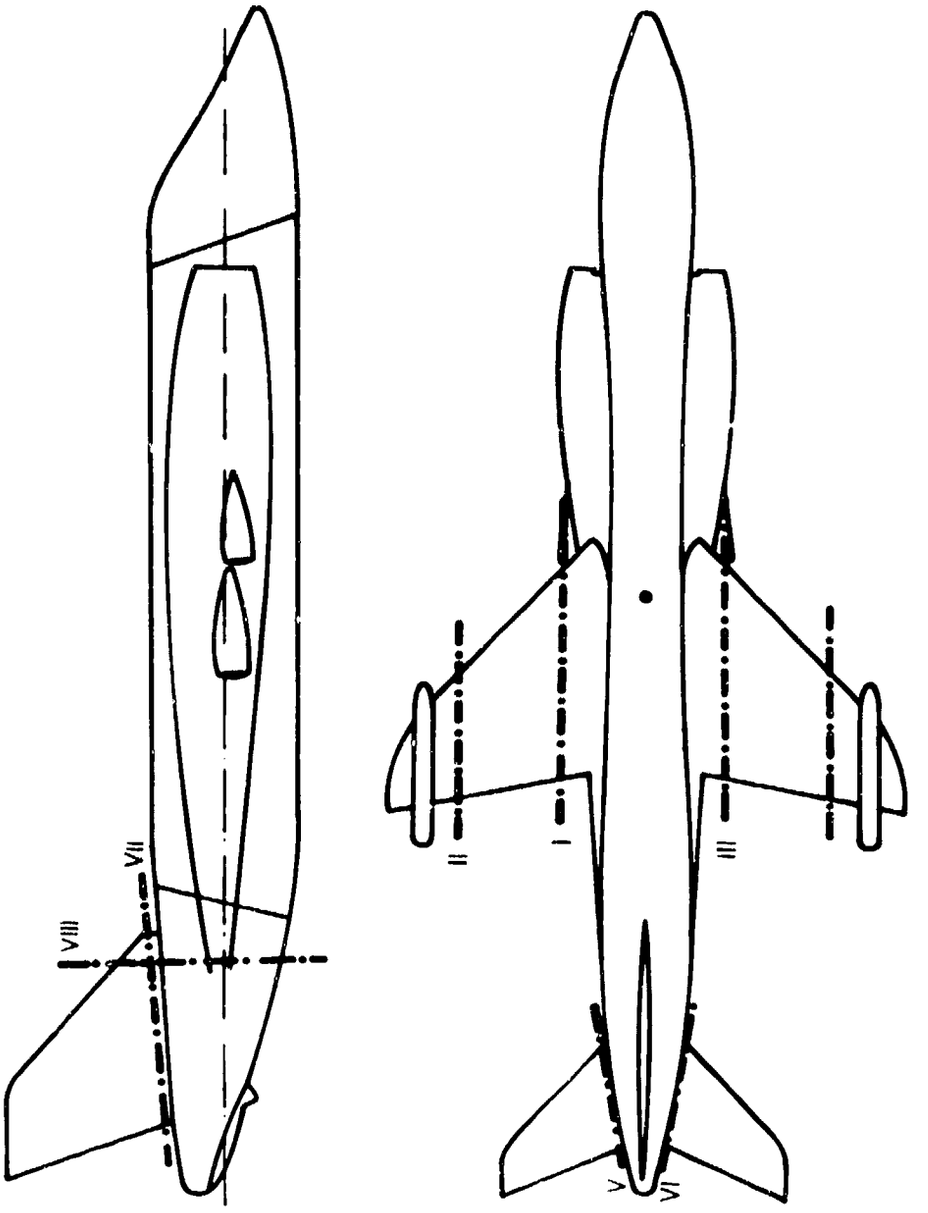

Fig. 9.2. - 1: VAK 191B V1 + V2
Position of measuring sections for load measurements during flight

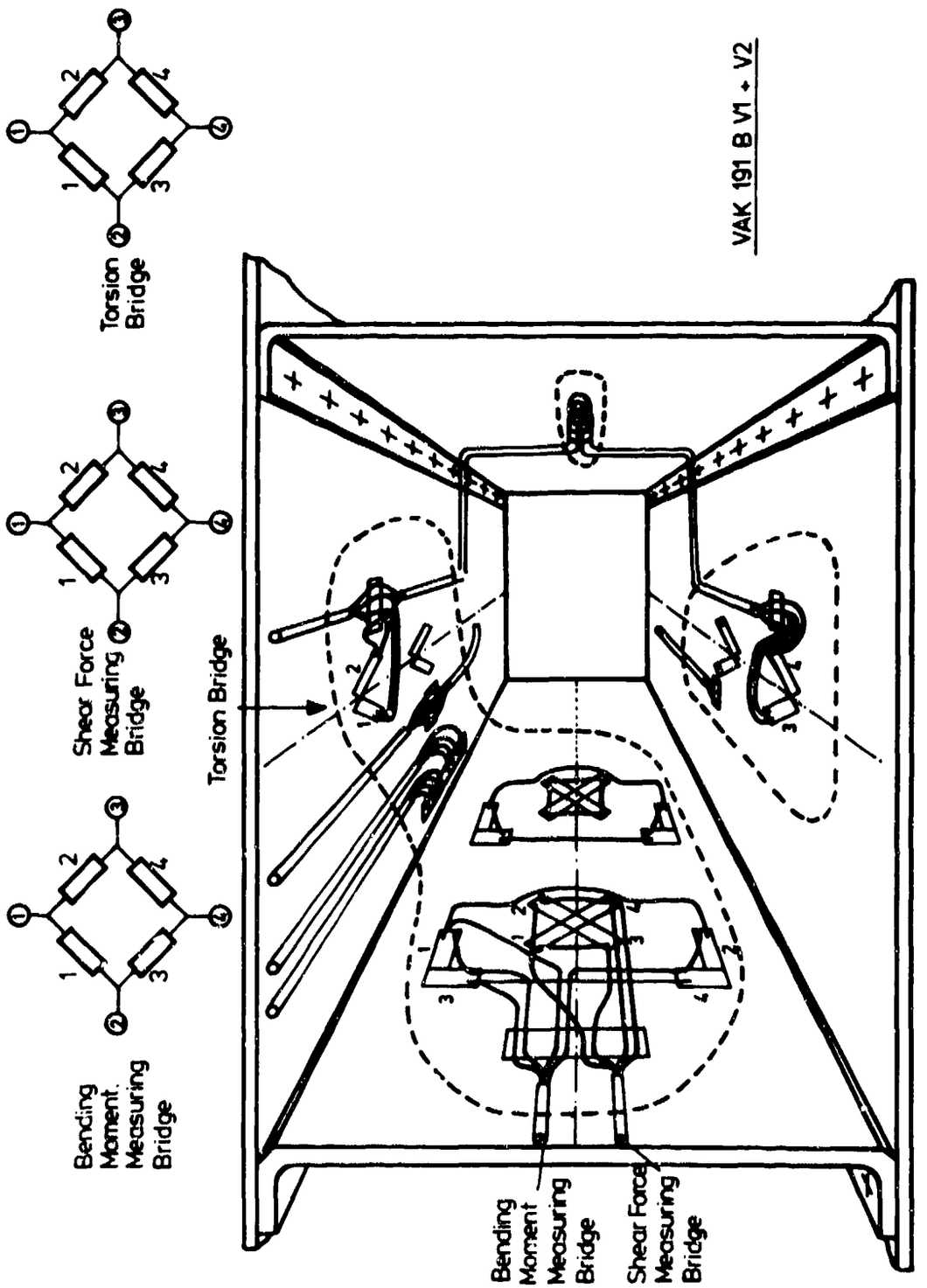

Fig. 9.2. - 2: View of a complete wing measuring point, spar and skin

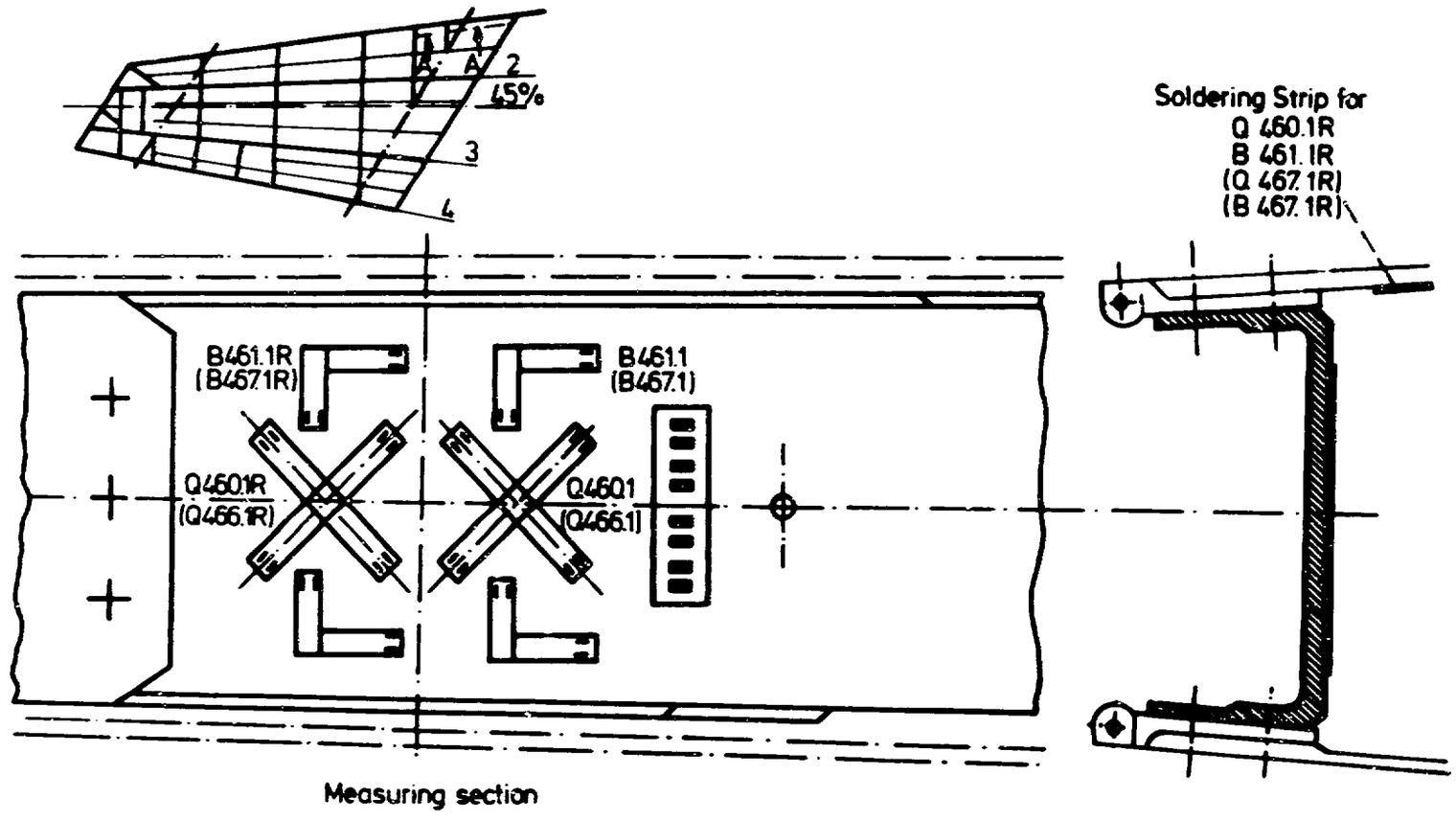

VAK 191B

Strain measuring points Wing
Bending moment and shear
force bridges

Fig. 9.2 - 3: Position of strain gauges on spar 1

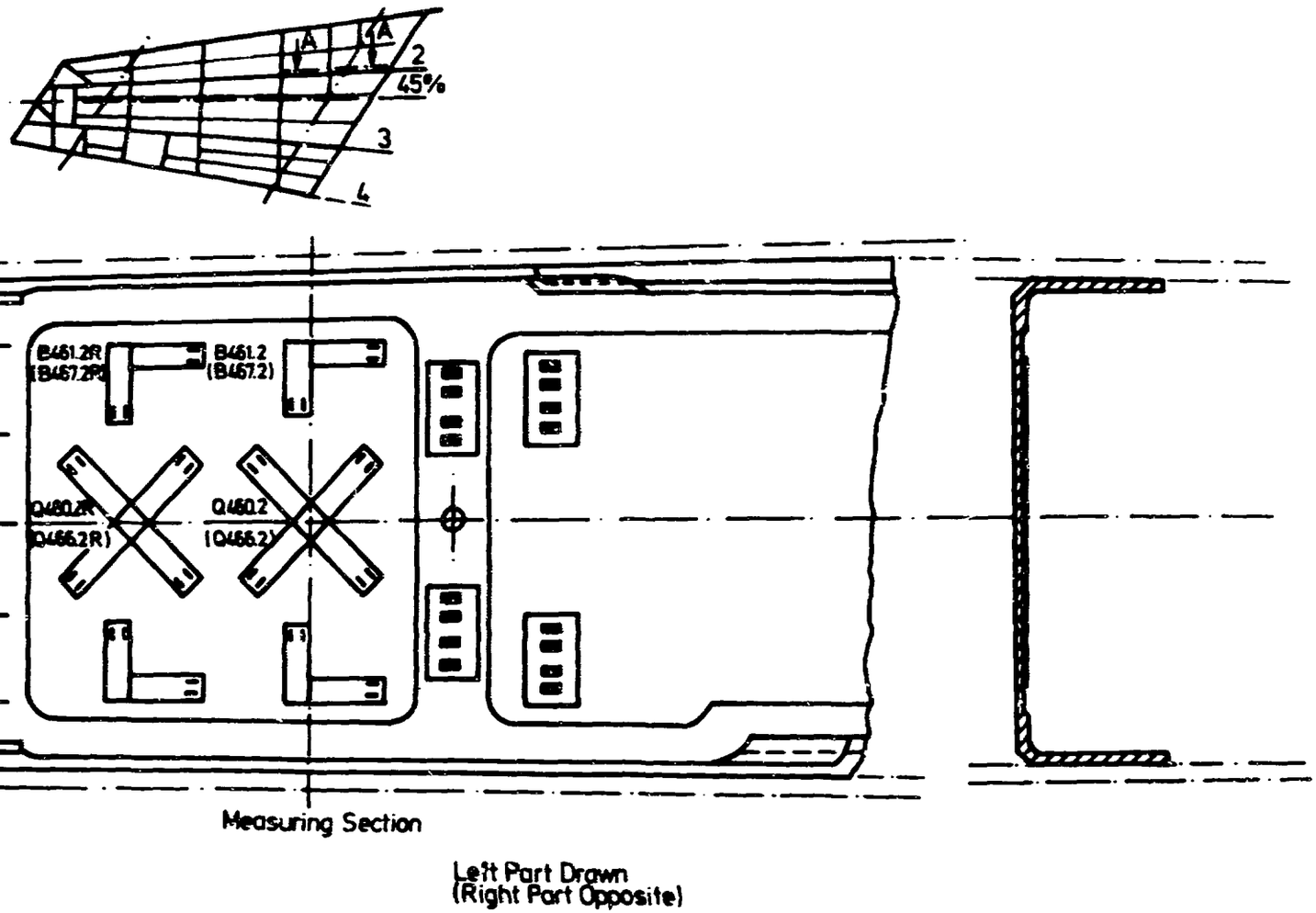

Fig. 9.2 - 4: Position of strain gauges on spar 2

VAK 191B

Strain measuring points Wing
Bending moment and shear
force bridges

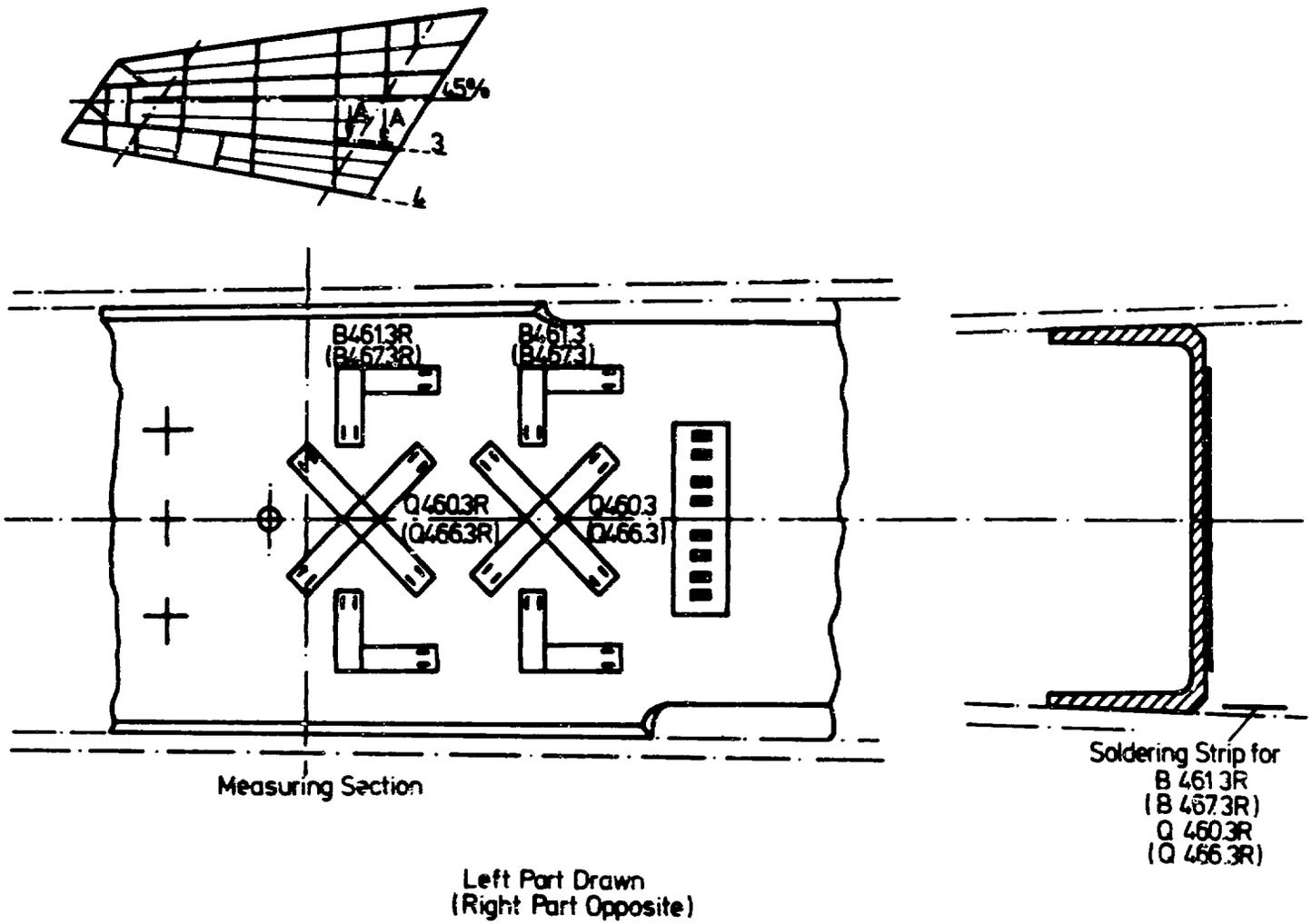

Fig. 9.2 - 5: Position of strain gauges on spar 3

VAK 191B

Strain measuring points Wing Bending moment and shear force bridges

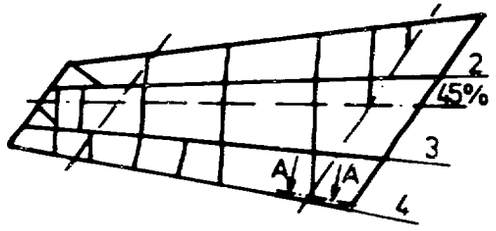

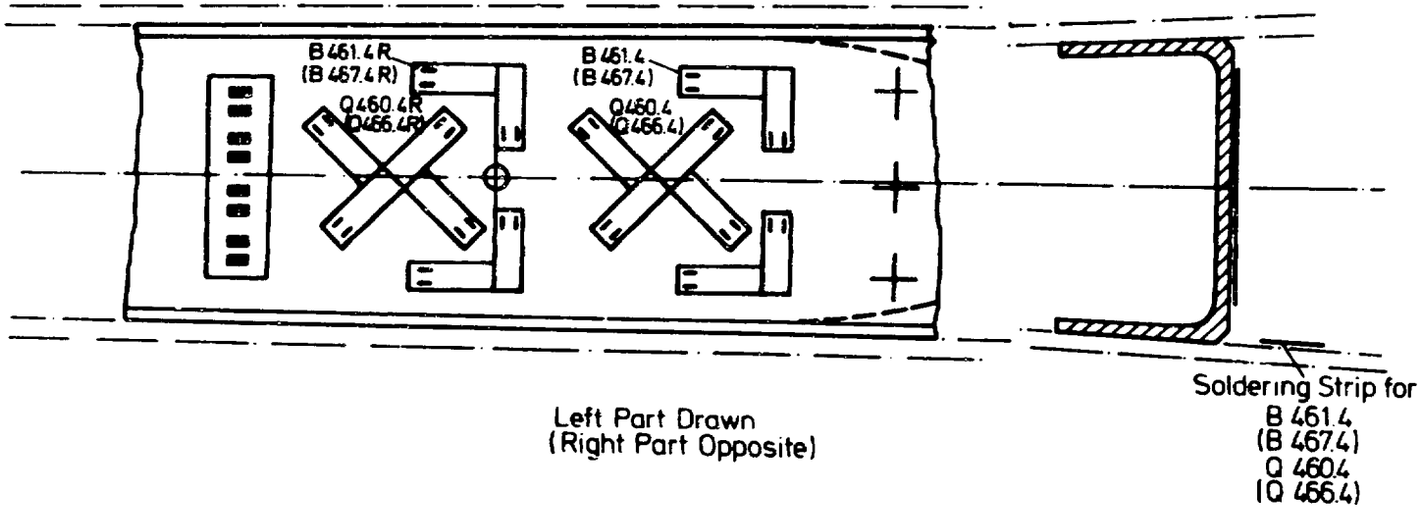

VAK 191B

Strain measuring points Wing Bending moment and shear force bridges

Fig. 9.2 - 6: Position of strain gauges on spar 4

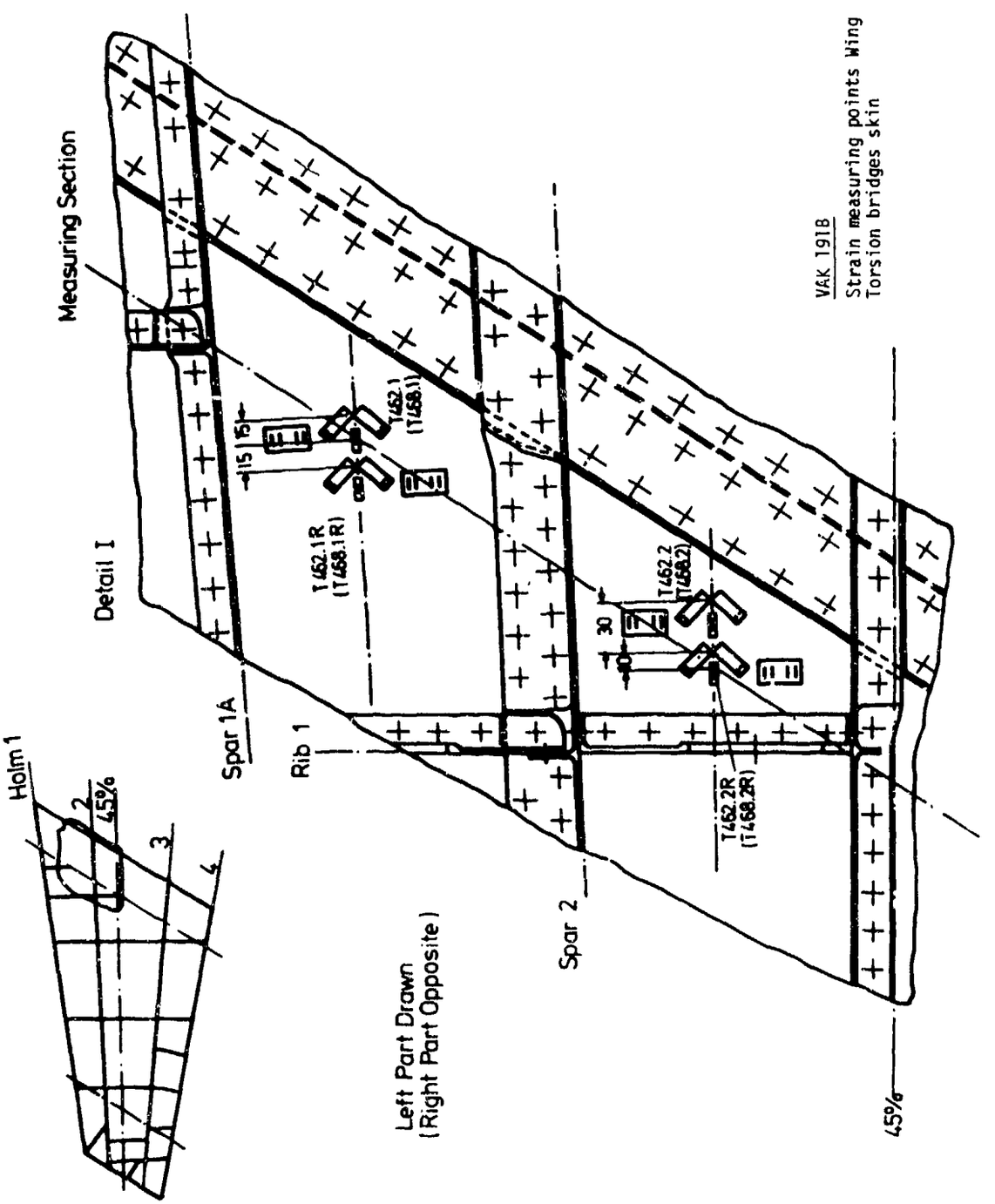

Fig. 9.2 - 7: Position of strain gauges on the skin at spar 2

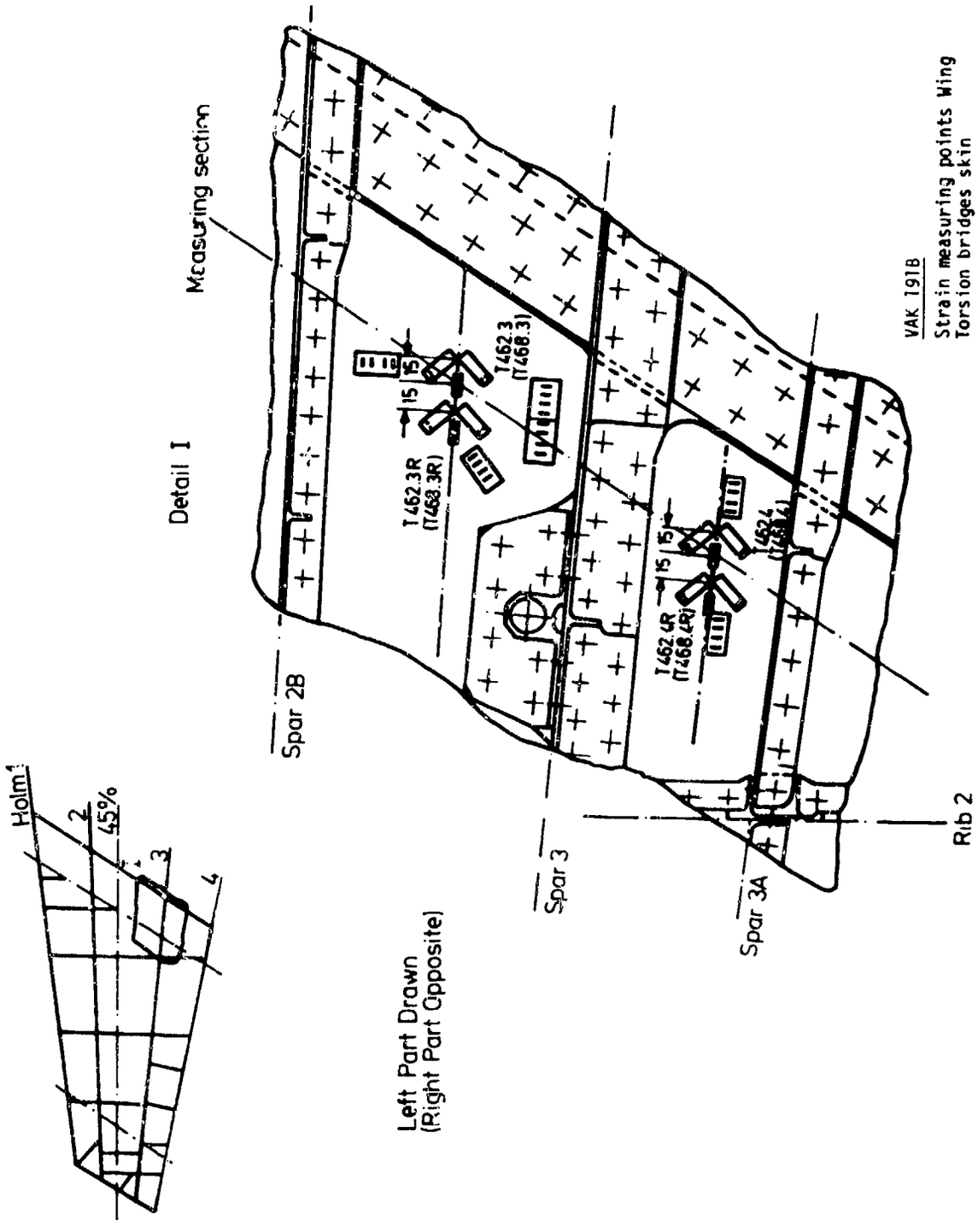

Fig. 9.2 - 8: Position of strain gauges on the skin at spar 3

AGARDograph No.160 Volume 7
Advisory Group for Aerospace Research and Development, NATO
STRAIN GAUGE MEASUREMENTS ON AIRCRAFT
E.Kottkamp, H.Wilhelm and D.Kohl
Published April 1976
150 pages

This AGARDograph is the seventh of the AGARD Flight Test Instrumentation Series, and is intended to give the test engineer a comprehensive description of the different aspects of strain and load measurements on aircraft. These measurements are of outstanding importance as they are the only practical means of determining material stresses during ground and flight tests.

This AGARDograph has been sponsored by the Flight Mechanics Panel of AGARD.

ISBN 92-835-1215-4

AGARD-AG-160 Vol.7
620.17:533.6.054:629.73.05

Aircraft
Strain measurement
Loads (forces)
Flight tests
Airborne equipment

AGARDograph No.160 Volume 7
Advisory Group for Aerospace Research and Development, NATO
STRAIN GAUGE MEASUREMENTS ON AIRCRAFT
E.Kottkamp, H.Wilhelm and D.Kohl
Published April 1976
150 pages

This AGARDograph is the seventh of the AGARD Flight Test Instrumentation Series, and is intended to give the test engineer a comprehensive description of the different aspects of strain and load measurements on aircraft. These measurements are of outstanding importance as they are the only practical means of determining material stresses during ground and flight tests.

This AGARDograph has been sponsored by the Flight Mechanics Panel of AGARD.

ISBN 92-835-1215-4

AGARD-AG-160 Vol.7
620.17:533.6.054:629.73.05

Aircraft
Strain measurement
Loads (forces)
Flight tests
Airborne equipment

AGARDograph No.160 Volume 7
Advisory Group for Aerospace Research and Development, NATO
STRAIN GAUGE MEASUREMENTS ON AIRCRAFT
E.Kottkamp, H.Wilhelm and D.Kohl
Published April 1976
150 pages

This AGARDograph is the seventh of the AGARD Flight Test Instrumentation Series, and is intended to give the test engineer a comprehensive description of the different aspects of strain and load measurements on aircraft. These measurements are of outstanding importance as they are the only practical means of determining material stresses during ground and flight tests.

This AGARDograph has been sponsored by the Flight Mechanics Panel of AGARD.

ISBN 92-835-1215-4

AGARD-AG-160 Vol.7
620.17:533.6.054:629.73.05

Aircraft
Strain measurement
Loads (forces)
Flight tests
Airborne equipment

AGARD
NATO ⊕ OTAN
7 RUE ANCELLE · 92200 NEUILLY-SUR-SEINE
FRANCE
Telephone 745-08-10 · Telex 610176

DISTRIBUTION OF UNCLASSIFIED AGARD PUBLICATIONS

AGARD does NOT hold stocks of AGARD publications at the above address for general distribution. Initial distribution of AGARD publications is made to AGARD Member Nations through the following National Distribution Centres. Further copies are sometimes available from these Centres, but if not may be purchased in Microfiche or Photocopy from from the Purchase Agencies listed below.

NATIONAL DISTRIBUTION CENTRES

BELGIUM
Coordonnateur AGARD – VSL
Etat-Major de la Force Aérienne
Caserne Prince Baudouin
Place Dailly, 1030 Bruxelles

CANADA
Defence Scientific Information Service
Department of National Defence
Ottawa, Ontario K1A 0Z2

DENMARK
Danish Defence Research Board
Østervoldgade 10
Copenhagen Ø

FRANCE
O.N.E.R.A. (Direction)
29 Avenue de la Division Leclerc
92 Châtillon sous Bagneux

GERMANY
Zentralstelle für Luft- und Raumfahrt-dokumentation und -information
D-8 München 86
Postfach 860880

GREECE
Hellenic Armed Forces Command
D Branch, Athens

ICELAND
Director of Aviation
c/o Flugrad
Reykjavik

ITALY
Aeronautica Militare
Ufficio del Delegato Nazionale all'AGARD
3, Piazzale Adenauer
Roma/EUR

LUXEMBOURG
See Belgium

NETHERLANDS
Netherlands Delegation to AGARD
National Aerospace Laboratory, NLR
P.O. Box 126
Delft

NORWAY
Norwegian Defence Research Establishment
Main Library
P.O. Box 25
N-2007 Kjeller

PORTUGAL
Direcção do Serviço de Material
da Força Aérea
Rua da Escola Politecnica 42
Lisbon
Attn: AGARD National Delegate

TURKEY
Department of Research and Development (ARGE)
Ministry of National Defence, Ankara

UNITED KINGDOM
Defence Research Information Centre
Station Square House
St. Mary Cray
Orpington, Kent BR5 3RE

UNITED STATES
National Aeronautics and Space Administration (NASA),
Langley Field, Virginia 23365
Attn: Report Distribution and Storage Unit

THE UNITED STATES NATIONAL DISTRIBUTION CENTRE (NASA) DOES NOT HOLD STOCKS OF AGARD PUBLICATIONS, AND APPLICATIONS FOR COPIES SHOULD BE MADE DIRECT TO THE NATIONAL TECHNICAL INFORMATION SERVICE (NTIS) AT THE ADDRESS BELOW.

PURCHASE AGENCIES

Microfiche or Photocopy

National Technical
Information Service (NTIS)
5285 Port Royal Road
Springfield
Virginia 22151, USA

Microfiche

Space Documentation Service
European Space Agency
114, Avenue Charles de Gaulle
92200 Neuilly sur Seine, France

Microfiche

Technology Reports
Centre (DTI)
Station Square House
St. Mary Cray
Orpington, Kent BR5 3RF
England

Requests for microfiche or photocopies of AGARD documents should include the AGARD serial number, title, author or editor, and publication date. Requests to NTIS should include the NASA accession report number. Full bibliographical references and abstracts of AGARD publications are given in the following journals:

Scientific and Technical Aerospace Reports (STAR),
published by NASA Scientific and Technical
Information Facility
Post Office Box 8757
Baltimore/Washington International Airport
Maryland 21240, USA

Government Reports Announcements (GRA),
published by the National Technical
Information Service, Springfield
Virginia 22161, USA

Printed by Technical Editing and Reproduction Ltd
Harford House, 7–9 Charlotte St, London W1P 1HD